université PARIS-SACLAY

Reconstructing the impacts of changes in land use on the transfers of sediments and contaminants in Southern Brazil and in Uruguay during the Anthropocene

Reconstruction des impacts des changements d'usage des sols sur les transferts de sédiments et de contaminants dans le Sud du Brésil et en Uruguay durant l'Anthropocène

Thèse de doctorat de l'Université Paris-Saclay

École doctorale n°129 : École doctorale Sciences de l'Environnement d'Île-de-France (SEIF)
Spécialité de doctorat : Géosciences
Graduate School : Géosciences, Climat, Environnement et Planètes
Référent : Université Versailles Saint-Quentin

Thèse préparée au **Laboratoire des Sciences du Climat et de l'Environnement (Université Paris-Saclay, CNRS, CEA, UVSQ, FRANCE)**, sous la direction d'**Olivier EVRARD**, Directeur de recherche CEA-LSCE, d'**Olivier Cerdan**, Directeur de recherche BRGM et d'**Anthony FOUCHER**, Chargé de recherche CEA-LSCE

Thèse soutenue à Paris-Saclay, le 22 septembre mois 2026, par

Amaury Bardelle

Composition du jury

Membres du jury avec voix délibérative

Christine HATTE Directrice de Recherche, Laboratoire des Sciences du Climat et de l'Environnement (LSCE), CEA-CNRS-UVSQ, Gif-sur-Yvette, France	Présidente
Nathalie DUBOIS Professeure, Eawag - Institut Fédéral Suisse des Sciences et Technologies de l'Eau	Rapporteure et Examinatrice
Kristof VAN OOST Professeur, Université catholique de Louvain	Rapporteur et Examinateur
Jean MINELLA Professeur, Department of Soils, Universidade Federal de Santa Maria	Examinateur

THESE DE DOCTORAT
NNT : 2026UPASJ017

université PARIS-SACLAY

ÉCOLE DOCTORALE
Sciences de l'Environnement d'Île-de-France (SEIF)

Titre : Reconstruction des impacts des changements d'usage des sols sur les transferts de sédiments et de contaminant dans le sud du Brésil et en Uruguay durant l'Anthropocène

Mots clés : datation, traçage sédimentaire, modélisation, érosion des sols, radionucléides

Résumé : L'Amérique du Sud en général et les biomes de la Pampa et de la Forêt Atlantique en particulier (Brésil, Argentine, Uruguay), ont connu une expansion et une intensification agricoles rapides depuis la fin du XXe siècle. Ces transformations incluent la conversion de paysages naturels en terres cultivées, l'adoption généralisée du semis direct et une augmentation marquée de l'utilisation de pesticides. Depuis 1985, les surfaces consacrées aux pâturages, aux terres cultivées et aux plantations forestières ont augmenté respectivement de 23 %, 160 % et 288 % en Amérique du Sud. Malgré leur ampleur, l'impact de ces changements sur l'érosion des sols et le transfert des sédiments reste insuffisamment quantifié, en raison de l'absence de suivi instrumental à long terme et d'archives permettant la reconstruction des processus passés. Cette thèse visait ainsi à reconstituer la redistribution des sols et les transferts de contaminants associés à différentes échelles spatiales et temporelles dans le sud de l'Amérique du Sud, en combinant des approches multi-proxies. Elle a permis d'évaluer la représentativité et la fiabilité de la méthode des inventaires de radionucléides pour quantifier l'érosion à l'échelle du versant, en analysant la variabilité spatiale, les potentiels biais et incertitudes méthodologiques de la méthode, et en comparant ces estimations à celles issues d'un modèle d'érosion distribué et évènementiel. L'impact des changements d'utilisation des sols a pu être étudié à partir de l'analyse d'archives prélevées dans deux lacs-réservoirs contrastés du bassin du fleuve Uruguay. Le réservoir de Salto Grande, situé à l'aval d'un bassin fortement anthropisé, permet d'étudier les dynamiques récentes (1980-2023) du transfert sédimentaire et de contaminants. À l'inverse, le réservoir de Rincón del Bonete fournit un enregistrement à plus long terme (1945-2025) de la transition entre paysages naturels et agricoles, en ce comprise l'évolution des pratiques culturales et de l'usage des pesticides. Les résultats montrent une forte variabilité spatiale de la redistribution des sols à l'échelle de la parcelle, avec des inventaires de radionucléides et des estimations d'érosion contrastées pour des profils collectés à proximité immédiate. Le choix du modèle de conversion impacte tant l'intensité reconstruite de la redistribution de sol que son signe (érosion ou accumulation). Dans le bassin de Salto Grande, les flux sédimentaires ont diminué de 61 % depuis les années 1980, tandis que la contribution de la partie sud du bassin aux sédiments du barrage a augmenté de 71% depuis les années 2000, en lien avec les aménagements hydrauliques, l'expansion agricole et la généralisation du semis direct. Une augmentation concomitante des flux de pesticides a également été observée. À plus long terme, l'archive sédimentaire de Rincón del Bonete indiquent l'occurrence d'une phase agricole initiale ayant un impact limité sur l'érosion des sols (1945–1991), suivie d'une diminution des apports sédimentaires lors de l'adoption du semis direct et de rotations avec pâturages (1991–2007), puis une augmentation récente de l'érosion et des flux sédimentaires (2007–2023) associée à l'intensification agricole et dissocié d'une variabilité naturelle. La détection de pesticides interdits, tels que le DDT, suggère une remobilisation de contaminants historiques liée à cette hausse récente de l'érosion. Ces travaux contribuent à améliorer la reconstruction des dynamiques d'érosion et de transfert sédimentaire dans une région où les données restent limitées, et soulignent la nécessité d'un suivi continu et de mesures agro-environnementales visant à limiter l'érosion des sols et la contamination par les pesticides.

Title : Reconstructing the impacts of changes in land use on the transfers of sediments and contaminants in Southern Brazil and in Uruguay during the Anthropocene

Keywords : dating, sediment tracing, modelling, soil erosion, radionuclides

Abstract : South America in general, and the Pampa and Atlantic Forest biomes (Uruguay, Argentina and Brazil) in particular, have undergone a rapid agricultural expansion and intensification since the late 20th century. These changes include the conversion of natural landscapes to cropland, the widespread adoption of no-tillage systems, simplification of landscapes and a marked increase in pesticide use. Since 1985, pasture, cropland, and forest plantation areas have increased by 23%, 160%, and 288%, respectively. Despite their magnitude, the implications of these transformations for soil erosion and sediment transfers remain insufficiently quantified, mainly because of the limited availability of long-term monitoring for their retrospective reconstruction. This thesis deployed multi-proxy approaches to reconstruct soil redistribution and sediment-associated contaminant transfers across a range of spatial and temporal scales in southern South America. A first objective was to evaluate the representativeness and reliability in fallout radionuclide inventory approaches for reconstructing erosion processes at the hillslope scale. This included assessing spatial variability and methodological limitations of radionuclide-based estimates, and comparing these estimates with outputs from a distributed erosion model. A second objective was to assess the impact of land-use change and agricultural intensification on sediment transfer dynamics investigating two contrasting reservoir systems within the Uruguay River basin. The Salto Grande reservoir, constructed in 1980, and draining a catchment already largely under agricultural use, was investigated to identify sediment sources and associated contaminant fluxes and examine the effects of no-tillage expansion and soybean monocropping (1980-2023). In contrast, the Rincón del Bonete reservoir, constructed in 1945 in a predominantly uncultivated basin, provides a longer-term record (1945-2023) of the transition from rather natural to more anthropogenic landscapes, including agricultural changes in tillage practices and increasing pesticide application. Results highlight substantial spatial variability in soil redistribution at the hillslope scale, with neighbouring cores yielding contrasting radionuclide inventories and erosion estimates. The choice of conversion model was found to significantly impact both the magnitude and the sign of soil redistribution. In the Salto Grande basin, sediment fluxes decreased by 61% since the 1980s, while the contribution from the southern part of the basin increased by 75% since the 2000s. These changes can be explained by the construction of dams upstream, agricultural expansion downstream, and the widespread adoption of monocropping no-tillage practices. Furthermore, an associated increase in pesticide fluxes was recorded. Over longer timescales, sediment records from Rincon del Bonete indicate an initial phase of limited impact despite the initiation of pesticide use (1945-1991), followed by a reduction in sediment delivery during the transition to no-tillage and pasture rotation (1991-2007), and subsequently (2007-2023) a renewed increase in sediment fluxes linked to large-scale land conversion and intensified herbicides application, largely decoupled from natural variability. The detection of banned pesticide compounds such as DDT further suggests the recent remobilisation of legacy contaminants. Overall, this work contributes to improving the reconstruction of soil erosion and sediment transfers in a data-scarce region since the onset of modern agriculture in South America and provides a framework for combining sediment archives, radionuclide tracers, and modelling tools. These results support a more robust assessment of the environmental impacts of agricultural development and highlight the need for continued monitoring and for the implementation of agri-environmental measures to mitigate soil erosion and pesticide contamination in Southern South America.

0.1 . Remerciements

Un peu plus de trois ans se sont écoulés depuis le début de ma thèse, qui n'aurait pas pu voir le jour sans l'aide de nombreuses personnes. J'ai toujours été meilleur pour rendre la pareille que pour rédiger de beaux remerciements, mais je tiens à remercier toutes celles et ceux qui ont contribué à l'aboutissement de ce travail.

Je souhaite tout d'abord remercier mes encadrants, les « Olivier » et Anthony.

Mes plus grands remerciements vont à mon directeur de thèse, Olivier Evrard, qui a su voir en moi le potentiel pour réaliser cette thèse, il y a un peu plus de trois ans, lors de notre premier rendez-vous en visioconférence. Sa présence, ses conseils et ses relectures rapides m'ont permis d'avancer efficacement, de mener à bien presque tous nos objectifs initiaux et de trouver en lui un bel exemple de ce que peut et doit être un chercheur. Merci également à Olivier Cerdan et Anthony foucher pour leur bienveillance et leur aide au travers de cette thèse. Je n'oublie pas non plus tous les moments conviviaux partagés en mission, lors de nos déjeuners et de nos pauses café. Il paraît qu'une nouvelle machine à café est arrivée dans notre salle de pause, je n'aurais donc pas le choix que de revenir au laboratoire l'essayer.

Je tiens ensuite à remercier les collègues avec qui j'ai passé la majeure partie de ces trois années. Je pense d'abord aux anciens doctorants, Rémi, Thomas et Camille, qui m'ont beaucoup appris à mon arrivée et m'ont fait vivre de « belles » expériences, à l'instar d'une visite des égouts parisiens. Je pense aussi à mon premier mon collègue de bureau, Paul, et encore Clément et Yang et les autres collègue de notre équipe avec qui nous avons pu échanger pendant de long moments pour refaire le monde ou plus simplement pour se soutenir dans ce long travail de thèse.

Puis il y a Romain, devenu mon collègue de bureau et ami, avec qui j'ai fait les quatre cents coups et sans qui cette thèse aurait sans doute pris une tout autre tournure. Sans rentrer d'avantages dans les détails qui resteront néanmoins dans mon esprit et dans mon coeur, merci à toi pour tout ce que tu m'as apporté. Enfin, Pierre-Alexis, parti étudier en postdoc au Japon, que nous n'avons d'abord connu qu'en visioconférence et que nous avons découvert à son retour en France. Romain et moi l'avons sans doute épuisé à force de lui poser des questions et de lui demander conseil. Pour cela, et pour tout ce que tu as fait pour nous, un très grand merci ! Merci à tous les deux donc, et j'espère que nous aurons l'occasion (ou que nous la créerons) de travailler de nouveau ensemble et que nous continuerons à entretenir les amitiés que nous avons nouées.

Merci aux collègues du BRGM, et tout particulièrement à Rosalie Vandrome, pour son implication dans ce projet de thèse, son expertise et sa façon d'aborder les choses. Grâce à elle, j'ai pu avancer sereinement et poser toutes les questions que je souhaitais. Merci également à Thomas Grangeron, qui m'a aidé à avancer, et à Claire Brugeron, dont l'aide administrative m'a grandement facilité les choses. Merci également aux collègues d'EDITEM et en premier lieu Pierre Sabatier qui aura notemment passé

de nombreuses heures pour nous aider dans la réalisation du package SedimentR.

Un grand merci à Fabio Schneider pour son aide lors de notre campagne d'échantillonnage au Brésil. Sans lui, cette étude n'aurait sans doute jamais vu le jour. Merci aussi à sa famille, qui nous a accueillis à bras ouverts pendant plusieurs jours. Ce fut une expérience incroyable avec toi et Gerald. J'espère avoir l'occasion de travailler de nouveau avec vous et de revoir ta famille au Brésil.

Merci aux chercheurs qui m'on acceuilli au Brésil et en Urguay, Jean Minella, Tales tiecher, Professor Inda, Rafael Ramon, Marcos Tassano et Mirel Cabrera et tous les autres et qui m'on beaucoup aidé pour mieux comprendre les zones que nous étudions et m'on permis de bien avancer.

Merci aux stagiaires, Nathan Martins et Robin Paillat, qui m'ont permis d'avancer plus rapidement sur certains sujets. J'espère que vous avez apprécié de travailler sur les projets que nous vous avions proposés et que cela pourra vous insipirer à l'avenir.

Je tiens aussi à remercier Irène Lefèvre pour l'aide qu'elle m'a apportée sur le plan scientifique, pour son franc-parler et pour sa capacité à nous mettre en contact avec d'autres chercheurs afin de faire avancer nos travaux. Je n'oublie pas non plus les nombreuses anecdotes et histoires du laboratoire qu'elle nous a racontées et qui nous ont beaucoup fait rire.

Je souhaite également remercier toutes les autres personnes avec qui j'ai eu l'occasion de travailler, notamment les chercheurs des projets AVATAR et CELEST LAB. Je préfère ne pas citer de noms, de peur d'en oublier, mais je vous remercie toutes et tous ! J'espère que nous aurons de nouveau l'occasion de travailler ensemble.

Je remercie Nathalie Dubois et Kristof Van Oost d'avoir accepté d'évaluer ce manuscrit en tant que rapporteurs, ainsi que Christine Hatte et Jean Minella d'avoir participé au jury de ma thèse en tant qu'examinateurs. Merci également aux membres de mes comités de pilotage, Gwenaël Hervé, Jean Minella et Marcos Tassano, pour leurs précieux conseils et leur aide tout au long de ce projet.

Je tiens finalement à remercier ma compagne, Sonya, qui m'a soutenu tout au long de cette thèse, ainsi que sa famille, qui m'a aidé à sortir de ma bulle et à me détendre.

Merci à ma famille, mes parents et mes grands-parents, mes sœurs et ma tante, pour votre soutien tout au long de cette thèse.

J'ai une pensée toute particulière pour tous mes grands-parents. Je pense à ma grand-mère, la seule à avoir pu voir ce travail achevé, et à mon grand-père, que j'espérais encore avoir près de nous à la fin, mais qui nous a quittés quelques mois trop tôt. Je sais que vous étiez tous fiers de moi, de là où vous me regardiez.

0.2 . Résumé de thèse en français

0.2.1 . Contexte

L'Amérique du Sud en général, et les biomes de la Pampa et de la Forêt Atlantique (Brésil, Argentine, Uruguay) en particulier, ont connu une expansion et une intensification rapides des pratiques agricoles depuis la fin du XXe siècle. Ces transformations se traduisent notamment par la conversion de milieux naturels en terres cultivées, l'adoption généralisée du semis direct et une augmentation marquée de l'utilisation de pesticides. Malgré leur ampleur, les conséquences de ces changements sur la redistribution des sols, les flux sédimentaires et les transferts de contaminants restent encore mal connues, en raison du manque de données temporelles et de dispositifs de suivi à grande échelle.

0.2.2 . Objectifs

Dans ce contexte, cette thèse vise à reconstituer les dynamiques de redistribution des sols et de transfert des contaminants associés à différentes échelles spatiales et temporelles dans le sud de l'Amérique du Sud, en développant et en appliquant une approche multi-proxies et multi-échelles. Elle s'articule autour de deux objectifs principaux.

Le premier objectif consiste à évaluer la représentativité et la fiabilité des approches basées sur l'échantillonnage de profils de sols pour reconstituer les processus d'érosion et de sédimentation à l'échelle du versant. Il s'agit d'analyser la variabilité spatiale des inventaires de radionucléides, d'identifier les biais liés aux conditions de dépôt et aux stratégies d'échantillonnage, et de préciser les limites méthodologiques associées à l'estimation des taux d'érosion à partir de ces traceurs radioactifs. Cet objectif inclut également une comparaison des taux d'érosion estimés à partir de modèles de conversion des inventaires de radionucléides avec ceux issus d'un modèle d'érosion distribué, contraint par des données hydrométéorologiques (pluie, débits, flux sédimentaires), afin de mieux quantifier l'érosion et d'interpréter les variations spatio-temporelles de ce processus.

Le second objectif vise à quantifier et à comprendre l'impact des changements d'usage des sols et de l'intensification agricole sur les dynamiques de transfert sédimentaire et de contaminants à l'échelle de grands bassins versants à travers les biomes de la Pampa et de la Forêt Atlantique (Figure 1). Il repose sur l'analyse d'archives sédimentaires lacustres issues de deux bassins contrastés. D'une part, l'étude du réservoir de Salto Grande (Figure 1), drainant un bassin transnational de 266,000 km^2, a pour objectif d'identifier les principales sources de sédiments, de retracer l'évolution des flux sédimentaires et des apports en contaminants, et d'évaluer l'impact des mutations agricoles majeures, telles que l'adoption du semis direct et l'expansion des cultures de soja. D'autre part, l'analyse du réservoir de Rincón del Bonete (Figure 1), caractérisé par un enregistrement sédimentaire de plus longue durée (1945-2023) et un bassin versant initialement peu anthropisé, vise à reconstituer la transition progressive depuis des paysages dominés par des couverts naturels vers des systèmes agricoles intensifs, et à évaluer les

effets combinés des changements de pratiques culturales et de l'usage croissant de pesticides sur la production et le transfert des sédiments depuis le milieu du XXe siècle.

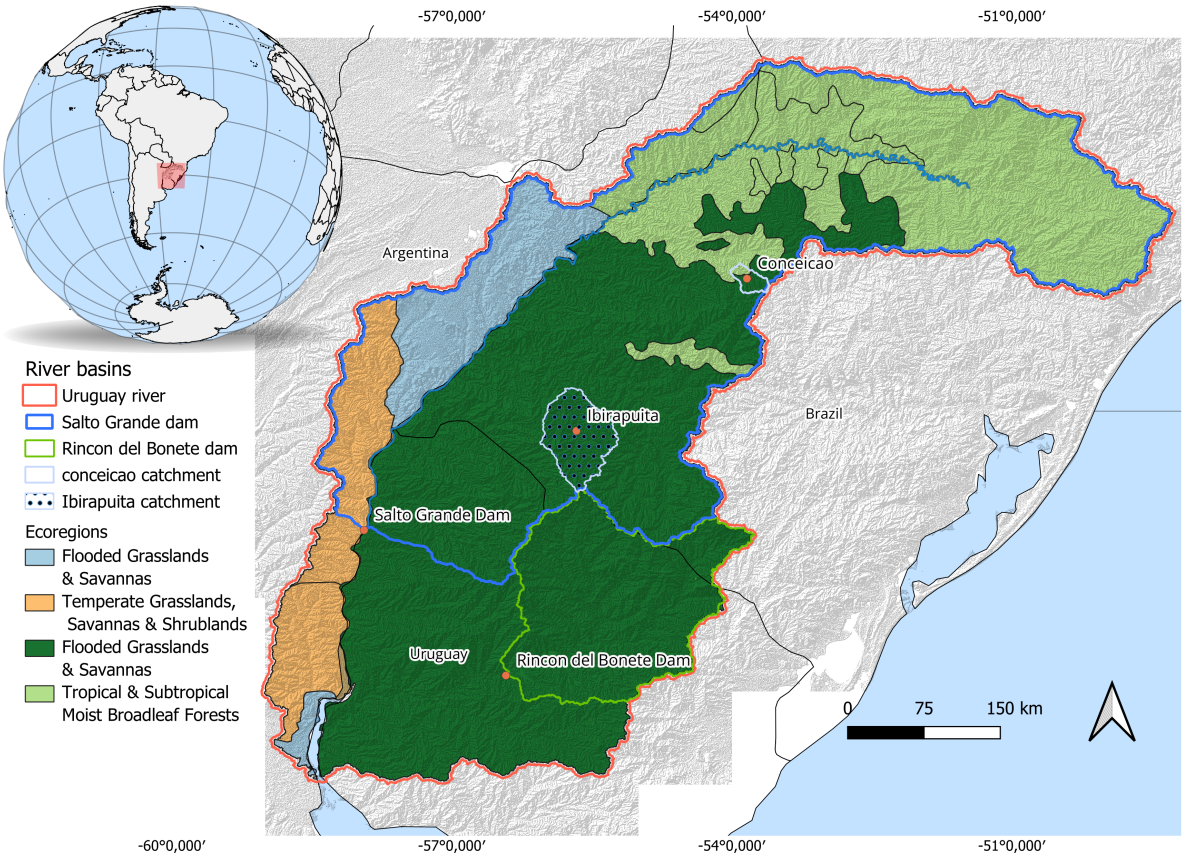

Figure 1: **Biomes** du bassin versant de la rivière Uruguay et **delimitation des bassins versants étudiés**. Fond de carte : OpenStreetMap

0.2.3 . Matériels & Méthodes

Cette approche repose sur l'acquisition et l'analyse de plusieurs types d'archives et de traceurs. Des carottes sédimentaires ont été prélevées dans les réservoirs de Salto Grande et de Rincón del Bonete (Figure 2), complétées par des carottes de sols et échantillons de sédiments en suspension issus de sous-bassins représentatifs des principales zones sources du réservoir de Salto Grande. Les séquences sédimentaires ont fait l'objet d'analyses à haute résolution incluant la granulométrie par diffraction laser, la densité apparente reconstruite à partir d'images de tomographie (CT-scan), ainsi que la teneur en carbone et azote et les signatures isotopiques du carbone. Pour la carotte du réservoir de Salto Grande, la composition minéralogique a également été déterminée par diffraction des rayons X et les propriétés magnétiques ont été utilisées comme traceurs pour les approches de fingerprinting des sources sédimentaires.

La chronologie des carottes sédimentaires a été établie à partir des activités en plomb 210 en excès mesurées par spectrométrie gamma, en appliquant un modèle CF:CS, permettant de reconstituer les taux d'accumulation sédimentaire au cours du temps. Ces reconstructions ont été couplées à des

mesures de contaminants, incluant un large spectre de pesticides analysés par chromatographie en phase gazeuse et liquide couplée à la spectrométrie de masse (GC-MS et LC-MS/MS) et ICPMS-MS pour les analyses de plutonium 239 et 240.

En complément, des données d'occupation et d'usage des sols à haute résolution spatiale (30 m) et temporelle (1985–2023) ont été mobilisées pour caractériser les dynamiques d'expansion agricole et de transformation des paysages. L'ensemble de ces observations a, enfin, été mis en perspective à l'aide d'un modèle hydrologique et sédimentaire distribué (WaterSed), permettant d'explorer la variabilité spatiale et temporelle des processus de ruissellement et de transfert sédimentaire, et de relier les signaux intégrés observés dans les archives aux dynamiques événementielles et saisonnières.

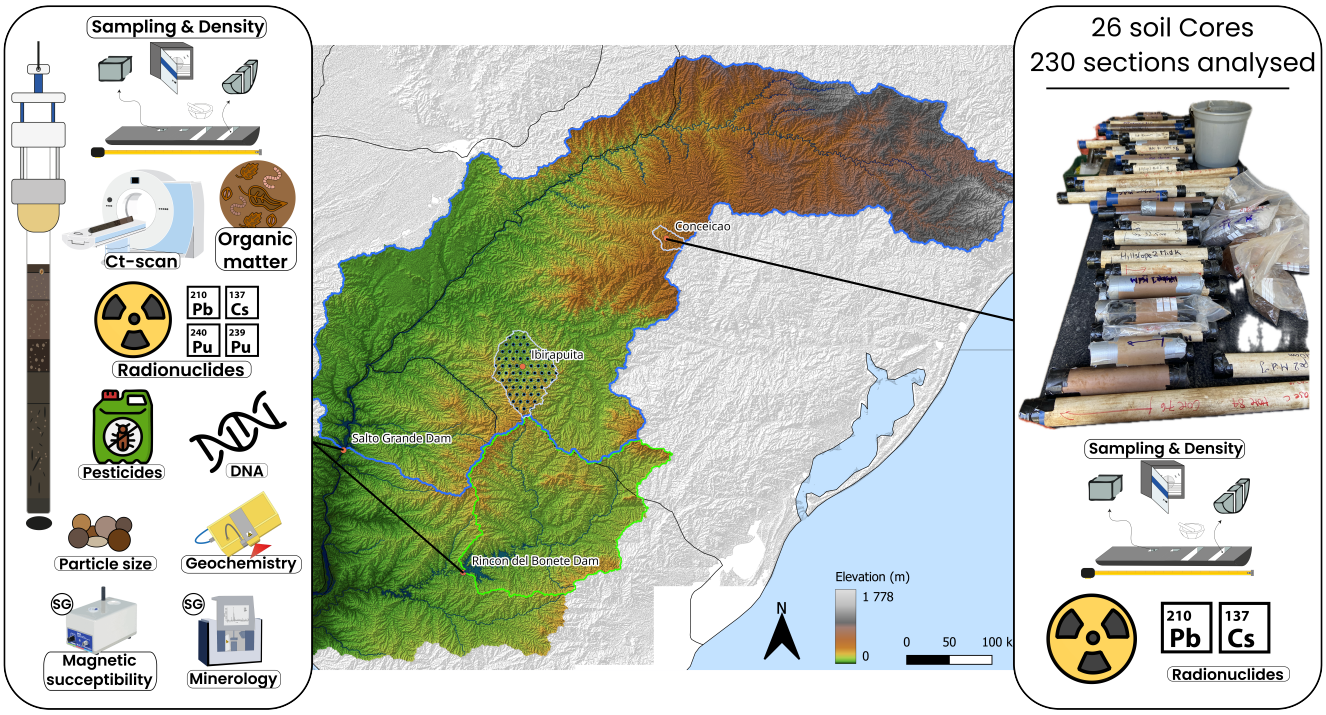

Figure 2: Analyses réalisées sur les carottes sédimentaires (à gauche), avec les analyses spécifiques à la carotte de Salto Grande indiquées par cercle muni des lettres « SG », ainsi que les analyses liées à la modélisation de la redistribution des sols dans le bassin de Conceição. Sur la carte, on discerne le modèle numérique de terrain du bassin du fleuve Uruguay montrant la localisation des bassins de Salto Grande (bleu), Rincón del Bonete (vert), Ibirapuitã (blanc avec points bleus) et Conceição (blanc). Fond de carte : **?**.

0.2.4 . Résultats

Dans son ensemble, cette thèse met en évidence l'intérêt d'approches multi-proxies et multi-échelles pour reconstruire les trajectoires environnementales dans des régions où les données environnementales historiques restent limitées. En combinant des analyses à différentes échelles spatiales, depuis la parcelle jusqu'aux grands bassins versants, elle montre que les changements d'usage des sols et des pratiques agricoles ont profondément modifié à la fois les processus d'érosion et les transferts de contaminants dans le sud de l'Amérique du Sud.

Dans un premier temps, cette thèse s'est attachée à évaluer la représentativité et la fiabilité des

approches basées sur les inventaires de radionucléides pour quantifier l'érosion des sols à l'échelle de la parcelle. Une campagne d'échantillonnage (voir figure 3) à haute résolution spatiale a mis en évidence la forte variabilité des inventaires de radionucléides (césium 137 et plomb 210 en excès) à l'échelle locale (12 x 12 m), conduisant à des estimations contrastées de la redistribution des sols. En effet, sur cette surface réduite, des zones à la fois en érosion et des zones de dépôt ont été identifiées alors même que tous les profils se trouvent en milieu de versant. Ces résultats soulignent les limites d'une interprétation à partir de profils prélevés de façon ponctuelle et le besoin de réaliser des composites pour l'étude de la redistribution des sols, mais confirment tout de même leur intérêt pour caractériser les tendances générales de redistribution des sols.



Figure 3: Photos de la campagne de terrain de 2024 dans le bassin versant de Conceição

En complément, un modèle hydrologique et sédimentaire dit distribué (WaterSed) a été mis en œuvre. Bien que la variabilité spatiale observée n'ait pas permis une calibration directe de celui-ci à partir des données de césium 137, le modèle reproduit les tendances hydrologiques et les variations du ruissellement, fournissant ainsi un cadre cohérent pour interpréter les processus hydrologiques et potentiellement hydrosédimentaires à l'échelle événementielle et saisonnière. Ce travail établit ainsi un lien entre les observations de terrain telles ques celles obtenues par l'analyse des carottes de sol et les reconstructions intégrées sur le long terme au travers de l'analyse des carottes sédimentaires lacustres.

Dans un second temps, la thèse a reconstruit les dynamiques du transfert sédimentaire et des contaminants à l'échelle de grands bassins versants à partir d'archives sédimentaires prélevées dans les réservoirs de barrages de la région ciblée. L'étude du réservoir de Salto Grande a permis de retracer l'évolution des flux sédimentaires et des apports en pesticides sur les dernières décennies, mais aussi d'identifier les principales zones sources de sédiments. Les résultats montrent une diminution globale des flux sédimentaires depuis les années 1980, accompagnée d'un changement des sources dominantes (depuis le nord vers le sud du bassin) depuis les années 2000, en lien avec les transformations agricoles et les aménagements hydrauliques réalisés dans le bassin.

Une troisième partie s'est ainsi attachée à mieux comprendre cette évolution. Pour ce faire, un second réservoir a été échantillonné, celui de Rincón del Bonete, dont le bassin versant, initialement peu anthropisé, fournit un enregistrement de plus longue durée des changements d'usage des sols. La re-

constitution des flux sédimentaires depuis les années 1950 met ainsi en évidence la succession de trois phases principales : (i) une période initiale caractérisée par un impact limité des activités agricoles conventionnelles, (ii) une phase de réduction des apports sédimentaires associée à l'adoption du semis direct et à certaines pratiques plus vertueuses de gestion des sols et, enfin, (iii) une phase récente d'augmentation de l'érosion et des flux sédimentaires en lien avec l'intensification agricole. La détection de pesticides, y compris de composés interdits tels que le DDT, suggère par ailleurs une remobilisation de stocks anciens de contaminants sous l'effet de cette accélération de l'érosion.

Un résultat majeur de la thèse est donc que la diminution des flux sédimentaires observée en aval d'un grand bassin versant tel que celui du fleuve Uruguay ne peut pas être interprétée de manière univoque comme un indicateur d'amélioration environnementale ou d'efficacité des pratiques de conservation des sols. Dans les bassins étudiés, cette diminution peut refléter, au contraire, des modifications des sources de sédiments, de la connectivité sédimentaire ou encore des changements dans les concentrations en contaminants, qui peuvent ainsi continuer à exercer des pressions écologiques significatives.

Ces travaux s'inscrivent dans un contexte régional où les systèmes agricoles ont bénéficié d'importants efforts de recherche et d'innovation, notamment à travers des institutions nationales dédiées. Toutefois, l'intensification des systèmes de production, soutenue par la demande internationale, continue d'exercer une pression forte sur les ressources en sols et en eau. Dans ce contexte, une meilleure prise en compte des impacts environnementaux des chaînes de production agricoles, ainsi que le renforcement des collaborations internationales et des cadres réglementaires, apparaissent comme des leviers importants pour accompagner des trajectoires de production davantage durables à l'avenir.

Contents

0.1 Remerciements . . . 3
0.2 Résumé de thèse en français . . . 5
0.2.1 Contexte . . . 5
0.2.2 Objectifs . . . 5
0.2.3 Matériels & Méthodes . . . 6
0.2.4 Résultats . . . 7

I General Introduction 23

1 General Introduction 25
1.1 Context and problem statement . . . 25
1.1.1 Context . . . 25
1.1.2 Problem statement . . . 27
1.2 Objectives and approach adopted . . . 30
1.2.1 objectives . . . 30
1.2.2 Approach adopted . . . 30
1.3 Context of this thesis . . . 32

II Materials and Methods 40

2 Material and Methods 42
2.1 Materials . . . 42
2.1.1 Study site . . . 42
2.1.2 Data sources . . . 43
2.1.3 Reconstruction of the land-use and land-cover . . . 43
2.1.4 Sample collection . . . 44
2.2 Methods . . . 45
2.2.1 Global Summary of methodologies . . . 45
2.2.2 Particle size analysis . . . 47
2.2.3 Density analysis . . . 47
2.2.4 Organic matter analysis . . . 47
2.2.5 Gamma spectrometry analysis . . . 48
2.2.6 Plutonium analysis . . . 48
2.2.7 Age model, Sediment and Pesticides fluxes . . . 48
2.2.8 Pesticides analysis . . . 48

2.2.9 DNA analysis . . . 50
2.2.10 Magnetic susceptibility analysis . . . 51
2.2.11 Sediment Fingerprinting . . . 52
2.2.12 Mineralogical composition . . . 52

III Small-scale variability in fallout radionuclide inventories and soil redistribution estimates in a cultivated catchment under contrasting management in Southernmost Brazil 57

3 Small-scale variability in fallout radionuclide inventories and soil redistribution estimates in a cultivated catchment under contrasting management in Southernmost Brazil 59

3.1 Introduction . . . 61
3.2 Materials and Methods . . . 63
3.2.1 Conceição river basin . . . 63
3.2.2 Methodology . . . 64
3.2.3 Density . . . 65
3.2.4 Gamma spectrometry analyses . . . 65
3.2.5 Soil redistribution rate calculation . . . 66
3.3 Results and Discussion . . . 67
3.3.1 Reference sites and modelling settings . . . 67
3.3.2 Hillslopes . . . 70
3.3.3 Soil redistribution modelling . . . 74
3.4 Discussion . . . 79
3.4.1 Spatial representativeness of ^{137}Cs and $^{210}Pb_{ex}$ inventories . . . 79
3.4.2 Effect of farming practices on the spatial variability of ^{137}Cs and $^{210}Pb_{ex}$ . . . 79
3.4.3 Soil redistribution modelling . . . 80
3.5 Conclusions . . . 81
3.6 Supplementary material . . . 83
3.6.1 Detailed Methodology . . . 83
3.6.2 Modern reference profiles . . . 85

IV Initial parametrisation of runoff for distributed conceptual model, WaterSed, in the Conceição catchment

91

4 Initial parametrisation of runoff for distributed conceptual model, WaterSed, in the Conceição catchment 93

4.1 Introduction . . . 94
4.2 Materials and Methods . . . 95
4.2.1 Study site . . . 95
4.2.2 Hydrological survey . . . 96
4.2.3 Methodology . . . 97
4.2.4 Indices calculated . . . 97
4.2.5 WaterSed simulations . . . 98
4.3 Results and Discussion . . . 99
4.3.1 Monitoring data analysis . . . 99
4.3.2 Events analysis . . . 101
4.3.3 Watersed runoff simulation . . . 103
4.4 Conclusions . . . 107

V Dramatic pesticide transfers fuelled by agricultural expansion in Southernmost Brazil. 109

5 Dramatic pesticide transfers fuelled by agricultural expansion in Southernmost Brazil. 111

5.1 Introduction . . . 112
5.2 Materials and methods . . . 116
5.2.1 Study site . . . 116
5.2.2 Data sources . . . 116
5.2.3 Reconstruction of the land-use and land-cover . . . 116
5.2.4 Sample collection . . . 117
5.2.5 Methodology . . . 117
5.3 Results . . . 119
5.3.1 Evolution of the land-use and land-cover . . . 119
5.3.2 Core description . . . 119
5.3.3 Geochemical analyses . . . 120
5.3.4 Gamma spectrometry and chronology . . . 120
5.3.5 Sediment source fingerprinting . . . 121
5.3.6 Pesticides . . . 122
5.4 Discussion . . . 124

5.4.1 Origin in changes of sedimentation rates from the 1980s to the 2020s 124
5.4.2 Evolution of the contamination from the 1980s to the 2020s 125
5.4.3 Possible future evolution of the agricultural expansion 126
5.5 Conclusion 127
5.6 Data Availability 127
5.7 Supplementary material 129
5.7.1 Evolution of the land-use and land-cover 129
5.7.2 Detailed core description 130
5.7.3 Magnetic Susceptibility 131
5.7.4 Mineralogical composition 132
5.7.5 Sediment Fingerprinting 133
5.8 Detailed pesticides results 133
5.8.1 Herbicides 133
5.8.2 Fungicides 134
5.8.3 Insecticides 134
5.9 Detailed Material and Methodology 137
5.9.1 Sediment source sampling 137
5.9.2 Particle size analysis 138
5.9.3 Density analysis 138
5.9.4 Statistics 139
5.9.5 Geochemical analysis 139
5.9.6 Organic matter analysis 139
5.9.7 Gamma spectrometry analysis 140
5.9.8 Magnetic susceptibility analysis 140
5.9.9 Mineralogical composition 140
5.9.10 Pesticides analysis 141

VI The hidden consequences of agricultural development: Soil degradation and pesticide contamination in the South American Pampa 148

6 The hidden consequences of agricultural development: Soil degradation and pesticide contamination in the South American Pampa. 150

6.1 Introduction 152
6.2 Materials and Methods 154
6.2.1 Study site 154
6.2.2 Data sources 156

6.2.3 Methodology . . . 156
6.3 Results and discussion . . . 161
6.3.1 Evolution of the land-use land-cover . . . 161
6.3.2 Sediment analyses . . . 163
6.3.3 Radionuclide analyses and age model . . . 165
6.3.4 Rainfall evolution . . . 169
6.3.5 Fluxes of sediments . . . 169
6.3.6 Pesticides . . . 173
6.4 Conclusions . . . 178
6.5 supplementary material . . . 180

VII General discussion, conclusion and perspectives 188

7 General discussion, conclusion and perspectives 190
7.1 Fluxes of sediments and historical contextualisation . . . 190
7.1.1 Brazil and the Salto Grande dam river basin . . . 190
7.1.2 Uruguay and the Rincon del Bonete dam river basin . . . 192
7.2 Integrating hillslope-scale variability to reservoir sediment records . . . 193
7.3 Agricultural intensification and conservation practices . . . 195
7.4 Socio-economic drivers, water resource and future trajectories . . . 197
7.5 Limitations and Perspectives for future research . . . 200
7.5.1 Methodological limitations . . . 201
7.5.2 Perspectives for future research . . . 202

VIII Supplementary material 210

A Supplementary material 212
A.1 Thesis timeline . . . 212

B SedimentR: Identifying major structures in sediment cores through clustering of XRF geochemical data. 215
B.1 Introduction to the package . . . 217
B.1.1 Fully automated workflow: `sedicore` . . . 218
B.1.2 First step: `charger` . . . 218
B.1.3 Second or Third step: `scale_data` . . . 221
B.1.4 Fourth step: `prop.select` . . . 222

B.1.5 Fifth step: `xrf_clust` . . . 224
B.1.6 Internal validation and stability assessment for clustering quality . . . 224
B.1.7 Sixth step: `visual.clust` . . . 230
B.2 Case studies using SedimentR . . . 232
B.2.1 Peguières case study: . . . 232
B.2.2 Validation of the clustering workflow using random variables . . . 238
B.2.3 Allos case study: . . . 239
B.3 Conclusions . . . 243
B.4 Supplementary Materials . . . 244

List of Figures

1 **Biomes** du bassin versant de la rivière Uruguay et **delimitation des bassins versants étudiés**. Fond de carte : OpenStreetMap 6

2 Analyses réalisées sur les carottes sédimentaires (à gauche), avec les analyses spécifiques à la carotte de Salto Grande indiquées par cercle muni des lettres « SG », ainsi que les analyses liées à la modélisation de la redistribution des sols dans le bassin de Conceição. Sur la carte, on discerne le modèle numérique de terrain du bassin du fleuve Uruguay montrant la localisation des bassins de Salto Grande (bleu), Rincón del Bonete (vert), Ibirapuitã (blanc avec points bleus) et Conceição (blanc). Fond de carte : **?**. 7

3 Photos de la campagne de terrain de 2024 dans le bassin versant de Conceição 8

1.1 **Biomes** of the Uruguay river basin and **delineation of the studied river basins** background map from OpenStreetMap 27

1.2 Pictures of the 2024 field campaign in the Conceição river basin 31

2.1 Digital elevation model of the Salto Grande, Ibirapuitã and Conceição river basins. Land-use and land-cover and source sample localisation analysed for magnetic susceptibility, background map from OpenStreetMap contributors (2024) 45

2.2 Analysis conducted on the sediment cores (left), with analyses specific to the Salto Grande core indicated by a circled “SG”, and analyses related to soil redistribution in the Conceição catchment. Digital elevation model of the Uruguay River basin showing the locations of the Salto Grande (blue), Rincón del Bonete (green), Ibirapuitã (white with blue dots), and Conceição (white) river basins. Background map from OpenStreetMap contributors (2024). 46

3.1 **Conceição river basin**, localisation in South America and general location of the sampling sites **H1 - Conventional tillage** and **H2 - No tillage** along with reference sites sampled **A,B and C**. Map of land-uses and covers in 2022 (from Mapbiomas Brazil), background map from OpenStreetMap and Google Imagerie, NASA 64

3.2 **Concept of the sampling strategy** with the example of hillslope **A** 65

3.3 Depth profiles of ^{137}Cs and $^{210}Pb_{ex}$ inventories at the three references sites, with - in the upper panels - the undisturbed references selected for soil redistribution modelling and - in the lower panels - the disturbed references that were not retained for further analysis . 68

3.4 Spatialised $^{210}Pb_{ex}$ inventories for hillslopes 1 and 2 in the Conceicão catchment. The left-hand maps show the location of the hillslopes within the catchment and the right-hand panels show the spatial distribution of measured inventories at the sampling locations. Circles represent total $^{210}Pb_{ex}$ inventories, with their size corresponding to the inventory classes shown in the legend ($Bq.m^{-2}$). Background imagery is from Google Satellite. . 70

3.5 Spatialised ^{137}Cs inventories for hillslopes 1 and 2 in the Conceicão catchment The left-hand maps show the location of the hillslopes within the catchment and the right-hand panels show the spatial distribution of measured inventories at the sampling locations. Circles represent total ^{137}Cs inventories, with their size corresponding to the inventory classes shown in the legend ($Bq.m^{-2}$). Background imagery is from Google Satellite. . . 71

3.6 Results of $^{210}Pb_{ex}$ inventories in $Bq.m^{-2}$. Inventories for each hillslope and for each depth increment in panel **A** and total inventory for each core and for each hillslope along with total reference inventories given in panel **B** 72

3.7 Results of ^{137}Cs inventories in $Bq.m^{-2}$. Inventories for each hillslope and for each depth increment in panel **A** and total inventory for each core and for each hillslope along with total reference inventories given in panel **B** 73

3.8 🄓, Soil redistribution modelling of H1 (in blue) and H2 (in orange) in $t.ha^{-1}.yr^{-1}$ based on $^{210}Pb_{ex}$ and ^{137}Cs inventories with proportional, MODERN and Radero modelling. 🄑, Boxplot of soil redistribution modelling per model and hillslope and only per model in $t.ha^{-1}.yr^{-1}$ based on $^{210}Pb_{ex}$ and ^{137}Cs inventories with proportional, MODERN and Radero modelling 78

3.1 Reference profile of $^{210}Pb_{ex}$ constructed with MODERN package, with A the raw mean profile, B the simulated smoothed profile, C simulated smoothed and ploughed profile, D simulated smoothed and deposited profile, E simulated smoothed, ploughed and deposited profile 85

3.2 Reference profile of ^{137}Cs constructed with MODERN package, with A the raw mean profile, B the simulated smoothed profile, C simulated smoothed and ploughed profile, D simulated smoothed and deposited profile, E simulated smoothed, ploughed and deposited profile 85

4.1 **Conceição river basin**, localisation in South America and map of land-uses and covers in 2022 (from Mapbiomas Brazil), background map from OpenStreetMap and Google Imagerie, NASA 96

4.2 Annual hydrological balance with discharge (m^3/s) in the top, rainfall (mm) in the middle and sediment load (kg) in the bottom 100

4.3 Seasonal hydrological balance with discharge (m^3/s) in the top, rainfall (mm) in the middle and sediment load (kg) in the bottom, with autumn in red, spring in blue, summer in green and winter in purple. 101

4.4 In the top, observed runoff coefficient for individual rainfall events. In the bottom, the calculated runoff coefficient plotted against total event rainfall. Marker size is proportional to the calculated net antecedent rainfall and ET for each event (between 0 and 714 mm). 103

4.5 Graph of observed and simulated runoff with watersed on the left, ET (red) and water storage (blue) parametrisations on the right of each simulation 106

4.6 Graph of observed and simulated runoff with WaterSed on the left, ET (red) and water storage (blue) fine-tuning parametrisations on the right 107

5.1 **Biomes** of the Salto Grande basin (A), **location of the study site**, in the river basin, in South America, map of land-uses and covers in 2022 (from Mapbiomas Argentina, Pampa and Brazil) with the location of Ibirapuitã and Conceição sub-basins (B) and coring location (S32°49.072', W56°24.008') (B), background map from OpenStreetMap 115

5.2 **Evolution of the land-use and land-cover in the Salto Grande river basin**, Main land-uses and land-covers from 1985 to 2022, data from Mapbiomas Argentina, Pampa and Brazil 119

5.3 Sediment characteristics along the SG03 sediment core, granulometry, Organic Matter (TOC and $\delta^{13}C$), elemental geochemistry (Mn measured at 30kV and Ti at 10kV) results and $^{210}Pb_{ex}$ age model. 120

5.4 Mean contributions of the two potential sediment sources - Southern basin part (in green on the right) and Northern basin part (in orange on the left) when running the Bayesian Mean Model using the FingR package 122

5.5 Total fluxes (in 10^{-9} mol.cm^{-2}.yr^{-1}) of insecticides without DDT, DDD and DDE (grey) and DDT + DDD + DDE (light purple), Ampa + glyphosate (light green) and total herbicides without AMPA and glyphosate (dark green), fungicides (red) as well as sediment fluxes (mass accumulation rate,MAR, in g.cm^2.yr^{-1}, brown) in the Salto Grande sediment core. 123

5.6 Spatialised main land-use and land-cover from 1985 to 2022, data from Mapbiomas Argentina, Pampa and Brazil and background map from OpenStreetMap contributors (2024) 129

5.7 Evolution of Total Nitrogen (TN) and Total organic Carbon (TOC) / TN ratios with depth in the core 131

5.8 Scatter plot of χ_{HF} & χ_{LF} magnetic susceptibility from Conceicão and Ibirapuitã (in dark cicrles and triangles respectively) and sediments from Salto Grande in colored circles depending on their year of supply to the Salto Grande reservoir, in m^3kg^{-1} 131

5.9 Mineralogical composition of the <2 mm fraction determined by X-ray Diffractometry, (**1**), relationship between the proportion of minerals in sediment samples (**2**) and proportion of quartz, kaolinite, hematite+goethite, and feldspar in sediment samples collected between 0-20 cm and between 20-55 cm (**3**). The point represents the average, and the whiskers represent the 95% confidence interval after bootstrapping with 5000 interactions. 132

5.10 Three step method tracer selection results with FingR package 133

5.11 Detailed fluxes (in 10^{-13} mol.cm^{-2}.yr^{-1}) of insecticides (grey), herbicides (green), and fungicides (red). Uncertainty for each pesticide is indicated alongside its range. 136

5.12 Digital elevation model of the Salto Grande, Ibirapuitã and Conceição river basins. Land-use and land-cover and source sample localisation analysed for magnetic susceptibility, background map from OpenStreetMap contributors (2024) 138

6.1 Location of the Rincón del Bonete River basin in South America, coring location (S32°49.072', W56°24.008') and map of land-uses and covers in 2022 (MapBiomas Pampa), background map from OpenStreetMap 155

6.2 Evolution of land-use and land-covers from 1985 to 2022 (MapBiomas Pampa) and representing area (in %) of pasture, grassland, temporary crop and forest plantation extracted from the MapBiomas dataset, background map from OpenStreetMap. The northwestern, southeastern and northeastern parts of the basin are shown for the 1985 map in light orange, red and blue 162

6.3 Results of Rincón del Bonete core analyses, including organic matter properties (TOC in % and TOC/TN), grain size distribution with D10, D50 and D90 values (dashed white lines) and bulk density values. 165

6.4 Rincón del Bonete core profile with $^{210}Pb_{ex}$, ^{137}Cs, $^{239+240}Pu$ activities ($Bq.kg^{-1}$), $^{240/239}Pu$ ratio and CFCS derived age model. Letters corresponding to historical events were added as well as the associated year 166

6.5 Fluxes of sediments (MAR, I) and result of Dunn test on the MAR for the different periods of sediment delivery (I) and mean annual fluxes of sediment and precipitation (II). Periods of sediment delivery identified with the breakpoint test and their corresponding agricultural phases were added, in green, conventional continuous cultivation, in blue, conventional cultivation with rotation (agriculture-pasture). In orange, no-tillage cultivation with rotation (agriculture-pasture) and in red, no-tillage continuous cultivation. 169

6.6 Fluxes (in 10^{-13} mol.cm^{-2}.yr^{-1}) of insecticides (grey), herbicides (green), and fungicides (red). Uncertainty for each pesticide is indicated alongside its range. The date of production is marked with a green circle, and the date of ban with a red cross 177

6.7 Synthesis of the main findings of this study and conceptual representation. The **Area affected by human activity** was derived from land-use land-cover analysis, **pesticide usage** from the pesticide analyses, **climatic and anthropogenic impacts** from the sediment flux/precipitation comparison, and the **sediment flux** and **breakpoint test dates** from MAR analysis. Results were categorised by period and expressed on a scale ranging from low to very high. 178

6.8 Correlation between measured density and CT scan values in blue in the top and CT scan values obtained in orange on the bottom part 181

6.9 Monthly precipitation in the Rincon del Bonete river basin as recorded in the TerraClimate dataset 182

6.10 Fluxes of Glyphosate in $10^{-13}.mol.cm^{-2}.yr^{-1} \pm 23.1\%$ 183

7.1 Localisation of the major Brazilian soybean producing states 198

A.1 Doctoral Training 212

A.2 Timeline of the PhD thesis 213

B.1 PCA of the Peguières core dataset showing the first two principal components (PC1 and PC2). Samples are grouped according to the identified clusters, with 95% confidence ellipses illustrating the dispersion of each cluster. 235

B.2 Results of the clustering workflow applied to the Peguières core dataset. The figure combines(i) a photo from the sediment archive; (ii) the sediment core age-depth model; (iii) Cesium-137 (^{137})Cs activity profiles used for chronological reconstruction; (iv) multi-proxy geochemical profiles relative to depth, alongside the associated clustering results; and (v) the clustered virtual core reconstruction. Together, these elements provide an integrated view of the sedimentary sequence, linking chronological information, geochemical variability, and data-driven stratigraphic clustering. 237

B.3 Comparison of clustering results obtained with and without PCA-based variable selection. The first approach retained the most influential variables according to cumulative explained variance and loading threshold criteria (A), whereas the second approach used the full dataset (B). 239

B.4 Results of the Allos clustering workflow implemented in the SedimentR package. The figure combines (i) a photo of the sediment core; (ii) geochemical profiles as a function of depth, alongside the associated clustering results; and (iii) the clustered virtual core reconstruction. 240

B.5 PCA of the Allos core dataset showing the first two components, with 95% confidence ellipses showing the dispersion of each cluster. Samples are grouped according to the identified clusters. 241

B.6 Allos comparison between the clustering result to identify flood events (orange square cluster 2/3) and the result from the previous study of Wilhelm et al. (2012)in light orange bands. 242

I

General Introduction

Chapter 1

General Introduction

1.1 . Context and problem statement

1.1.1 . Context

Soils are a fundamental interface supporting ecosystems and human societies by providing the physical basis for agricultural production, while also regulating water, nutrient, and carbon cycles (Keesstra et al. 2016). However, the expansion and mechanisation of agriculture, together with the increasing reliance on agricultural inputs including pesticides, can substantially modify soil properties, hydrological pathways, and biogeochemical processes. In subtropical agricultural regions, water erosion intensified by agricultural activities is a major driver of soil degradation, with both on-site impacts, such as soil, water storage, and nutrient losses, and off-site consequences, including the transfer of sediment, nutrients, and contaminants to rivers and reservoirs (Bertol et al. 2017; Londero et al. 2018; Ramos et al. 2019; Bennett et al. 2001; Golosov and Walling 2019).

In this context, South America has become one of the major agricultural production regions worldwide and has experienced extensive land-use and land-cover changes over recent decades. These transformations have largely been driven by the expansion of pasture, cropland, and tree plantations over natural ecosystems that previously supported high levels of biodiversity and ecological resilience (Oliveira et al. 2017; Zalles et al. 2021). Since 1985, pasture, cropland, and plantation areas have increased by 23%, 160%, and 288%, respectively, while natural vegetation has declined, including tree cover at the South American scale and grasslands in southern Brazil. These changes have contributed to increasing pressure on soils, habitats, and aquatic systems (Foley et al. 2005; Zurbriggen et al. 2020).

In the Pampa and Atlantic forest biomes, agricultural development has not only expanded cultivated areas but also transformed farming practices. The generalisation from tillage-based systems to no-tillage agriculture after 2000, often associated with intensive herbicide use, with the implementation and removal of terraces, has strongly modified landscapes at both local and regional scales (Merotto et al. 2022). Although no-tillage systems may reduce direct soil disturbance and surface erosion, their environmental effects remain context-dependent, particularly where they are combined with simplified crop rotations, high chemical inputs, and increased hydrological connectivity between fields and drainage networks (Didoné et al. 2014).

Several local studies have provided valuable evidence of soil redistribution and soil degradation in the Pampa biome using the technique of fallout radionuclide inventories and found that 37 to 51.7% of the soils from a first catchment and 34.2 to 63.6% of the soils from a second catchment exceeded the modelled tolerable erosion rate of 7 and 9 $t.ha^{-1}.yr^{-1}$ respectively for the first and second catchments. In addition, Beretta-Blanco et al. (2019) observed decreases in soil pH, soil organic carbon, and exchange-

able base content at the experimental station of the *Instituto Nacional de Investigacion Agropecuaria* at La Estanzuela, despite the adoption of no-tillage systems between 2002 and 2004. These findings indicate that changes in farming systems may affect not only rates of soil loss, but also soil chemical fertility and longer-term soil functioning.

The consequences of agricultural intensification extend beyond cultivated hillslopes. Sediment- and nutrient-enriched runoff can be transferred downstream, where it may contribute to eutrophication and water-quality degradation. In southern South America, nutrient inputs have been associated with toxic cyanobacterial blooms, which have affected the capacity of some water bodies to meet public health standards since 2010 (Kruk et al. 2023). In parallel, pesticide use in modern agriculture raises additional concerns as active ingredients and their metabolites can be transferred through soils, surface waters, groundwater, and vegetation, with potential effects on aquatic ecosystems, biodiversity, and human populations (Aktar et al. 2009). For instance, Skidmore et al. (2023) reported a statistically significant association between the expansion of soybean production and increased paediatric leukaemia, with exposure pathways likely linked to contamination of water supplies. However, the environmental risk associated with pesticide use depends on multiple factors, including the amount and location of application, partitioning among environmental compartments, degradation rates, metabolite formation, and toxicity to exposed organisms (Van Der Werf 1996).

Despite this growing number of studies, important knowledge gaps remain. In particular, few studies investigated the evolution of fluxes of sediments and contaminants southern South America after World War II. Existing studies provide valuable catchment-scale evidence of soil redistribution, soil chemical degradation, and water-quality impacts, but few datasets allow these processes to be assessed jointly over large spatial (multiple thousand kilometres) and temporal scales (multiple decades). In particular, the lack of long-term monitoring data (>10 years) limits the reconstruction of historical erosion dynamics, sediment provenance, and pesticide-related pressures.

These limitations are particularly important in regions that have undergone a rapid agricultural transformation but that remain less studied than more emblematic South American ecosystems. Indeed, while the Amazon region often dominates public and scientific attention, other regions with essential ecological functions remain comparatively overlooked, including the Pampa biome (Figure 1.1) (Dinerstein et al. 2017; Andrade et al. 2023). In this context, the Uruguay river basin, covering both the Pampa and the Atlantic Forest biomes within one of South America's most productive agricultural zones, represents an area of particular interest on which the current thesis focuses on.

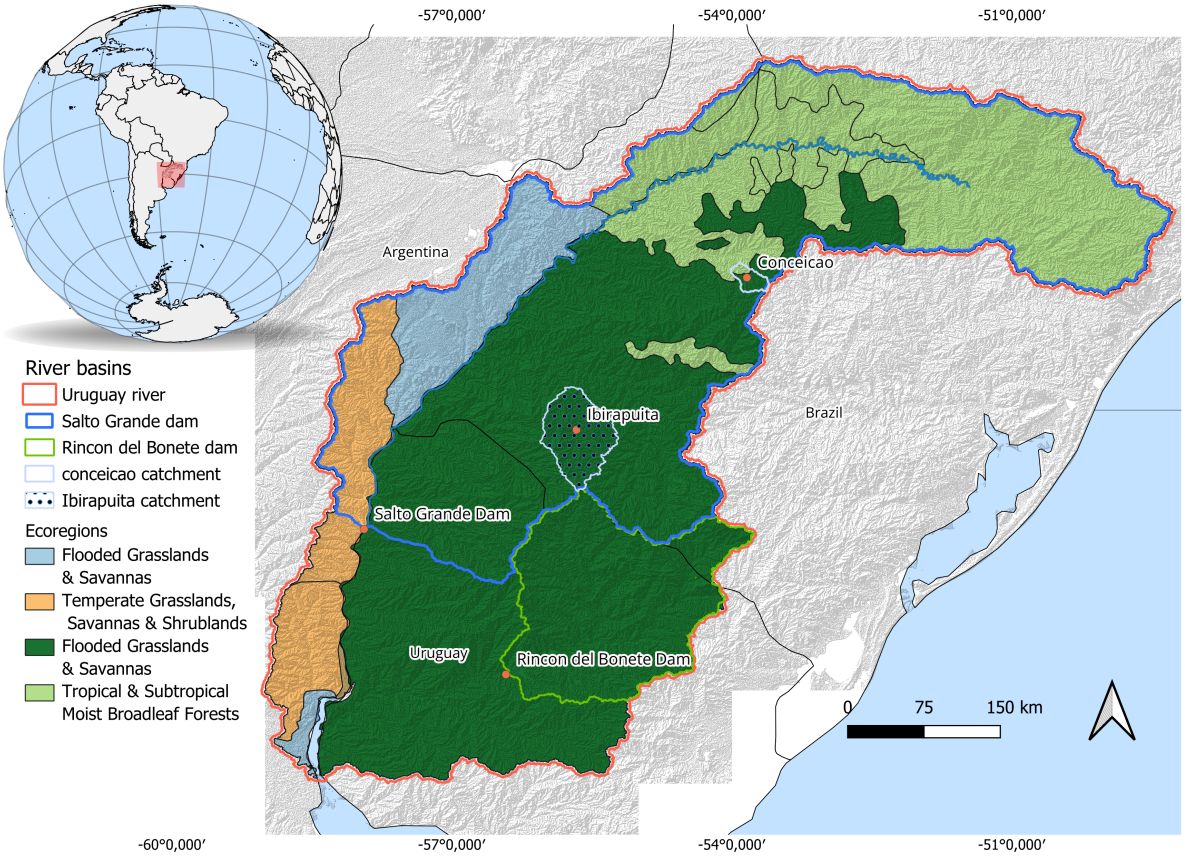

Figure 1.1: **Biomes** of the Uruguay river basin and **delineation of the studied river basins** background map from OpenStreetMap

1.1.2 . Problem statement

Over the past decade, several studies conducted in southern Brazil have investigated the effects of agricultural activities on sediment and contaminant dynamics at the catchment scale, including in the Arvorezinha (Minella et al. 2014, 2017) ($1.19\ km^2$), Guaporé (Le Gall et al. 2017; Tiecher et al. 2017; Zafar et al. 2016; Didoné et al. 2014) ($2\,000\ km^2$), and Conceição (Tiecher et al. 2018; Didoné et al. 2014, 2017, 2019, 2021) ($800\ km^2$) catchments. These studies consistently identified croplands as major sources of sediments and associated contaminants, largely because of insufficient or inadequately implemented soil conservation practices. However, existing studies in the region have often focused on individual contaminants and fewer attempts have been made to jointly reconstruct sediment fluxes, contaminant transfers, and their links to land-use and agricultural practice changes at the scale of the largest river basins of South America.

As a result, large uncertainties remain regarding the long-term dynamics of soil redistribution and associated sediment and contaminant transfers in response to recent agricultural expansion and intensification. In order to resolve these uncertainties, there is a need for approaches that can integrate sediment fluxes and contaminant records within a consistent chronological reconstruction, and relate them to documented changes in land use and farming practices across large and heterogeneous catchments.

To this end, retrospective studies using reservoir sediment cores may provide a powerful means to reconstruct long-term environmental changes in the absence of continuous monitoring, as demonstrated by Foucher et al. (2023); Dearing and Jones (2003). In fact, these records of sediment and contaminant fluxes, were shown to allow the reconstruction of historical trajectories of soil erosion, nutrient inputs, and pesticide contamination over different timescales in the Northern Hemisphere. In contrast, very few records, few studies are available in the Southern Hemisphere (Foucher et al. 2023; Garcia-Rodrıguez et al. 2002).

For this type of reconstruction, chronological assessment of the sediment cores is of upmost importance and is often achieved through modelling using the method of natural unsupported or excess lead-210 ($^{210}Pb_{ex}$, derived from atmospheric fallout of radon-222 decay products). Furthermore, the initial validation of the modelling typically relies on cesium-137 (^{137}Cs) activities, a radionuclide released during atmospheric nuclear bomb tests mainly conducted between 1945 and 1963 (when the United States of America (USA), the Former Soviet Union (FSU) signed the 1963 moratorium enforcing the limitation of atmospheric nuclear bomb testing) and then conducted from 1966 and 1974 by France and until 1980 by China. Along with ^{137}Cs, other radionuclides such as plutonium-239 (^{239}Pu) and plutonium-240 (^{240}Pu) were deposited globally during this period (United Nations Scientific Committee on the Effects of Atomic Radiation 2000; Bennett 2002).

Beyond sediment core reconstructions, several complementary methods have been developed to quantify soil redistribution across different spatial and temporal scales to help developing effective soil conservation strategies. These include direct field-based measurements of runoff and sediment transport using erosion plots or sediment traps (Hudson 1993; Morgan 2006), fallout radionuclide inventory methods (Walling et al. 1993; Walling and He 1999; Mabit et al. 2008), and empirical or process-based erosion models. The Universal Soil Loss Equation and its revised versions remain among the most widely used empirical approaches for estimating sheet and rill erosion (Wischmeier, W. H. and Smith, O.D. 1978; Renard, K. G. et al. 1997). Other models, including WEPP, LISEM, and WaterSed, aim to represent erosion processes more explicitly by simulating runoff generation, sediment detachment, transport, and deposition (Nearing et al. 1989; De Roo et al. 1996; Merritt et al. 2003). However, these approaches are limited by their dependence on input data quality, parameter uncertainty, and their difficulty in representing spatial variability and long-term soil redistribution at the plot scale.

Fallout radionuclide techniques provide an alternative, as they are based on measured inventories that integrate soil redistribution over multiple decades. As such, they offer an empirical means of constraining net erosion and deposition patterns that complement model-based approaches. Since the development of profile distribution, mass balance, and diffusion-migration models, these methods have been applied in a wide range of agricultural and natural environments (Walling and Quine 1992; XINBAO et al. 1990; Walling and He 1999; Ritchie and Ritchie 2008). They can provide spatially-distributed estimates of both

erosion and accumulation, and are therefore valuable for testing erosion models and assessing land-use impacts at hillslope or catchment scales (Porto et al. 2009). However, their interpretation is sensitive to assumptions about initial fallout homogeneity, the definition of local reference inventories, and the redistribution of radionuclides by tillage or bioturbation (Parsons and Foster 2013, 2011; Mabit et al. 2013) and there is therefore a lack of data regarding the representativity of soil cores.

1.2 . Objectives and approach adopted

1.2.1 . objectives

The objectives of this thesis were :

- First to evaluate the representativeness and reliability of soil core sampling for reconstructing erosion and sedimentation processes (at the hillslope scale). This objective focused on identifying spatial variability, depositional biases, and methodological limitations associated with the collection and analysis of soil cores used to infer historical erosion rates. Then, to compare these estimated erosion rates with a process-based erosion model using data records of rain, water flow and sediment load in order to improve the quantitative estimation of soil erosion.

- Secondly, to assess the impact of land-use change and agricultural intensification on sediment transfer dynamics in the biomes of the Southernmost part of Brazil, i.e. the Pampa and Atlantic forest. This objective was subdivided into two different studies with specific objectives ; The study of the very large Salto Grande river basin with the main objective to identify the origin of the sediments supplied to the dam reservoir as well as to quantify the impact of the transition from conventional to no-tillage agricultural practices, the massive development of monocropping of soybean and the associated contaminants in the region and the expected changes for the future. Then, the study of sediment accumulated behind one of the oldest dams in South America, the Rincon del Bonete dam (constructed in the 1940s) to evaluate the transition from natural to anthropogenic landscapes, the shift from conventional tillage to no-tillage systems, and the growing application of pesticides, and determine how these changes have impacted sediment production and transport since the onset of modern agriculture.

1.2.2 . Approach adopted

The overall goal of this thesis was therefore to develop multi-proxy methodologies to understand and provide novel insights - on broad spatial and temporal scales - into the impacts of agricultural development, land-use land-cover as well farming practices changes on soil redistribution and the transfer of sediment and associated contaminants in South America.

In South America in general, and in the Pampa and Atlantic forest biomes in particular, retrospective reconstructions are associated with major challenges, including the limited number of lakes and reservoirs suitable for sediment coring operations in this target region. Additional parameters, such as the reservoir size, the extent of its drainage area, and the year of reservoir construction, must also be considered when selecting potential sampling sites.

Foucher et al. (2023) successfully identified a reservoir in Uruguay, the Rincon del Bonete reservoir (Figure 1.1), that meets these criteria and collected a sediment core to investigate the impacts of

landscape modifications on sediment supply. However, their analysis was restricted to the recent period comprised between 1990 and 2020 as the core did not reach the bottom of the reservoir and they could not investigate earlier changes in land-use, land-cover and agricultural practices (i.e., tillage transition and increasing pesticide use).

Another reservoir was identified since 2018, the Salto Grande reservoir. However, this reservoir is shared between Uruguay and Argentina, therefore it took time to obtain the authorisations from the binational commission in charge of the dam (https://www.saltogrande.org). Then, the covid-19 pandemic travel regulations delayed the organisation of the campaign to conduct the sampling campaign in this reservoir. Agriculture was already widespread in the basin at the time of the dam construction. However, technicians and engineers who manage the Salto Grande Hydroelectric Power Plant, built on the Uruguay River in 1980, have recently reported siltation and eutrophication of the reservoir (Ramon 2021). Large quantities of sediments have accumulated and their specific source within the basin remained unknown (Ramon 2021). In contrast, the Rincon del Bonete river basin was mostly natural and less impacted by human activities when the dam was constructed and has since then experienced major changes in land-use, land-cover and agricultural practices.

These two sites, draining contrasted areas of the Uruguay river basin with distinct temporal agricultural developments, therefore emerged for the reconstruction of the sediment and contaminant transfers with regard to the changes that occurred in this region, including the impacts of land-use land-cover and agricultural practice changes.

Furthermore, to evaluate the representativeness and reliability of soil core sampling for reconstructing erosion and sedimentation processes at the hillslope scale, a high-density sampling design within two 12 m $\times$ 12 m midslope plots in cultivated Brazilian hillslopes was conducted in 2024 (see pictures in figure 1.2).



Figure 1.2: Pictures of the 2024 field campaign in the Conceição river basin

1.3 . Context of this thesis

This PhD thesis is part of a broader series of investigations conducted on soil erosion in South America and more specifically in Southern Brazil and follows up on previous efforts made by Chaboche (2021) and Ramon (2021) since 2018. Accordingly, this PhD thesis was part of two larger projects :

- The AVATAR (https://avatar-project.unibas.ch/en/) project, the acronym of which standing for 'A re-Vised dATing framework for quantifying geomorphological processes during the AnthRopocene'. This project was elaborated between multiple collaborators in Europe, EDYTEM (Environnements, Dynamiques et Territoires de la Montagne and Savoie Mont-blanc University), LSCE (Laboratory for Climate and Environmental Sciences), BRGM (French geological survey), WSL (Swiss Federal Research Institute for Forest, Snow and Landscape) and Basel university as well as the Spiez laboratory https://www.spiezlab.admin.ch/en. This project was partly motivated by the work of Chaboche et al. (2022) who showed that fallout radionuclides from French atmospheric tests should be considered to avoid any misinterpretation in sediment core dating in the 20-45° latitudinal band and that there was a need to refine the chronology of the reconstruction of environmental processes in this region of the world. This project also follows up on Ramon (2021)'s PhD thesis who deployed sediment fingerprinting techniques in Southern Brazil. Artificial fallout radionuclides from nuclear weapons testing and, more locally, from nuclear power plant accidents are found ubiquitously in the environment around the world and they provide the privileged marker candidates ("golden spikes") of the Anthropocene stratigraphic layers. The onset of their emissions coincided with the period of Great Acceleration (Steffen et al. 2015) that took place after World War II and that is characterised by an increase in soil degradation, which was mostly triggered by land use change. Particle-bound radiocaesium and plutonium are widely used to date modern sediment archives and reconstruct soil redistribution rates during this period. However, the fallout chronology is better constrained in the Northern Hemisphere, and much less is known regarding the timing and the spatial distribution of their deposition in the Southern Hemisphere (Chaboche 2021).

  Within this context, the **AVATAR project** aims to improve the understanding of the spatial and temporal distribution of fallout radionuclides (^{137}Cs and ^{239}Pu and ^{240}Pu) across the Southern Hemisphere by compiling existing datasets and refining their interpretation, particularly in regions where fallout histories remain poorly documented.

  This thesis contributed to this project by using ^{239}Pu and ^{240}Pu to validate the chronology of the Rincon del Bonete reservoir sediment record, which permitted the interpretation of the sediment dynamics, soil redistribution, and associated contaminant transfers in the catchment. Although the refined fallout baselines developed within the AVATAR project were not directly implemented, the approach adopted here is consistent with the project's objectives, as it illustrates the need for

improved fallout radionuclide chronologies in the Southern hemisphere and provides a practical example of sediment records reconstruction.

- CELESTE lab, an international research project from CNRS (referred to as 'IRP' standing for "International Research Project") and the acronym of which standing for "Investigating the impact of climate and land use change on soil and water resources in the so-called Southern Cone Region, located in Southern Brazil, Uruguay and Northeastern Argentina", and understudied compared to other regions of the South-American continent such as the Amazon.

This PhD thesis was therefore also characterised by the multiple national and international collaborations that emerged from both projects, leading to engaging discussions and meaningful outcomes, while at the same time requiring thoughtful efforts to harmonise the multiple contributions.

Manuscript Structure

The results of this thesis are presented in a chapter of materials and methods then 3 chapters of results, which were written following the format of scientific articles and their structure was adapted to the journals styles. The final chapter of this thesis presents a synthesis and discussion of the results, along with perspectives for future research.

The first chapter focused on the representativeness of soil sampling for fallout radionuclide soil redistribution analysis. During the first year of this thesis, a high-density sampling campaign was implemented at a small spatial scale within two erosion sites in Southern Brazil located on cultivated hillslopes under conventional and no-tillage practices. This approach aimed to evaluate how well individual soil cores capture spatial variability of radionuclide inventories and, consequently, how representative they are for estimating soil redistribution.

An extension of this chapter was made on the implementation of a distributed erosion model, WaterSed, in this catchment. The hydrological balance was parametrised, as it conditions both runoff generation and the associated fluxes of suspended sediment.

Chapter two introduces a change in spatial scale and was dedicated to a multi-proxy analysis of the sediment archive from the Salto Grande reservoir, which permitted the first long-term reconstruction of land degradation and pesticide fluxes as well as the origin of the sediments supplied to the reservoir from the 266,000 km^2 Uruguay river transnational basin (Brazil, Argentina and Uruguay).

Chapter three was then dedicated to the retrospective reconstruction of sediment fluxes since the 1950s in the Rincon del Bonete river basin, in the Pampa region in Uruguay through a multi-proxy analysis including that of key pesticides on a sediment archive collected in a dam reservoir inaugurated in 1945. These findings provided long-term insights into the environmental consequences of the changes in land-use, land-cover and farming practices since the mid-twentieth century in this relatively understudied region.

Bibliography

Aktar, W., Sengupta, D., and Chowdhury, A. (2009). Impact of pesticides use in agriculture: their benefits and hazards. *Interdisciplinary Toxicology*, 2(1):1–12.

Andrade, B. O., Dröse, W., Aguiar, C. A. D., Aires, E. T., Alvares, D. J., Barbieri, R. L., Carvalho, C. J. B. D., Bartz, M., Becker, F. G., Bencke, G. A., Beneduzi, A., Silva, J. B., Blochtein, B., Boldrini, I. I., Boll, P. K., Bordin, J., Silveira, R. M. B. D., Martins, M. B., Bosenbecker, C., Braccini, J., Braun, B., Brito, R., Brown, G. G., Büneker, H. M., Buzatto, C. R., Cavalleri, A., Cechin, S. Z., Colombo, P., Constantino, R., Costa, C. F. D., Dalzochio, M. S., Oliveira, M. G. D., Dias, R. A., Santos, L. A. D., Duarte, A. D. F., Duarte, J. L. P., Durigon, J., Da Silva, M. E., Ferreira, P. P. A., Ferreira, T., Ferrer, J., Ferro, V. G., Fontana, C. S., Freire, M. D., Freitas, T. R. O., Galiano, D., Garcia, M., Dos Santos, T. G., Gomes, L. R. P., Gonzatti, F., Gottschalk, M. S., Graciolli, G., Granada, C. E., Grings, M., Guimarães, P. S., Heydrich, I., Iop, S., Jarenkow, J. A., Jungbluth, P., Käffer, M. I., Kaminski, L. A., Kenne, D. C., Kirst, F. D., Krolow, T. K., Krüger, R. F., Kubiak, B. B., Leal-Zanchet, A. M., Loebmann, D., Lucas, D. B., Lucas, E. M., Luza, A. L., Machado, I. F., Madalozzo, B., Maestri, R., Malabarba, L. R., Maneyro, R., Marinho, M. A. T., Marques, R., Marta, K. D. S., Martins, D. D. S., Martins, G. D. S., Martins, T. R., Mello, A. S. D., Mello, R. L., Mendonça Junior, M. D. S., Morais, A. B. B. D., Moreira, F. F. F., Moreira, L. F. B., Moura, L. D. A., Nervo, M. H., Ott, R., Paludo, P., Passaglia, L. M. P., Périco, E., Petzhold, E. S., Pires, M. M., Poppe, J. L., Quintela, F. M., Raguse-Quadros, M., Pereira, M. J. R., Renner, S., Ribeiro, F. B., Ribeiro, J. R. I., Rodrigues, E. N. L., Rodrigues, P. E. S., Romanowski, H. P., Ruschel, T. P., Saccol, S. D. S. A., Savaris, M., Silveira, F. S., Schmitz, H. J., Siegloch, A. E., Siewert, R. R., Silva Filho, P. J. S. D., Soares, A. G., Somavilla, A., Sperotto, P., Spies, M. R., Tirelli, F. P., Tozetti, A. M., Verrastro, L., Vogel Ely, C., Da Silva, A. Z., Zank, C., Zefa, E., and Overbeck, G. E. (2023). 12,500+ and counting: biodiversity of the Brazilian Pampa. *Frontiers of Biogeography*, 15(2).

Bennett, B. G. (2002). WORLDWIDE DISPERSION AND DEPOSITION OF RADIONUCLIDES PRODUCED IN ATMOSPHERIC TESTS:. *Health Physics*, 82(5):644–655.

Bennett, E. M., Carpenter, S. R., and Caraco, N. F. (2001). Human Impact on Erodable Phosphorus and Eutrophication: A Global Perspective: Increasing accumulation of phosphorus in soil threatens rivers, lakes, and coastal oceans with eutrophication. *BioScience*, 51(3):227–234.

Beretta-Blanco, A., Pérez, O., and Carrasco-Letelier, L. (2019). Soil quality decrease over 13 years of agricultural production. *Nutrient Cycling in Agroecosystems*, 114(1):45–55.

Bertol, I., Luciano, R. V., Bertol, C., and Bagio, B. (2017). Nutrient and Organic Carbon Losses, Enrichment Rate, and Cost of Water Erosion. *Revista Brasileira de Ciência do Solo*, 41:e0160150. Publisher: Sociedade Brasileira de Ciência do Solo.

Chaboche, P.-A. (2021). *Amélioration de la chronologie des retombées initiales de radionucléides pour reconstruire les taux de redistribution de sol dans les bassins versants agricoles d'Amérique du Sud*. phdthesis, Université Paris-Saclay.

Chaboche, P.-A., Pointurier, F., Sabatier, P., Foucher, A., Tiecher, T., Minella, J. P., Tassano, M., Hubert, A., Morera, S., Guédron, S., Ardois, C., Boulet, B., Cossonnet, C., Cabral, P., Cabrera, M., Chalar, G., and Evrard, O. (2022). 240Pu/239Pu signatures allow refining the chronology of radionuclide fallout in South America. *Science of The Total Environment*, 843:156943.

De Roo, A. P. J., Wesseling, C. G., and Ritsema, C. J. (1996). Lisem: A Single-Event Physically Based Hydrological and Soil Erosion Model for Drainage Basins. I: Theory, Input and Output. *Hydrological Processes*, 10(8):1107–1117. _eprint: https://onlinelibrary.wiley.com/doi/pdf/10.1002/%28SICI%291099-1085%28199608%2910%3A8%3C1107%3A%3AAID-HYP415%3E3.0.CO%3B2-4.

Dearing, J. A. and Jones, R. T. (2003). Coupling temporal and spatial dimensions of global sediment flux through lake and marine sediment records. *Global and Planetary Change*, 39(1):147–168.

Didoné, E. J., Gomes Minella, J. P., and Allasia Piccilli, D. G. (2021). How to model the effect of mechanical erosion control practices at a catchment scale? *International Soil and Water Conservation Research*, 9(3):370–380.

Didoné, E. J., Gomes Minella, J. P., Andres Schneider, F. J., Londero, A. L., Lefèvre, I., and Evrard, O. (2019). Quantifying the impact of no-tillage on soil redistribution in a cultivated catchment of Southern Brazil (1964–2016) with 137Cs inventory measurements. *Agriculture, Ecosystems & Environment*, 284:106588.

Didoné, E. J., Minella, J. P. G., and Evrard, O. (2017). Measuring and modelling soil erosion and sediment yields in a large cultivated catchment under no-till of Southern Brazil. *Soil and Tillage Research*, 174:24–33.

Didoné, E. J., Minella, J. P. G., Reichert, J. M., Merten, G. H., Dalbianco, L., de Barrros, C. A. P., and Ramon, R. (2014). Impact of no-tillage agricultural systems on sediment yield in two large catchments in Southern Brazil. *Journal of Soils and Sediments*.

Dinerstein, E., Olson, D., Joshi, A., Vynne, C., Burgess, N. D., Wikramanayake, E., Hahn, N., Palminteri, S., Hedao, P., Noss, R., Hansen, M., Locke, H., Ellis, E. C., Jones, B., Barber, C. V., Hayes, R., Kormos, C., Martin, V., Crist, E., Sechrest, W., Price, L., Baillie, J. E. M., Weeden, D., Suckling, K., Davis, C., Sizer, N., Moore, R., Thau, D., Birch, T., Potapov, P., Turubanova, S., Tyukavina, A., de Souza, N., Pintea, L., Brito, J. C., Llewellyn, O. A., Miller, A. G., Patzelt, A., Ghazanfar, S. A., Timberlake, J., Klöser, H., Shennan-Farpón, Y., Kindt, R., Lillesø, J.-P. B., van Breugel, P., Graudal, L., Voge, M.,

Al-Shammari, K. F., and Saleem, M. (2017). An Ecoregion-Based Approach to Protecting Half the Terrestrial Realm. *BioScience*, 67(6):534–545.

Foley, J. A., DeFries, R., Asner, G. P., Barford, C., Bonan, G., Carpenter, S. R., Chapin, F. S., Coe, M. T., Daily, G. C., Gibbs, H. K., Helkowski, J. H., Holloway, T., Howard, E. A., Kucharik, C. J., Monfreda, C., Patz, J. A., Prentice, I. C., Ramankutty, N., and Snyder, P. K. (2005). Global Consequences of Land Use. *Science*, 309(5734):570–574.

Foucher, A., Tassano, M., Chaboche, P.-A., Chalar, G., Cabrera, M., Gonzalez, J., Cabral, P., Simon, A.-C., Agelou, M., Ramon, R., Tiecher, T., and Evrard, O. (2023). Inexorable land degradation due to agriculture expansion in South American Pampa. *Nature Sustainability*.

Garcia-Rodrıguez, F., Mazzeo, N., Sprechmann, P., Metzeltin, D., Sosa, F., Renom, M., Scharf, B., and Gaucher, C. (2002). Paleolimnological assessment of human impacts in Lake Blanca, SE Uruguay. *Journal of Paleolimnology*.

Golosov, V. and Walling, D. E. (2019). Erosion and sediment problems: Global Hotspots.

Hudson, N. (1993). *Field measurement of soil erosion and runoff*. Number 68 in FAO soils bulletin. Food and Agriculture Organization of the United Nations, Rome.

Keesstra, S. D., Bouma, J., Wallinga, J., Tittonell, P., Smith, P., Cerdà, A., Montanarella, L., Quinton, J. N., Pachepsky, Y., van der Putten, W. H., Bardgett, R. D., Moolenaar, S., Mol, G., Jansen, B., and Fresco, L. O. (2016). The significance of soils and soil science towards realization of the United Nations Sustainable Development Goals. *SOIL*, 2(2):111–128.

Kruk, C., Segura, A., Piñeiro, G., Baldassini, P., Pérez-Becoña, L., García-Rodríguez, F., Perera, G., and Piccini, C. (2023). Rise of toxic cyanobacterial blooms is promoted by agricultural intensification in the basin of a large subtropical river of South America. *Global Change Biology*, 29(7):1774–1790.

Le Gall, M., Evrard, O., Dapoigny, A., Tiecher, T., Zafar, M., Minella, J. P. G., Laceby, J. P., and Ayrault, S. (2017). Tracing Sediment Sources in a Subtropical Agricultural Catchment of Southern Brazil Cultivated With Conventional and Conservation Farming Practices. *Land Degradation & Development*, 28(4):1426–1436. _eprint: https://onlinelibrary.wiley.com/doi/pdf/10.1002/ldr.2662.

Londero, A. L., Minella, J. P. G., Deuschle, D., Schneider, F. J. A., Boeni, M., and Merten, G. H. (2018). Impact of broad-based terraces on water and sediment losses in no-till (paired zero-order) catchments in southern Brazil. *Journal of Soils and Sediments*, 18(3):1159–1175.

Mabit, L., Benmansour, M., and Walling, D. E. (2008). Comparative advantages and limitations of the fallout radionuclides 137Cs, 210Pbex and 7Be for assessing soil erosion and sedimentation. *Journal of Environmental Radioactivity*, 99(12):1799–1807.

Mabit, L., Meusburger, K., Fulajtar, E., and Alewell, C. (2013). The usefulness of 137Cs as a tracer for soil erosion assessment: A critical reply to Parsons and Foster (2011). *Earth-Science Reviews*, 127:300–307.

Merotto, A., Gazziero, D. L. P., Oliveira, M. C., Scursoni, J., Garcia, M. A., Figueroa, R., and Turra, G. M. (2022). Herbicide use history and perspective in South America. *Advances in Weed Science*, 40(spe1):e020220050.

Merritt, W., Letcher, R., and Jakeman, A. (2003). A review of erosion and sediment transport models. *Environmental Modelling & Software*, 18(8-9):761–799.

Minella, J. P., Merten, G. H., Barros, C. A., Ramon, R., Schlesner, A., Clarke, R. T., Moro, M., and Dalbianco, L. (2017). Long-term sediment yield from a small catchment in southern Brazil affected by land use and soil management changes. *Hydrological Processes*, 32(2):200–211. _eprint: https://onlinelibrary.wiley.com/doi/pdf/10.1002/hyp.11404.

Minella, J. P. G., Walling, D. E., and Merten, G. H. (2014). Establishing a sediment budget for a small agricultural catchment in southern Brazil, to support the development of effective sediment management strategies. *Journal of Hydrology*, 519:2189–2201.

Morgan, R. P. C. (2006). *Soil erosion and conservation*. Blackwell, Malden, Mass., 3. ed., [nachdr.] edition.

Nearing, M. A., Foster, G. R., Lane, L. J., and Finkner, S. C. (1989). A Process-Based Soil Erosion Model for USDA-Water Erosion Prediction Project Technology. *Transactions of the ASAE*, 32(5):1587–1593.

Oliveira, T. E. D., Freitas, D. S. D., Gianezini, M., Ruviaro, C. F., Zago, D., Mércio, T. Z., Dias, E. A., Lampert, V. D. N., and Barcellos, J. O. J. (2017). Agricultural land use change in the Brazilian Pampa Biome: The reduction of natural grasslands. *Land Use Policy*, 63:394–400.

Parsons, A. J. and Foster, I. D. L. (2011). What can we learn about soil erosion from the use of 137Cs? *Earth-Science Reviews*, 108(1):101–113.

Parsons, A. J. and Foster, I. D. L. (2013). The assumptions of science: A reply to Mabit et al. (2013). *Earth-Science Reviews*, 127:308–310.

Porto, P., Walling, D. E., Callegari, G., and Capra, A. (2009). Using caesium-137 and unsupported lead-210 measurements to explore the relationship between sediment mobilisation, sediment delivery and sediment yield for a Calabrian catchment. *Marine & Freshwater Research*, 60(7):680–689.

Ramon, R. (2021). *Quantifying sediment source contributions in contrasted agricultural catchments (Uruguay River, Southern Brazil)*. PhD thesis, Universit{\'e} Paris-Saclay ; Universidade Federal do Rio Grande do Sul (Porto Alegre, Br{\'e}sil).

Ramos, M. C., Lizaga, I., Gaspar, L., Quijano, L., and Navas, A. (2019). Effects of rainfall intensity and slope on sediment, nitrogen and phosphorous losses in soils with different use and soil hydrological properties. *Agricultural Water Management*, 226:105789.

Renard, K. G., Foster, G. R., Weesies, G. A., McCool, D. K., and Yoder, D. C. (1997). *Predicting Soil Erosion by Water: A Guide to Conservation Planning with the Revised Universal Soil Loss Equation*, volume 703. United States Department of Agriculture, agriculture handbook edition.

Ritchie, J. C. and Ritchie, C. A. (2008). BIBLIOGRAPHY OF PUBLICATIONS OF 137CESIUM STUDIES RELATED TO EROSION AND SEDIMENT DEPOSITION. *USDA*.

Skidmore, M. E., Sims, K. M., and Gibbs, H. K. (2023). Agricultural intensification and childhood cancer in Brazil. *Proceedings of the National Academy of Sciences*, 120(45):e2306003120.

Steffen, W., Broadgate, W., Deutsch, L., Gaffney, O., and Ludwig, C. (2015). The trajectory of the Anthropocene: The Great Acceleration. *The Anthropocene Review*, 2(1):81–98.

Tiecher, T., Minella, J. P. G., Caner, L., Evrard, O., Zafar, M., Capoane, V., Le Gall, M., and Santos, D. R. d. (2017). Quantifying land use contributions to suspended sediment in a large cultivated catchment of Southern Brazil (Guaporé River, Rio Grande do Sul). *Agriculture, Ecosystems & Environment*, 237:95–108.

Tiecher, T., Minella, J. P. G., Evrard, O., Caner, L., Merten, G. H., Capoane, V., Didoné, E. J., and dos Santos, D. R. (2018). Fingerprinting sediment sources in a large agricultural catchment under no-tillage in Southern Brazil (Conceição River). *Land Degradation & Development*, 29(4):939–951. _eprint: https://onlinelibrary.wiley.com/doi/pdf/10.1002/ldr.2917.

United Nations Scientific Committee on the Effects of Atomic Radiation (2000). *Sources and effects of ionizing radiation. 1: Sources*. Number 2000 in Report of the United Nations Scientific Committee on the Effects of Atomic Radiation. United Nations, New York.

Van Der Werf, H. M. (1996). Assessing the impact of pesticides on the environment. *Agriculture, Ecosystems & Environment*, 60(2-3):81–96.

Walling, D. and Quine, T. (1992). The use of caesium-137 measurements in soil erosion surveys. *Erosion and sediment monitoring programmes in river basins. Proc. international symposium, Oslo, 1992*.

Walling, D. E. and He, Q. (1999). Improved Models for Estimating Soil Erosion Rates from Cesium-137 Measurements. *Journal of Environmental Quality*, 28(2):611–622. _eprint: https://acsess.onlinelibrary.wiley.com/doi/pdf/10.2134/jeq1999.00472425002800020027x.

Walling, D. E., Quine, T. A., and Department of Geography, U. o. E. U. K. (1993). Use of caesium-137 as a tracer of erosion and sedimentation: Handbook for the application of the caesium-137 technique. UK Overseas Development Administration research scheme R4579. Technical Report INIS-XA-N–179, Department of Geography, University of Exeter (United Kingdom).

Wischmeier, W. H. and Smith, O.D. (1978). AH_537 Predicting Rainfall Soil Losses.

XINBAO, Z., HIGGITT, D. L., and WALLING, D. E. (1990). A preliminary assessment of the potential for using caesium-137 to estimate rates of soil erosion in the Loess Plateau of China. *Hydrological Sciences Journal*, 35(3):243–252. Publisher: Taylor & Francis _eprint: https://doi.org/10.1080/02626669009492427.

Zafar, M., Tiecher, T., de Castro Lima, J. A. M., Schaefer, G. L., Santanna, M. A., and dos Santos, D. R. (2016). Phosphorus seasonal sorption-desorption kinetics in suspended sediment in response to land use and management in the Guaporé catchment, Southern Brazil. *Environmental Monitoring and Assessment*, 188(11):643.

Zalles, V., Hansen, M. C., Potapov, P. V., Parker, D., Stehman, S. V., Pickens, A. H., Parente, L. L., Ferreira, L. G., Song, X.-P., Hernandez-Serna, A., and Kommareddy, I. (2021). Rapid expansion of human impact on natural land in South America since 1985. *Science Advances*, 7(14):eabg1620.

Zurbriggen, C., González-Lago, M., Baraibar, M., Baethgen, W., Mazzeo, N., and Sierra, M. (2020). Experimentation in the Design of Public Policies: The Uruguayan Soils Conservation Plans. *Iberoamericana – Nordic Journal of Latin American and Caribbean Studies*, 49(1):52–62.

II

Materials and Methods

Chapter 2

Material and Methods

2.1 . Materials

2.1.1 . Study site

Two main river basins were explored during this thesis, the Salto Grande dam and the Rincon del Bonete dam river basins, both being tributaries of the particularly widespread Uruguay river river basin. First, the Salto Grande (SG) dam, located along the border between Uruguay and Argentina, was investigated. At the SG dam, the Uruguay river drains an transnational surface area of approximately 266,000 km^2 (Figure 5.1, Ramon (2021)). Of this area, 70% is located in southern Brazil, 20% in Argentina and 10% in Uruguay. Land-use in the river basin is primarily agricultural, with intensive farming production in the Brazilian states of Rio Grande do Sul (RS) and Santa Catarina (SC). Small farms (< 50 ha) predominate in the hilly upper parts of the basin while larger properties (mostly < 100 ha) dominate the lower areas, primarily used for the production of soybeans (*Glycine max*), corn (*Zea mays*), and wheat (*Triticum Aestivum*). Similar land uses are observed in Argentina, where plantations of mate (*Ilex paraguariensis*), tea (*Camellia sinensis*), and eucalyptus (*Eucalyptus globulus*) prevail (Ramon 2021). In the alluvial plain, larger farms (> 100 ha) dominate in the southwestern regions of RS and northern Uruguay. These regions are mostly used for extensive ranching and irrigated rice production. The southernmost part of the Argentinian part is made up of flooded grasslands and savannahs. This extremely flat region has hydromorphic soils, which are ideal for pastures and commercial forest plantations used for wood and cellulose extraction.

Second, the Rincón del Bonete catchment that was investigated afterwards is also transboundary with 9% of its surface area being located in Brazil and 91% in Uruguay. It is located within the Pampa biome, mainly in the central and northern regions of Uruguay (figure 6.1) with hilly to rolling landscapes.

The Rincón del Bonete catchment has two major tributaries including Rio Tacuarembó and Rio Negro (figure 6.1). These two rivers drain very contrasting landscapes with distinct reliefs, geologies and soil types, reflecting the occurrence of different ecoregions (Arocena et al. 2022). On the one hand, the Rio Negro, in the western part of the river basin, drains a region characterised by the presence of mudstones and limestones that support the formation of Mollisols, or dark soils, which are rich in organic matter, silt, and clay and that are mainly used for crop cultivation. In contrast, the Rio Tacuarembó drains a region mainly composed of Alfisols, underlied by sandstones, characterised by leached and weathered acidic soils with low organic matter content, showing the country's lowest fertility, or shallow sandy or coarser soils with rock outcrops and loose stones on the surface, predominantly used for forest plantations (Arocena et al. 2022).

Overall, land-use in the Rincón del Bonete catchment remained dominated by natural herbaceous

vegetation (61%) in 2023. In addition, the catchment was also occupied with cropland cultivated using no-tillage practices (14%), forest plantations (11%), natural forests (5%), wetlands (4%), water bodies (3%) and non-vegetated areas (1%) (figure 6.1).

Furthermore, the Rincón del Bonete catchment drains into a reservoir whose surface area varies between 465-1495 km^2 (1140 km^2 in optimal conditions). Built in 1937 and inaugurated in 1945, this reservoir is used to generate electric power in Uruguay. Importantly, the Rincón del Bonete reservoir has never been emptied or dredged since its creation. This reservoir is the largest freshwater body in Uruguay (5 km^3 of water storage) with a ratio of 25-33 km^2 of drainage basin per km^2 of reservoir, thereby exceeding the storage capacity of the other reservoirs in the country, including the large Salto Grande and Palmar dams, with respective reservoir surfaces of 783 and 320 km^2 (World Lake Database - 2025).

2.1.2 . Data sources

2.1.3 . Reconstruction of the land-use and land-cover

Land-use and land-cover were reconstructed in the Salto Grande river basin using a freely available set of maps provided by the MapBiomas network. As no dataset was available for the entire Salto Grande river basin, the maps were reconstructed based on multiple MapBiomas datasets : Mapbiomas Argentina, Pampa and Brazil (Mapbiomas Argentina, Pampa and Brazil).

Land-use was reconstructed in the Rincon del Bonete river basin using the set of maps provided by the MapBiomas network (MapBiomas Pampa) for the Pampa biome for the 1985-2022 period (Baeza et al. 2022). The river basin data were retrieved from the maps published for each year during this period. In the last version of MapBiomas, a distinction was made between permanent pasture and temporary crops. Permanent pastures were defined by MapBiomas as the "cultivation of perennial herbaceous forage species, that persist for more than one year", while temporary crops were defined as the "cultivation of annual herbaceous species that are planted and harvested within one year". Corresponding increase and decrease percentages were calculated following equation 6.1.

The land-use and land-cover maps used in this thesis are derived from the most recent available versions. These products provide annual land-use and land-cover data from 1985 to 2023 at a 30-m spatial resolution across a comprehensive set of classes including forest, pasture, cropland, urban areas, and water bodies in Uruguay and more specific classes in Brazil, with consistent temporal coverage. These datasets were therefore proven to be valuable for reconstructing trends in agricultural expansion, deforestation and other land-use changes driven by human activity across the broader regions of southern Brazil, northern Argentina, and Uruguay (Souza et al. 2020; Baeza and Paruelo 2020; Baeza et al. 2022). Its annual temporal resolution makes it particularly suitable for analysing long-term land-use patterns and evaluating the effects of environmental and agricultural policies across this diverse and dynamic landscape. Although the datasets provide robust insights into broad trends, cautious interpretation of

specific land-cover transitions is required for identifying fine-scale transitions or mixed-use landscapes.

2.1.4 . Sample collection

Sediment cores

Three sediment cores were collected from the Salto Grande dam (Figure 1.1) during fieldwork conducted in December 2022 (IGSN number: 10.58052/IEFOU002F). A gravity corer equipped with 90 mm PVC liners and a floating platform, which was made available by the Salto Grande dam authorities, were used for that purpose. The analyses were conducted on the longest core, SG03, showing a length of 73.5 cm.

A 48 cm long sediment (22-BONETE-03) core was also collected in December 2022 in the Rincón del Bonete reservoir, (Figure 1.1, IGSN number: 10.58052/IEFOU002D) by local researchers using a Uwitec gravity corer available at the Universidad de la República (Montevideo, Uruguay) equipped with 90 mm PVC liners on a floating platform and by hammering. The sediment core was collected in the original Rio Negro river channel. This channel was identified with a sonar, at 2.5 km from the dam (figure 6.1, under 20 m water depth) to ensure a reconstruction of the complete sedimentation history since the dam creation.

Sediment source sampling

Potential sediment sources from two upstream sub-catchments, which were defined as representative of the two major zones that may supply sediment to the Uruguay river (Tales Tiecher 2015; Ramon 2021), including the Northern basaltic plateau and the Southern Pampa, were collected during a previous PhD (Ramon 2021). The goal was to characterise and compare their respective sediment properties, in order to determine their relative contributions to the sediment accumulated in the dam reservoir, and their potential variations throughout time. Tales Tiecher (2015) and Ramon (2021) collected suspended sediments close to, or at the outlet of the Conceição river basin in 2012 and Ibirapuitã river basin in 2021, respectively.

Conceição river basin The Conceição River basin (Figure 2.1), located on the basaltic plateau of Rio Grande do Sul and covering approximately 804.3 km^2 is representative of the northern area of the Salto Grande river basin (Ramon 2021). The soils found in the area are mainly Ferrasols (80%) although Nitisols (18%), and Acrisols (2%) can also be found. Altitudes range from 270 to 480 m, and the terrain consists of gentle slopes (9$\%$) at the highest points of the basin and moderate to steep slopes near the river and drainage channels. The land is primarily used for cropland and is mainly cultivated with soybeans (*Glycine max*) under a no-tillage system in the summer. During the winter, wheat (*Triticum aestivum*), oats (*Avena sativa* and *Avena strigosa*) and ryegrass (*Lolium multiflorum*) are cultivated for grain production, as feed for dairy cattle feed or to cover the soil (Ramon 2021). However, inadequate soil management in these areas under the no-tillage system has resulted in high erosion rates in recent

decades (Didoné et al. 2019). Pastures used for raising cattle occupy 12% of the river basin's surface area, while forests cover only 5%. Only perennial pastures were sampled in the study.

Ibirapuitã river basin Located in the south of the Salto Grande river basin, the Ibirapuita sub-basin (Figure 2.1) covers an area of 5943 km^2 and is representative of the lower part of the river basin (Ramon 2021). This basin is comprised between 70 and 370 m of altitudes (only 15% of the river basin is between 280 and 370 m and in the headwaters of the basin). The catchment is dominated by shallow Regosols and sandy Acrisols, which are mainly occupied by the native grasslands that are typical of the Pampa biome (81%, Figure 2.1).

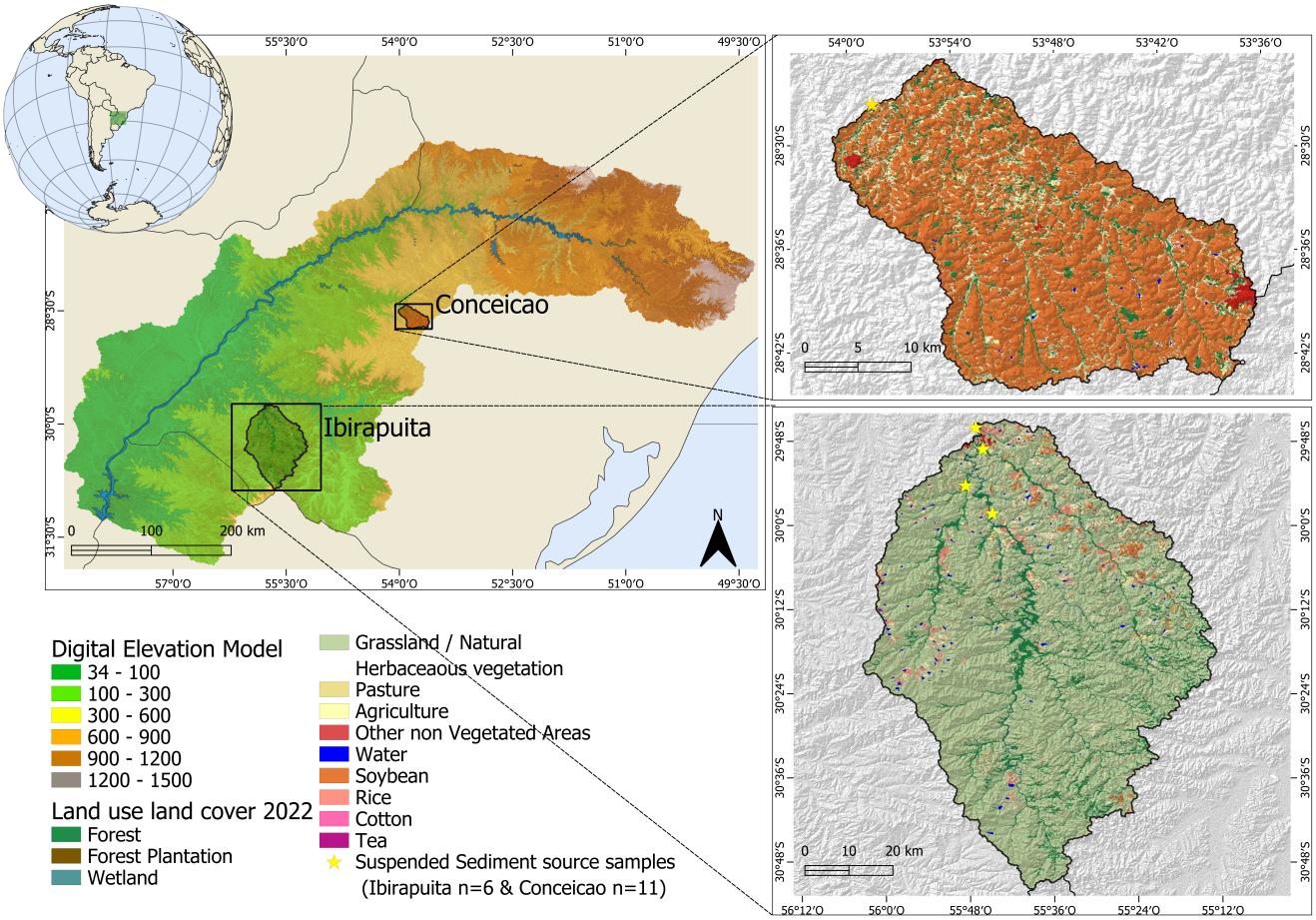

Figure 2.1: Digital elevation model of the Salto Grande, Ibirapuitã and Conceição river basins. Land-use and land-cover and source sample localisation analysed for magnetic susceptibility, background map from OpenStreetMap contributors (2024)

2.2 . Methods

2.2.1 . Global Summary of methodologies

Resolution of the different analyses conducted on the sediment cores and their respective units are summarized in table 2.1 along with graphical representation of analyses conducted (Figure 2.2). The methodology applied for each studied parameter is partly detailed in this section. However, details on

the methodology applied for each type of measurement can be found in the chapters where they have been applied.

Analysis conducted	Studied parameters	Resolution	Units	Conducted at
Particle size analysis	D10, D50, D90	1 cm	μm	LSCE*
CT-scanner	Relative density	0.625 mm	Hounsfield	DOSEO platform*
Bulk density	Bulk density	1 cm	$g.cm^{-3}$	LSCE*
Organic matter analysis	TOC, TN, δ^{13}Corg	1 cm	% + ‰	LSCE/IEES**
XRF Geochemical analysis	Mg, Al, Si, P, S, Cl, Ar, K, Ca, Ti, V, Cr, Co, Mn, Fe, Co, Rh, Ni, Cu, Zn, Ga, As, Br, Rb, Sr, Y, Zr	0.5 mm	counts per second	LSCE*
Gamma spectrometry analysis	$^{210}Pb_{ex}$, ^{137}Cs	1 - 1.5 cm	$Bq.kg^{-1}$	LSCE*
Plutonium Analysis	^{239}Pu, ^{240}Pu	1 - 1.5 cm	$Bq.kg^{-1}$	Basel/Spiez laboratory***
Magnetic susceptibility analysis	high (χ_{HF}) and low χ_{LF} frequencies magnetic susceptibility	1-1.5 cm	m^3kg^{-1}	UFRGS*
Pesticide analysis	See Table 2.2 for full list	2-4 cm	$mol.cm^{-2}.yr^{-1}$	EDYTEM**
Fluxes of sediments	MAR	0.625 mm	$g.cm^{-2}.yr^{-1}$	LSCE*
X-ray diffractometry	Mineralogical composition	1-1.5 cm	angstroms (Å)	UFRGS***

Table 2.1: Summary of analyses conducted, parameters studied, resolution of the data, measurement units and laboratory where they were conducted. * Analysis conducted by A. Bardelle with the help or guidance from researchers or technicians ** Preparation of samples by A. Bardelle, and analysis conducted by other researchers or technicians *** Analysis conducted by other researchers or technicians

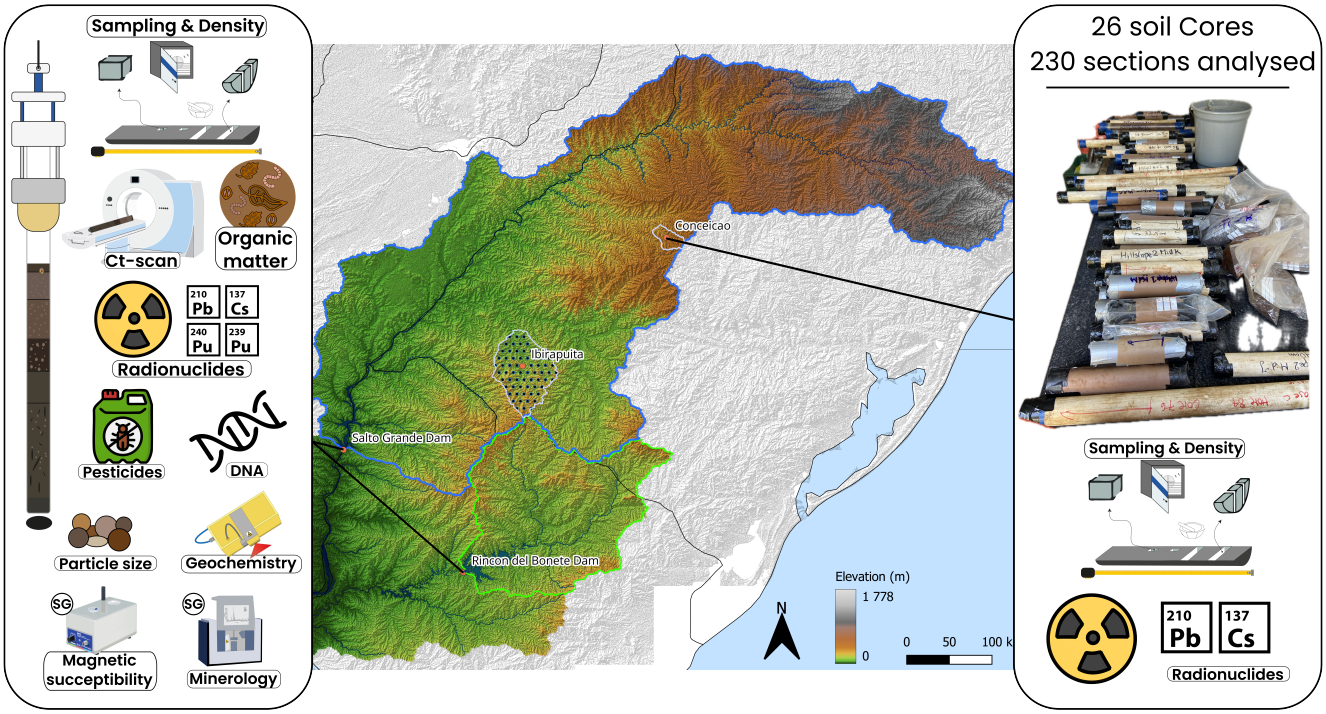

Figure 2.2: Analysis conducted on the sediment cores (left), with analyses specific to the Salto Grande core indicated by a circled “SG”, and analyses related to soil redistribution in the Conceição catchment. Digital elevation model of the Uruguay River basin showing the locations of the Salto Grande (blue), Rincón del Bonete (green), Ibirapuitã (white with blue dots), and Conceição (white) river basins. Background map from OpenStreetMap contributors (2024).

2.2.2 . Particle size analysis

Particle size analysis was conducted on fresh sediment at centimetre-scale resolution using a laser diffraction particle size analyser (Mastersizer 3000 with Hydro LV, Malvern Panalytical). The particle size distribution was assessed over a range of 0.01 µm to 3500 µm and the proportion of particles smaller than 10%, 50% and 90%, respectively, were recorded as D10, D50 and D90 indices.

2.2.3 . Density analysis

Relative density of the sediments was recorded at 0.488 mm intervals using a Computer Tomography scanner (CT-scan), and images were recorded using the GE Discovery CT750 HD equipment available at the DOSEO platform (French Atomic Energy and Alternative Energy Commission, CEA Paris-Saclay, France). Relative density (grey values) was extracted from the recorded images using the free software ImageJ. Discrete Dry Bulk Density (DBD) was measured on multiple samples of fresh sediment using a volume of 1.7 cm^3 (V) in an acrylic cube. The cubes were filled with fresh sediment, and their humid weight (m_{humid} in g) was recorded. Then, they were oven-dried at 40°C for 48 to 96 hours, and their dry weight (m_{dry} in g) was measured. DBD (in $g.cm^3$) was calculated using the following equation 2.1.

$$\rho_b = \frac{m_{\text{dry}}}{V} \tag{2.1}$$

The measured DBD was correlated with the mean relative density values recorded for the samples. The DBD was then reconstructed for the entire sequences following the procedure proposed by Foucher et al. (2021, 2023).

2.2.4 . Organic matter analysis

For both the Salto Grande and Rincon del Bonete cores, the total organic carbon (TOC) and nitrogen (TN), as well as the stable carbon (δ^{13}C) isotope ratios of organic and clay-bound organic matter were measured. However, different methods were used to analyse sediment from both sites. For the Salto Grande dam, the measurements were performed using a continuous flow Elementar® VarioPyro cube elemental analyzer (EA) coupled to a Micromass® Isoprime Isotope Ratios mass Spectrometer (IRMS) at the Institute of Ecology and Environmental Science of Paris. Oxygen for combustion was injected at a rate of 30 ml.min^{-1} for 70 s, and the reduction and combustion furnaces were set to temperatures of 850 °C and 1120 °C, respectively (Agnihotri et al. 2014). Analytical precision and repeatability were controlled using tyrosine samples that were calibrated against international standards (Coplen et al. 1983).

For the Rincon del Bonete dam, contents were measured using an elemental analyser (Flash HT 2000) coupled to an isotope ratio mass spectrometer Advantage delta V via a conflow IV interface from Thermo Scientific. The EA-IRMS instrument was calibrated against two standards (i.e., EMAP2 and USGS24). Analytical precision and repeatability were assessed via the analysis of reference material

(Low Organic Standard and High Organic Standard).

2.2.5 . Gamma spectrometry analysis

Gamma spectrometry measurements for the Salto Grande sediment core were conducted using coaxial HPGe detectors (Canberra/Ortec®), which are available at the Laboratoire des Sciences du Climat et de l'Environnement (Gif-sur-Yvette, France). For the Rincon del Bonete dam, as less material quantity was available for analysis, the samples were measured using a 'well' type HPGe detector (Canberra/Ortec®) available at the Modane underground laboratory, a subterranean low-background laboratory located within the Fréjus Road Tunnel, near Modane, France. This laboratory is shielded from cosmic radiation by 1700 m of rocks and is only equipped with very low activity materials and copper-lead shielded detectors to achieve ultra-low background in order to analyse low-radioactivity samples in the best conditions.

All measurements were corrected for the background level as well as for detector and geometry efficiencies. Activities were also decay-corrected to the sampling date.

2.2.6 . Plutonium analysis

Based on the vertical distribution of ^{137}Cs activities in the Rincon del Bonete sediment core, 16 samples among those analysed in gamma spectrometry were selected for additional plutonium analyses (^{239}Pu, ^{240}Pu). Measurements were conducted at the Spiez Laboratory in Switzerland following the methodology established by Röllin et al. (2022).

2.2.7 . Age model, Sediment and Pesticides fluxes

The sediment core chronology was established using the activities of $^{210}Pb_{ex}$ measured in the cores. The *serac* R package for ShortlivEd RAdionuclide Chronology (Bruel and Sabatier 2020) was used to establish the age model via the Constant Flux Constant Sedimentation (CF:CS) model.

Sediment fluxes (MAR, Mass Accumulation Rate,$g.cm^{-2}.yr^{-1}$) were reconstructed by multiplying the Sediment Accumulation Rate (SAR, $cm.yr^{-1}$) obtained from the CF:CS age model by the high-resolution DBD calibrated from the CT scan values ($g.cm^{-3}$) (equation 2.2).

$$\mathrm{MAR}\ (\mathrm{g\,cm^{-2}\,yr^{-1}}) = \mathrm{Sedimentation\ rate}\ (\mathrm{cm\,yr^{-1}}) \cdot \mathrm{DBD}\ (\mathrm{g\,cm^{-3}}) \tag{2.2}$$

2.2.8 . Pesticides analysis

A total of 16 pesticides and their metabolites (Table 2.2), which are commonly reported in the literature in environmental samples of the region of interest (López et al. 2012; Mañay et al. 2004; Palladino et al. 2023; Rodríguez-Bolaña et al. 2024), were measured at EDYTEM Laboratory (Univ. Savoie Mont-Blanc, France)

Pesticide fluxes were derived from the sediment fluxes. Therefore, the moles of pesticides were

converted into fluxes by multiplying the pesticide concentrations with the MAR (equation 2.3).

$$\text{Fluxes of pesticides } (\text{mol}\,\text{cm}^{-2}\,\text{yr}^{-1}) = \text{Pesticides } (\text{mol}\,\text{g}^{-1}) \cdot \text{MAR } (\text{g}\,\text{cm}^{-2}\,\text{yr}^{-1}) \tag{2.3}$$

The set of samples used for pesticides analysis was freeze-dried in an ALPHA 1-2 LD plus (CHRIST®) freeze dryer for 24 to 48h, depending on the quantity of sample available The pesticides were then extracted using the QuEChERS method; the Quick, Easy, Cheap, Effective, Rugged, and Safe extraction kit and method (Perestrelo et al. 2019). Pesticide concentrations were obtained via Gas and Liquid Chromatography coupled with Mass Spectrometry (GC-MS for Endosulfan, Chlopryrifos Ethyl, DDT,DDD, DDE, and Mirex and LC-MS/MS for S-Metolachlor, Simazine, Atrazine, Diruon, 2.4-D, Tebuconazole, Imidacloriprid and Friponil). Glyphosate and AMPA were analysed using a rapid LC-MS/MS method with a Polypore H+ column without derivatisation, which demonstrated a good selectivity and sensitivity.

Pesticide	Abbreviation	IUPAC name	Familly	Marketed in	Source
2,4-Dichlorophenoxyacetic acid	2,4-D	2,4-Dichlorophenoxyacetic acid	Organic compound	1940	Merotto et al. (2022)
Atrazine	Atrazine	6-chloro-N^2-ethyl-N^4-(propan-2-yl)- 1,3,5-triazine-2,4-diamine	Triazine	1958	(Heri et al. 2008)
Simazine	Simazine	6-chloro-N^2,N^4-diethyl-1,3,5-triazine-2,4-diamine	Triazine	1956	(Heri et al. 2008)
Diuron	DCMU	3-(3,4-dichlorophenyl)-1,1-dimethylurea	Phenylurea	1954	(Woodford 1957)
S-Metolachlor	S-Metolachlor	(S)-2-chloro-N-(2-ethyl-6-methylphenyl)-N-[(2S)-1-methoxypropan-2-yl]acetamide	Urea	1976	(United States Environmental Protection Agency 1995)
Tebuconazole	Tebuconazole	(RS)-1-(4-chlorophenyl)-4,4-dimethyl-3-(1H-1,2,4-triazol-1-ylmethyl)pentan-3-ol	Neonicotinoid	1989	McInnes et al. (2023)
Imidacloprid	IMI	1-[(6-chloro-3-pyridinyl)methyl]-N-nitroimidazolidin-2-ylideneamine	Neonicotinoid	1985	Jeschke et al. (2019)
Endosulfan	Endosulfan	dodecachlorooctahydromethanetriyl benzodioxathiepine oxide	Organochlorine	1954	United States Environmental Protection Agency (2002)
Fipronil	Fipronil	5-Amino-1-[2,6-dichloro-4-(trifluoromethyl)phenyl]-4-(trifluoromethylsulfinyl)-1H-pyrazole-3-carbonitrile	Phenylpyrazole	1990	Jeschke et al. (2019)
Chlorpyrifos Ethyl	Chlorpyrifos Ethyl	O,O-Diethyl O-(3,5,6-trichloropyridin-2-yl) phosphorothioate	Organochlorine	1965	Rauh et al. (2011)
Dichlorodiphényltrichloroéthane	DDT	1,1'-(2,2,2-Trichloroethane-1,1-diyl)bis(4-chlorobenzene)	Organochlorine	1945	Mellanby (1992)
Dichlorodiphényldichloroéthane	DDD	1,1'-(2,2-Dichloroethane-1,1-diyl)bis(4-chlorobenzene)	Metabolite of DDT	-	-
Dichlorodiphényldichloroéthylène	DDE	1,1'-(2,2-Dichloroethene-1,1-diyl)bis(4-chlorobenzene)	Metabolite of DDT	-	-
Glyphosate	Glyphosate	N-(phosphonomethyl)glycine	Phosphonate	1974	Baer and Marcel (2014)
AMPA	AMPA	(Aminomethyl)phosphonic acid	Metabolite of glyphosate	-	-
Mirex	Mirex	dodecachloropentacyclo[5.3.0.$0^{2,6}$.$0^{3,9}$.$0^{4,8}$]decane	Organochlorine	1958	

Table 2.2: Complete list of 16 pesticides with their abbreviations, International Union of Pure and Applied Chemistry (IUAPC) names and classifications. Molecules were found on PubChem (https://pubchem.ncbi.nlm.nih.gov/)

2.2.9 . DNA analysis

Environmental DNA was analysed by E-Biom in Namur, Belgium. Three layers of 1-cm width were collected at 2-3, 11-12 and 35-36 cm depths for the Rincon del Bonete core and 10-11, 30-31 and 40-41 cm depths for the Salto Grande core in a controlled environment at the University of Namur to limit the risk of contamination. A water recipient was placed and used as a control sampling. eDNA was retrieved using a commercial kit (Nucleospin soil -Macherey-Nagel). A second extraction was applied following ISO 11063:2020 procedure and DNA was purified following INRAE's methodology. PCR were realised 8 times as per recommended for rare eDNA analyses on regions of interest. ITS, trnL, rbcL markers regions for the plants and 12S, 16S and 18S marker regions for Vertebrates, Eukaryotes and

Metazoa were amplified. Primers for each combination of markers-sample containing a specific tag allowed mutliplex of the different amplicons obtained. 1.5 $\%$ agarose gel was used in order to check the amplicons quality. Those meeting sufficient quality requirements were purified and sequenced on a Illumina sequencing platform. Control samples allowed for the detection of transfer of eDNA from one sample to another or that of external eDNA introduced during sampling or eDNA extraction. Amplification control allowed for detection of eDNA introduction during the genetic library preparation step.

The sequenced DNA were assigned their corresponding marker-sample combination, and the low quality sequences were removed. Sequencing errors were corrected and the sequences were clustered using a percentage of similarity of 97$\%$. A naive Bayesian classifier was used in order to assign the taxonomy of the sequences based on the genetic databases NCBI (Schoch et al. 2020) and SILVA (Quast et al. 2012). Finally, a standardisation step was applied as to compare samples among them in spite of the observed variations in terms of genetic material abundance.

Statistical analyses were conducted on R using MicrobiotaProcess package (Xu et al. 2023) as well as E-Biom developed scripts.

Quality control shows that the concentration and quality of extracted eDNA was sufficient to validate analysis procedures. Qualitative PCRs conducted at least twice per control sample using both pure and 10 times diluted samples showed sequences of human and beef origin for which it is impossible to determine whether they were introduced from the environment to the samples and control samples or whether they were actually present in the samples of interest and transmitted to the control samples. The ubiquity of these two species in the world makes it impossible to determine the origin of this DNA. Besides, sequences of *Broussonetia papyrifera* were found in the control samples. Originating from east Asia and being sensitive to cold, there is a high probability that the DNA came from the samples. Finally, artefact sequences were detected in the control samples. These sequences can appear during PCR when the quantity of DNA to replicate is not sufficient. Amplifications of sufficient quality were obtained for all the markers except Prosser (rbcL) and Taberlet (trnL). On the one hand, regarding Prosser, amplicons were obtained but did not match the right size, meaning that the target DNA was present but in insufficient quantity compared to less specific DNA. On the other hand, no amplification were obtained for Taberlet. The second extraction realised to obtain better amplicons for Prosser and Taberlet did not show better result and the amplicons were discarded.

2.2.10 . Magnetic susceptibility analysis

The magnetic properties of the Salto Grande sediment core and soil source samples were measured using a Bartington MS2B Dual Frequency sensor. Two grams of each sample were measured three times at high and low frequencies (4.7 and 0.47 kHz, respectively) to obtain the mass-specific magnetic susceptibility at high and low frequencies ($\chi_{HF} - m^3kg^{-1}$ and $\chi_{LF} - m^3kg^{-1}$).

2.2.11 . Sediment Fingerprinting

A sediment fingerprinting analysis of the core was conducted in accordance with the recommendations of Chalaux-Clergue et al. (2024) and using the freely available FingR package from Chalaux-Clergue and Bizeul (2025). The magnetic susceptibility parameters were used as potential fingerprints in this analysis, as these allowed a good discrimination between soils of the upper and lower parts of the river basin represented by those collected in the Conceição and Ibirapuitã sub-catchments, as initially demonstrated by Ramon (2021).

2.2.12 . Mineralogical composition

The mineralogical composition of the Salto Grande core air-dried fine-earth (ADFE) fraction ($<$2 mm) was determined by X-ray Diffractometry (XRD) on a Bruker D2 Phaser spectrometer equipped with a Lynxeye™ fast linear detector and the software Diffrac.Suite™.

Bibliography

Agnihotri, R., Kumar, R., Prasad, M. V. S. N., Sharma, C., Bhatia, S. K., and Arya, B. C. (2014). Experimental Setup and Standardization of a Continuous Flow Stable Isotope Mass Spectrometer for Measuring Stable Isotopes of Carbon, Nitrogen and Sulfur in Environmental Samples. *MAPAN*, 29(3):195–205.

Arocena, R., Castro, M., and Chalar, G. (2022). Ecological integrity assessment of streams in the light of natural ecoregions and anthropic land use. *Environmental Monitoring and Assessment*, 194(10):748.

Baer, K. and Marcel, B. (2014). Glyphosate. In *Encyclopedia of Toxicology*, pages 767–769. Elsevier.

Baeza, S. and Paruelo, J. M. (2020). Land Use/Land Cover Change (2000–2014) in the Rio de la Plata Grasslands: An Analysis Based on MODIS NDVI Time Series. *Remote Sensing*, 12(3):381.

Baeza, S., Vélez-Martin, E., De Abelleyra, D., Banchero, S., Gallego, F., Schirmbeck, J., Veron, S., Vallejos, M., Weber, E., Oyarzabal, M., Barbieri, A., Petek, M., Guerra Lara, M., Sarrailhé, S., Baldi, G., Bagnato, C., Bruzzone, L., Ramos, S., and Hasenack, H. (2022). Two decades of land cover mapping in the Río de la Plata grassland region: The MapBiomas Pampa initiative. *Remote Sensing Applications: Society and Environment*, 28:100834.

Bruel, R. and Sabatier, P. (2020). serac: an R package for ShortlivEd RAdionuclide chronology of recent sediment cores. *Journal of Environmental Radioactivity*, 225:106449.

Chalaux-Clergue, T. and Bizeul, R. (2025). FingR: A Support for Sediment Source Fingerprinting Studies. Language: en.

Chalaux-Clergue, T., Bizeul, R., Batista, P. V. G., Martínez-Carreras, N., Laceby, J. P., and Evrard, O. (2024). Sensitivity of source sediment fingerprinting to tracer selection methods. *SOIL*, 10(1):109–138. Publisher: Copernicus GmbH.

Coplen, T. B., Kendall, C., and Hopple, J. (1983). Comparison of stable isotope reference samples. *Nature*, 302(5905):236–238.

Didoné, E. J., Gomes Minella, J. P., Andres Schneider, F. J., Londero, A. L., Lefèvre, I., and Evrard, O. (2019). Quantifying the impact of no-tillage on soil redistribution in a cultivated catchment of Southern Brazil (1964–2016) with 137Cs inventory measurements. *Agriculture, Ecosystems & Environment*, 284:106588.

Foucher, A., Evrard, O., Cerdan, O., Chabert, C., Lefèvre, I., Vandromme, R., and Salvador-Blanes, S. (2021). Deciphering human and climatic controls on soil erosion in intensively cultivated landscapes after 1950 (Loire Valley, France). *Anthropocene*, 34:100287.

Foucher, A., Tassano, M., Chaboche, P.-A., Chalar, G., Cabrera, M., Gonzalez, J., Cabral, P., Simon, A.-C., Agelou, M., Ramon, R., Tiecher, T., and Evrard, O. (2023). Inexorable land degradation due to agriculture expansion in South American Pampa. *Nature Sustainability*.

Heri, W., Carroll, B., Parshley, T., and Nabors, J. B. (2008). Production, Development, and Registration of Triazine Herbicides. In *The Triazine Herbicides*, pages 31–43. Elsevier.

Jeschke, P., Witschel, M., Krämer, W., and Schirmer, U., editors (2019). *Modern Crop Protection Compounds*. Wiley, 1 edition.

López, S. L., Aiassa, D., Benítez-Leite, S., Lajmanovich, R., Mañas, F., Poletta, G., Sánchez, N., Simoniello, M. F., and Carrasco, A. E. (2012). Pesticides Used in South American GMO-Based Agriculture. In *Advances in Molecular Toxicology*, volume 6, pages 41–75. Elsevier.

Mañay, N., Rampoldi, O., Alvarez, C., Piastra, C., Heller, T., Viapiana, P., and Korbut, S. (2004). Pesticides in Uruguay. In Ware, G. W., Albert, L. A., Crosby, D. G., De Voogt, P., Hutzinger, O., Knaak, J. B., Mayer, F. L., Morgan, D. P., Park, D. L., Tjeerdema, R. S., Yang, R. S. H., and Gunther, F. A., editors, *Reviews of Environmental Contamination and Toxicology*, volume 181, pages 111–138. Springer New York, New York, NY.

McInnes, E. F., Papineni, S., Rinke, M., Schorsch, F., and Marxfeld, H. A. (2023). Agrochemicals. In *Haschek and Rousseaux's Handbook of Toxicologic Pathology, Volume 3*, pages 727–763. Elsevier.

Mellanby, K. (1992). *The DDT story*. British Crop Protection Council, Farnham, Surrey, UK.

Merotto, A., Gazziero, D. L. P., Oliveira, M. C., Scursoni, J., Garcia, M. A., Figueroa, R., and Turra, G. M. (2022). Herbicide use history and perspective in South America. *Advances in Weed Science*, 40(spe1):e020220050.

OpenStreetMap contributors (2024). Planet dump retrieved from https://planet.osm.org.

Palladino, C., García, I., and Fernández, G. (2023). Pesticide dependence and associated risks in Uruguayan agriculture: limitations in its approach. *Agrociencia Uruguay*, 27:e1156.

Perestrelo, R., Silva, P., Porto-Figueira, P., Pereira, J. A., Silva, C., Medina, S., and Câmara, J. S. (2019). QuEChERS - Fundamentals, relevant improvements, applications and future trends. *Analytica Chimica Acta*, 1070:1–28.

Quast, C., Pruesse, E., Yilmaz, P., Gerken, J., Schweer, T., Yarza, P., Peplies, J., and Glöckner, F. O. (2012). The SILVA ribosomal RNA gene database project: improved data processing and web-based tools. *Nucleic Acids Research*, 41(D1):D590–D596.

Ramon, R. (2021). *Quantifying sediment source contributions in contrasted agricultural catchments (Uruguay River, Southern Brazil)*. PhD thesis, Universit{\'e} Paris-Saclay ; Universidade Federal do Rio Grande do Sul (Porto Alegre, Br{\'e}sil).

Rauh, V., Arunajadai, S., Horton, M., Perera, F., Hoepner, L., Barr, D. B., and Whyatt, R. (2011). Seven-Year Neurodevelopmental Scores and Prenatal Exposure to Chlorpyrifos, a Common Agricultural Pesticide. *Environmental Health Perspectives*, 119(8):1196–1201. Publisher: Environmental Health Perspectives.

Rodríguez-Bolaña, C., Pérez-Parada, A., Niell, S., Heinzen, H., and De Mello, F. T. (2024). Comparative deterministic and probabilistic approaches for assessing the aquatic ecological risk of pesticides in a mixed land use basin: A case study in Uruguay. *Science of The Total Environment*, 910:168704.

Röllin, S., Corcho-Alvarado, J. A., Sahli, H., Putyrskaya, V., and Klemt, E. (2022). High-resolution records of cesium, plutonium, americium, and uranium isotopes in sediment cores from Swiss lakes. *Environmental Science and Pollution Research*, 29(57):85777–85788.

Schoch, C. L., Ciufo, S., Domrachev, M., Hotton, C. L., Kannan, S., Khovanskaya, R., Leipe, D., Mcveigh, R., O'Neill, K., Robbertse, B., Sharma, S., Soussov, V., Sullivan, J. P., Sun, L., Turner, S., and Karsch-Mizrachi, I. (2020). NCBI Taxonomy: a comprehensive update on curation, resources and tools. *Database: The Journal of Biological Databases and Curation*, 2020:baaa062.

Souza, C. M., Z. Shimbo, J., Rosa, M. R., Parente, L. L., A. Alencar, A., Rudorff, B. F. T., Hasenack, H., Matsumoto, M., G. Ferreira, L., Souza-Filho, P. W. M., De Oliveira, S. W., Rocha, W. F., Fonseca, A. V., Marques, C. B., Diniz, C. G., Costa, D., Monteiro, D., Rosa, E. R., Vélez-Martin, E., Weber, E. J., Lenti, F. E. B., Paternost, F. F., Pareyn, F. G. C., Siqueira, J. V., Viera, J. L., Neto, L. C. F., Saraiva, M. M., Sales, M. H., Salgado, M. P. G., Vasconcelos, R., Galano, S., Mesquita, V. V., and Azevedo, T. (2020). Reconstructing Three Decades of Land Use and Land Cover Changes in Brazilian Biomes with Landsat Archive and Earth Engine. *Remote Sensing*, 12(17):2735.

Tales Tiecher (2015). *Fingerprinting sediment sources in agricultura catchments in Southern Brazil*. PhD thesis, Federal University of Rio Grande do Sul. Publisher: Unpublished.

United States Environmental Protection Agency (1995). metolachlor.pdf. Reregistration Eligibility Decision (RED) Metolachlor EPA 738-R-95-006, United States Environmental Protection Agency.

United States Environmental Protection Agency (2002). endosulfan_red.pdf. Reregistration Eligibility Decision (RED) Endosulfan EPA 738-R-02-013, United States Environmental Protection Agency.

Woodford, E. K. (1957). The Toxic Action of Herbicides. *Outlook on Agriculture*, 1(4):145–154.

Xu, S., Zhan, L., Tang, W., Wang, Q., Dai, Z., Zhou, L., Feng, T., Chen, M., Wu, T., Hu, E., and Yu, G. (2023). MicrobiotaProcess: A comprehensive R package for deep mining microbiome. *The Innovation*, 4(2):100388.

III

Small-scale variability in fallout radionuclide inventories and soil redistribution estimates in a cultivated catchment under contrasting management in Southernmost Brazil

Chapter 3

Small-scale variability in fallout radionuclide inventories and soil redistribution estimates in a cultivated catchment under contrasting management in Southernmost Brazil

Multiple studies were conducted on the Conceição river basin, in the Atlantic Forest biome, to assess the impact of no-tillage on soil redistribution at the scale of the plot Didoné et al. (2019); Tales Tiecher (2015). Chaboche (2021) tried to apply the same techniques they used at the scale of the entire river basin, with sampling designed based on compact strata analysis, the creation of geographic blocks on the studied area (using only the DEM). This second study showed that, while part of the variability of radionuclide inventories can be explained with multiple environmental covariates, uncertainties remained to explain the full variance of these inventories, also that compact strata sampling design did not account for the full covariates range.

Graphical abstract

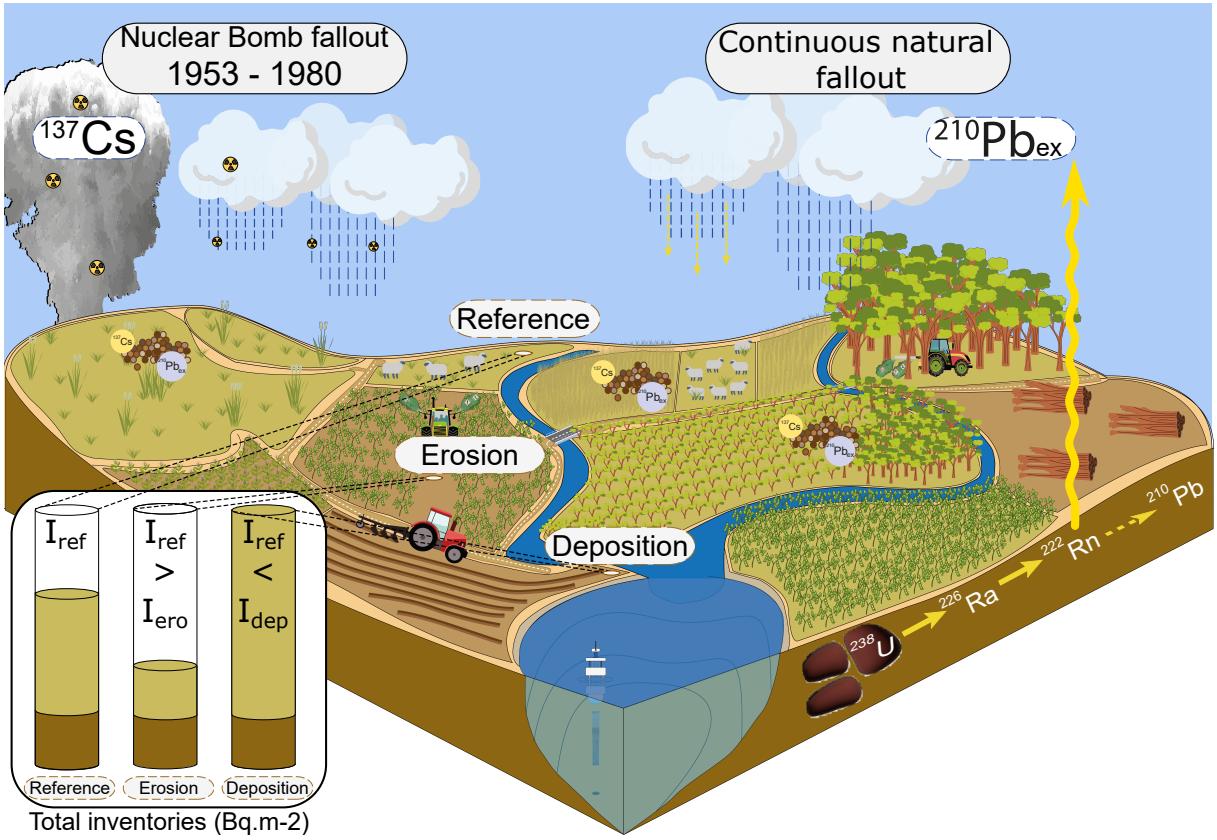

Amaury Bardelle[1], Pierre-Alexis Chaboche[1], Gerald Dicen[2], Fabio Schneider[3], Mirel Cabrera[4], Marcos Tassano[4,5], Jean Paolo Gomes Minella[6], Rosalie Vandrome[7], Anthony Foucher[1], Olivier Cerdan[7], Christine Alewell[1], Olivier Evrard[1]

[1]Laboratoire des Sciences du Climat et de l'Environnement (LSCE, IPSL), Université Paris-Saclay, UMR 8212 (CEA, CNRS, UVSQ),Gif-sur-Yvette,91190,France
[2]Environmental Geosciences, University of Basel, Basel, 4056, Switzerland
[3] Identité et différenciation de l'espace, de l'environnement et des sociétés (IDEES - UMR 6266), Université de Caen Normandie, France
[4]Laboratorio de Radioquímica, Área de Radiofarmacia, Centro de Investigaciones Nucleares. Facultad de Ciencias, Universidad de la República, Montevideo, Uruguay
[5]Instituto de Investigacion Una Salud, Universidad de la República, Montevideo, Uruguay
[6]Department of Soils, Universidade Federal de Santa Maria, Santa Maria, F-45060, Brazil
[7]Risk and Prevention Division, Bureau de Recherches Géologiques et Minières (BRGM), Orléans, F-45060, France

Abstract

Fallout radionuclide techniques are widely used to estimate soil redistribution during the last several decades. While it is known that results may vary depending on model choice and parametrisation and the reference profiles, the representativity of the sampled cores is often overlooked. This study applied a high-density sampling design within two 12 m $\times$ 12 m midslope plots in cultivated Brazilian hillslopes to assess small-scale variability in ^{137}Cs and ^{210}Pb$_{ex}$ inventories. The sites differed in agricultural management, with one hillslope under conventional tillage and the other under no-tillage since the 2000 with a history of ploughing and terracing. Results show a strong plot-scale variability, with neighbouring cores yielding contrasting inventories and redistribution estimates, particularly for ^{210}Pb$_{ex}$. Current farming practices appear to be the most important parameter influencing radionuclide depth distributions, although interpretation is complicated by a rather complex and undocumented history of land-use changes. Model choice also affected results: under conventional tillage, ^{137}Cs Proportional, Modern and RadeRo models agreed on the sign of redistribution (erosion or deposition) but provided variable values of redistribution magnitude, whereas under no-tillages practices, both magnitude and sign of redistribution varied among models. ^{210}Pb$_{ex}$ results under conventional tillage, are more heterogenous probably due to the tillage operations while under no-tillage practices, redistribution rates were lower and more homogeneous probably due to the compaction of the soils, increased runoff and decreased infiltration.

These findings indicate that isolated cores may not adequately represent soil redistribution at the hillslope scale in complex cultivated settings. Nevertheless, fallout radionuclide methods remain useful for identifying local patterns for decadal timescales. While robust hillslope-scale estimates would require denser sampling or composites, improved reference inventories, and explicit consideration of model uncertainty, this study highlights the possible use of ^{210}Pb$_{ex}$ for recent analysis of the impact of agricultural practices on soil quality and redistribution.

3.1 . Introduction

Soils are fundamental for human societies, providing the foundation for food production, water regulation and nutrient cycles, as well as for supporting biodiversity (FAO & ITPS 2015). Their degradation poses serious risks to food security and ecosystem services, with soil erosion representing one of the most pressing threats. Erosion can remove the fertile topsoil layer far faster than it can be naturally regenerated under conventional intensive agriculture (Montgomery 2007), reducing agricultural productivity, and contributing to carbon losses and accelerating sedimentation in lower landscape positions and river systems. Recent studies highlighted that unsustainable land use and intensive farming practices are accelerating these processes worldwide, threatening the long-term capacity of soils to sustain human needs (Pimentel and Burgess 2013; Amundson et al. 2015).

Developing effective soil conservation strategies requires a robust quantification of soil erosion rates. Multiple methods were developed at different spatial and temporal scales to quantify soil erosion through direct field-based measurements of runoff and sediment transport; such as with erosion plots or sediment traps (Hudson 1993; Morgan 2006), fallout radionuclides (Walling et al. 1993; Walling and He 1999; Mabit et al. 2008); or empirical and process-based erosion models. Among these, the Universal Soil Loss Equation and its revised versions remain among the most widely used empirical approaches for estimating sheet and rill erosion (Wischmeier, W. H. and Smith, O.D. 1978; Renard, K. G. et al. 1997), but other models exist such as WEPP, LISEM or WaterSed (https://watersed.fr/) providing more explicitly process-based representations of runoff generation, sediment detachment, transport, and deposition (Nearing et al. 1989; De Roo et al. 1996; Merritt et al. 2003).

Since their formalisation in the early 1990s through the development of multiple methods relying on fallout radionuclide analyses such as profile distribution (estimation of soil erosion or deposition by comparing the shape and depth distribution of a fallout radionuclide profile with an undisturbed reference profile) or mass balance (estimation of soil redistribution by comparing the total fallout radionuclide inventory at a site with a reference inventory while accounting for inputs, decay, mixing, and losses or gains through time), have been widely applied across agricultural and natural landscapes worldwide (Walling and Quine 1992; XINBAO et al. 1990; Walling and He 1999; Ritchie and Ritchie 2008). Their popularity stems from their ability to estimate spatially-distributed, pluri-decadal soil redistribution rates (including both erosion and accumulation), without the need for continuous monitoring. This makes them particularly valuable for validating erosion models and assessing land-use impacts at the hillslope or at the catchment scale(Porto et al. 2009). Fallout radionuclide (FRN) inventory techniques have become standard methods for quantifying soil erosion and sediment redistribution for timescales ranging from the mid-1950s until present (Cabrera et al. 2023), overcoming key limitations of traditional plot or outlet-based measurements that often fail to capture spatial variability and long-term dynamics of soil redistribution (IAEA 2014). FNRs are generally divided into naturally occurring radionuclides, such as $^{210}Pb_{ex}$ ($t_{1/2}$ =

22.3 years) and ^{7}Be ($t_{1/2}$ = 53,22 days), falling continuously with precipitation onto the soil and artificial radionuclides such as $^{239+240}Pu$ (respectively $t_{1/2}$ = 24,110 and 6561 years) and ^{137}Cs ($t_{1/2}$ = 30 years) that were emitted into this environment during atmospheric nuclear bomb testing (1954-1980). Based on this difference in emission period, natural and artificial radionuclides may be used to reconstruct erosion for different timescales (Cabrera et al. 2023). Indeed, while $^{210}Pb_{ex}$ has longer time window than ^{137}Cs (the past 50–60 years for ^{137}Cs and up to 100 years for $^{210}Pb_{ex}$), these radionuclides have contrasting sensitive behaviours, with $^{210}Pb_{ex}$ being more sensitive to recent redistribution events (of its last period of disintegration, 22.3 yr) than 137Cs, being more sensitive to the past erosion and depositional events (Cabrera et al. 2023)). Nevertheless, the application of FRN techniques relies on multiple assumptions regarding the spatially uniform character of initial fallout deposition, the selection and representativeness of undisturbed reference sites, and the effects of tillage-induced mixing or bioturbation on radionuclide depth profiles. All of these assumptions have been the subject of sustained methodological debate (Parsons and Foster 2013, 2011; Mabit et al. 2013).

Early applications demonstrated the potential of FRN techniques as a sediment tracer for estimating long-term soil loss (IAEA 2014), leading to the development of two broad classes of conversion models. Empirical models establish regression relationships between observed soil loss rates and relative radionuclide inventory depletion (Elliott et al. 1990), whereas theoretical models are based on mass-balance principles that describe the conservation and redistribution of ^{137}Cs under simplified representations of erosion and sediment transport processes (Brown et al. 1981; Walling and Quine 1992; Walling and He 1999). Most theoretical approaches rely on three key assumptions: (1) the spatially uniform character of initial fallout deposition, (2) the rapid and irreversible adsorption of ^{137}Cs to soil constituents, and (3) a redistribution that is driven exclusively by soil movement. However, these assumptions have been increasingly questioned (Parsons and Foster 2011). Experimental and field studies have shown that ^{137}Cs transfer from rainfall to the soil can be spatially heterogeneous due to vegetation interception, micro-topography, infiltration variability, and the preferential removal of radionuclides by suspended sediment during runoff events (Parsons and Foster 2011; Zhang 2015, 2023). Such processes may partly violate the preliminary hypothesis of spatially homogeneous initial inventories and can lead to a substantial overestimation of erosion rates when ignored, with theoretical models overpredicting long-term soil loss by several hundreds of percent in some catchments (Zhang 2023). In parallel, numerous studies have highlighted a large spatial variability in reference and sampling site inventories, showing typically high coefficients of variation (Sutherland (1996) found median coefficient of variation of about 20% in numerous studies for references sites), yet this variability associated with sampling design and model application has often been overlooked (Parsons and Foster 2011). Recent methodological advances have therefore emphasised the need to conduct statistically robust sampling strategies, the interest to analyse replicates beyond spatial correlation distances and to propagate uncertainties, and the use of

improved mass-balance models that explicitly take into account potential radionuclide losses during transfer (Mabit et al. 2013; Zhang et al. 2019; Zhang 2023; Evrard et al. 2020). While these developments reinforced the trust in FRN techniques as powerful tools for reconstructing long-term soil redistribution, there is a clear need to better understand the spatial representativeness, the processes and uncertainties associated with these techniques.

To address the question of sampling representativity, two erosion sites were selected along hillslopes cultivated under contrasting farming practices within the Conceição catchment, an intensively cultivated basin of approximately 800 km^2 in Rio Grande do Sul, in the southernmost State of Brazil. Erosion and sediment transfers in this catchment have been previously investigated, providing a valuable framework for examining soil redistribution at finer spatial scales (Didoné et al. 2014, 2021, 2019).

Overall, the objectives of this study were threefold : 1) characterise the spatial representativeness of cores collected in a close vicinity for both ^{137}Cs and $^{210}Pb_{ex}$ inventories along two agricultural hillslopes, 2) evaluate the effect of conventional and no-tillage agricultural practices on ^{137}Cs and $^{210}Pb_{ex}$ spatial and/or depth variability, and 3) conduct a sensitivity analysis to quantify the impact of such variability on erosion models outputs. The implications of these results for future FRN-based applications deployed to quantify soil redistribution during the last several decades will then be discussed.

3.2 . Materials and Methods

3.2.1 . Conceição river basin

The Conceição River basin is located on the southern plateau of Rio Grande do Sul, covering an area of approximately 804.3 km^2. The soils found in the area are mainly Ferrasols (80%) although Nitisols (18%) and Acrisols (2%) can also be found. Altitudes range from 270 to 480 m, and the terrain consists of gentle slopes (9%) at the highest points of the basin and moderate to steep slopes near the river and drainage channels (up to a maximum of 20%). The land is primarily used for cropland and is mainly cultivated with soybeans (*Glycine max*) under a no-tillage system in summer. During winter, wheat (*Triticum aestivum*), oats (*Avena sativa* and *Avena strigosa*) and ryegrass (*Lolium multiflorum*) are cultivated for grain production, as feed for dairy cattle or as a cover crop (Ramon 2021), (Figure 3.1).

Studied hillslopes The characteristics of the two hillslopes were described by Didoné et al. (2019). Both hillslopes (hillslope 1, H1 and hillslope 2, H2, **A** and **B** in Figure 3.1 respectively) are composed of Ferralsols, and are respectively 100 and 260 m long with respective slope gradients of 13.8 and 11.4%. The two hillslopes were initially covered by native forests and progressively deforested in the 1960s (Didoné et al. 2019). H1 was managed under conventional tillage (ploughed once every one to two years, depending on the crop grown) until nowadays with ploughing depth of 20 cm. H2 was managed under conventional tillage as H1 until 1980 and transitioned to the no-tillage system (5 cm chiselling once

a year) with terraces until 1990 and devoid of terraces since then and until 2023 when the cores were collected.

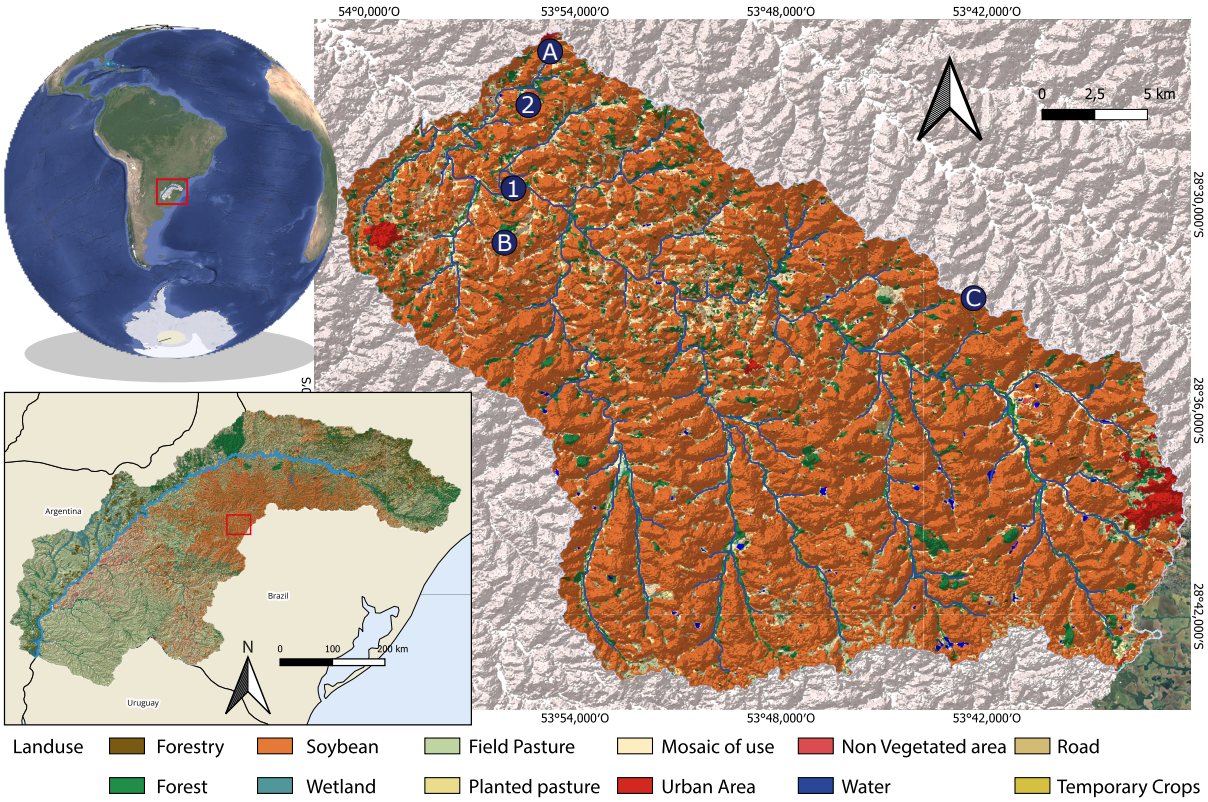

Figure 3.1: **Conceição river basin**, localisation in South America and general location of the sampling sites **H1 - Conventional tillage** and **H2 - No tillage** along with reference sites sampled **A,B and C**. Map of land-uses and covers in 2022 (from Mapbiomas Brazil), background map from OpenStreetMap and Google Imagerie, NASA

3.2.2 . Methodology

Sample collection

Samples were collected using a Cobra TT vibro-corer equipped with a 1 m long, 50 mm diameter PVC liner as well as manual corer equipped with a 50 cm long, 50 mm diameter PVC liner, following the spatial pattern illustrated in figure 3.2. The two hillslopes were selected and sampled at the same locations as those sampled by Didoné et al. (2017) in 2016 using their GPS coordinates. In total, 26 soil cores were collected, including 13 cores in the middle portion of each slope, located systematically 2 meters apart from each other following a grid pattern as described in figure 3.2. This sampling strategy was also constrained by the DEM resolution (12.5m), which represents the best resolution available to date in this area, with the objective to quantify the variability of $^{210}Pb_{ex}$ and ^{137}Cs inventories within one DEM grid cell.

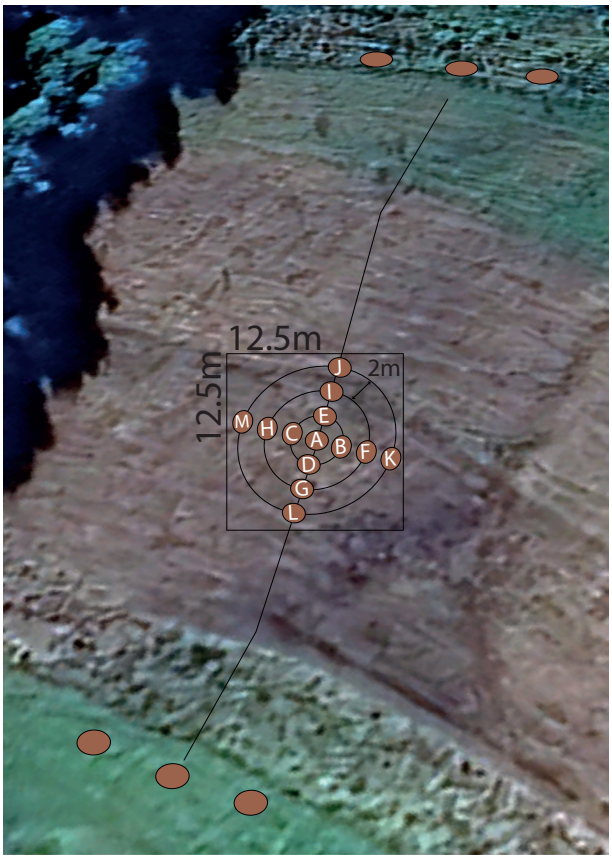

Figure 3.2: **Concept of the sampling strategy** with the example of hillslope **A**

Analyses

The cores were opened and sampled following depth, collecting increments every 5 cm. The subsamples were oven-dried at 40° during at least 24 h, grounded, sieved to 2 mm and weighted before and after drying to measure the density (the sieved particles exceeding 2 mm in size were also weighted before being removed).

3.2.3 . Density

The density of each layer of each core was calculated independently following equation Eq. 3.1.

$$\text{Dry bulk density}_{layer\ x}(\text{kg m}^{-3}) = \frac{\text{Dry weight of the section (kg)}_{layer\ x}}{\pi.\text{core radius}^2(\text{m}^2).\text{Sampling rate(m)}} \tag{3.1}$$

3.2.4 . Gamma spectrometry analyses

Once dried, samples were placed in polyethylene boxes with a standardised geometry, and weighted. Gamma spectrometry measurements were conducted using coaxial HPGe detectors (Mirion/Ortec®), which are available at the Laboratoire des Sciences du Climat et de l'Environnement (Gif-sur-Yvette, France). The activities of lead-210 in excess ($^{210}Pb_{ex}$) were calculated by subtracting the activities of two Radium-226 daughters, Lead-214 (average count at 295.2 and 351.9 keV) and Bismuth-214 (609.3

keV), from the total ^{210}Pb activities detected at 46.5 keV. ^{137}Cs activities were measured at 661.7 keV. All the activities were decay-corrected to the sampling date (i.e. 22/06/2024 for H1 and 14/06/2024 for H2).

All measurements were corrected for background levels determined every two months and for detector and geometry efficiencies. Furthermore, uncertainties associated with sample mass measurements were propagated to the final activity uncertainties. An additional relative uncertainty of 5% was included for all radionuclide activity estimates to account for potential matrix effects, including photo self-attenuation within the samples.

Quality assurance was ensured through the regular analysis of certified reference materials issued by the International Atomic Energy Agency (https://analytical-reference-materials.iaea.org/radionuclides), measured under the same analysis geometry, sample preparation and analytical workflow as the investigated samples. The reference materials analysed for calibration and quality assurance included are detailed in 3.6.1.

Inventories of $^{210}Pb_{ex}$ and ^{137}Cs were calculated following equation 3.2

$$\text{Inventory } (\text{Bq.m}^{-2}) = \text{ Radionuclide activity } (\text{Bq.kg}^{-1}).\text{Dry bulk density } (\text{kg.m}^{-3}).\text{Depth increment}(\text{m}) \tag{3.2}$$

3.2.5 . Soil redistribution rate calculation

The rates of redistribution were calculated for each core and hillslope using three approaches: the proportional model, a commonly used linear model (Zhang 2023); the MODERN model (Modelling Deposition and Erosion rates with RadioNuclides), which accounts for the depth distribution of fallout radionuclides (FRNs) at the reference site and can be adapted to site-specific conditions (Arata et al. 2016); and the RadEro model (Catalá et al. 2025). The MODERN and RadEro models were implemented using the freely available R packages `modeRn` and `RadEro`, respectively. Proportional and MODERN models were applied for both ^{137}Cs and $^{210}Pb_{ex}$ whereas Radero model was applied for ^{137}Cs only.

The proportional model was applied by implementing the following equation 3.3:

$$Y \ \left(\text{t.ha}^{-1}.\text{yr}^{-1}\right) = -10\frac{B_d D_L X}{100TP} \tag{3.3}$$

where Y is the soil redistribution rate in $t.ha^{-1}.yr^{-1}$, B_d is the mean soil bulk density (kg.m^{-3}), D_L is the mean tillage depth (m), T is the time elapsed since the onset of ^{137}Cs fallout or tillage, and P is the particle-size correction factor, expressed as the ratio between the ^{137}Cs activity of mobilised sediment and that of the original soil. The term X represents the relative change in ^{137}Cs inventory compared with the reference inventory and was calculated as:

$$X = 100\frac{A_{\text{ref}} - A}{A_{\text{ref}}} \tag{3.4}$$

where A_{ref} is the reference inventory and A is the inventory measured at the sampling point. Positive values of X indicate a depletion of the inventory relative to the reference site, whereas negative values reflect inventory enrichment. In this study, P was set to 1 for both hillslopes.

Three reference sites with 3 replicates each time were sampled in this study (figure 3.1, **A, B & C**). As demonstrated by Cabrera et al. (2023) since both ^{137}Cs and $^{210}Pb_{ex}$ have different periods of fall-out and deposition, a distinction was made between both radionuclides to verify the relevance of the reference profiles. In fact, ^{137}Cs was deposited during the main nuclear fallout (i.e. from the global detection in 1953 to the peak of maximum fallout in the Southern Hemisphere in 1964–1965) while $^{210}Pb_{ex}$ is deposited continuously. Accordingly, a ^{137}Cs undisturbed reference profile should also represent a $^{210}Pb_{ex}$ undisturbed reference profile. However, the contrary may not be true as true as the disturbance might have taken place prior to the $^{210}Pb_{ex}$ deposition. Furthermore, the reference sites were selected based on the landscape position (a flat site with no obvious disturbances) and selected after their gamma spectrometry analysis based on depth-distribution criteria (the profile must be undisturbed, with most of the fallout radionuclide inventory concentrated in the first few centimetres of the soil and show a rapid decrease with depth)

3.3 . Results and Discussion

3.3.1 . Reference sites and modelling settings

^{137}Cs ranged between 340 and 775 $Bq.m^{-2}$ with standard deviation of 149 $Bq.m^{-2}$ in the reference sites with mean and median of 514 and 498 $Bq.m^{-2}$ and avariation coefficient of 29.0%. While at reference site 1 (Figure 3.1), cores A, B and C showed the expected reference profile with accumulation in the upper 5 to 15 cm (Figure 3.3), at reference sites 2 and 3, cores A, B and C appeared to be disturbed, with a maximum inventory found in deeper layers (10-25 cm), which likely indicates the occurrence of deposition. Accordingly, this profile was found not to be representative of an undisturbed fallout accumulation profile. Therefore, only the cores A, B and C at site 1 were considered as a reference for ^{137}Cs for the remainder of the study, with mean and median of 382.4 and 385.5 with standard deviation of 40.6 and a variation coefficient of 10.6%.

Nevertheless, these reference values remain in the range of the inventories found by Didoné et al. (2019) at the same reference site 1 (327.1 ± 62.4 $Bq.m^{-2}$, decay-corrected to the sampling date of this study following equation 3.7). They validated this reference site based on those of another study conducted 200 km away showing very similar total inventories of 315± 22.25 (Minella et al. 2014). No major controls (e.g., strong precipitation gradients or orographic effects) are expected to significantly influence the spatial pattern of 137Cs fallout in this area (Didoné et al. 2019). As a comparison, these results also fall in the same range as the reference found by Tassano et al. (2025), with values between 357.8 and 365.4 $Bq.m^{-2}$ across Uruguay (from approximately 350 to 750 km away from this study's reference

sites). These studies therefore allow to validate this study's selected reference sites at the local (Didoné et al. 2019) and regional scales (Minella et al. 2014; Tassano et al. 2025).

As for $^{210}Pb_{ex}$, total inventory values ranged between 4 008 and 11 725 $\pm$ 1 363 $Bq.m^{-2}$ at the reference sites with mean and median of 7 716 and 7 353 $Bq.m^{-2}$ and a variation coefficient of 31.7% (Figure 3.3). For $^{210}Pb_{ex}$, first the same cores selected for ^{137}Cs were retained, then core 3 from reference site B, and core 1 from reference site C were considered undisturbed profiles and retained. Reference sites B cores 1 and 2 and reference sites C, cores 2 and 3 appeared to be disturbed, with a maximum inventory found either in deeper layers (10-25 cm) or 2 to 3 times the maximum inventories found in the other cores, which likely indicates the occurrence of deposition. Accordingly, these profiles were found not to be representative of an undisturbed fallout accumulation profile. Selected reference sites ranged between 4 008 and 7 353 $Bq.m^{-2}$ with mean and median of 5 997 and 6 511 $Bq.m^{-2}$, standard deviation of 1 363 $Bq.m^{-2}$ and coefficient of variation of 22.7%

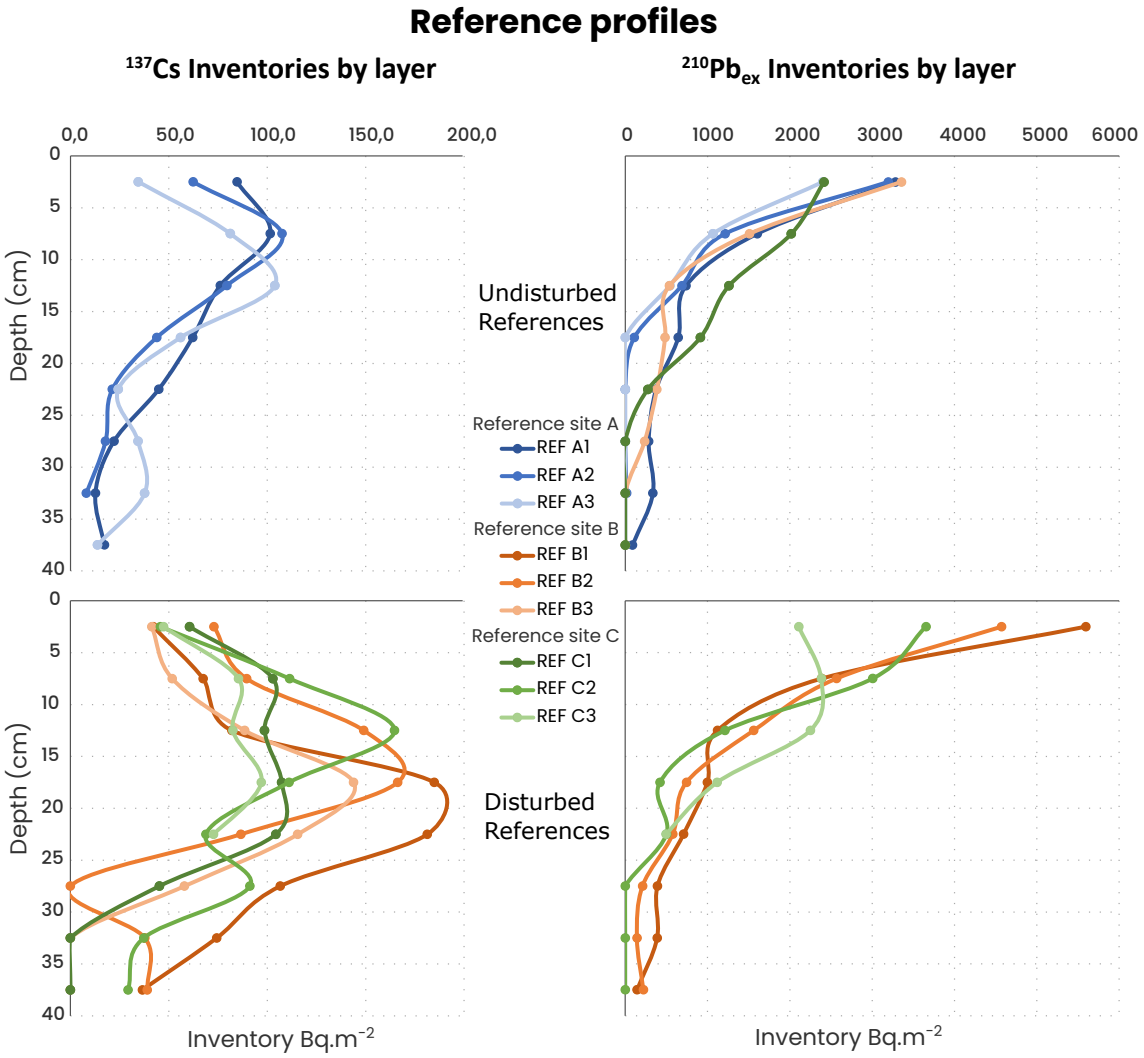

Figure 3.3: Depth profiles of ^{137}Cs and $^{210}Pb_{ex}$ inventories at the three references sites, with - in the upper panels - the undisturbed references selected for soil redistribution modelling and - in the lower panels - the disturbed references that were not retained for further analysis

For the proportional and RadEro models, only the total mean reference inventory (the sum of the inventory found for each layer) is used. Therefore, the reference inventory was calculated using cores from reference site A from the present study together with published reference inventories from Didoné et al. (2019) and Minella et al. (2014). This approach increased the number of available reference inventories while retaining sites considered to be comparable to the present study area and provided a final mean total inventory of 358.0 $Bq.m^{-2}$ associated with a variation coefficient of 12.3%.

For RadEro, a Southern Hemisphere ^{137}Cs fallout chronicle was approximated from the Health and Safety Laboratory (1977) report and adapted to the local conditions based on the selected reference inventories. Because relatively few monitoring stations were operational in the Southern Hemisphere before 1960, part of the early ^{137}Cs fallout record was not directly measured. ^{137}Cs fallout was therefore estimated from ^{90}Sr records from the Buenos Aires station ((Health and Safety Laboratory 1977), the closest to the studied region) by assuming a ^{137}Cs/^{90}Sr fission yield ratio of 1.5 (United Nations Scientific Committee on the Effects of Atomic Radiation 2000). The fallout chronicle was first normalized by calculating the relative contribution of each year to the total fallout. These relative contributions were then used to distribute the local reference inventory across time, with decay corrections applied to each year. This assumption and local corrections allowed the construction of a continuous fallout input function for the RadEro simulations, although it also represents a source of uncertainty. Indeed, the ^{137}Cs/^{90}Sr ratio may vary spatially and temporally (Sherrill et al. 1975). As a result, the reconstructed early ^{137}Cs fallout chronicle should be interpreted as an approximation rather than a directly measured record as part of the fallout was not recorded (from 1952/3 to 1959 and from 1977 to 1982) and the station used is located 800 km from the studied region. These uncertainties are particularly relevant for the oldest part of the fallout record (1952-1959) and may affect RadEro-derived redistribution rates.

For MODERN, only the reference cores mentioned above (reference site A cores 1, 2, 3 for ^{137}Cs and reference site A cores 1, 2, 3, reference site B core 3 and reference site C core 1 for $^{210}Pb_{ex}$) from the current research were used because the model requires a depth-resolved reference profile and the previous studies had different depth increments. For both radionuclides, the reference depth profile was built within the MODERN package. Two smoothing layers were added at the base of the profile to represent possible downward redistribution by migration, diffusion processes or bioturbation (references). Depositional layers were also added using the package functionality to take into account possible areas of deposition along the hillslopes. For both radionuclides, the values of deposition were assessed from the reference sites that showed clear signs of deposition. For ^{137}Cs, an initial MODERN simulation was performed for H1 using the 'ploughed' reference profile, with ploughing parametrised over the upper 0.20 m. However, this configuration produced mostly unresolved outputs, including `NA` values or multiple possible solutions for multiple cores. These outputs prevented a consistent interpretation of redistribution rates across H1. Therefore, the final MODERN simulations for H1 were performed using the

non-ploughed reference profile, which provided more stable and interpretable model results. In contrast, for the $^{210}Pb_{ex}$ modelling with MODERN and the proportional models, tillage depths of 0.20 m for H1 and 0.05 m for H2 were retained, which were consistent with the local farmers practices.

3.3.2 . Hillslopes

$^{210}Pb_{ex}$ inventories

$^{210}Pb_{ex}$ inventories ranged between 2 361 and 15 822 $\pm$ 3 233 $Bq.m^{-2}$ for hillslope H1 with mean and median values of 7 004 and 6 670 $Bq.m^{-2}$. In contrast, $^{210}Pb_{ex}$ inventories were slightly lower and ranged from 2 292 to 12 351 $\pm$ 2 635 $Bq.m^{-2}$ for hillslope H2 with mean and median values of 4 635 and 4 010 $Bq.m^{-2}$ respectively. Both hillslopes show a much higher variability than those found at the reference sites with variation coefficients of 46.4 and 56.8% in H1 and H2, respectively.

The detection depths of $^{210}Pb_{ex}$ varied depending on farming practices and were found from 30 cm to the top of the core in H1 and from 15 cm in H2 . H1 profiles show a decreasing trend of $^{210}Pb_{ex}$ from 20 to 30 cm while H2 shows an enrichment of the top-layer from 0 to 5 cm and then a decrease down to 10 - 15 cm.

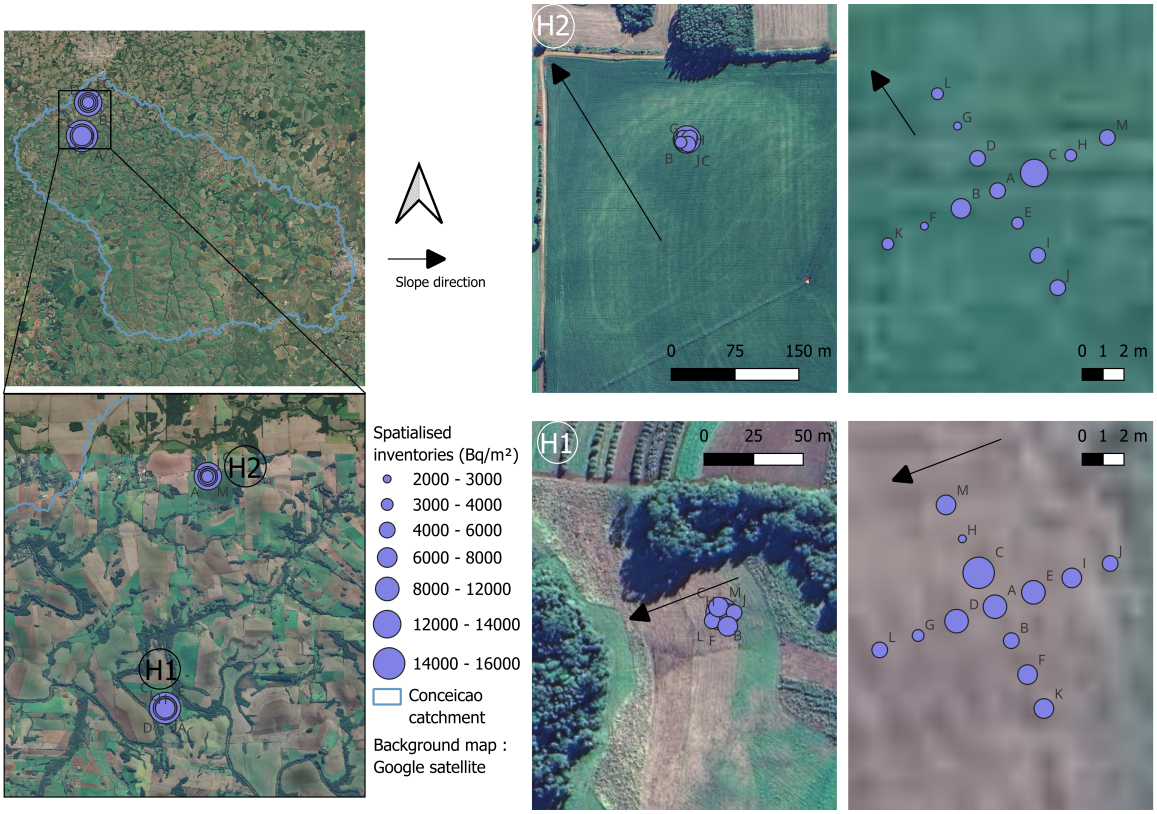

Figure 3.4: Spatialised $^{210}Pb_{ex}$ inventories for hillslopes 1 and 2 in the Conceicão catchment. The left-hand maps show the location of the hillslopes within the catchment and the right-hand panels show the spatial distribution of measured inventories at the sampling locations. Circles represent total $^{210}Pb_{ex}$ inventories, with their size corresponding to the inventory classes shown in the legend ($Bq.m^{-2}$). Background imagery is from Google Satellite.

^{137}Cs inventories

^{137}Cs inventories ranged between 88 and 499 $\pm$ 132 $Bq.m^{-2}$ in hillslope H1 with mean and median of 205 and 143 $Bq.m^{-2}$ while ^{137}Cs inventories were lower and ranged from 37 to 349 $\pm$ 76 $Bq.m^{-2}$ in hillslope H2 with mean and median of 153 and 135 $Bq.m^{-2}$, respectively.

Mean inventories in both hillslopes are comparable with those inventories found by (Didoné et al. 2019) with mean ^{137}Cs inventories of 138 and 253 $Bq.m^{-2}$ after decay-correction (205 and 152 $Bq.m^{-2}$ in this study) respectively for H1 and H2.

As for $^{210}Pb_{ex}$, both hillslopes show a high variability of ^{137}Cs inventories with variation coefficients of 64.2 % and 49.7 % in H1 and H2, respectively. ^{137}Cs was detected from a depth of 30 cm to the top of the core in H1 and from 20 cm depth in H2. Except for two reversed profiles in H1 (H1-C and -D) probably from tillage operations and a slight enrichment of ^{137}Cs in the layer from 5 to 10 cm depth, profiles of both hillslopes show a homogeneous distribution of ^{137}Cs.

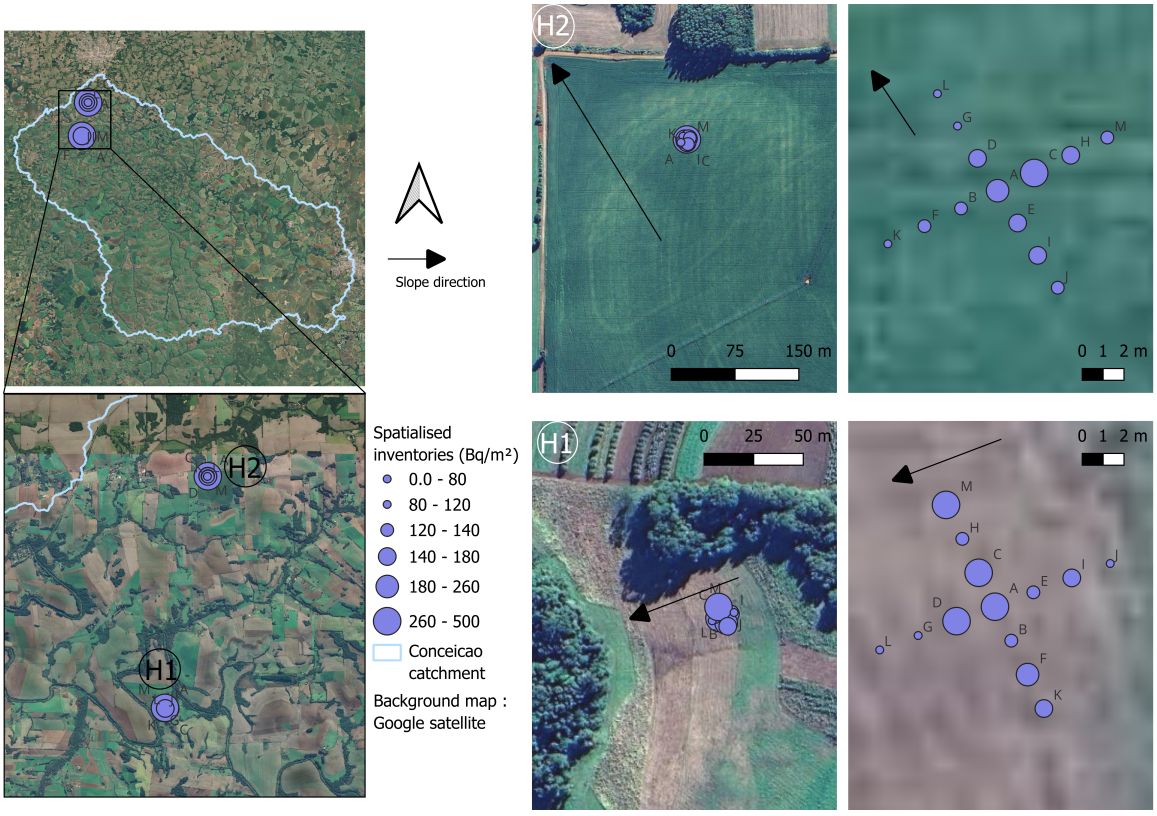

Figure 3.5: Spatialised ^{137}Cs inventories for hillslopes 1 and 2 in the Conceicão catchment The left-hand maps show the location of the hillslopes within the catchment and the right-hand panels show the spatial distribution of measured inventories at the sampling locations. Circles represent total ^{137}Cs inventories, with their size corresponding to the inventory classes shown in the legend ($Bq.m^{-2}$). Background imagery is from Google Satellite.

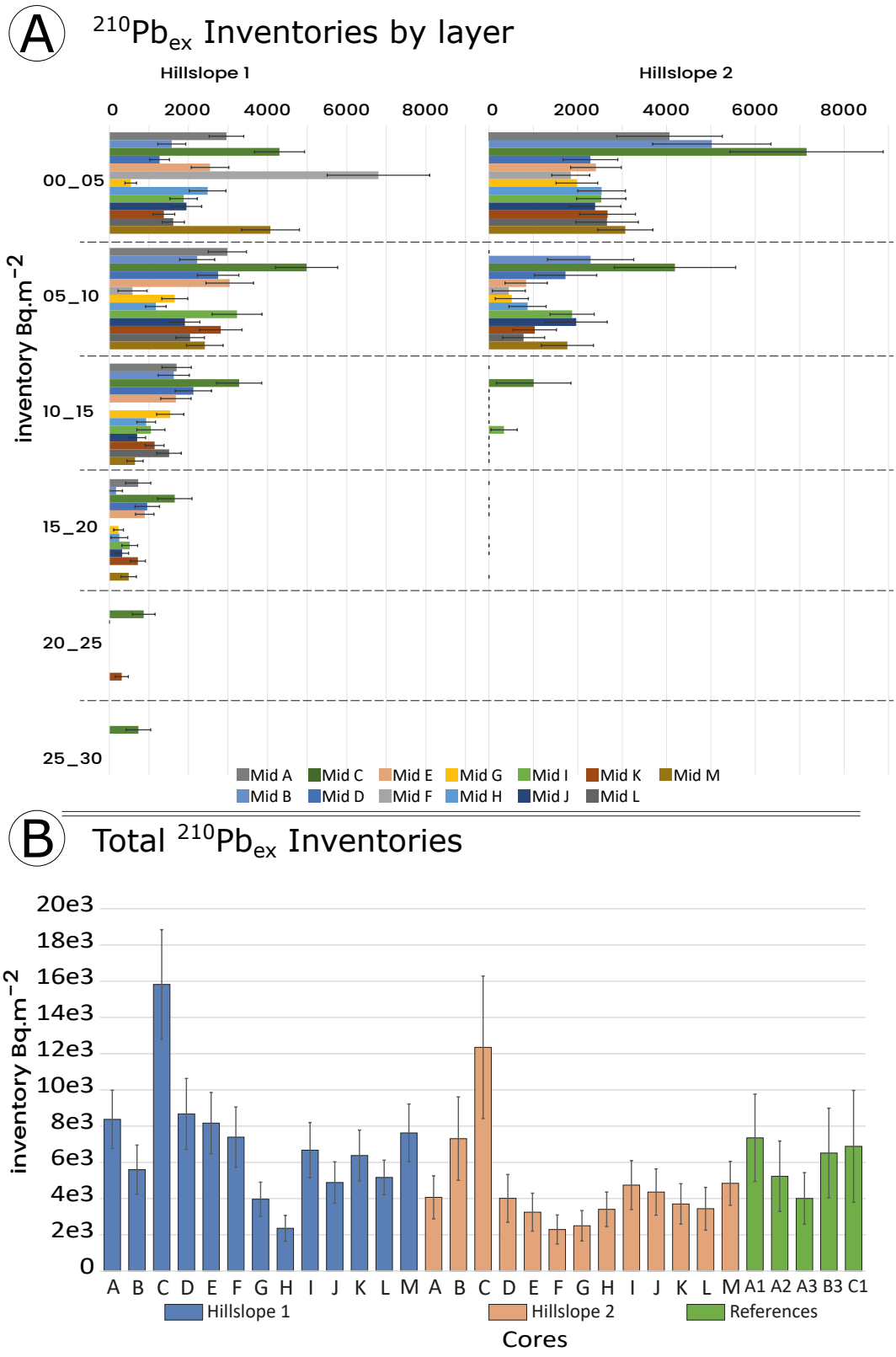

Figure 3.6: Results of $^{210}Pb_{ex}$ inventories in $Bq.m^{-2}$. Inventories for each hillslope and for each depth increment in panel **A** and total inventory for each core and for each hillslope along with total reference inventories given in panel **B**

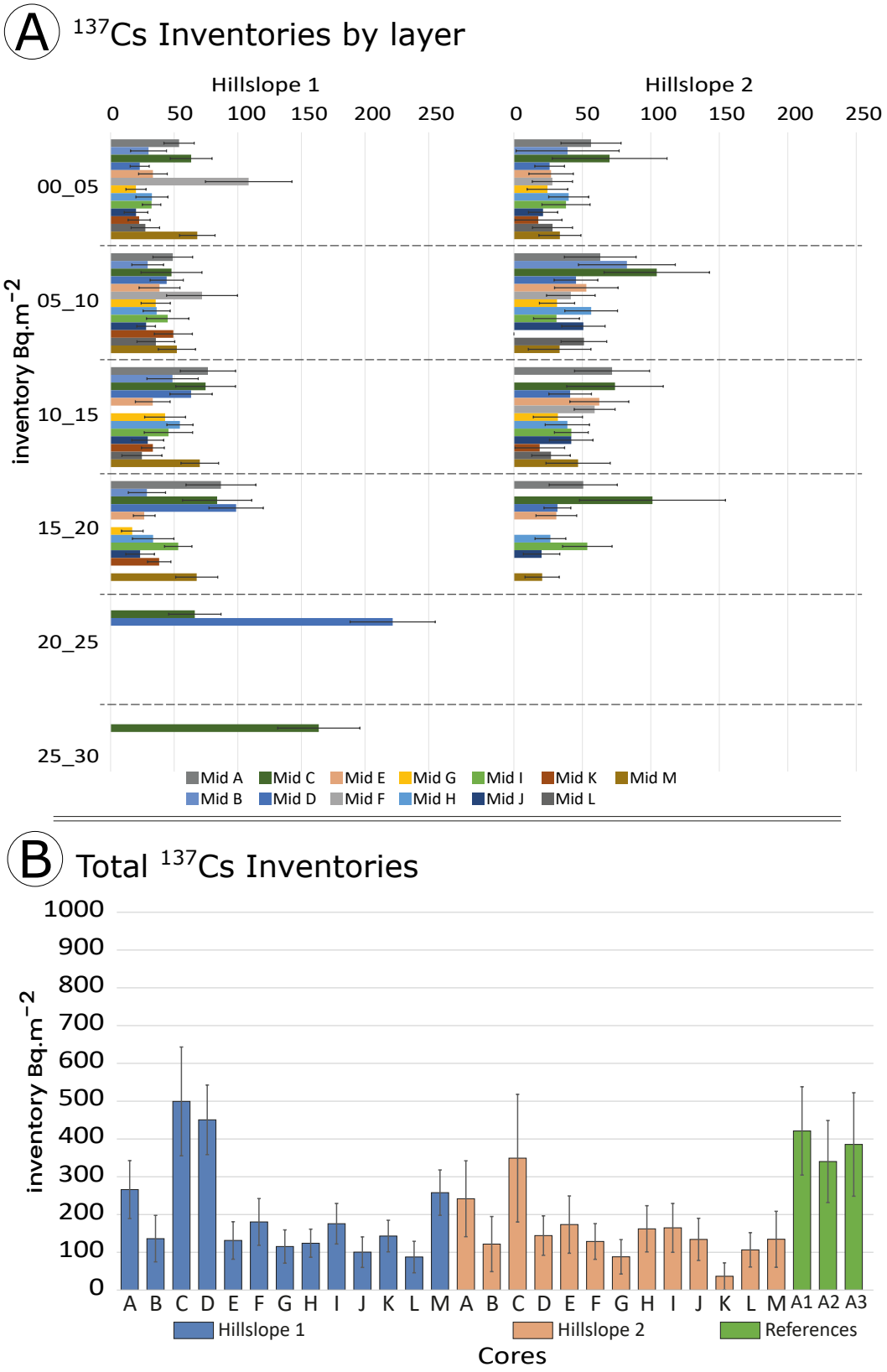

Figure 3.7: Results of ^{137}Cs inventories in $Bq.m^{-2}$. Inventories for each hillslope and for each depth increment in panel **A** and total inventory for each core and for each hillslope along with total reference inventories given in panel **B**

3.3.3 . Soil redistribution modelling

For both hillslopes, the soil cores were collected in midslope areas within a zone of 12 m $\times$ 12 m. The results therefore represent small-scale spatial variability around these midslope positions. The results show significant variability in modelled soil redistribution rates for each midslope area. This variability was found both between neighbouring cores and between conversion models applied to the same radionuclide inventory. The MODERN reference profile constructed in the package is given in supplementary material (annexes figure 3.1 & 3.2)

Redistribution rates estimated with $^{210}Pb_{ex}$ inventories

For H1, the $^{210}Pb_{ex}$ proportional model produced both positive and negative redistribution estimations, ranging from approximately -25.6 to 96.0 $t.ha^{-1}.yr^{-1}$ (Figure 3.8 I & II). Positive values were obtained for cores A, C, D, E, F, I, K, and M, whereas negative values were obtained for cores B, G, H, J, and L. The highest positive value was observed for core A, while the most negative value was found for core H.

The $^{210}Pb_{ex}$ MODERN model produced a wider range of values for H1, from approximately -107.8 to 87.1 $t.ha^{-1}.yr^{-1}$ (Figure 3.8 II). Strong negative values were estimated for cores B, D, G, H, J and K, whereas positive values were obtained for cores A, C, E, F, I, L, and M (Figure 3.8 I). The highest positive value was obtained for core F, while the lowest negative value was found for core H. Compared with the proportional model, MODERN amplified the contrasts between cores, especially for the most negative estimates.

For H2, the $^{210}Pb_{ex}$ proportional model yielded mostly negative values, ranging from approximately -5.8 to 15.3 $t.ha^{-1}.yr^{-1}$ (Figure 3.8 I & II). Most cores showed low negative redistribution estimates, while core B and C showed a clear positive value.

The $^{210}Pb_{ex}$ MODERN modelling for H2 produced a broader range of values than the proportional model, from approximately -28.7 to 32.0 $t.ha^{-1}.yr^{-1}$ (Figure 3.8 II). Positive values were obtained for cores A, B, C and M, whereas negative values were obtained for cores D to L (Figure 3.8 I). The highest positive value was obtained for core C, while the most negative value was found for core G. As for H1, the MODERN model showed higher magnitude and contrasted redistribution estimates than the proportional model.

Redistribution rates estimated with ^{137}Cs inventories

For H1, with ^{137}Cs, the three models yielded the same general pattern in terms of the sign of redistribution, with all cores showing negative redistribution rates except for cores C and D, for which all three models indicate positive redistribution rates suggesting that for the H1 midslope area results were not affected by the choice of conversion model (Figure 3.8 I). However, the magnitude of redistribution between models was significantly different. The proportional model provided values ranging from approximately

-41.4 to 23.2 $t.ha^{-1}.yr^{-1}$, the MODERN model generated estimates from approximately -86.7 to 25.6 $t.ha^{-1}.yr^{-1}$, and the Radero model provided results from -13.7 to 13.9 $t.ha^{-1}.yr^{-1}$ (Figure 3.8 II). The MODERN model generally produced the highest absolute values, whereas Radero provided more moderate estimates.

For H2, the ^{137}Cs proportional model produced negative estimates for all cores, ranging from approximately -8.6 to -0.35 $t.ha^{-1}.yr^{-1}$ (Figure 3.8 I). The values were less negative than those obtained for H1, showing weaker apparent inventory depletion in the H2 midslope plot using this model (Figure 3.8 II).

The ^{137}Cs MODERN modeling for H2 produced both positive and negative values, ranging from approximately -134.8 to 23.9 $t.ha^{-1}.yr^{-1}$ (Figure 3.8 I & II). All other cores showed negative values except core B, which showed a positive redistribution estimate. This model therefore indicates stronger spatial contrasts across H2 than the proportional ^{137}Cs model, with one locally positive estimate occurring within an otherwise negative redistribution pattern.

The Radero model for H2 produced only negative values, ranging from approximately -38.2 to -20.7 $t.ha^{-1}.yr^{-1}$ (Figure 3.8 I & II). As for the proportional model, these values showed a consistent negative redistribution signal across the H2 midslope area.

Because Hillslopes I and II in Didoné et al. (2019) correspond to H1 and H2 in the present study, their ^{137}Cs MBM-2 results can be compared directly. For H1, Didoné et al. (2019) reported erosion rates of -28 ± 7 $t.ha^{-1}.yr^{-1}$ (Mg.ha^{-1}.yr^{-1}, equivalent to $t.ha^{-1}.yr^{-1}$) at the summit and -57 ± 15 $t.ha^{-1}.yr^{-1}$ at the backslope, with deposition of 201 ± 2 $t.ha^{-1}.yr^{-1}$ at the toeslope. For H2, they reported lower erosion rates of -25 ± 8 and -18 ± 16 $t.ha^{-1}.yr^{-1}$ at the summit and backslope, respectively, with deposition of 120 ± 12 $t.ha^{-1}.yr^{-1}$ at the toeslope.

The present ^{137}Cs estimates are broadly consistent with the erosional pattern reported by Didoné et al. (2019), but their magnitude varies substantially among conversion models. In H1, the proportional and MODERN estimates partly overlap with the MBM-2 summit and backslope rates, whereas Radero gives more moderate values. In H2, the proportional model produces lower erosion estimates than those reported by Didoné et al. (2019), while Radero is closer to their reported range. The MODERN model gives the strongest contrast, particularly in H2, where the most negative value substantially exceed the MBM-2 rates of -25 ± 8 and -18 ± 16 $t.ha^{-1}.yr^{-1}$ reported for the summit and backslope.

Compared with plot-based erosion studies, the radionuclide-derived estimates obtained here are relatively high. Previous studies in comparable agricultural settings reported soil losses of approximately 6.1 to 13 $t.ha^{-1}.yr^{-1}$ (Cogo et al. 2003; Beutler et al. 2003), while values of 13 to 15 $t.ha^{-1}.yr^{-1}$ have been reported for similar clayey soils under conventional tillage (Bertoni and Neto Francisco Lombardi 2008; Bertol and Almeida 2000). These values are close to the estimated tolerable soil-loss range for Ferralsols in southern Brazil, varying approximately from 12 to 15 $t.ha^{-1}.yr^{-1}$ (Eltz et al. 1984; Bertol and

Almeida 2000; Cogo et al. 2003). Several estimates from the present study exceed this range, especially those obtained with the MODERN model. The maximum negative values reached $-107.8\ t.ha^{-1}.yr^{-1}$ for $^{210}Pb_{ex}$ in H1 and $-134.8\ t.ha^{-1}.yr^{-1}$ for ^{137}Cs in H2. These high values may indicate intense local soil redistribution, but they may also reflect methodological differences between plot monitoring and fallout radionuclide approaches. Plot monitoring generally quantifies short-term gross soil loss over small delineated areas, whereas fallout radionuclide inventories estimate net redistribution over decadal timescales and are sensitive to spatial variability in inventory depletion and accumulation.

Comparison between H1 and H2

The two hillslopes show different redistribution rates across the sampled midslope areas and for each radionuclide. For H1, the ^{137}Cs results show a consistent pattern in terms of the sign of redistribution across the three models. Most cores show negative redistribution rates. However, cores C and D show positive redistribution rates in all three models. This suggests that the distinction between mostly depleted inventory points and locally enriched points across the H1 midslope plot was weakly affected by the choice of ^{137}Cs conversion model. However, the magnitude of the estimates differs substantially among models, with MODERN producing the largest absolute values and Radero producing more moderate values.

The $^{210}Pb_{ex}$ results for H1 show a more heterogeneous pattern than the ^{137}Cs results. Both the proportional and MODERN $^{210}Pb_{ex}$ models produced positive and negative redistribution estimates, but MODERN amplified the contrasts between cores, especially for the most negative estimates (cores G, H, and J). This indicates that the results for H1 were both dependent of the radionuclide considered and the model used. While ^{137}Cs inventories were associated with mostly negative redistribution rates with some positive values (cores C and D), the use of $^{210}Pb_{ex}$ led to more spatially variable rates within the same midslope plot.

For H2, the ^{137}Cs proportional and Radero models produced negative estimates for all cores, indicating a consistently negative redistribution signal. The same results were obtained with MODERN for ^{137}Cs except for one positive estimate (core B). The MODERN model introduced stronger spatial contrast in H2, with one locally positive value. The $^{210}Pb_{ex}$ proportional model also yielded mostly negative redistribution rates, except for one positive rate (core C), whereas the MODERN modelling with $^{210}Pb_{ex}$ yielded positive rates for cores A, B, C, K, L, and M and negative rates for cores D to J.

Overall, H1 and H2 differ in both the sign structure and magnitude of radionuclide-derived redistribution. H1 shows a more consistent ^{137}Cs pattern across models, with positive estimates restricted to cores C and D. H2 shows a more model-dependent ^{137}Cs pattern, because only MODERN led to a positive value, at core B. However, this comparison should be made with caution because both hillslopes are managed with different agricultural practices.

Effect of model selection

Model choice strongly influenced the estimated redistribution rates. For both radionuclides, MODERN generally produced larger absolute values and stronger contrasts between neighbouring cores than the proportional model. This effect was particularly clear for $^{210}Pb_{ex}$, for which MODERN produced a wider range of redistribution estimates on both hillslopes.

For H1, the three ^{137}Cs models agreed on the sign of redistribution, with positive values for cores C and D and negative values for the remaining cores. However, the magnitude of the estimations differed substantially among models. Therefore, the spatial pattern of ^{137}Cs-derived erosion and accumulation was comparatively robust in H1, whereas the estimated intensity of redistribution remained model-dependent.

For H2, model choice affected both the magnitude and, in one case, the sign of the ^{137}Cs-derived estimates. The proportional and Radero models indicated negative redistribution for all cores, whereas MODERN produced a positive estimate for core B. This indicates that the H2 ^{137}Cs interpretation was more sensitive to model choice than H1.

Comparison between ^{137}Cs and $^{210}Pb_{ex}$

The ^{137}Cs and $^{210}Pb_{ex}$ results did not produce identical redistribution patterns. In H1, the ^{137}Cs models indicated a mostly negative pattern, with positive values restricted to cores C and D. In contrast, the $^{210}Pb_{ex}$ models indicated a more mixed pattern, with several positive and negative estimates across the plot.

In H2, the ^{137}Cs proportional and Radero models indicated consistently negative redistribution, whereas the ^{137}Cs MODERN model produced one positive value at core B. The $^{210}Pb_{ex}$ results were more variable. The proportional model produced mainly negative estimates, with positive values at cores B and C, whereas MODERN produced positive estimates for cores A, B, C, K, L, and M and negative estimates for cores D to J.

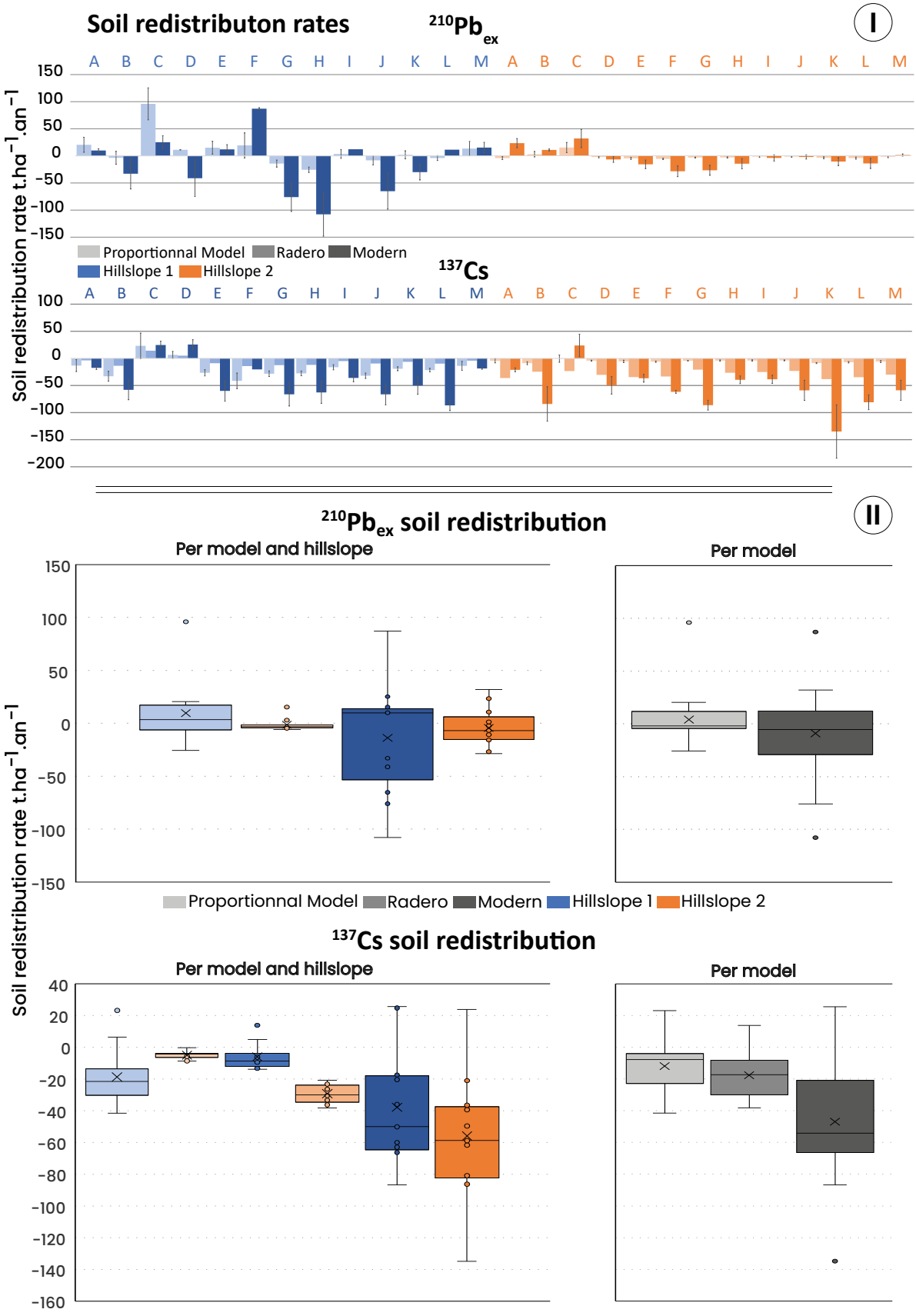

Figure 3.8: Φ, Soil redistribution modelling of H1 (in blue) and H2 (in orange) in $t.ha^{-1}.yr^{-1}$ based on $^{210}Pb_{ex}$ and ^{137}Cs inventories with proportional, MODERN and Radero modelling. Φ, Boxplot of soil redistribution modelling per model and hillslope and only per model in $t.ha^{-1}.yr^{-1}$ based on $^{210}Pb_{ex}$ and ^{137}Cs inventories with proportional, MODERN and Radero modelling

3.4 . Discussion

FNR techniques are often applied following a systemic sampling on the summit, backslope and toeslope of the studied hillslopes with only one or two references. This study relied on the dense sampling of soil cores at two sites impacted by erosion, along hillslopes cultivated with conventional or no-tillage practices in order to better understand the representativeness of the cores used to apply FNR techniques as well as the effect of farming practices.

3.4.1 . Spatial representativeness of ^{137}Cs and $^{210}Pb_{ex}$ inventories

While mean inventories might be comparable, this study demonstrates that erosion sites exhibit pronounced small-scale variability for both ^{137}Cs and $^{210}Pb_{ex}$ inventories. Indeed, variation coefficients of 64% and 46% for H1 and 50% and 57% for H2 were found with ^{137}Cs and $^{210}Pb_{ex}$ inventories, respectively.

Multiple factors can explain such large variability in ^{137}Cs inventories at local scale. First, it is difficult to find reliable information on when these hillslopes were first cultivated and what was their previous land use/cover. Didoné et al. (2019) found that these hillslopes were covered with native forest and progressively cultivated. However, the temporality of this change remains unclear. Therefore, during the main ^{137}Cs fallout period (i.e. from the global detection in 1953 to the end of the french nuclear bomb test in 1974 Guillevic et al. (2026)), part of it might have been retained by the native forest, which generated a higher heterogeneity of ^{137}Cs distribution in the soils. Furthermore, the transition for H2 from conventional tillage to no-tillage as well as the construction and then the removal of terraces (1980-1990), have influenced the hydrological behaviour of these hillslopes. In addition, the induced concentration of the flows might have further affected the ^{137}Cs inventories across this hillslope.

Although it could be argued that having a higher-resolution DEMs and additional environmental covariates might help to explain part of this variability, such an approach would require a density of spatial data that is most often unavailable or incompatible with the rapid assessment of soil erosion magnitude for which fallout radionuclide methods are often implemented. The high number of samples and the additional information required to achieve reliable estimates under these conditions undermines the practicality of using $^{210}Pb_{ex}$ and ^{137}Cs as rapid and reliable tools for quantifying and spatialising soil erosion in these conditions and in this region of Brazil.

Finally, while $^{210}Pb_{ex}$ also exhibit high heterogeneity in terms of total inventories, the layers inventories can give important information on the effects of farming practices as discussed in the following paragraph.

3.4.2 . Effect of farming practices on the spatial variability of ^{137}Cs and $^{210}Pb_{ex}$

While this study highlights the high small-scale variability observed at erosion sites, it also reveals systematic differences between sites that can likely be attributed to contrasting agricultural practices. In-

deed, $^{210}Pb_{ex}$ and ^{137}Cs give information on soil redistribution during different time periods (Cabrera et al. 2023). While ^{137}Cs was deposited only during atmospheric nuclear bomb testing, $^{210}Pb_{ex}$ is constantly deposited with rainfall and is therefore more influenced by recent and current agricultural practices.

H1 exhibits $^{210}Pb_{ex}$ depth profiles that are characteristic of conventional tillage practices, including the occurrence of inverted or mixed profiles, such as those observed in the mid-slope cores, which are consistent with tillage-induced soil mixing. In contrast, H2 displays profiles that are more typical of no-tillage systems, with compaction of the upper soil layers, reduced infiltration capacity, and a significant enrichment of $^{210}Pb_{ex}$ in the near-surface horizon.

At the hillslope scale, H1 shows greater spatial homogeneity in $^{210}Pb_{ex}$ inventories compared to H2, where profiles reflect the expected exponential decrease of $^{210}Pb_{ex}$ with depth driven by atmospheric deposition. These differences can be explained by the influence of farming practices on the soil structure and hydrological pathways. No-tillage systems tend to promote surface compaction and enhanced runoff, leading to more heterogeneous radionuclide redistribution, whereas conventional tillage increases infiltration, and promotes vertical mixing, resulting in more homogeneous $^{210}Pb_{ex}$ inventories.

Besides the actual agricultural practices, H2 might have been influenced by past operations. Indeed, while it is cultivated nowadays under no-tillage, this hillslope was ploughed in the past, which influenced the distribution of ^{137}Cs along the hillslope and in the investigated soil profiles. Furthermore, soils of hillslope H2 might have been redistributed during the creation and destruction of the terraces, which may have led to some local soil accumulation and redistribution.

In this area where massive changes occurred recently and where it is difficult to quantify the ^{137}Cs inventories variability, the use of $^{210}Pb_{ex}$ may then provide the best tracer to conduct such pluridecadal soil redistribution quantification.

3.4.3 . Soil redistribution modelling

The results highlight two major sources of uncertainty in fallout radionuclide-based soil redistribution estimates: sampling representativeness and model choice. Although fallout radionuclide methods are widely used to reconstruct soil redistribution, their interpretation depends on the assumption that sampled cores adequately represent local inventory patterns. The strong variability observed among neighbouring cores within the 12 m $\times$ 12 m plots shows that this assumption may be problematic in cultivated hillslopes affected by tillage, terracing, and recent changes in agricultural practices such as those investigated in the study area of Southern Brazil.

This finding is consistent with those of previous studies showing strong spatial variability in ^{137}Cs and ^{210}Pb$_{ex}$ inventories along cultivated slopes and catchments (Mabit et al. 2008; Cabrera et al. 2023). It also agrees with studies from southern Brazil showing that soil redistribution patterns are strongly influenced by agricultural management and by the transition from conventional tillage to no-tillage systems (Didoné et al. 2019; Minella et al. 2014). However, the present study adds that substantial variability can occur

over very short distances, meaning that individual cores may not be sufficient to infer hillslope- and ctachment- scale redistribution rates.

Model selection further influenced the results of soil redistribution. MODERN generally produced larger absolute values and stronger contrasts between cores than the proportional model (+270.8% and 146.4% for ^{137}Cs and ^{210}Pb$_{ex}$ respectively with mean redistribution). This result is consistent with previous work showing that fallout radionuclide-derived redistribution rates are sensitive to the assumptions and parameters embedded in conversion models, including reference inventory, fallout history, vertical mixing, radionuclide migration (Jagercikova et al. 2015, 2014), particle-size correction, and tillage depth (Walling and He 1999; Mabit et al. 2008; Arata et al. 2016; Zhang 2015; IAEA 2014).

The disagreement between ^{137}Cs and ^{210}Pb$_{ex}$ also suggests that the two radionuclides provide complementary although different information. ^{137}Cs mainly reflects soil redistribution since the onset and peak period of atmospheric nuclear weapons fallout, whereas ^{210}Pb$_{ex}$ is supplied continuously to the soil surface and can therefore provide information over a different, and potentially more recent, effective timescale (Cabrera et al. 2023). This may make ^{210}Pb$_{ex}$ useful in landscapes affected by recent management changes, but its interpretation requires caution and may also be affected by vertical migration, bioturbation, and local profile disturbance (Mabit et al. 2008; Zhang et al. 2019).

Overall, the redistribution rates estimated in this study fall within the broad range of values reported for comparable agricultural hillslopes, but the highest MODERN-derived estimates exceed both the site-specific MBM-2 values of (Didoné et al. 2019) and plot-based erosion rates reported for similar soils of Southern Brazil.

This type of fallout-radionuclide approach remains valuable for assessing medium- to long-term soil redistribution in agricultural hillslopes, although the current results show that it should not rely on a single tracer, conversion model, or isolated core. Future applications should treat model choice as a source of uncertainty rather than as a technical detail, and should use sampling designs that are dense enough to capture plot-scale variability. Combining several radionuclides, testing multiple conversion models, and comparing neighbouring cores or slope-position replicates can help distinguish robust redistribution patterns from model-sensitive or locally disturbed estimates.

3.5 . Conclusions

By applying a high-density fallout radionuclide sampling strategy within two 12 m $\times$ 12 m midslope plots, this study tested to what extent individual soil cores are representative for estimating soil redistribution in cultivated hillslopes in southern Brazil. The combined use of ^{137}Cs and ^{210}Pb$_{ex}$ inventories, together with the implementation of several conversion models, showed that cores collected in a close vicinity can show contrasting radionuclide inventories (coefficients of variation of 64% and 46% for H1 and 50% and 57% for H2 were found with ^{137}Cs and $^{210}Pb_{ex}$ inventories, respectively) and modelled soil

redistribution rates over very short distances (2 m).

Furthermore, the comparison between H1 and H2 showed that this heterogeneity is likely influenced by differences in land-use history and agricultural practices. H1, under conventional tillage, showed evidence of stronger vertical mixing in the $^{210}Pb_{ex}$ profiles, whereas H2, currently under no-tillage, displayed patterns that are more consistent with near-surface radionuclide enrichment and greater local variability.

The redistribution models also produced contrasting results. For H1, the ^{137}Cs estimates showed a clear agreement in terms of redistribution sign, as all three models led to positive estimates for cores C and D and negative estimates for the other cores. However, the magnitude of the estimated redistribution differed substantially among models. For H2, the interpretation was more model-dependent. The proportional and Radero ^{137}Cs models produced negative estimations for all cores, whereas MODERN produced one positive estimation and stronger negative values for other cores.

Overall, this study showed that radionuclide inventories and modelled redistribution rates vary substantially over short distances. However, $^{210}Pb_{ex}$ may provide useful complementary information on recent soil redistribution and farming-practice effects, particularly where ^{137}Cs inventories are difficult to interpret because of historical land-cover change or past soil disturbances such as those induced by the creation and destruction of terraces. Although results deduced from inventory conversions for both radionuclides remain affected by reference inventory uncertainty, local spatial variability, and model assumptions, major findings could be found. $^{210}Pb_{ex}$ inventories for H1, under conventional tillage, are more heterogenous probably due to the tillage operations while for H2, under no-tillage practices, redistribution rates are lower and more homogeneous probably due to the compaction of the soils, increased runoff and decreased infiltration. This was possible to infer from $^{210}Pb_{ex}$ inventories as this tracer gives information on a more recent period when the changes in land-use and farming practices occurred. Using both radionuclide inventories complementing each other, it could then be possible to infer more information about farming practices and their impacts on soil redistribution in the field. Future applications in similar environments should therefore include denser or on the contrary composite reference-site sampling and sampling designs taking into account this small-scale variability to infer hillslope scale sediment redistribution.

3.6 . Supplementary material

3.6.1 . Detailed Methodology

Gamma spectrometry quality assessment

- IAEA-375
- IAEA-465 Baltic Sea Sediment
- IAEA-444 Chinese Soil
- IAEA-384 Fangataufa Sediment
- IAEA-372 Chernobyl Grass
- IAEA-385 Irish Sea Sediment
- IAEA-447 Moss Soil
- IAEA-135
- IAEA-312 Stream sediment
- IAEA-313 Stream sediment
- IAEA-314 Stream sediment
- IAEA-Soil 6
- IAEA-RGTh-1
- IAEA-RGU-1

These reference materials include soil, sediment, vegetation, and uranium/thorium standards covering a broad range of radionuclide activities. Detector performance and analytical reproducibility were assessed through repeated measurements of the certified reference material IAEA-444 “Chinese Soil”, with particular attention to ^{137}Cs and $^{210}Pb_{ex}$, which constitute the main radionuclides investigated in this study. Method accuracy was evaluated by comparing the mean activities obtained from repeated measurements of the certified reference material with their corresponding certified or information values (Eq. 3.5) performed throughout the period 2024-2026 with their certified or information values, while analytical precision was quantified as the relative standard deviation (RSD, %) derived from replicate certified reference material measurements over the same period (Eq. 3.6).

$$\text{Relative Bias } (\%) = \frac{\mathrm{A}^{-} - \mathrm{A}_{\mathrm{cert}}}{\mathrm{A}_{\mathrm{cert}}} \times 100 \tag{3.5}$$

where A^{-}represents the arithmetic mean of the specific activities ($Bq.kg^{-1}$) obtained from repeated measurements of the certified reference material for the radionuclides considered, and A_cert is the certified specific activity ($Bq.kg^{-1}$).

$$\text{RSD } (\%) = \frac{\sigma}{\mathrm{A}^{-}} \times 100 \tag{3.6}$$

where RSD (%) represents the relative standard deviation of the specific activities measured for the radionuclides under consideration, and σ is the standard deviation of the repeated measurements.

Radionuclide	Certified / Information values	Standard combined uncertainty
	$Bq.kg^{-1}$	$Bq.kg^{-1}$
$^{210}Pb_{ex}$	48.0	1.6
^{137}Cs	68.5	1.4

Table 3.1: Reference activities of ^{137}Cs (certified value) and $^{210}Pb_{ex}$ (information value) for the IAEA-444 reference material (Chinese soil), decay-corrected to 15 October 2007.

Detector	Number of measurements	^{137}Cs			^{210}Pb		
		Mean ± SD	Relative Bias	RSD	Mean ± SD	Relative Bias	RSD
		$Bq.kg^{-1}$	(%)	(%)	$Bq.kg^{-1}$	(%)	(%)
1	7	66.9 ± 1.2	-2.4	1.7	42.8 ± 1.8	-10.9	4.2
2	6	66.4 ± 0.5	-3.1	0.7	38.7 ± 1.2	-19.4	3.5
3	4	67.0 ± 0.7	-2.2	1.1	42.6 ± 3.8	-11.4	9.0
4	8	68.4 ± 2.3	-0.1	3.3	40.6 ± 1.9	-15.5	4.7
All	**25**	**67.0 ± 1.4**	**-2.2**	**2.0**	**41.3 ± 2.7**	**-13.9**	**6.6**

Table 3.2: Summary statistics of repeated measurements of the IAEA-444 reference material performed on the four HPGe detectors at the Laboratoire des Sciences du Climat et de l'Environnement between 2024 and 2026, decay-corrected to 15 October 2007.

Decay correction

$$^{137}\mathrm{Cs}\ (\mathrm{Bq.m^{-2}}) = {}^{137}Cs(\mathrm{Bq.m^{-2}}).e^{(-\lambda.t)} \tag{3.7}$$

With $\lambda = \frac{ln(2)}{^{137}Cs\ t^{1/2}}$

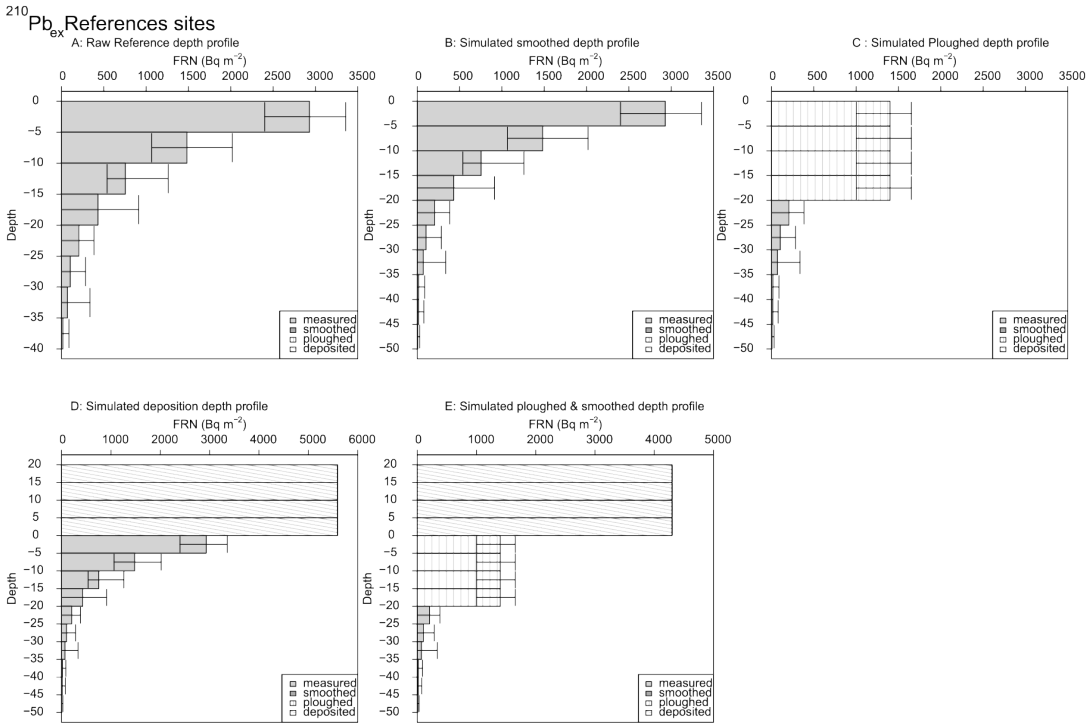

Figure 3.1: Reference profile of $^{210}Pb_{ex}$ constructed with MODERN package, with A the raw mean profile, B the simulated smoothed profile, C simulated smoothed and ploughed profile, D simulated smoothed and deposited profile, E simulated smoothed, ploughed and deposited profile

3.6.2 . Modern reference profiles

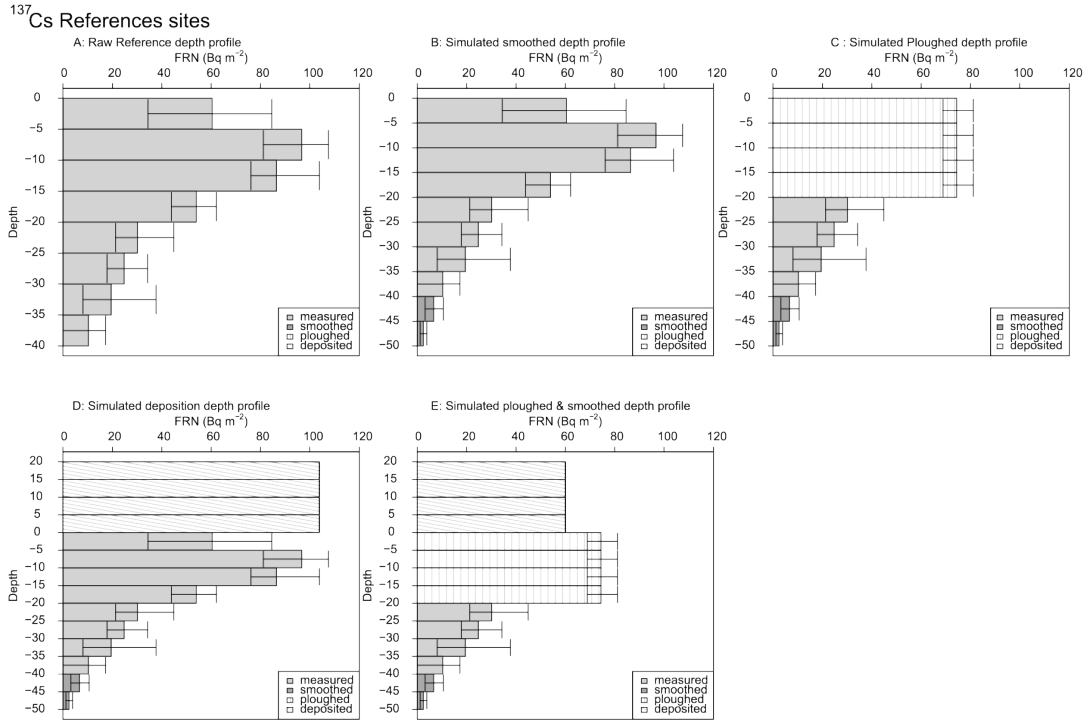

Figure 3.2: Reference profile of ^{137}Cs constructed with MODERN package, with A the raw mean profile, B the simulated smoothed profile, C simulated smoothed and ploughed profile, D simulated smoothed and deposited profile, E simulated smoothed, ploughed and deposited profile

Bibliography

Amundson, R., Berhe, A. A., Hopmans, J. W., Olson, C., Sztein, A. E., and Sparks, D. L. (2015). Soil and human security in the 21st century. *Science*, 348(6235):1261071.

Arata, L., Meusburger, K., Frenkel, E., A'Campo-Neuen, A., Iurian, A.-R., Ketterer, M. E., Mabit, L., and Alewell, C. (2016). Modelling Deposition and Erosion rates with RadioNuclides (MODERN) – Part 1: A new conversion model to derive soil redistribution rates from inventories of fallout radionuclides. *Journal of Environmental Radioactivity*, 162-163:45–55.

Bertol, I. and Almeida, J. A. (2000). Tolerância de perda de solo por erosão para os principais solos do estado de Santa Catarina. *Revista Brasileira de Ciência do Solo*, 24:657–668. Publisher: Sociedade Brasileira de Ciência do Solo.

Bertoni, J. and Neto Francisco Lombardi (2008). *Conservação do Solo*. Ícone Editora. Google-Books-ID: d0xaEQAAQBAJ.

Beutler, J. F., Bertol, I., Veiga, M., and Wildner, L. P. (2003). Perdas de solo e água num Latossolo Vermelho aluminoférrico submetido a diferentes sistemas de preparo e cultivo sob chuva natural. *Revista Brasileira de Ciência do Solo*, 27:509–517. Publisher: Sociedade Brasileira de Ciência do Solo.

Brown, R. B., Kling, G. F., and Cutshall, N. H. (1981). Agricultural Erosion Indicated by 137Cs Redistribution: II. Estimates of Erosion Rates. *Soil Science Society of America Journal*, 45(6):1191–1197. _eprint: https://acsess.onlinelibrary.wiley.com/doi/pdf/10.2136/sssaj1981.03615995004500060036x.

Cabrera, M., Sanabria, R., González, J., Cabral, P., Tejeda, S., Zarazua, G., Melgar-Paniagua, E., and Tassano, M. (2023). Using 137Cs and 210Pbex to assess soil redistribution at different temporal scales along with lithogenic radionuclides to evaluate contrasted watersheds in the Uruguayan Pampa grassland. *Geoderma*, 435:116502.

Catalá, A., Latorre, B., Gaspar, L., and Navas, A. (2025). Estimating soil redistribution rates with the RadEro model: A physically based compartmental model for 137Cs analysis in an R package. *Environmental Modelling & Software*, 192:106551.

Chaboche, P.-A. (2021). *Amélioration de la chronologie des retombées initiales de radionucléides pour reconstruire les taux de redistribution de sol dans les bassins versants agricoles d'Amérique du Sud*. phdthesis, Université Paris-Saclay.

Cogo, N. P., Levien, R., and Schwarz, R. A. (2003). Perdas de solo e água por erosão hídrica influenciadas por métodos de preparo, classes de declive e níveis de fertilidade do solo. *Revista Brasileira de Ciência do Solo*, 27:743–753. Publisher: Sociedade Brasileira de Ciência do Solo.

De Roo, A. P. J., Wesseling, C. G., and Ritsema, C. J. (1996). Lisem: A Single-Event Physically Based Hydrological and Soil Erosion Model for Drainage Basins. I: Theory, Input and Output. *Hydrological Processes*, 10(8):1107–1117. _eprint: https://onlinelibrary.wiley.com/doi/pdf/10.1002/%28SICI%291099-1085%28199608%2910%3A8%3C1107%3A%3AAID-HYP415%3E3.0.CO%3B2-4.

Didoné, E. J., Gomes Minella, J. P., and Allasia Piccilli, D. G. (2021). How to model the effect of mechanical erosion control practices at a catchment scale? *International Soil and Water Conservation Research*, 9(3):370–380.

Didoné, E. J., Gomes Minella, J. P., Andres Schneider, F. J., Londero, A. L., Lefèvre, I., and Evrard, O. (2019). Quantifying the impact of no-tillage on soil redistribution in a cultivated catchment of Southern Brazil (1964–2016) with 137Cs inventory measurements. *Agriculture, Ecosystems & Environment*, 284:106588.

Didoné, E. J., Minella, J. P. G., and Evrard, O. (2017). Measuring and modelling soil erosion and sediment yields in a large cultivated catchment under no-till of Southern Brazil. *Soil and Tillage Research*, 174:24–33.

Didoné, E. J., Minella, J. P. G., Reichert, J. M., Merten, G. H., Dalbianco, L., de Barrros, C. A. P., and Ramon, R. (2014). Impact of no-tillage agricultural systems on sediment yield in two large catchments in Southern Brazil. *Journal of Soils and Sediments*.

Elliott, G. L., Campbell, B. L., and Loughran, R. J. (1990). Correlation of erosion measurements and soil caesium-137 content. *International Journal of Radiation Applications and Instrumentation. Part A. Applied Radiation and Isotopes*, 41(8):713–717.

Eltz, F., Cassol, E., Guerra, M., and Abrão, P. (1984). Perdas de solo e água por erosão em diferentes sistemas de manejo e coberturas vegetais em solo São Pedro (Podzólico Vermelho-Amarelo) sob chuva natural. *Revista Brasileira de Ciência do Solo*, 8(2):245–249.

Evrard, O., Chaboche, P.-A., Ramon, R., Foucher, A., and Laceby, J. P. (2020). A global review of sediment source fingerprinting research incorporating fallout radiocesium (137Cs). *Geomorphology*, 362:107103.

FAO & ITPS (2015). Status of the World's Soil Resources: Main Report. *Food and Agriculture Organization*.

Guillevic, F., Gastineau, R., Evrard, O., Sabatier, P., Bardelle, A., Chaboche, P.-A., Foucher, A., Achaga, R., Ruiz-Fernández, A. C., Sanchez-Cabeza, J.-A., Tassano, M., Cabrera, M., Quicke, J. A., Chalar, G., Van Daele, M., Moreno-Allende, V., Moernaut, J., Haberzettl, T., Corcho Alvarado, J. A., Röllin, S.,

Sahli, H., Kobler, J., Dicen, G., and Alewell, C. (2026). Plutonium isotopes as time-markers in South American lake sediments: identifying pre- and post-1959 and French test periods.

Health and Safety Laboratory (1977). Health and Safety Laboratory environmental quarterly. Final tabulation of monthly /sup 90/Sr fallout data: 1954–1976. Technical Report HASL-329, 7291252, U. S. Energy Research and Developnent Administration.

Hudson, N. (1993). *Field measurement of soil erosion and runoff*. Number 68 in FAO soils bulletin. Food and Agriculture Organization of the United Nations, Rome.

IAEA, editor (2014). *Guidelines for using fallout radionuclides to assess erosion and effectiveness of soil conservation strategies*. IAEA, Vienna. OCLC: 1039239887.

Jagercikova, M., Cornu, S., Le Bas, C., and Evrard, O. (2015). Vertical distributions of 137Cs in soils: a meta-analysis. *Journal of Soils and Sediments*, 15(1):81–95.

Jagercikova, M., Evrard, O., Balesdent, J., Lefèvre, I., and Cornu, S. (2014). Modeling the migration of fallout radionuclides to quantify the contemporary transfer of fine particles in Luvisol profiles under different land uses and farming practices. *Soil and Tillage Research*, 140:82–97.

Mabit, L., Benmansour, M., and Walling, D. E. (2008). Comparative advantages and limitations of the fallout radionuclides 137Cs, 210Pbex and 7Be for assessing soil erosion and sedimentation. *Journal of Environmental Radioactivity*, 99(12):1799–1807.

Mabit, L., Meusburger, K., Fulajtar, E., and Alewell, C. (2013). The usefulness of 137Cs as a tracer for soil erosion assessment: A critical reply to Parsons and Foster (2011). *Earth-Science Reviews*, 127:300–307.

Merritt, W., Letcher, R., and Jakeman, A. (2003). A review of erosion and sediment transport models. *Environmental Modelling & Software*, 18(8-9):761–799.

Minella, J. P. G., Walling, D. E., and Merten, G. H. (2014). Establishing a sediment budget for a small agricultural catchment in southern Brazil, to support the development of effective sediment management strategies. *Journal of Hydrology*, 519:2189–2201.

Montgomery, D. R. (2007). Soil erosion and agricultural sustainability. *Proceedings of the National Academy of Sciences*, 104(33):13268–13272.

Morgan, R. P. C. (2006). *Soil erosion and conservation*. Blackwell, Malden, Mass., 3. ed., [nachdr.] edition.

Nearing, M. A., Foster, G. R., Lane, L. J., and Finkner, S. C. (1989). A Process-Based Soil Erosion Model for USDA-Water Erosion Prediction Project Technology. *Transactions of the ASAE*, 32(5):1587–1593.

Parsons, A. J. and Foster, I. D. L. (2011). What can we learn about soil erosion from the use of 137Cs? *Earth-Science Reviews*, 108(1):101–113.

Parsons, A. J. and Foster, I. D. L. (2013). The assumptions of science: A reply to Mabit et al. (2013). *Earth-Science Reviews*, 127:308–310.

Pimentel, D. and Burgess, M. (2013). Soil Erosion Threatens Food Production. *Agriculture*, 3(3):443–463.

Porto, P., Walling, D. E., Callegari, G., and Capra, A. (2009). Using caesium-137 and unsupported lead-210 measurements to explore the relationship between sediment mobilisation, sediment delivery and sediment yield for a Calabrian catchment. *Marine & Freshwater Research*, 60(7):680–689.

Ramon, R. (2021). *Quantifying sediment source contributions in contrasted agricultural catchments (Uruguay River, Southern Brazil)*. PhD thesis, Universit{\'e} Paris-Saclay ; Universidade Federal do Rio Grande do Sul (Porto Alegre, Br{\'e}sil).

Renard, K. G., Foster, G. R., Weesies, G. A., McCool, D. K., and Yoder, D. C. (1997). *Predicting Soil Erosion by Water: A Guide to Conservation Planning with the Revised Universal Soil Loss Equation*, volume 703. United States Department of Agriculture, agriculture handbook edition.

Ritchie, J. C. and Ritchie, C. A. (2008). BIBLIOGRAPHY OF PUBLICATIONS OF 137CESIUM STUDIES RELATED TO EROSION AND SEDIMENT DEPOSITION. *USDA*.

Sherrill, R. D., Sumerlin, N. G., Beck, J. N., and Kuroda, P. K. (1975). Variation of the Ratio of Cesium-137 to Strontium-90 in the Atmosphere. *Health Physics*, 28(4):335.

Sutherland, R. A. (1996). Caesium-137 soil sampling and inventory variability in reference locations: A literature survey. *Hydrological Processes*, 10(1):43–53. _eprint: https://onlinelibrary.wiley.com/doi/pdf/10.1002/%28SICI%291099-1085%28199601%2910%3A1%3C43%3A%3AAID-HYP298%3E3.0.CO%3B2-X.

Tales Tiecher (2015). *Fingerprinting sediment sources in agricultura catchments in Southern Brazil*. PhD thesis, Federal University of Rio Grande do Sul. Publisher: Unpublished.

Tassano, M., Cabral, P., and Cabrera, M. (2025). Inventario de cesio-137 y plomo-210 en suelos de referencia del centro-oeste de Uruguay: base para estudios de erosión y vigilancia radiológica. *INNOTEC*, 29:1–19.

United Nations Scientific Committee on the Effects of Atomic Radiation (2000). *Sources and effects of ionizing radiation. 1: Sources*. Number 2000 in Report of the United Nations Scientific Committee on the Effects of Atomic Radiation. United Nations, New York.

Walling, D. and Quine, T. (1992). The use of caesium-137 measurements in soil erosion surveys. *Erosion and sediment monitoring programmes in river basins. Proc. international symposium, Oslo, 1992*.

Walling, D. E. and He, Q. (1999). Improved Models for Estimating Soil Erosion Rates from Cesium-137 Measurements. *Journal of Environmental Quality*, 28(2):611–622. _eprint: https://acsess.onlinelibrary.wiley.com/doi/pdf/10.2134/jeq1999.00472425002800020027x.

Walling, D. E., Quine, T. A., and Department of Geography, U. o. E. U. K. (1993). Use of caesium-137 as a tracer of erosion and sedimentation: Handbook for the application of the caesium-137 technique. UK Overseas Development Administration research scheme R4579. Technical Report INIS-XA-N–179, Department of Geography, University of Exeter (United Kingdom).

Wischmeier, W. H. and Smith, O.D. (1978). AH_537 Predicting Rainfall Soil Losses.

XINBAO, Z., HIGGITT, D. L., and WALLING, D. E. (1990). A preliminary assessment of the potential for using caesium-137 to estimate rates of soil erosion in the Loess Plateau of China. *Hydrological Sciences Journal*, 35(3):243–252. Publisher: Taylor & Francis _eprint: https://doi.org/10.1080/02626669009492427.

Zhang, X. C., Polyakov, V. O., Liu, B. Y., and Nearing, M. A. (2019). Quantifying geostatistical properties of 137Cs and 210Pbex at small scales for improving sampling design and soil erosion estimation. *Geoderma*, 334:155–164.

Zhang, X. J. (2015). New Insights on using Fallout Radionuclides to Estimate Soil Redistribution Rates. *Soil Science Society of America Journal*, 79(1):1–8. _eprint: https://acsess.onlinelibrary.wiley.com/doi/pdf/10.2136/sssaj2014.06.0261.

Zhang, X. J. (2023). Evaluating and improving 137Cs technology for estimating soil erosion using soil loss data measured during 1954–2015. *Earth-Science Reviews*, 247:104619.

IV

Initial parametrisation of runoff for distributed conceptual model, WaterSed, in the Conceição catchment

Chapter 4

Initial parametrisation of runoff for distributed conceptual model, WaterSed, in the Conceição catchment

The high small-scale variability observed in radionuclide-derived soil redistribution rates, together with the sensitivity of the results to model assumptions, highlight the need for approaches that better capture the spatial organisation of erosion and sediment transfers under changing agricultural practices. In this context, distributed models such as WaterSed offer a complementary framework by integrating topography, land use, and soil types to simulate spatial patterns of erosion, deposition, and sediment delivery, and this approach is explored in the following chapter.

Amaury Bardelle[1], Rosalie Vandrome[2], Thomas Grangeon[2], Jean Paolo Gomes Minella[4], Anthony Foucher[1], Olivier Cerdan[2], Christine Alewell[5], Olivier Evrard[1]

[1]Laboratoire des Sciences du Climat et de l'Environnement (LSCE, IPSL), Université Paris-Saclay, UMR 8212 (CEA, CNRS, UVSQ),Gif-sur-Yvette,91190,France
[2]Risk and Prevention Division, Bureau de Recherches Géologiques et Minières (BRGM), Orléans, F-45060, France
[3]Identité et différenciation de l'espace, de l'environnement et des sociétés (IDEES - UMR 6266),Université de Caen Normandie, France
[4]Department of Soils, Universidade Federal de Santa Maria, Santa Maria, F-45060, Brazil
[5]Environmental Geosciences, University of Basel, Basel, 4056, Switzerland

4.1 . Introduction

Soils play a central role in food production, water regulation, nutrient cycling, and biodiversity conservation (FAO & ITPS 2015). Their degradation threatens both agricultural productivity and ecosystem services, with water erosion representing one of the most important drivers of soil loss. By removing fertile topsoil faster than it can be naturally regenerated under most intensive agricultural systems, erosion reduces soil fertility, exports organic carbon and nutrients, and contributes to sedimentation in downstream water bodies (Montgomery 2007). These processes are often intensified by unsustainable land use, reduced vegetation cover, and intensive farming practices, which increase runoff and sediment detachment (Pimentel and Burgess 2013; Amundson et al. 2015).

A reliable quantification of soil erosion is required to assess land degradation and support conservation planning. Erosion can be estimated using field measurements, sediment monitoring, tracer-based approaches, empirical models, or process-based models. Field observations provide essential reference data but are often spatially-limited and difficult to extrapolate.

There are currently three major families of models, arbitrarily classified here based on their representation of space:

- So-called "global" models. A widely used example is the USLE (Universal Soil Loss Equation; Wischmeier, W. H. and Smith, O.D. (1978)). The USLE describes the mass of soil transferred to the outlet of a plot under given conditions. It does not explicitly describe either the study area or the transfer processes.

- So-called "semi-distributed" models, typically the SWAT model and its variations (Arnold et al. 1998; Bieger et al. 2017). This type of model describes processes within hydrological units assumed to be homogeneous (sub-catchments). Each unit describes runoff and suspended sediment production (e.g., via a global model such as USLE). These models are therefore semi-explicit in space; they do not reproduce interactions between entities.

- So-called "distributed" models, which describe the processes of water and soil particle production and transport at the grid cell scale. the processes are thus described at every point within the study

area. These approaches include both so-called “physically-based” models, such as PSEM_2D (Nord and Esteves 2005) or EROSION3D (Schindewolf et al. 2013), and “process-based” models, such as WaterSed (Landemaine et al. 2023).

The WaterSed model was initially envisaged to complement the soil cores studies. Soil cores provide valuable historical perspectives on sediment sources and long-term erosion dynamics, but they do not capture seasonal to event-scale variability or the spatial heterogeneity of erosion processes. In contrast, process-based modelling enables the simulation of erosion and sediment transfer continuously in time and across the catchment, allowing the identification of spatial patterns, temporal dynamics of individual rainfall events, and the relative contribution of different landscape units under varying hydrometeorological conditions. Therefore the model was parametrised using monitored hydrological events, while accounting for seasonal variability, in order to better constrain the interpretation of long-term soil redistribution rates derived from sediment cores. As a first step, the hydrological balance was parameterised, as it conditions both runoff generation and the associated fluxes of suspended sediment.

4.2 . Materials and Methods

4.2.1 . Study site

The Conceição River basin is located on the southern plateau of Rio Grande do Sul, covering an area of approximately 804.3 km^2. The soils found in the area are mainly Ferrasols (80%) although Nitisols (18%) and Acrisols (2%) can also be found. Altitudes range from 270 to 480 m, and the terrain consists of gentle slopes (9%) at the highest points of the basin and moderate to steep slopes near the river and drainage channels (maximum recorded 20%). The land is primarily used for cropland and is mainly cultivated with soybeans (Glycine max) under a no-tillage system in summer. During winter, wheat (Triticum aestivum), oats (Avena sativa and Avena strigosa) and ryegrass (Lolium multiflorum) are cultivated for grain production, as feed for dairy cattle or as a cover crop (Ramon 2021), (Figure 4.1).

No-tillage is applied on more than 80% of the cropland, without the implementation of additional erosion control measures such as terraces, strip cropping, vegetated ridges, or contour farming. Other land uses including forests, wetlands, and urban areas cover less than 15% of the total catchment surface area. The riparian areas found along the permanent river network are narrow ($<$10 m wide) and affected by cattle trampling, which prevents them from providing effective traps to stop sediment originating from upper parts of the catchment. The current land cover distribution in the catchment was used to define a business-as-usual (BAU) scenario representative of the conditions found in areas dedicated to intensive grain farming in southern Brazil.

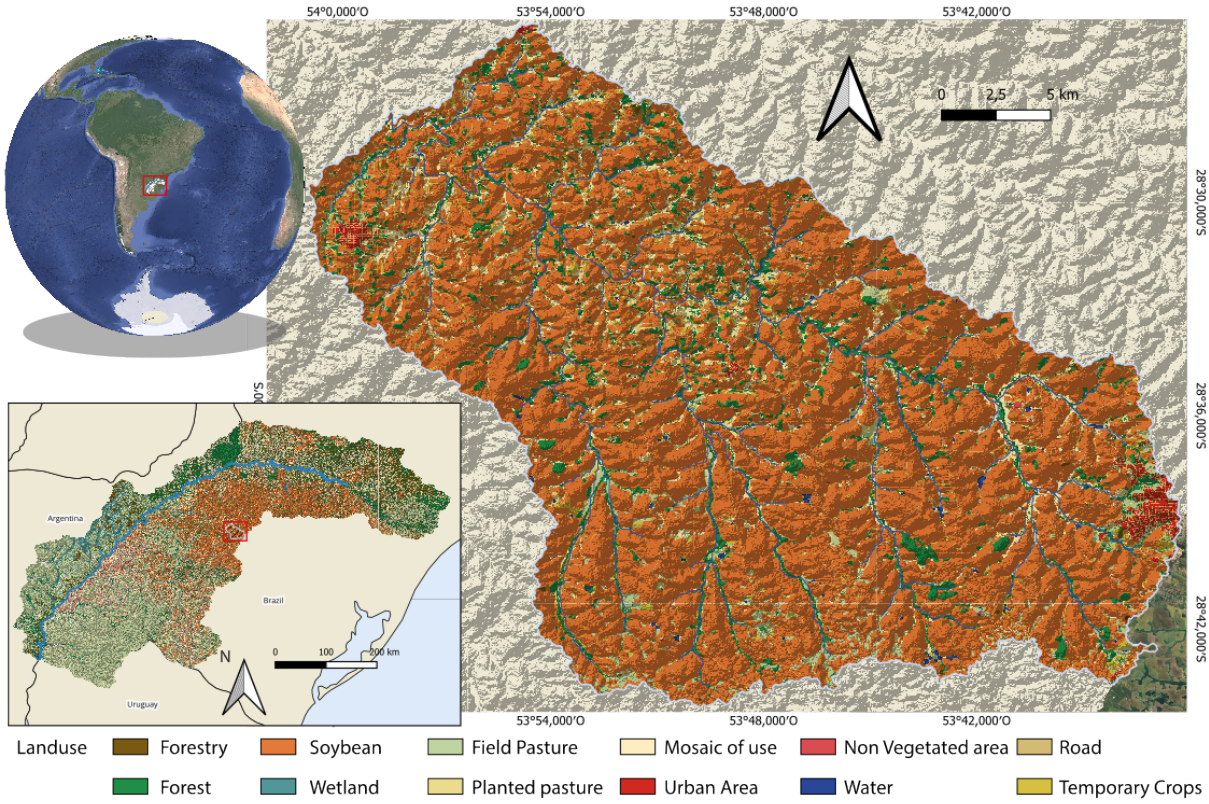

Figure 4.1: **Conceição river basin**, localisation in South America and map of land-uses and covers in 2022 (from Mapbiomas Brazil), background map from OpenStreetMap and Google Imagerie, NASA

4.2.2 . Hydrological survey

All the hydrological data used along this study were acquired prior to this study and most of the data was already published by Didoné et al. (2017).

The water discharge (Q) and suspended sediment concentration (SSC) were monitored at the catchment outlet using automatic equipments that recorded the water level and turbidity every 10 min through a pressure water level sensor and a turbidimeter (Hydrological monitoring station Model SL-2000, Solar®, Brazil), respectively. The Q was calculated from the water level data using a rating curve. The turbidity sensor was properly calibrated with SSC measured data obtained from samples of the water and sediment mixture collected during rainfall-runoff events and in a daily based schedule used for determination of SSC in the laboratory.

The Conceição river basin was equipped for monitoring in 2011 and surveyed until 2019 and multiple years of rainfall, flow and suspended sediments data were therefore collected at the outlet of the basin. Some disturbances with the measurement tools prevented from correctly collecting data in 2012 and 2013.

Suspended sediment concentration (SSC) data were acquired in 10-min intervals indirectly using a turbidimeter. Signals (mV) were converted into NTU by using Polymer bead calibration solutions, and the NTU was converted into SSC by using the SSC equation obtained from daily manual samples using a

DH-48 sampler (USGS). Samples collected during flood events were brought back to the Sedimentology Laboratory at the Federal University of Santa Maria, Brazil, to determine SSC after evaporation and filtration of the samples. In addition to the traditional sampling methods, a turbidity meter was used to increase the frequency of measurements. It was calibrated using SSC data acquired simultaneously. Suspended solid discharge SSD ($kg.s^{-1}$) was estimated by multiplying instantaneous Q ($L.s^{-1}$) and SSC ($g.L^{-1}$) data. SSD was then used to calculate sediment yield (SY; $t.year^{-1}$)

4.2.3 . Methodology

For the event identification, only the 2014-2017 years were used as too much data was lacking for the other studied years. Hydrological events were then identified using the hydroEvents package in R. Baseflow separation was first performed on the discharge time series using a recursive digital filter (baseflowB function) with a filter parameter $\alpha = 0.999$ and three passes. Quickflow was then obtained as the difference between total discharge and estimated baseflow. A high α value was selected to ensure a smooth baseflow separation and avoid overestimation of quickflow during low-flow periods.

Rainfall events were extracted using a peak-over-threshold (POT) approach applied to precipitation data, with a minimum rainfall threshold of 1 mm and a minimum inter-event time of 80 minutes. Similarly, discharge events were identified from the quickflow series using a POT approach with a threshold defined as the 90th percentile of quickflow and a minimum inter-event separation of 80 minutes.

Rainfall and discharge events were subsequently paired using the pairEvents function, allowing for a maximum lag of 200 minutes between rainfall and corresponding discharge responses. Event boundaries were further extended by $\pm$ 80 minutes to ensure full coverage of hydrological responses.

This procedure resulted in a set of 57 paired rainfall–runoff events used for subsequent analysis.

Then, events were manually checked, 8 events were removed due to issues with the measurements of the rainfall or discharge or because the event's runoff coefficient was higher than 1 with no apparent issues in measurements (for study sites of this size, it is possible that the number of hydrological stations was too low to capture all the precipitations occurring in the catchment). 3 events (7,35 and 36) showed distinct multipeaks and were divided into 7 events (7a, 7b, 35a, 35b, 35c and 36a and 36b).

When low punctual inconsistencies were found in the dataset, the values were corrected with simple linear correlation.

The baseflow of the river was also manually corrected for some well defined events, however the baseflow was not corrected when the events were manually divided.

4.2.4 . Indices calculated

For each rainfall and runoff event combination, hydrometeorological variables were analysed at a 10-minute resolution. Event-based time series of precipitation, discharge, baseflow, and suspended sediment concentration were used to characterise catchment response.

Event rainfall was quantified as total precipitation depth, and its temporal distribution was described using cumulative precipitation. Runoff response was characterised through hydrograph analysis, including peak discharge and time to peak.

Direct runoff (quickflow) was estimated as the difference between total flow and baseflow, and expressed as an equivalent runoff depth normalised by catchment area. A runoff coefficient based on quickflow was calculated to quantify the proportion of rainfall contributing to direct runoff (eq. 4.1).

Several approaches were tested to estimate rainfall duration. First, event duration was defined as the total time interval during which rainfall was recorded. Second, a spatially-distributed duration was derived by accounting for the infiltration capacity at the pixel scale and comparing it with rainfall intensity, so that only time periods during which rainfall intensity exceeded local infiltration capacity were considered effective.

All metrics were computed consistently across events to enable inter-event comparison of hydrological and sediment dynamics. The inter-event rain and evapotranspiration were computed in-between events to take into account the available water storage and the saturation of the soils.

$$\text{runoff coeff} = \frac{\text{quick flow volume}}{\frac{\text{total precip}}{1000} * \text{watershed area m}^2} \tag{4.1}$$

4.2.5 . WaterSed simulations

The aim was first to calibrate the spatial representations of the WaterSed model against ^{137}Cs measurements from Chapter 3. However, the high small-scale variability observed in the measurements prevented a robust spatial calibration and the model was therefore parametrised using monitored hydrological events, while accounting for seasonal variability, in order to better constrain the interpretation of long-term soil redistribution rates derived from sediment cores.

The model takes into account the main components of the water balance, including rainfall input, infiltration, soil water storage, percolation, evapotranspiration (ET), and runoff generation. First, the hydrological balance of the catchment needs to be assessed, as sediment export is closely linked to runoff generation and its temporal variability. Only the year 2014 was modelled and the parametrisation focused on soil water storage capacity, infiltration capacity and ET. Infiltration capacity values were defined using order-of-magnitude estimates derived from field knowledge of soil properties within the catchment (forest $50\ mm.h^{-1}$, crops $15\ mm.h^{-1}$, plains $12\ mm.h^{-1}$, roads $4\ mm.h^{-1}$, river $3\ mm.h^{-1}$). The model was used to test different hypotheses about the hydrological response of the catchment. For each event, the water storage was calculated from the previous event by increasing or decreasing its depth based on inter-event rains, percolation and evapotranspiration (ET). Model performance was evaluated by comparing simulated and observed runoff volumes for individual events. Agreement was assessed using the coefficient of determination (R^2) and comparison to the 1:1 line, together with a qualitative evaluation of

bias and dispersion.

4.3 . Results and Discussion

4.3.1 . Monitoring data analysis

The hydrological balance of the Conceição catchment shows clear differences between years in rainfall, discharge, and sediment export over the study period (2011–2017, Figure 4.2). Annual rainfall was the lowest in 2013 and higher during 2015–2017, with the highest value observed in 2016. Discharge followed the general pattern of rainfall variability, although the relationship was not proportional, suggesting differences in runoff response between years, potentially reflecting shifts between excess infiltration runoff (Hortonian), when rainfall intensity exceeds soil infiltration capacity, and excess saturation runoff, which occurs when soils become fully saturated.

The highest annual rainfall occurred in 2016; however, discharge did not reach its maximum during this year. Similar or higher discharge values were observed in 2015 and 2017 under lower or comparable rainfall amounts, indicating that annual runoff response varied over the study period, likely reflecting differences in antecedent moisture conditions, soil water storage, and catchment connectivity. After a careful examination of the dataset, several rainfall events recorded during spring in 2016 appear to be affected by measurement or processing inconsistencies. Specifically, a high number of rainfall records was identified for individual events, exceeding the expected temporal resolution of one measurement every 10 minutes. This suggests a potential issue either with the acquisition system or with subsequent data aggregation. As a result, rainfall totals for these events are likely overestimated and were removed from the subsequent WaterSed simulations.

Sediment export showed stronger contrasts between years than discharge. Moderate sediment loads were observed between 2012 and 2016, whereas a much higher value occurred in 2017. This increase was not proportional to that of annual rainfall or discharge, suggesting that sediment export was influenced not only by water fluxes but also by sediment availability and transfer pathways within the catchment.

At the seasonal scale (Figure 4.3), rainfall and discharge were generally higher during winter and spring and lower during summer. This seasonal pattern was observed over several years, although it became less regular during the wetter period that took place from 2015 to 2017, when elevated values occurred across several seasons.

Seasonal sediment export did not always coincide with the highest seasonal rainfall or discharge. This suggests that part of the sediment response may be affected by temporary storage and remobilisation within the catchment. In this agricultural basin, dominated by no-tillage practices, Ferralsols, and limited riparian forest cover ($<$10m Didoné et al. (2017)) affected by cattle trampling (preventing them from providing effective traps to stop sediment originating from upper parts of the catchment), these patterns

may reflect changes in surface connectivity, soil moisture conditions, and the availability of mobilisable sediment.

Overall, the annual and seasonal balances indicate that the catchment response cannot be described by rainfall amount alone. While discharge broadly follows rainfall variability, sediment export appears to depend on additional controls related to sediment availability and hydrological connectivity.

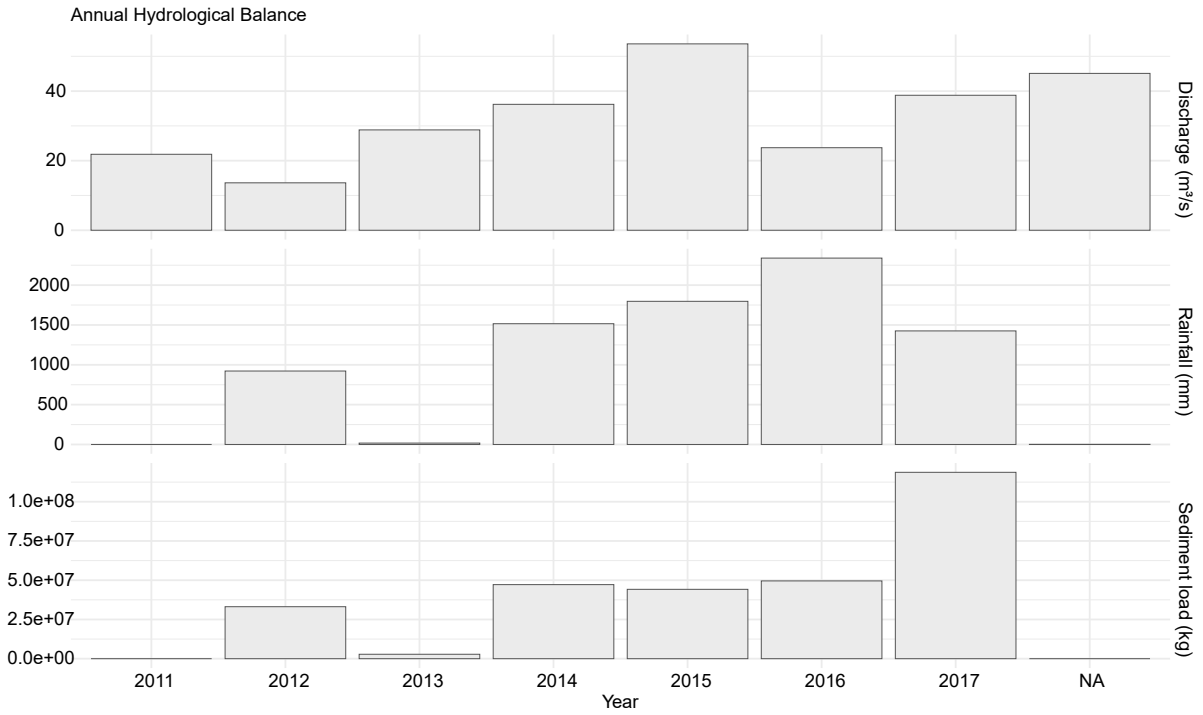

Figure 4.2: Annual hydrological balance with discharge (m^3/s) in the top, rainfall (mm) in the middle and sediment load (kg) in the bottom



Figure 4.3: Seasonal hydrological balance with discharge (m^3/s) in the top, rainfall (mm) in the middle and sediment load (kg) in the bottom, with autumn in red, spring in blue, summer in green and winter in purple.

4.3.2 . Events analysis

The event-scale analysis (Figure 4.4) provides a detailed view of rainfall–runoff response over the 2014–2017 period. Individual events show substantial variability in rainfall amount, peak discharge, quick flow, time to peak, and runoff coefficient, indicating that event response cannot be explained by rainfall depth alone.

Total precipitation per event was generally moderate, with most events being below approximately 100 mm, although a limited number of higher-magnitude events were observed. This distribution indicates that the dataset is dominated by small to medium events, with relatively few extreme events.

Event-scale monitoring for the 2014–2015 period indicates a relatively consistent runoff response, with several events exhibiting moderate to high runoff coefficients under conditions of elevated antecedent rainfall. This clustering suggests reduced catchment storage during this period, allowing a larger fraction of rainfall to contribute to runoff. In contrast, low runoff coefficients are less frequent for comparable rainfall depths, indicating a more efficient hydrological response. These patterns are consistent with a strong influence of antecedent wetness on runoff generation.

Overall, these results indicate that rainfall amount alone is insufficient to explain catchment response. While larger rainfall events can generate higher runoff volumes and peak flows, the magnitude and effi-

ciency of the response depend strongly on antecedent conditions and internal catchment states.

The observed tendency towards lower runoff coefficients during higher-magnitude events may reflect differences in rainfall characteristics and soil hydrological response. In particular, larger events in the dataset were generally associated with lower average intensities, which may have allowed greater infiltration and reduced rainfall excess compared to shorter, high-intensity events. This interpretation is consistent with the contrast between infiltration-excess runoff during intense storms and more gradual soil water replenishment during prolonged events.

In addition, larger events may involve a shift in dominant runoff generation processes, with a greater contribution of subsurface flow or delayed saturation, although this cannot be confirmed with the available data. The role of antecedent soil moisture remains critical, as similar rainfall amounts may produce contrasting responses depending on initial conditions. In addition to hydrometeorological controls, land surface conditions linked to agricultural practices provide an additional source of variability in event response. Based on previous studies of this river basin (Didoné et al. 2017; Ramon 2021), the agricultural calendar in the catchment can be divided into three main periods, which likely influence soil protection, runoff generation, and sediment transfer. The first period extends from September to November, following the winter season and corresponding to the preparation and sowing of summer crops. During this phase, soils are relatively exposed because of field operations and the sparse crop cover of the soil. This period also coincides with more intense rainfall, making the catchment more sensitive to erosion and sediment mobilisation.

The second period corresponds to the main summer crop growing season, when crops are established and vegetation cover increases. During this stage, the soil surface is generally better protected by crop cover, which may reduce direct raindrop impact, surface runoff, and sediment detachment.

The third period corresponds to the post-harvest and winter period, after the summer crops have been harvested and before the following summer crop cycle begins. Rainfall is generally less intense during this period, and the presence of crop residues or winter cover may limit erosion processes compared with the sowing period.

These seasonal differences in land cover and agricultural operations are important for interpreting event-scale response. Events occurring during the sowing period may produce higher sediment mobilisation for a given rainfall amount, whereas events during periods of established crop cover may show a more limited sediment response and higher infiltration due to increased soil protection.

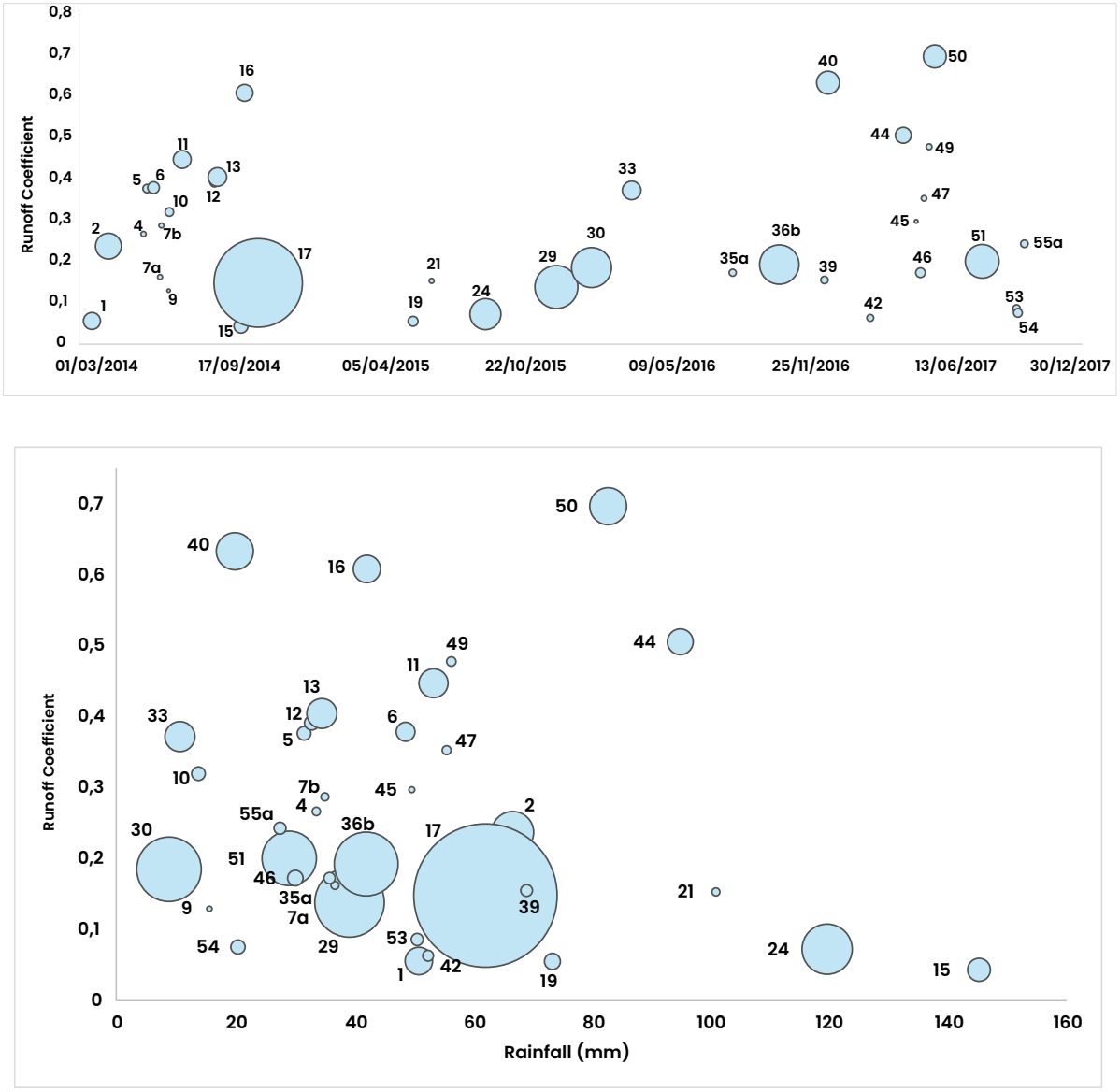

Figure 4.4: In the top, observed runoff coefficient for individual rainfall events. In the bottom, the calculated runoff coefficient plotted against total event rainfall. Marker size is proportional to the calculated net antecedent rainfall and ET for each event (between 0 and 714 mm).

4.3.3 . Watersed runoff simulation

To illustrate the ability of the model to reproduce the main hydrological trends, we have chosen, three parametrisations that were tested to evaluate the ability of the model to reproduce event-scale runoff. First, initial water storage and infiltration capacity values based on field knowledge of the catchment (Figure 4.5.1) were used, resulting in a moderate agreement between simulated and observed runoff (R^2 = 0.51). However, simulated runoff was overestimated, and a substantial dispersion around the 1:1 line was observed, indicating limited predictive accuracy of each event. Several events (e.g., Event 3, Event 7a, Event 14) plot well above the 1:1 line, indicating overestimation, whereas others (e.g., Event 2, Event 12, Event 16) fall below it, indicating an underestimation. The magnitude of deviation from the 1:1 line tends to increase with increasing event values, with the largest discrepancies being observed for

high-magnitude events.

Secondly, simulating the runoff with an increased water storage (Figure 4.5.2), an improvement of the alignment of simulated values with the 1:1 line was obtained. However, runoff remained overestimated overall. In addition, once the storage capacity was exceeded, the model produced widespread runoff, suggesting an overly abrupt transition to saturation-excess conditions.

Thirdly, with increased evapotranspiration and baseline water storage (Figure 4.5.3), results showed a marked decrease of model performance (R^2 = 0.058). Runoff was systematically underestimated, and the deviation from the 1:1 line increased significantly. Overall, the model reproduced the order of magnitude of runoff but remained sensitive to parametrisation choices, and particularly of water storage, evapotranspiration and percolation.

These examples of models test results highlight that runoff generation in the catchment is strongly controlled by the balance between soil water storage, infiltration capacity, and losses (evapotranspiration and percolation). The first configuration demonstrates that a reasonable first-order representation of runoff dynamics can be achieved using physically plausible parameter values. However, the systematic overestimation suggests that either storage capacity or loss terms are underestimated. Increasing the water storage improved the fit to observed data but introduces unrealistic hydrological behaviour. The rapid and widespread runoff generation once storage is filled indicates that the model may overestimate saturation-excess processes, without adequately representing spatial heterogeneity in soil moisture or infiltration. Conversely, increasing evapotranspiration reduced runoff too strongly, leading to a systematic underestimation. This indicates that evapotranspiration cannot be treated as a constant or overly dominant loss term, and likely needs to vary temporally as it has been done in this study.

Overall, these results suggest that a relatively high storage capacity combined with temporally variable evapotranspiration is required to reproduce observed runoff dynamics. The model appears to be capable of capturing intra-annual variability and event-scale trends, but its performance depends on a careful balance between storage and loss processes. At this stage, the model provides a proof of concept that such an approach can reproduce the temporal variability of runoff at the catchment scale. However, further work is required to refine parametrisation, particularly the evapotranspiration dynamics (seasonal variability), the soil water storage capacity as a function of land use and soil properties and the infiltration processes under varying saturation conditions. Future developments could include incorporating land use changes and soil management practices, as well as increasing spatial resolution to explicitly represent hydraulic structures and landscape heterogeneity.

The variability observed between simulated and reference values indicates that model performance remains event-dependent, even after iterative fine-tuning of key parameters (Figure 4.6). The updated simulations, which incorporate adjustments to soil water storage and evapotranspiration (ET) based on the previous configurations, show an improved structuring of the simulated and observed values rela-

tionship, although a tendency toward overestimation persists, particularly for higher-magnitude events. This suggests that the main controls on runoff generation are reasonably captured, but that their relative weighting, especially between storage, infiltration, and losses, still requires refinement.

Some intermediate events remain underestimated, indicating that the model only partially captures threshold behaviour. These processes are known to produce non-linear responses controlled by antecedent moisture conditions and the expansion of saturated areas (Western et al. 2002; Ali and Roy 2010). The coexistence of over- and underestimation across events with different magnitudes highlights the sensitivity of the system to parameter choices and reinforces the importance of accurately representing the balance of water storage capacity and evapotranspiration and percolation.

The coefficient of determination (R^2 = 0.47) is consistent with that obtained with previous simulations and indicates that, while first-order trends are reproduced, a substantial proportion of variability remains unexplained. Accordingly, these results show the intrinsic complexity of the system and the limits of the current parametrisation. In particular, the adjustments performed here represent an initial step toward constraining the orders of the balance between evapotranspiration, soil water storage, and runoff production.

The occurrence of small-scale hydraulic structures within the catchment, such as field check dams and roadside infiltration ditches, may also contribute to the observed variability in model performance. These features temporarily store runoff and locally modify soil moisture and flow paths, delaying the development of connected saturated areas and introducing threshold-like responses (Ali and Roy 2010). However, as these elements operate at spatial scales that are smaller than the model resolution (12 m × 12 m), they are not explicitly represented. In this large catchment (800 km²), their cumulative effect may still influence hydrological response, but this cannot be directly assessed within the current modelling framework.

Overall, these results demonstrate that the model provides a coherent representation of the catchment water balance and captures the main orders of magnitude of event-scale runoff. The fine-tuning undertaken here represents an initial but necessary step in model development. Further improvements will require a more systematic exploration of parameter space and a better representation of spatial and temporal variabilities in key processes, particularly, land use practices (in time and space) and its effect on evapotranspiration and soil moisture dynamics. Such developments are beyond the scope of the present study and would justify a dedicated, more comprehensive investigation.

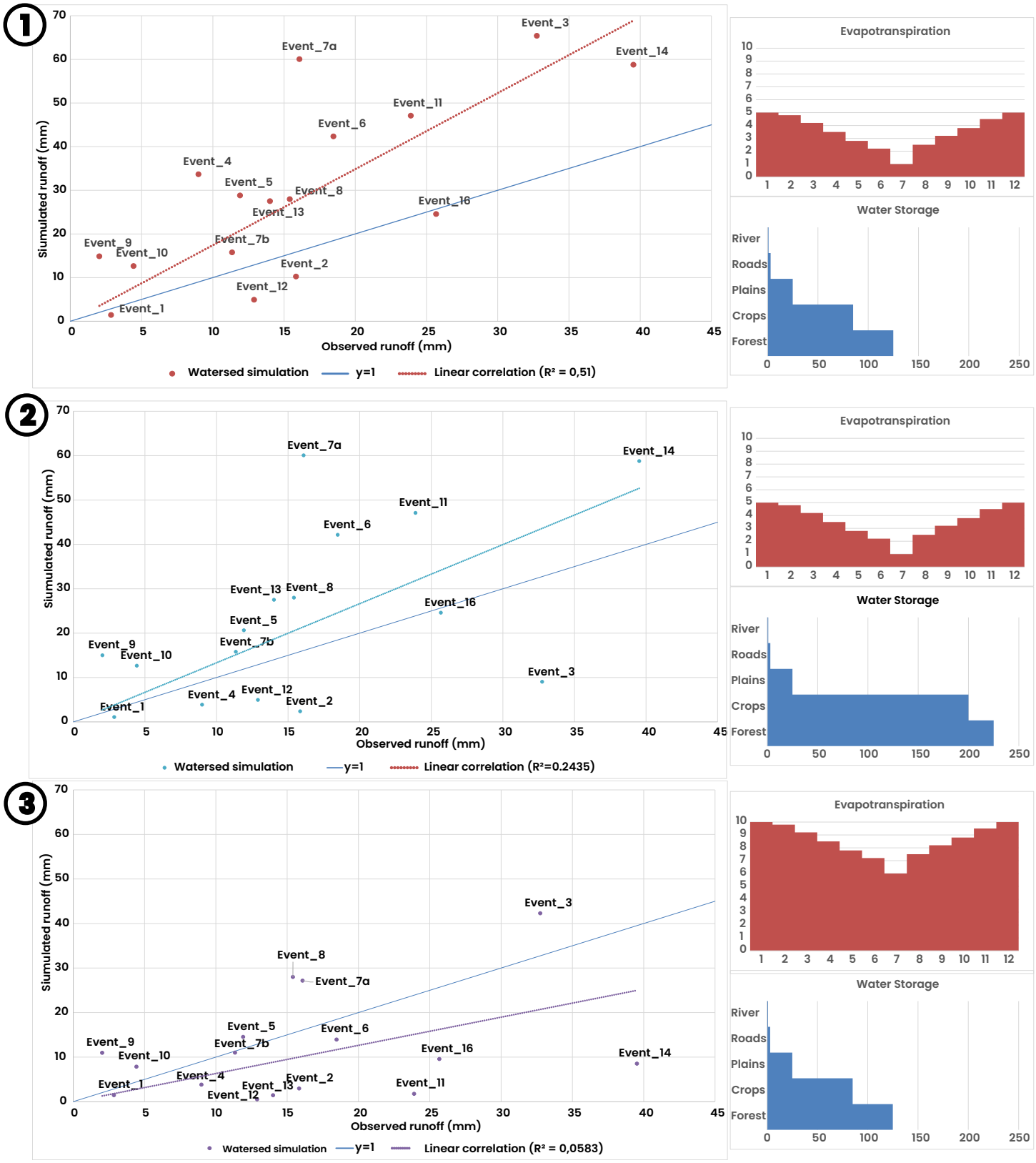

Figure 4.5: Graph of observed and simulated runoff with watersed on the left, ET (red) and water storage (blue) parametrisations on the right of each simulation

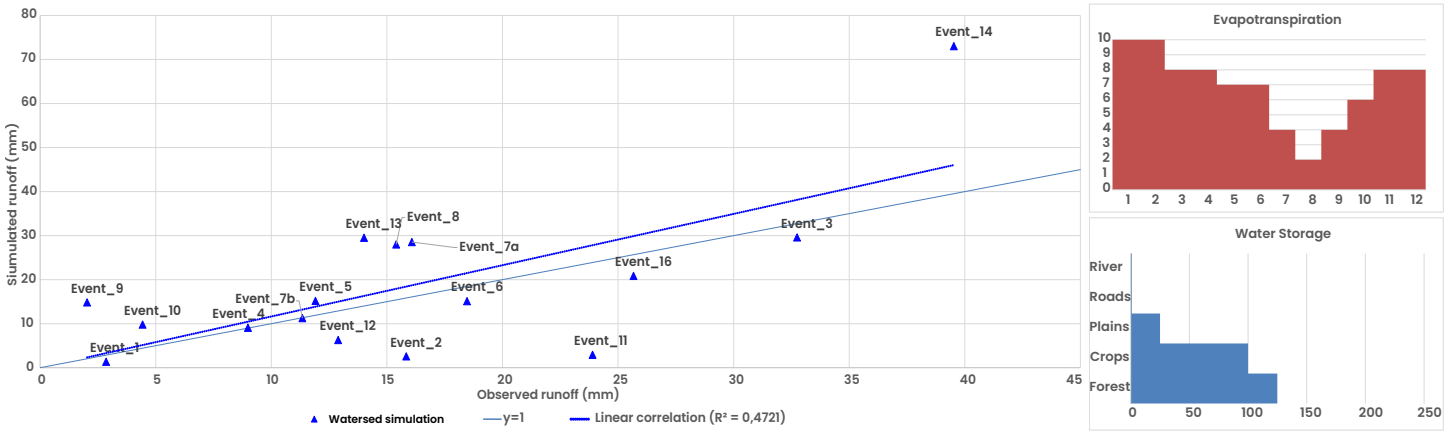

Figure 4.6: Graph of observed and simulated runoff with WaterSed on the left, ET (red) and water storage (blue) fine-tuning parametrisations on the right

4.4 . Conclusions

Taken together, these results indicate that the hydrological and sediment dynamics of the Conceição catchment are primarily governed by internal catchment states rather than by rainfall magnitude alone. Both the analysis of the monitoring and the modelling converge toward the conclusion that antecedent moisture conditions, soil water storage, and the temporal evolution of percolation and ET exert a first-order control on runoff generation and, by extension, sediment transfer. In this context, the WaterSed model successfully reproduces the general magnitude and intra-annual variability of runoff.

This provides a valuable link with the longer-term, multi-annual sedimentary signals derived for following the sediment cores studies, bridging short-term process dynamics and integrated erosion rates over historical timescales. At this stage, the modelling approach therefore constitutes a proof of concept that distributed models can be used to interpret intra-annual variability that cannot be resolved from soil profiles alone.

Further developments are nevertheless required to extend this framework. In particular, improving the representation of soil water storage variability, land management practices, and vegetation dynamics, as well as explicitly incorporating erosion processes (e.g., distinguishing between concentrated and diffuse erosion), will be necessary steps toward a more comprehensive description of soil erosion and sediment redistribution. Such developments are ultimately needed to address the spatial variability of erosion.

Bibliography

Ali, G. A. and Roy, A. G. (2010). Shopping for hydrologically representative connectivity metrics in a humid temperate forested catchment. *Water Resources Research*, 46(12). _eprint: https://agupubs.onlinelibrary.wiley.com/doi/pdf/10.1029/2010WR009442.

Amundson, R., Berhe, A. A., Hopmans, J. W., Olson, C., Sztein, A. E., and Sparks, D. L. (2015). Soil and human security in the 21st century. *Science*, 348(6235):1261071.

Arnold, J. G., Srinivasan, R., Muttiah, R. S., and Williams, J. R. (1998). LARGE AREA HYDROLOGIC MODELING AND ASSESSMENT PART I: MODEL DEVELOPMENT[1]. *JAWRA Journal of the American Water Resources Association*, 34(1):73–89.

Bieger, K., Arnold, J. G., Rathjens, H., White, M. J., Bosch, D. D., Allen, P. M., Volk, M., and Srinivasan, R. (2017). Introduction to SWAT +, A Completely Restructured Version of the Soil and Water Assessment Tool. *JAWRA Journal of the American Water Resources Association*, 53(1):115–130.

Didoné, E. J., Minella, J. P. G., and Evrard, O. (2017). Measuring and modelling soil erosion and sediment yields in a large cultivated catchment under no-till of Southern Brazil. *Soil and Tillage Research*, 174:24–33.

FAO & ITPS (2015). Status of the World's Soil Resources: Main Report. *Food and Agriculture Organization*.

Landemaine, V., Cerdan, O., Grangeon, T., Vandromme, R., Laignel, B., Evrard, O., Salvador-Blanes, S., and Laceby, J. P. (2023). Saturation-excess overland flow in the European loess belt: An underestimated process? *International Soil and Water Conservation Research*, 11(4):688–699.

Montgomery, D. R. (2007). Soil erosion and agricultural sustainability. *Proceedings of the National Academy of Sciences*, 104(33):13268–13272.

Nord, G. and Esteves, M. (2005). PSEM_2d: A physically based model of erosion processes at the plot scale. *Water Resources Research*, 41(8):2004WR003690.

Pimentel, D. and Burgess, M. (2013). Soil Erosion Threatens Food Production. *Agriculture*, 3(3):443–463.

Ramon, R. (2021). *Quantifying sediment source contributions in contrasted agricultural catchments (Uruguay River, Southern Brazil)*. PhD thesis, Universit{\'e} Paris-Saclay ; Universidade Federal do Rio Grande do Sul (Porto Alegre, Br{\'e}sil).

Schindewolf, M., Schmidt, J., and Von Werner, M. (2013). Modeling Soil Erosion and resulting Sediment Transport into Surface Water Courses on Regional Scale. *Zeitschrift für Geomorphologie, Supplementary Issues*, 57(1):157–175.

Western, A. W., Grayson, R. B., and Blöschl, G. (2002). Scaling of Soil Moisture: A Hydrologic Perspective. *Annual Review of Earth and Planetary Sciences*, 30(Volume 30, 2002):149–180. Publisher: Annual Reviews.

Wischmeier, W. H. and Smith, O.D. (1978). AH_537 Predicting Rainfall Soil Losses.

V

Dramatic pesticide transfers fuelled by agricultural expansion in Southernmost Brazil.

Chapter 5

Dramatic pesticide transfers fuelled by agricultural expansion in Southernmost Brazil.

The investigation of soil core representativity provided an important methodological perspective for interpreting the analyses of reservoir sediment cores. While the sediment cores from Rincon del Bonete and Salto Grande integrate sediment and contaminant signals at the scale of large agricultural basins, the hillslope scale study showed that sediment production and redistribution can be highly heterogeneous over distances of only a few metres. Indeed, the high-density sampling of two 12 m $\times$ 12 m midslope plots showed a strong variability in ^{137}Cs and ^{210}Pb$_{ex}$ inventories and in modelled redistribution rates between neighbouring cores. This indicates that individual soil cores may record very local redistribution processes rather than a spatially representative hillslope signal. Therefore, the sediment exported to rivers and ultimately accumulated in reservoirs should not be interpreted as the record of uniform erosion across cultivated hillslopes. Instead, it likely reflects the contribution of connected source areas, including locations where runoff concentrates, gullies develop, terraces modify flow pathways, or soil structure and properties are altered by farming practices.

This chapter differs in structure from the others because it was initially developed as a full-length research article and subsequently condensed to meet the requirements of the target journal. This shortened, publication-oriented organisation was retained, reflecting the successive stages of structuring, synthesis, and revision inherent to this process.

Graphical Abstract

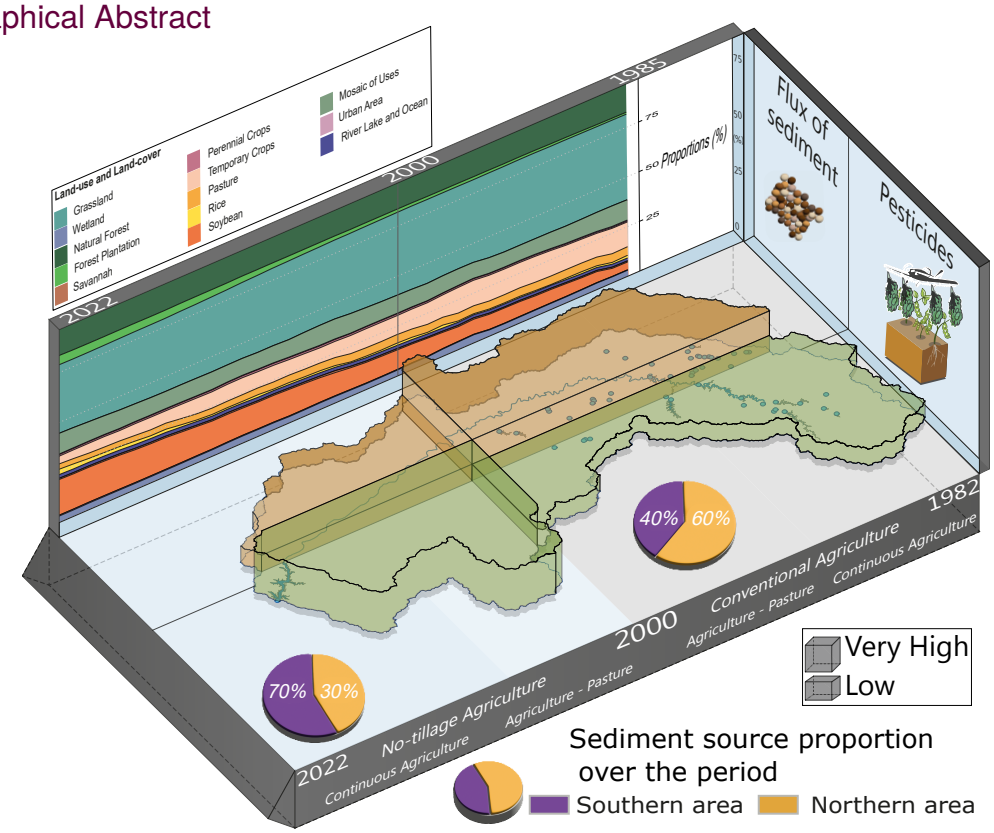

Amaury Bardelle[1], Renaldo Gastineau[2,3], Tales Tiecher[4], Guillermo Chalar[5], Mirel Cabrera[6], Marcos Tassano[6,7], Jean Paolo Gomes Minella[8], Alberto Vasconcellos Inda[4], Nathalie Cottin[2], Pierre Sabatier[2], Anthony Foucher[1], Olivier Cerdan[9], Christine Alewell[10], Olivier Evrard[1]

[1]Laboratoire des Sciences du Climat et de l'Environnement (LSCE, IPSL), Université Paris-Saclay, UMR 8212 (CEA, CNRS, UVSQ),Gif-sur-Yvette,91190,France
[2]EDYTEM, Université Savoie Mont Blanc, CNRS, Bâtiment Pôle Montagne, 5 bd de la mer Caspienne, Le Bourget du Lac,73376, France
[3]International Research Institute of Disaster Science, Tohoku University,468-1 Aramaki Aza-Aoba, Aoba-ku, Sendai, Miyagi, 980-8572, Japan
[4]Department of Soil Science, Faculty of Agronomy, Universidade Federal do Rio Grande do Sul, Bento Gonçalvez Avenue 7712, Porto Alegre, Rio Grande do Sul State, 91540-000, Brazil
[5]Instituto de Ecología y Ciencias Ambientales, Sección Limnología, Facultad de Ciencias, Universidad de la República, Montevideo, Uruguay
[6]Laboratorio de Radioquímica, Área de Radiofarmacia, Centro de Investigaciones Nucleares. Facultad de Ciencias, Universidad de la República, Montevideo, Uruguay
[7]Instituto de Investigacion Una Salud, Universidad de la República, Montevideo, Uruguay
[8]Department of Soils, Universidade Federal de Santa Maria, Santa Maria, F-45060, Brazil
[9]Risk and Prevention Division, Bureau de Recherches Géologiques et Minières (BRGM), Orléans, F-45060, France
[10]Environmental Geosciences, University of Basel, Basel, 4056, Switzerland

Accepted: Under review

Published: Under review



Abstract

The emergence of South America as one of the world's leading agricultural producers has led to significant environmental changes including in the Pampa Biome. However, the impact of this development remains understudied. Here, a multi-proxy analysis of a sediment archive from the Salto Grande reservoir, incorporating pesticide, geochemistry and magnetic measurements, enabled the first long-term reconstruction of land degradation and pesticide fluxes in the very large Uruguay river transnational basin (comprising Brazil, Argentina and Uruguay) since 1982. Sediment fluxes have largely decreased and the main region of the sediment provenance changed since the 2000s, with an increasing proportion of material originating from the southern part of the basin. These changes coincide with dam construction in the north, agricultural expansion in the south and the widespread adoption of no-tillage practices. This change in farming practices induced an increase of pesticide fluxes, thereby representing potential ecological risks. In the context, trade deals such as those between the European Union and the European Free Trade Association and Mercosur, combined with the anticipated increase in the area dedicated to soybean and cellulose production, may contribute to the further expansion of agriculture and intensify related ecological threats.

5.1 . Introduction

Over the past five decades, South America has experienced some of the most significant land-use and land-cover changes worldwide, and these were largely driven by the rapid expansion of agriculture. Pasture, cropland, and tree plantations have spread across the continent, often replacing natural ecosys-

tems that previously supported high levels of biodiversity and ecological resilience (Oliveira et al. 2017; Zalles et al. 2021). Since 1985 CE, the area of pasture has grown by 23%, the area of cropland by 160%, and that of forest plantations by almost 288%, highlighting the extensive scale of this transformation. However, this agricultural intensification has come at a substantial environmental cost: native vegetation has been progressively reduced, with natural tree cover in South America declining by 16% and natural grasslands in Southern Brazil decreasing by 26% (Zurbriggen et al. 2020). These changes accelerated soil degradation and drove biodiversity loss and the fragmentation of natural habitats, thereby undermining the provision of ecosystem services at regional and continental scales (Foley et al. 2005).

Alongside extensive land-use change, South America, and particularly the Río de la Plata Basin, have undergone a shift from conventional tillage-based systems to no-tillage agriculture from the 1990s onwards (Derpsch et al. 2010), with a strong acceleration in the 2000s. No-tillage is expected to increase soil cover and imply crop diversification when a conservation agriculture system (referred to as 'Sistema de Plantio Direto na Palha com Qualidade' in Brazil) is implemented, having a minimal environmental footprint. However, this transition was not observed in the target region in the context of decreasing herbicide costs and the widespread adoption of genetically modified (GM) crops resistant to glyphosate such as soybean and corn (Merotto et al. 2022). This shift created a heavy dependence of farmers on herbicide-based weed control, leading to unprecedented application rates, and consequently, the proliferation of herbicide-resistant weeds, threatening the sustainability of agricultural production over the longer term (Merotto et al. 2022). Intensive glyphosate application also disrupts soil microbial communities, and its metabolites lead to additional ecological and human-health concerns (Gandhi et al. 2021). Notably, (Skidmore et al. 2023) documented a significant rise in pediatric leukemia linked to soybean expansion, likely reflecting increased pesticide exposure through exposure to contaminated supply water.

While the Amazon region often captures the attention of the general public, other regions playing essential ecological roles such as the Pampa (Figure 5.1.A) yet remain understudied (Dinerstein et al. 2017; Andrade et al. 2023). In this context, the Uruguay river basin, covering both the Pampa and the Atlantic Forest biomes within one of South America's most productive agricultural zones, represents an area of particular interest.

Retrospective analyses of reservoir sediment cores were shown to provide a robust and powerful means to reconstruct long-term environmental dynamics in data scarce regions, and have effectively traced back ecological and environmental changes as well as contaminant dynamics and pesticide transfers across diverse environmental settings and temporal scales (Garcia-Rodrıguez et al. 2002; Sabatier et al. 2014; Foucher et al. 2021b; Bizeul et al. 2025).

In the current research, sediment and pesticide transfers were reconstructed across the Uruguay river Basin since the 1980s (Figure 5.1.B). A sediment core was collected in the Salto Grande Reservoir (Figure 5.1.C), which river basin lies within one of Brazil's most productive agricultural zones, the State of

Rio Grande do Sul, the first and second producer of rice and soybean in Brazil, respectively (Brazillian agricultural projection 2023-2024 to 2033-2034, Ministry of Agriculture and Livestock). This region has been undergoing a large-scale expansion of soybean and other crops since the 1980s. Geochemical and sedimentological analyses of the core enabled the quantification of soil erosion rates and the retrospective reconstruction of changes in pesticide usage and remobilisation through agricultural development. Reference material from two sub-basins representative of the northern and southern sectors of the Salto Grande basin were sampled to derive information on sediment provenance within the basin, and the occurrence of potential changes of this provenance with time.

The originality of the current research lies in the multiproxy reconstruction of sediment and pesticide dynamics in relation to environmental and socio-economic trends, which is almost unique in a region where historical archives and data are scarce. More specifically, the main objective of the current research was to reconstruct the temporal evolution of erosion rates and associated pesticide fluxes from 1982 to 2023 in the Uruguay basin in response to changes in land use and agricultural practices. The socio-economic reasons for these changes were also investigated.

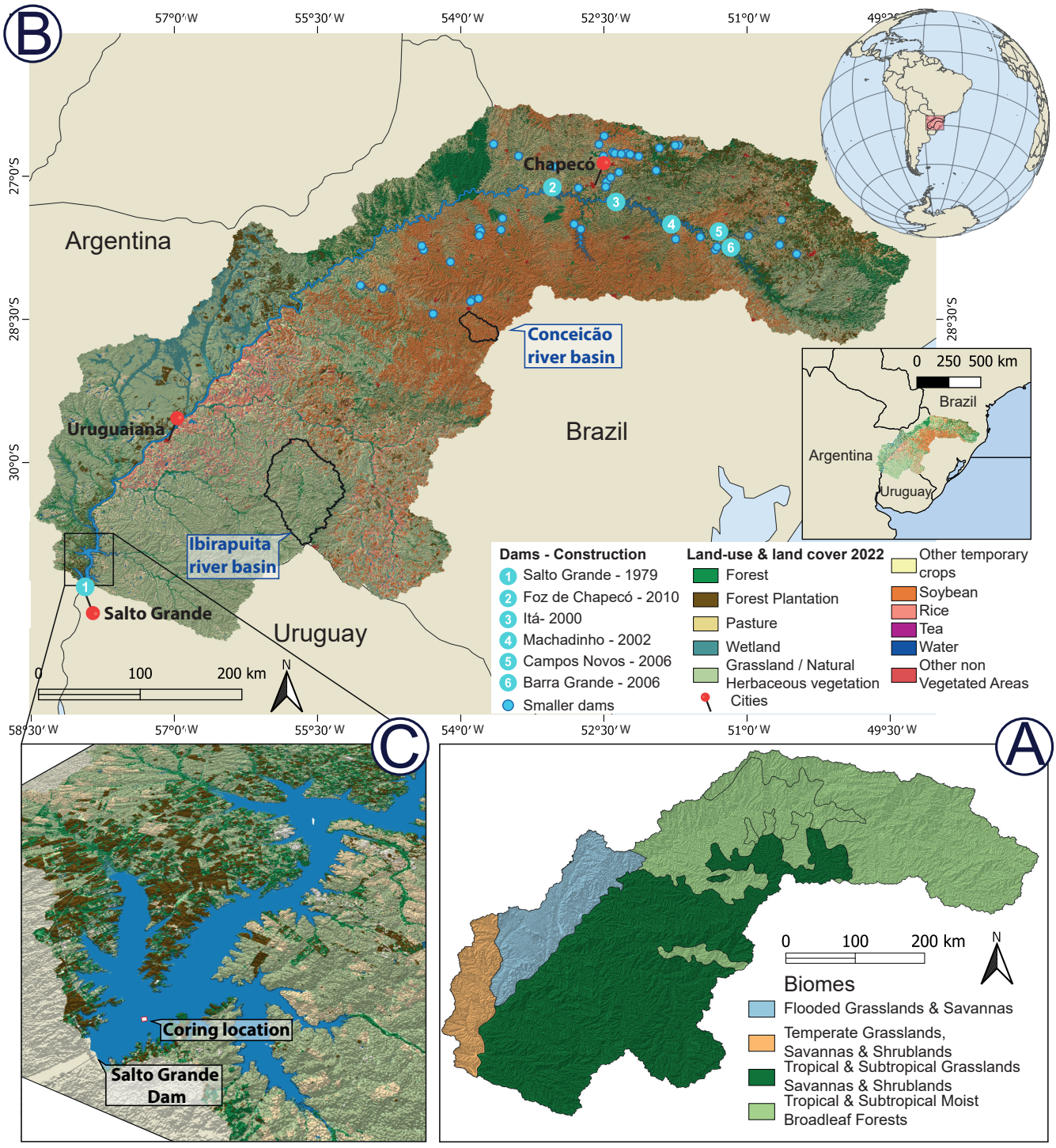

Figure 5.1: **Biomes** of the Salto Grande basin (A), **location of the study site**, in the river basin, in South America, map of land-uses and covers in 2022 (from Mapbiomas Argentina, Pampa and Brazil) with the location of Ibirapuitã and Conceição sub-basins (B) and coring location (S32°49.072', W56°24.008') (B), background map from OpenStreetMap

5.2 . Materials and methods

5.2.1 . Study site

The study site was located on the Uruguay river at the Salto Grande (SG) dam, along the border between Uruguay and Argentina. At the SG dam, the Uruguay river drains an transnational surface area of approximately 266,000 km^2 (Figure 5.1, Ramon (2021)). Of this area, 70% is located in southern Brazil, 20% in Argentina and 10% in Uruguay. Land-use in the river basin is primarily agricultural, with intensive farming production in the Brazilian states of Rio Grande do Sul (RS) and Santa Catarina (SC). Small farms (< 50 ha) predominate in the hilly upper parts of the basin while larger properties (mostly < 100 ha) dominate the lower areas, primarily used for the production of soybeans (*Glycine max*), corn (*Zea mays*), and wheat (*Triticum Aestivum*). Similar land uses are observed in Argentina, where plantations of mate (*Ilex paraguariensis*), tea (*Camellia sinensis*), and eucalyptus (*Eucalyptus globulus*) prevail (Ramon 2021). In the alluvial plain, larger farms (> 100 ha) dominate in the southwestern regions of RS and northern Uruguay. These regions are mostly used for extensive ranching and irrigated rice production. The southernmost part of the Argentinian part is made up of flooded grasslands and savannahs. This extremely flat region has hydromorphic soils, which are ideal for pastures and commercial forest plantations used for wood and cellulose extraction. The reservoir of the Salto Grande dam spends over 783 km^2 (between 500-1500 km^2) with a mean depth of 6.4 m.

5.2.2 . Data sources

5.2.3 . Reconstruction of the land-use and land-cover

Land-use and land-cover were reconstructed in the investigated catchment using a freely available set of maps provided by the MapBiomas network. As no dataset was available for the entire Salto Grande river basin, the maps were reconstructed based on multiple MapBiomas datasets : Mapbiomas Argentina, Pampa and Brazil (Mapbiomas Argentina, Pampa and Brazil).

The land-use and land-cover maps used in this study are derived from the most recent available versions. These products provide annual land-use and land-cover data from 1985 to 2023 at a 30-m spatial resolution across a comprehensive set of classes including forest, pasture, cropland, urban areas, and water bodies with consistent temporal coverage. These datasets were therefore proven to be valuable for reconstructing trends in agricultural expansion, deforestation and other land-use changes driven by human activity across the broader regions of southern Brazil, northern Argentina, and Uruguay (Souza et al. 2020; Baeza and Paruelo 2020). Its annual temporal resolution makes it particularly suitable for analysing long-term land-use patterns and evaluating the effects of environmental and agricultural policies across this diverse and dynamic landscape. Although the datasets afford robust insights into broad trends, cautious interpretation of specific land-cover transitions is required for identifying fine-scale tran-

sitions or mixed-use landscapes.

5.2.4 . Sample collection

Sediment core

Three sediment cores were collected from the Salto Grande dam during fieldwork conducted in december 2022 (IGSN number: 10.58052/IEFOU002F). A gravity corer equipped with 90 mm PVC liners and a floating platform, which was made available by the Salto Grande dam authorities, were used for that purpose. The analyses were conducted on the longest core, SG03, showing a length of 73.5 cm.

Sediment source sampling

Potential sediment sources from two upstream sub-catchments, which were defined as representative of the two major zones that may supply sediment to the Uruguay river (Tales Tiecher 2015; Ramon 2021), including the Northern basaltic plateau and the Southern Pampa, were collected. The goal was to characterise and compare their respective sediment properties, in order to determine their relative contributions to the sediment accumulated in the dam reservoir, and their potential variations throughout time. Tales Tiecher (2015) and Ramon (2021) collected suspended sediments close to, or at the outlet of the Conceição river basin in 2012 and Ibirapuitã river basin in 2021, respectively (5.9.1).

5.2.5 . Methodology

Resolution of the different analyses conducted on the sediment core and their respective units are summarized in table 5.1. The specific methodology applied for each studied parameter is detailed in supplementary material (5.9)

Analysis conducted	Studied parameters	Resolution	Units
Particle size analysis	D10, D50, D90	1 cm	μm
CT-scanner	Relative density	0.625 mm	Grey value
Bulk density	Bulk density	1 cm	$g.cm^{-3}$
Organic matter analysis	TOC, TN, δ^{13}Corg	1 cm	% + ‰
XRF Geochemical analysis	Mg, Al, Si, P, S, Cl, Ar, K, Ca, Ti, V, Cr, Co, Mn, Fe, Co, Rh, Ni, Cu, Zn, Ga, As, Br, Rb, Sr, Y, Zr	0.5 mm	counts per second
Gamma spectrometry analysis	$^{210}Pb_{ex}$, ^{137}Cs	1 - 1.5 cm	$Bq.kg^{-1}$
Magnetic susceptibility analysis	high (χ_{HF}) and low χ_{LF} frequencies magnetic susceptibility	1-1.5 cm	m^3kg^{-1}
Pesticide analysis	See Table 5.3 for full list	2-4 cm	$mol.cm^{-2}.yr^{-1}$
Fluxes of sediments	MAR	0.625 mm	$g.cm^{-2}.yr^{-1}$
X-ray diffractometry	Mineralogical composition	1-1.5 cm	angstroms (Å)

Table 5.1: Summary of analyses conducted, parameters studied, resolution of the data, and measurement units.

Age model, Sediment and Pesticides fluxes

The sediment core chronology was established using the activities of $^{210}Pb_{ex}$ measured in a set of 16 samples of dried material collected along the core. Depth increments of 1.5 cm were taken every five cm down to 60 cm (n=13), with additional samples collected at depths of 17.5, 22.5 and 70 cm. The *serac* R package for ShortlivEd RAdionuclide Chronology (Bruel and Sabatier 2020) was used to establish the age model via the Constant Flux Constant Sedimentation (CF:CS) model.

Sediment fluxes (MAR, Mass Accumulation Rate,$g.cm^{-2}.yr^{-1}$) were reconstructed by multiplying the Sediment Accumulation Rate (SAR, $cm.yr^{-1}$) obtained from the CF:CS age model by the high-resolution DBD calibrated from the CT scan values ($g.cm^{-3}$) (equation 5.1).

$$\text{MAR } (g.cm^{-2}.yr^{-1}) = \text{Sedimentation rate } (cm.yr^{-1}) \cdot \text{DBD } (g.cm^{-3}) \tag{5.1}$$

A total of 16 pesticides and their metabolites (Table 5.3), which are commonly reported in the literature of the region of interest (López et al. 2012; Mañay et al. 2004; Palladino et al. 2023; Rodríguez-Bolaña et al. 2024), were measured at EDYTEM Laboratory (Univ. Savoie Mont-Blanc, France) .

To conduct the pesticide analyses, the second half of the core collected as described above was sampled following 2-cm depth increments from 0 to 25 cm and then following 4-cm depth increments from 25 cm to 55 cm.

Pesticide fluxes were derived from the sediment fluxes. Therefore, the moles of pesticides were converted into fluxes by multiplying the pesticide concentrations with the MAR (equation 5.2).

$$\text{Fluxes of pesticides } (\text{mol.cm}^{-2}.\text{yr}^{-1}) = \text{Pesticides } (\text{mol.g}^{-1}) \cdot \text{MAR } (\text{g.cm}^{-2}.\text{yr}^{-1}) \tag{5.2}$$

Sediment Fingerprinting

The sediment fingerprinting analysis of the core was conducted in accordance with the recommendations of Chalaux-Clergue et al. (2024) and using the freely available FingR package from Chalaux-Clergue and Bizeul (2025). The magnetic susceptibility parameters were used in the fingerprinting analysis, as these allowed a good discrimination between the upper and lower parts of the river basin, as initially demonstrated by Ramon (2021). The three-step method described by Chalaux-Clergue et al. (2024) was applied to select the tracers used for fingerprinting. This method first involves a range test to identify conservative properties. Secondly, a Kruskal–Wallis H test is applied to identify discriminant properties. Finally, a discriminant function analysis (DFA) or a principal component analysis (PCA) with forward stepwise selection based on the Wilk's lambda criterion is applied to identify the best subset of predictors amongst the identified tracers (i.e. conservative and discriminant properties). The Bayesian Mean Model was then applied to calculate sediment source contributions along the Salto Grande sediment core for

successive 1-cm increments characterised for their magnetic susceptibility properties. The performance of the model was assessed using virtual mixtures created with the FingR package.

5.3 . Results

5.3.1 . Evolution of the land-use and land-cover

In 1985 Common Era (CE), the Salto Grande river basin was already used for agriculture, with 19.3% of the river basin used either for cultivating soybean (3.9%), rice (1.4%), 'other' temporary crops (13%) and forest plantations (1%), although a large part of the river basin was still occupied by natural habitats, grasslands (43.1%), native forest (17.4%), pasture (4.3%) and savannahs (0.5%, Figure 5.2).

Nowadays, the agricultural activities account for 29.9% of the of the total river basin's area, including soybean (17.9%), forest plantation (4.6%), rice (2.7%) and other temporary crops (3.8%) while natural habitats such as grasslands occupy 34.4% of the river basin Figure 5.2).

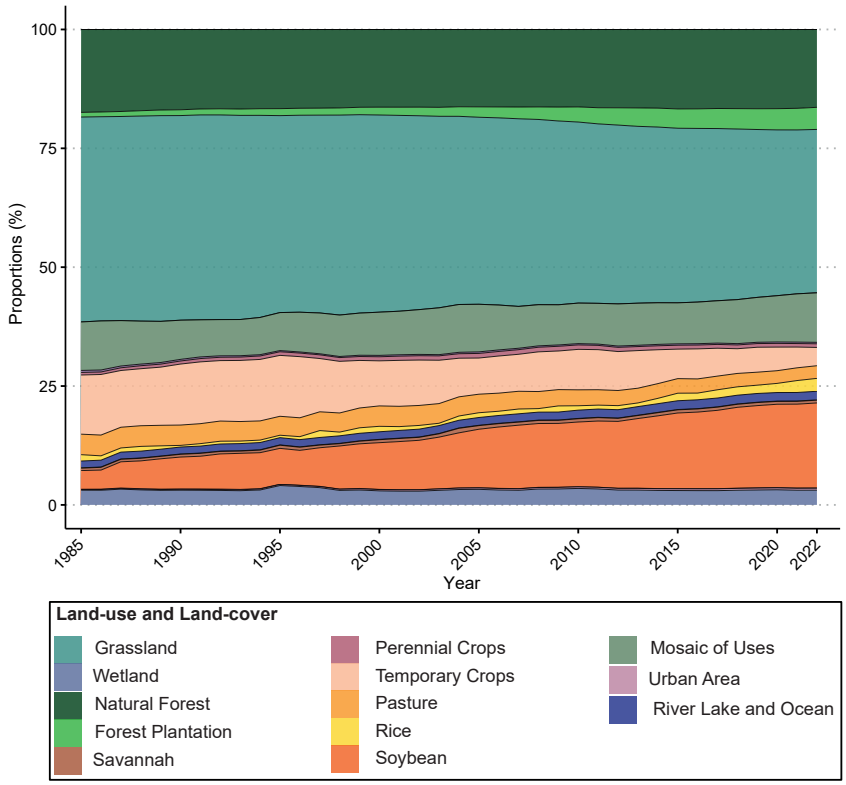

Figure 5.2: **Evolution of the land-use and land-cover in the Salto Grande river basin**, Main land-uses and land-covers from 1985 to 2022, data from Mapbiomas Argentina, Pampa and Brazil

5.3.2 . Core description

The core collected and referred to as SG03 was composed of two units, the sediment sequence (0-52 cm), composed of homogenous fine particles (D10, D50 and D90 indices of 0.6 $\pm$ 0.02, 6.3 $\pm$ 0.08 and 42.4 $\pm$ 7.14 µm, respectively, Figure 5.3) and the soil exposed before the dam construction from 52 to 73.5 cm. TOC concentrations in the sediments ranged from 1.98 to 4.14 g C.kg^{-1} (4.61 to 5.77 g C.kg^{-1}

in the soil, Figure 5.3). δ^{13}C ranged from -22.5‰ to -15.3‰ in the sediments (23.3‰ to 24.6‰ in the soil Figure 5.3). The values obtained are consistent with those of a mix of C_3 and C_4 vegetation, both being naturally found in the Salto Grande river basin (Overbeck et al. 2007). A more detailed description of the core is provided in supplementary material (5.7.2).

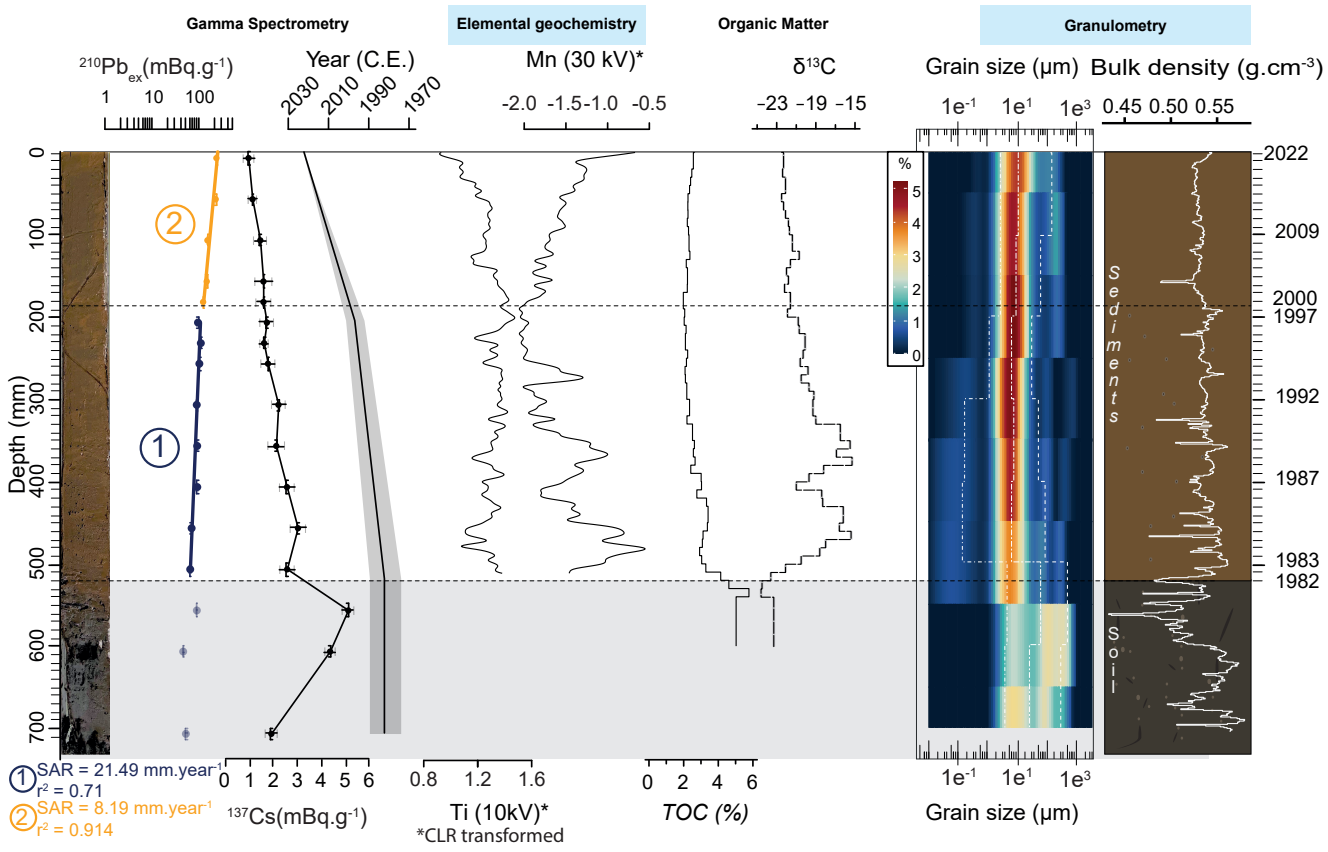

Figure 5.3: Sediment characteristics along the SG03 sediment core, granulometry, Organic Matter (TOC and $\delta^{13}C$), elemental geochemistry (Mn measured at 30kV and Ti at 10kV) results and $^{210}Pb_{ex}$ age model.

5.3.3 . Geochemical analyses

Geochemical analyses reveal the occurrence of two phases in the sediment sequence with low increases of Titanium (Ti) and decreasing Manganese (Mn) counts from 19-52 cm, with the observation of significant Mn peaks at 48, 35 and 26 cm followed by a decrease of Ti and an increase of Mn from 0-19 cm (Figure 5.3). These variations reflect periods of higher (19-52 cm) and lower (0-19 cm) terrigenous contributions (5.9.5) and a possible shift in sediment provenance or a change in redox conditions in the lake (5.9.5).

5.3.4 . Gamma spectrometry and chronology

The $^{210}Pb_{ex}$ activities along the SG03 core decreased following two linear trends (r^2 = 0.71 from 19-52 cm and r^2 = 0.9 from 0-19 cm, Figure 5.3). The change in sedimentation rates was fixed based on the Ti and Mn variations and the distribution of the $^{210}Pb_{ex}$ activity data. Based on the Constant Flux Constant Sedimentation model (Bruel and Sabatier 2020), the base of the lake sediment sequence at

52 cm was dated to 1982 (±6 years), which is consistent with the dam inauguration year (1979). An average sedimentation rate (SAR) of 21.5 ± 4.6 $mm.yr^{-1}$ was found from 19-52 cm, while a rate of 8.2 ± 1.5 $mm.yr^{-1}$ was found from 0-19 cm (Figure 5.3).

^{137}Cs was detected from the bottom to the surface of the core with activities ranging between 0.9 and 5.0 $Bq.kg^{-1}$ (at 55 cm depth). The relatively low values of ^{137}Cs found in the sediment sequence (0-52 cm) are consistent with the dating of the bottom of the sediments sequence to 1982 CE. The bottom unit consists of soil exposed before the dam construction, relatively enriched in ^{137}Cs (52-73.5 cm) with a peak at 55 cm, corresponding to a typical soil profile with higher levels of nuclear bomb fallout in the uppermost soil layer (Foucher et al. 2021a).

5.3.5 . Sediment source fingerprinting

The potential of multiple tracing properties (including radionuclides, elemental geochemistry and visible spectroscopy) to identify sediment provenance in the region has been tested (Tales Tiecher 2015; Ramon 2021). Nevertheless, the best discrimination was achieved through the use of magnetic properties and mineralogical composition. Reference material from the two sub-basins of interest, i.e. the southern and northern sections of the Salto Grande River basin (5.8) showed indeed distinct magnetic signatures. These properties were therefore compared to those of Salto Grande reservoir sediment and used to calculate shifts in the relative contributions of sources.

The northern area shows an elevated susceptibility in both high and low frequencies ($\chi_{HF-North}$ $[9.15.e^{-6}$ - $1.93.e^{-5}]$ and $\chi_{LF-North}$ $[9.87.e^{-6}$ - $1.98.e^{-5}]$ m^3kg^{-1}), while the southern area is almost non-responsive in both high and low frequencies ($\chi_{HF-South}$ $[2.73.e^{-7}$ - $7.08.e^{-7}]$ and $\chi_{LF-South}$ $[3.80.e^{-7}$ - $7.84.e^{-7}]$ m^3kg^{-1}). According to the magnetic susceptibility map of Rio Grande do Sul provided by Ramos et al. (2021), a clear decrease in susceptibility is observed from the north to the south of the State. This pattern reflects contrasting lithologies : soils of the northern part were formed on the basaltic Paraná/Serra Geral formation, rich in Fe oxides, the weathering of which generated fine ferrimagnetic particles, and thus strong soil magnetic signatures (Fodor, 1985). Conversely, in the south, soils are mainly derived from andesite and schist, which are materials depleted in oxides and characterised by a low magnetic susceptibility, which explains their low magnetic signatures.

The validity of this hypothesis is confirmed by the fact that the magnetic signature of sediments from the Salto Grande reservoir lies in-between both end-members ($\chi_{HF-Salto\ Grande}$ $[1.73.e^{-6}$ - $8.98.e^{-6}]$ and $\chi_{LF-Salto\ Grande}$ $[1.87.e^{-6}$ - $9.82.e^{-6}]$ m^3kg^{-1}). Furthermore, a shift in signature can be observed throughout time : sediments that deposited between 1983-2000 show a signature closer to that of the northern sub-basin material while sediments that deposited in more recent years (i.e., 2000-2023) show a signature closer to that of the southern sub-basin material. This shift is further supported by temporal changes in mineralogical composition, with the lower part of the sediment sequence (20–52 cm) containing higher proportions of kaolinite and iron oxides (hematite + goethite) than the upper section (0–20

cm), while the opposite pattern is observed for quartz (5.9).

A three-step method (Chalaux-Clergue et al. 2024), testing the conservativeness, the discriminant power, and selecting the best set of tracers, confirmed that magnetic susceptibility measured at high and low frequencies provided the optimal suite of tracers for distinguishing material from both source regions (5.10). An un-mixing model was then applied to estimate the proportions of sediment derived from the northern and southern parts of the basin in each depth increment of the core.

Results of this Bayesian Mean Model showed the occurrence of two periods with distinct dominant contributions from both sources. A first period, from 1982-2000, was dominated by the northern area contribution while the second period, from 2000-2023, showed an important shift towards a stronger contribution of the southern area.

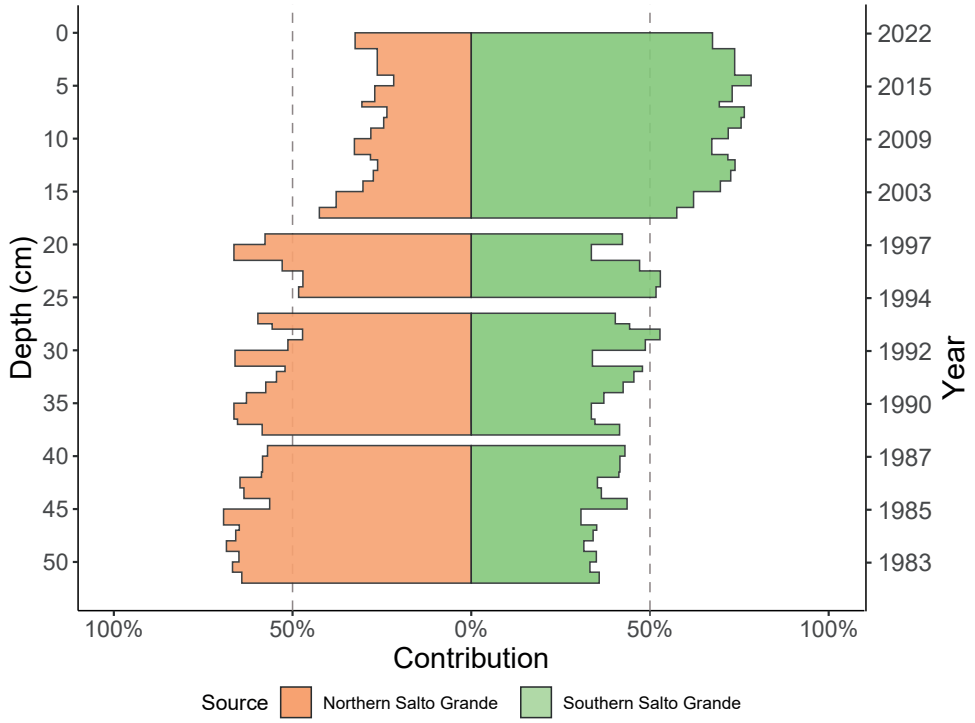

Figure 5.4: Mean contributions of the two potential sediment sources - Southern basin part (in green on the right) and Northern basin part (in orange on the left) when running the Bayesian Mean Model using the FingR package

5.3.6 . Pesticides

All the 16 pesticides analysed were detected in variable concentrations along the core, and contrasting fluxes ($mol.cm^{-2}.yr^{-1}$, Figure 5.5) were therefore calculated depending on the substance and period considered. Since post-depositional mobility may be an issue for all pesticides, the first detection depth and production date, or marketing authorisation, of each compound (Table 5.3) in Brazil, Argentina, and Uruguay were compared to the pesticide downcore profiles for those substances for which this data was available. Only the sums of broad categories of pesticides (i.e., insecticides, herbicides, fungicides) are shown in this section. The detailed pesticide results are presented in the supplementary material, (5.8), along with the corresponding graphs (5.11).

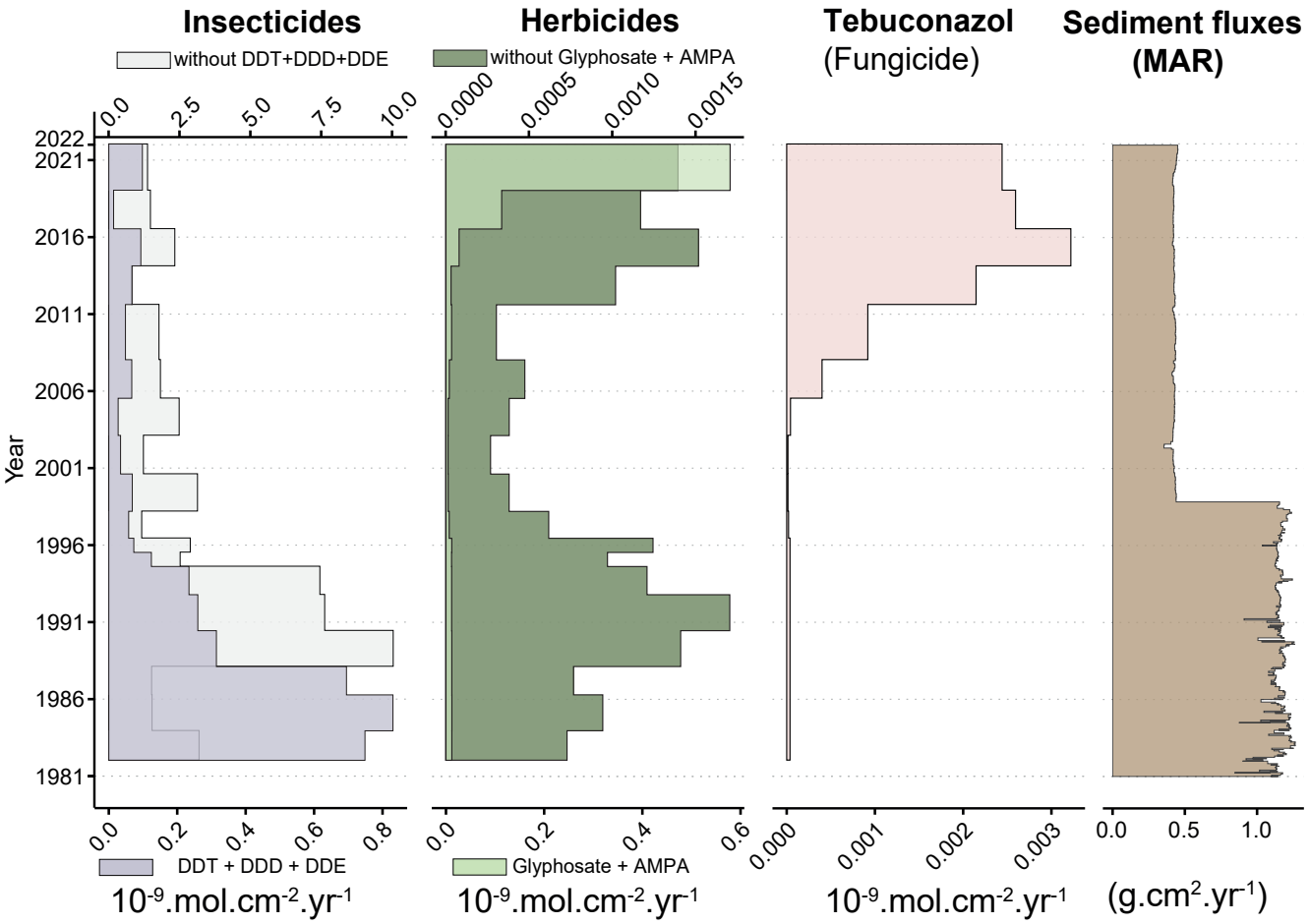

Figure 5.5: Total fluxes (in 10^{-9} mol.cm^{-2}.yr^{-1}) of insecticides without DDT, DDD and DDE (grey) and DDT + DDD + DDE (light purple), Ampa + glyphosate (light green) and total herbicides without AMPA and glyphosate (dark green), fungicides (red) as well as sediment fluxes (mass accumulation rate,MAR, in g.cm^2.yr^{-1}, brown) in the Salto Grande sediment core.

Three periods of herbicide and insecticide inputs are observed (Figure 5.5). The first period, from 1982 to the mid-1990s, shows a high usage of insecticides and herbicides and a low usage of fungicides. Then, from 2000 to 2005, a lower input of pesticides is observed for all categories of substances. Finally, from 2005 onward, an increase in herbicides and fungicides is found along with a continuous decrease of insecticides.

More specifically, records obtained during the first period are consistent with a high usage of broad-spectrum herbicides (diuron and s-metolachlor, 5.11 and one selective herbicide, 2,4-D) and insecticides (chlorpyrifos ethyle, endosulfan, and mirex, 5.11), while the second period shows a high usage of selective herbicides (simazine, atrazine 5.11) and broad-spectrum products with glyphosate and the use of mostly broad-spectrum insecticides (chlorpyrifos ethyle, imidacloprid, and fipronil, 5.11) along with mirex, mainly used in forest plantations (5.11).

Risk characterisation ratios (RCRs), were calculated from measured pesticide concentrations and their respective predicted no effect concentration in the sediments ($PNEC_{sediment}$) values (Table 5.2, with values $>$1 indicating a potential ecological risk). Most substances, including glyphosate, AMPA and

mirex, were associated with RCRs < 1, suggesting no apparent ecological risk under present conditions. In contrast, several substances exceeded this threshold. Atrazine (RCR = 1.06) slightly exceeded the corresponding PNEC value, while chlorpyrifos ethyl (RCR = 9.36) and fipronil (RCR = 16.4) indicated higher ratios, suggesting potential effects on benthic organisms. The pesticides that exceeded the most the PNEC values in the uppermost 2 cm of the sediment core correspond to legacy pollutants: endosulfan (RCR = 400) and DDT (RCR = 677) along with it's metabolites DDD and DDE (RCR = 1.9 - 30 and RCR = 0.5 - 3, respectively, depending on the isomers), which could potentially pose a very high risk to benthic communities.

5.4 . Discussion

Through a comprehensive and original multi-proxy approach, this study revealed how the construction of dams, land-use and land-cover transitions, the massive introduction of GM crop monocultures and the shift to no-tillage practices influenced the reduction of sediment fluxes and changes in contaminants observed in the vast and understudied region of the Pampa biome.

5.4.1 . Origin in changes of sedimentation rates from the 1980s to the 2020s

Major changes in sediment properties and detrital inputs were observed before and after 2000 CE (Figure 5.3). Several hypotheses may be put forward to explain this shift.

Firstly, in the late 1990s, five major dams and a series of smaller dams were constructed on the upper Salto Grande river (Figure 5.1). The decline in MAR observed after 2000 (Figure 5.5) may partly reflect sediment trapping by these structures, which likely intercept a substantial fraction of upstream sediment (Cantalice et al. 2015).

Secondly, beyond dam sediment trapping, reduced sediment fluxes may originate from shifts in farming practices. No-tillage was adopted to limit severe soil losses (Didoné et al. 2019; Fuentes-Llanillo et al. 2021). However, the implementation of no-tillage alone (without crop rotations, contour farming, etc.) over the long term may lead to soil sealing and compaction inducing increased runoff, which can concentrate downslope and initiate gully erosion, thereby mobilising subsoil material (Didoné et al. 2017, 2019; Bernardi et al. 2024). This change in dominant soil erosion processes is likely reflected by the ^{137}Cs activities in the core (Figure 5.3). Indeed, following nuclear fallout, ^{137}Cs accumulated predominantly in topsoils Chaboche (2021). The decreasing activities observed throughout the core then likely reflect either the prior removal of these upper horizons or the increased mobilisation of deeper subsoil layers depleted in fallout radionuclides. Such patterns are consistent with increased runoff and the shift from diffuse to concentrated erosion across the basin (Evrard et al. 2020; Londero et al. 2021).

Thirdly, historical land-use maps show a catchment southward expansion of agricultural land since 1985 (5.6). Sediment fingerprinting (Figure 5.4) corroborates this trend, revealing a growing contribution of sediments from the southern part of the river basin, which is consistent with these land-use shifts.

These hypotheses are not mutually exclusive and it is most likely that the combination of all these factors culminated in the observed changes in the sediment fluxes.

5.4.2 . Evolution of the contamination from the 1980s to the 2020s

Brazil has risen among the world's largest pesticide consumers, largely driven by intensive agriculture and the predominance of GM crops resistant to herbicides (mostly glyphosate). The sediment core reflects this evolution, preserving a chronological record of pesticide inputs.

Based on the results regarding land-use and land-cover changes and the increase of the proportion of sediment originating from the southern part of the river basin, it is hypothesised that the rise of herbicides after 2010 likely results from the massive transformation of the Pampa from natural grassland to cropland and the generalisation of monocroping under no-tillage without the associated soil conservation measures expected to be implemented in the region (Merotto et al. 2022). Furthermore, the increase of the fungicide analysed (tebuconazol) may reflect the expansion of the soybean cultivation area in the region from the mid-2000s (Figure 5.5).

Furthermore, atrazine, chlorpyryfos ethyl, fipronil, S-metolachlor, endosulfan and DDT showed RCR values exceeding 1, which indicates a potential ecological risk (5.2).

Resurgence of DDT (RCR = 677.1) was recorded in the uppermost centimetres of the core corroborating the widespread herbicide use. This resurgence likely originated from remobilised legacy residues stored in the soils and associated with widespread applications for vector control programs targeting malaria and yellow fever shortly after World War II.

Moreover, most of the studied pesticides are still currently authorised to be used in the region (López et al. 2012; Merotto et al. 2022).

The general decrease in the use of insecticides from the late 1990s until the late 2000s (Figure 5.5) could be attributed to the implementation of integrated pest management (Hoffmann-Campo et al. 2003), which might have allowed the reduction of the use of insecticides. However, despite rising national insecticide imports (FAO Statistics), concentrations declined in the core. This discrepancy may be attributable to the limited set of compounds that were analysed, which may have excluded substitute insecticides. Alternatively, newly used insecticides may be more biodegradable or less prone to sorption, limiting their accumulation in soils and sediments.

The decrease of most of the herbicides fluxes in the 2000s (Figure 5.5) could correspond to the initial introduction of conservation agriculture systems (integrated no-tillage systems with multiple measures to maintain soil and soil health), which limited erosion and thus transfers of herbicides, while the increase after 2007 could correspond to the longer-term effects of the use of no-tillage in monocropping systems without the expected associated soil conservation measures leading to increasing soil compaction and run-off production, thereby leading to accelerated herbicide transfers. Furthermore, a significant increase of glyphosate and its metabolite AMPA has been recorded since 2008, coinciding with the expansion of

GM soybean crops in the region. Mirex was an exception. Indeed, fluxes of this widely used insecticide remained potentially widely used in forest plantations across the basin. Although concentrations of this insecticide did not exceed the sediment PNEC values and therefore did not pose a major risk for benthic communities, it is forbidden in multiple countries including the United States of America since 1976 (Metcalf 2000) and more recently in Europe (European Commission - Pesticides database) because of its limited biodegradation as well as its acute bioaccumulation. Its continued usage in the region could therefore have detrimental consequences on the environment over the long term.

Furthermore, since its filling in 1979, the Salto Grande Reservoir has exhibited persistent eutrophic conditions (Quirós and Luchini 1982; Berón 1990), reflecting chronic nutrient enrichment and recurrent phytoplankton blooms. These conditions have intensified since the early 2000s (Chalar 2006, 2009), in response to the expansion of intensive agriculture and livestock production across the basin. Eutrophication is strongly linked to nutrient inputs from agrosystems (Chalar 2006; Kruk et al. 2023), as cropland and pasture expansion have generated increased runoff and that of nutrients, pesticides, and contaminants, especially during heavy rainfall or flood events. Such phenomena amplify contaminant transport into tributaries and the reservoir (Chalar 2009; O'Farrell et al. 2012; Kruk et al. 2023). In 2024, for example, extreme flooding in the Guaíba river basin submerged large areas of Porto Alegre, the capital and largest city of Rio Grande do Sul, depositing potentially contaminated sediments across the metropolitan region (Mantovani et al. 2025).

The evidence therefore suggests that the Salto Grande Reservoir has been contaminated following the culmination of long-term land-use intensification and the increase in hydrological connectivity between agricultural landscapes and river systems. It also outlines emerging concerns for currently used pesticides such as chlorpyrifos ethyle, mirex, fipronil or more recent compounds.

This study was restricted to the analysis of 16 pesticides, and future research should be conducted to enlarge the scope including compounds introduced more recently.

5.4.3 . Possible future evolution of the agricultural expansion

Agricultural land covered 19.3% of the basin surface area in 1985 and 29.9% in 2022. While this surface area represents one third of the basin nowadays, agricultural areas dedicated to soybean cultivation and the production of cellulose from forest plantations are projected to further increase by 25.1% and 24.5% between 2023 and 2033 in Brazil, respectively (Brazilian agricultural projection 2023-2024 to 2033-2034, Ministry of Agriculture and Livestock)

Furthermore, the Mercosur Treaty, the regional customs union comprising Argentina, Bolivia, Brazil, Paraguay and Uruguay permitted the elimination of tariffs between these countries and facilitated large-scale commodity flows. Beyond the region, Brazil stands to benefit from external Mercosur agreements, including the EU-Mercosur trade deal (political agreement signed in 2024) with the European Union, and the Mercosur-EFTA free trade agreement with EFTA members (Iceland, Liechtenstein, Norway and

Switzerland). These agreements intend to reduce trade barriers for key commodities such as soybean and beef, thereby granting an easier access to European markets (Wieslaw 2025). Furthermore, the implementation of bilateral protocols, in particular with China, resulted in the emergence of new sanitary and phytosanitary markets for meat and crops (Ministério da Agricultura e Pecuária). These mechanisms serve to reduce export costs, harmonise regulations, and attract foreign investments. Consequently, this could create strong incentives for the further intensification and expansion of export-oriented agriculture in Brazil and particularly in the soybean-dominated agricultural regions including the Pampa.

In light of the environmental challenges already identified in this study and the alarming projections of land use and cover changes by 2033, our study underscores the urgent need for clear agricultural policies and the monitoring of land use and management to enforce sustainable and "good"/virtuous agricultural practices. Future research should also take advantage of the numerous dams and reservoirs along the Uruguay river and to its estuary, in order to assess more specifically sediment transport, contaminant retention, and their eventual transfer from agricultural headwaters to downstream ecosystems.

5.5 . Conclusion

Overall, the Salto Grande sediment record shows that sediment delivery, sediment provenance and pesticide fluxes changed together, but not in the same direction. Sediment accumulation rates were higher from 1982 to 2000 and lower thereafter. Over the same period, fingerprinting indicates a shift from predominantly northern sediment sources before 2000 to a greater contribution from the southern part of the basin after 2000. The construction of upstream dams may have reduced sediment delivery from the north by trapping material, while agricultural expansion in the south is consistent with the growing southern contribution. The widespread adoption of no-tillage practices may also have contributed to lower sediment fluxes, although the record does not isolate the effect of this practice from dam construction and other land-use changes.

Pesticide fluxes followed a more varied pattern: inputs were generally lower during the early 2000s, then herbicide and fungicide fluxes increased from the mid-2000s, while insecticide fluxes generally declined. The later rise in herbicides coincides with the expansion of soybean cultivation and the widespread use of no-tillage, often without the complementary conservation measures associated with conservation agriculture. Thus, lower sediment delivery did not correspond to lower pesticide transfer. The record instead suggests that upstream reservoirs and changing agricultural practices altered sediment storage, source contributions and pesticide transport in different ways across the basin.

5.6 . Data Availability

Both previously published (suspended sediment sources) and original (Salto Grande core and analyses) data were used for this study. All original results obtained from analysis of the core are freely

available on datagouv.fr.

5.7 . Supplementary material

5.7.1 . Evolution of the land-use and land-cover

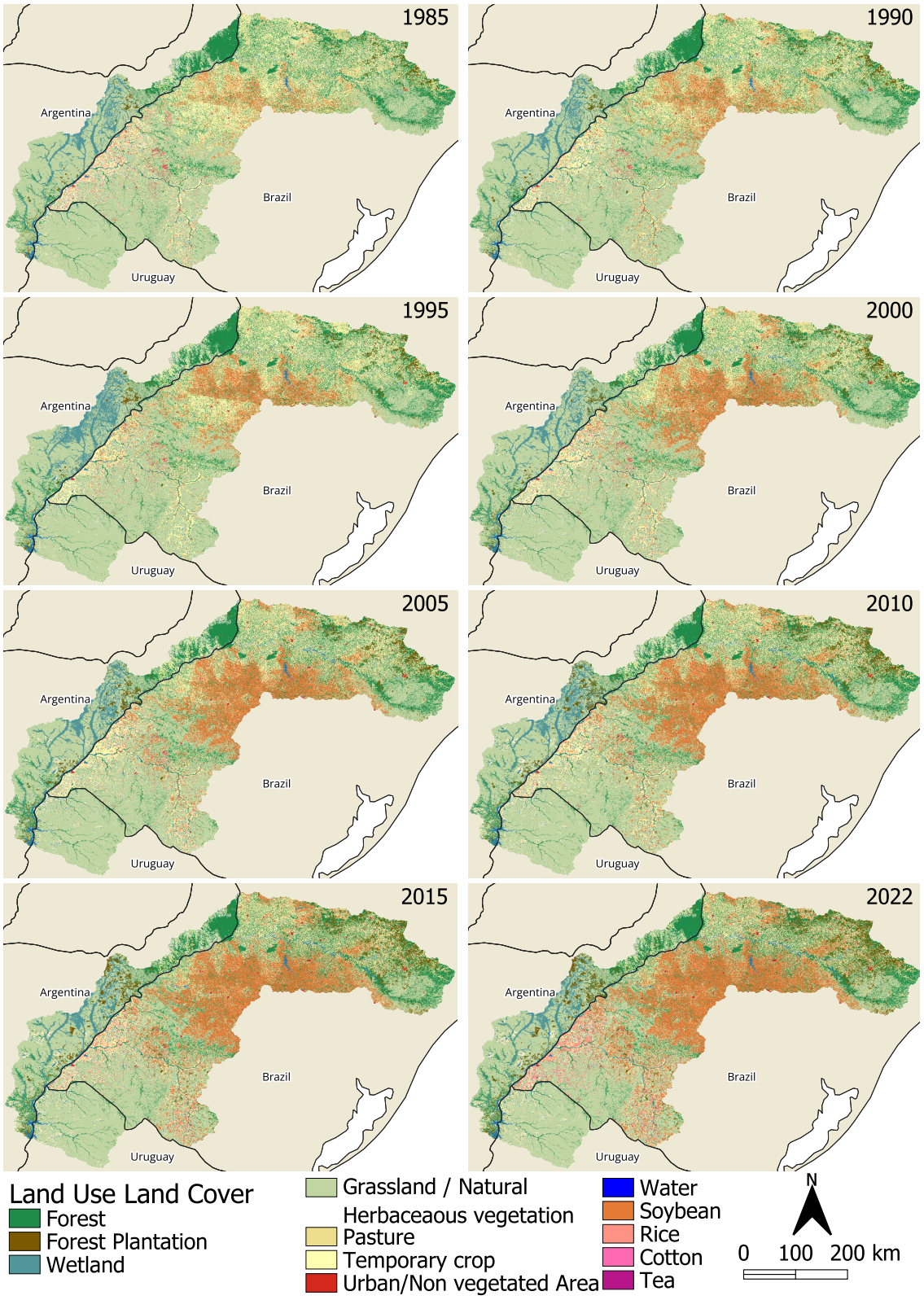

Figure 5.6: Spatialised main land-use and land-cover from 1985 to 2022, data from Mapbiomas Argentina, Pampa and Brazil and background map from OpenStreetMap contributors (2024)

5.7.2 . Detailed core description

Visual inspection revealed the occurrence of three units within the SG03 sediment core (Figure 5.3). The deepest unit (60-73.5 cm) consisted of very dark, silty material, overlaid by a darker silty layer (52-60 cm) containing plant debris. Mean grain-size indices for these two units (52-73.5 cm) were D10 = 2.9 ± 0.06 µm, D50 = 33.9 ± 2.8 µm, and D90 = 303.9 ± 38.1 µm. Based on grain-size data and the occurrence of plant residues, this interval was interpreted as corresponding to exposed soil before the dam construction.

The upper 0-52 cm sedimentary units was composed of homogeneous brown silty clays (Figure 5.3). Finer particles are found between 30-52 cm, low and homogeneous grain size was recorded with mean D10, D50 and D90 indices of 0.6 $\pm$ 0.02, 6.3 $\pm$ 0.08 and 42.4 $\pm$ 7.14 µm, respectively. An increase in size was recorded from 0-30 cm with a mean of 2.6 $\pm$ 0.03, 10.5 $\pm$ 0.2 and 111.3 $\pm$ 9.4 µm for D10, D50 and D90, respectively.

TOC concentrations in the sediments ranged from 1.98 to 4.14 g C.kg^{-1} in the sediments (4.61 to 5.77 g C.kg^{-1} in the soil, Figure 5.3). A strong decline of TOC was observed from 4.14 $gC.kg^{-1}$ to 3.01 $gC.kg^{-1}$ from 40-50 cm. Then, TOC contents further declined by 19.5% from 0-40 cm although some additional trends can be observed. Two peaks of TOC were indeed observed at 45 and 35 cm. TOC reached its lowest value around 19 cm with 1.98 $gC.kg^{-1}$, before an increase up to 2.64 $gC.kg^{-1}$ in the uppermost centimetres.

δ^{13}C ranged from -22.5‰to -15.3‰in the sediments (23.3 to 24.6‰in the soil Figure 5.3). The minimum δ^{13}C values found in the bottom of the sediments. As for TOC, several trends can be observed. Strong variations of δ^{13}C were observed before and after 52 cm with two significant peaks that occurred around 45 cm and 35 cm, with peaks of respectively -15.4‰ and -15.3‰. A global decrease and stabilization occurred after these two peaks to a value of around -22‰.

Sedimentary δ^{13}C reflects the proportion of C_3 versus C_4 vegetation, both coexisting in the Salto Grande river basin (Overbeck et al. 2007). C_4 plants display values of –16 to –10 ‰, while C_3 vegetation lies between –33 and –24 ‰, partly overlapping with lacustrine organic matter. The region supports roughly 50–70 % C_4 cover (Powell and Still 2009), consistent with mean signatures around –20 ‰.

Changepoint testing of the CT-scan derived dry bulk density profile (calibration $r^2 = 0.73$) revealed two stratigraphic units. Average DBD amounted to 0.54 $\pm$ 0.02 $g.cm^{-3}$ from 19-52 cm, followed by a more homogeneous interval above 19 cm with a mean of 0.53 $\pm$ 0.01 $g.cm^{-3}$. A notable increase was recorded in the uppermost 5 cm (Figure 5.3).

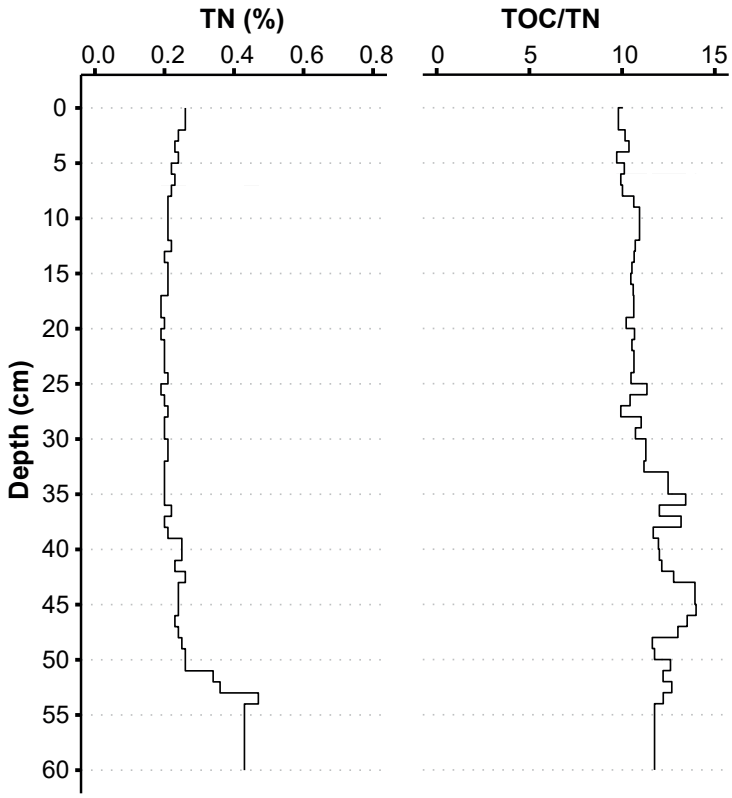

Figure 5.7: Evolution of Total Nitrogen (TN) and Total organic Carbon (TOC) / TN ratios with depth in the core

5.7.3 . Magnetic Susceptibility

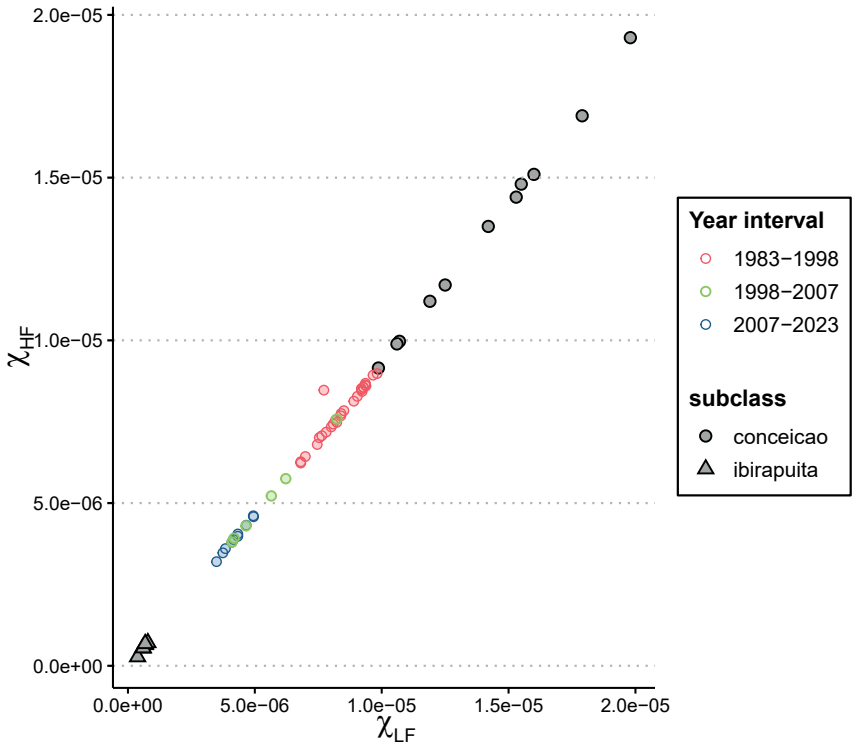

Figure 5.8: Scatter plot of χ_{HF} & χ_{LF} magnetic susceptibility from Conceicão and Ibirapuitã (in dark cicrles and triangles respectively) and sediments from Salto Grande in colored circles depending on their year of supply to the Salto Grande reservoir, in m^3kg^{-1}

5.7.4 . Mineralogical composition

The mineralogical composition changed along the first 55 cm of depth (5.9.1). From the bottom to the top of the core, there was a decrease in the proportion of kaolinite and iron oxides (hematite + goethite), while the proportion of quartz increased. These relationships are more evident in the correlations between the proportions of the minerals (5.9.2). Comparing the most superficial section (0-20 cm) with the intermediate section (20-55 cm), it becomes more evident that older sediments have a higher proportion of kaolinite and iron oxides (hematite + goethite), which are predominant minerals in soils developed in the northern part of the basin (5.9.3). On the other hand, the more recent sediments have a higher proportion of quartz, which is more common in soils found in the southern part of the watershed.

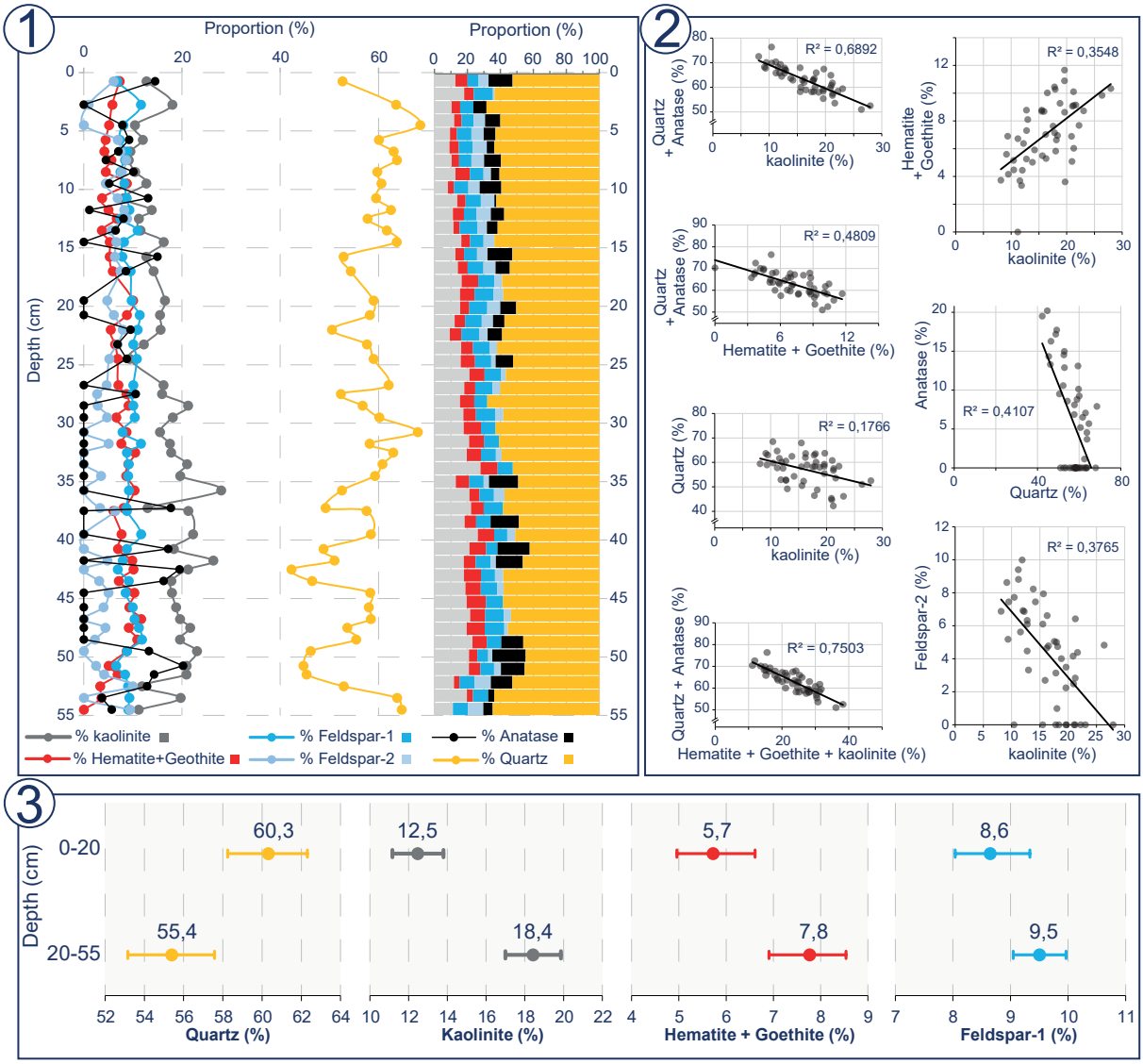

Figure 5.9: Mineralogical composition of the <2 mm fraction determined by X-ray Diffractometry, (**1**), relationship between the proportion of minerals in sediment samples (**2**) and proportion of quartz, kaolinite, hematite+goethite, and feldspar in sediment samples collected between 0-20 cm and between 20-55 cm (**3**). The point represents the average, and the whiskers represent the 95% confidence interval after bootstrapping with 5000 interactions.

5.7.5 . Sediment Fingerprinting

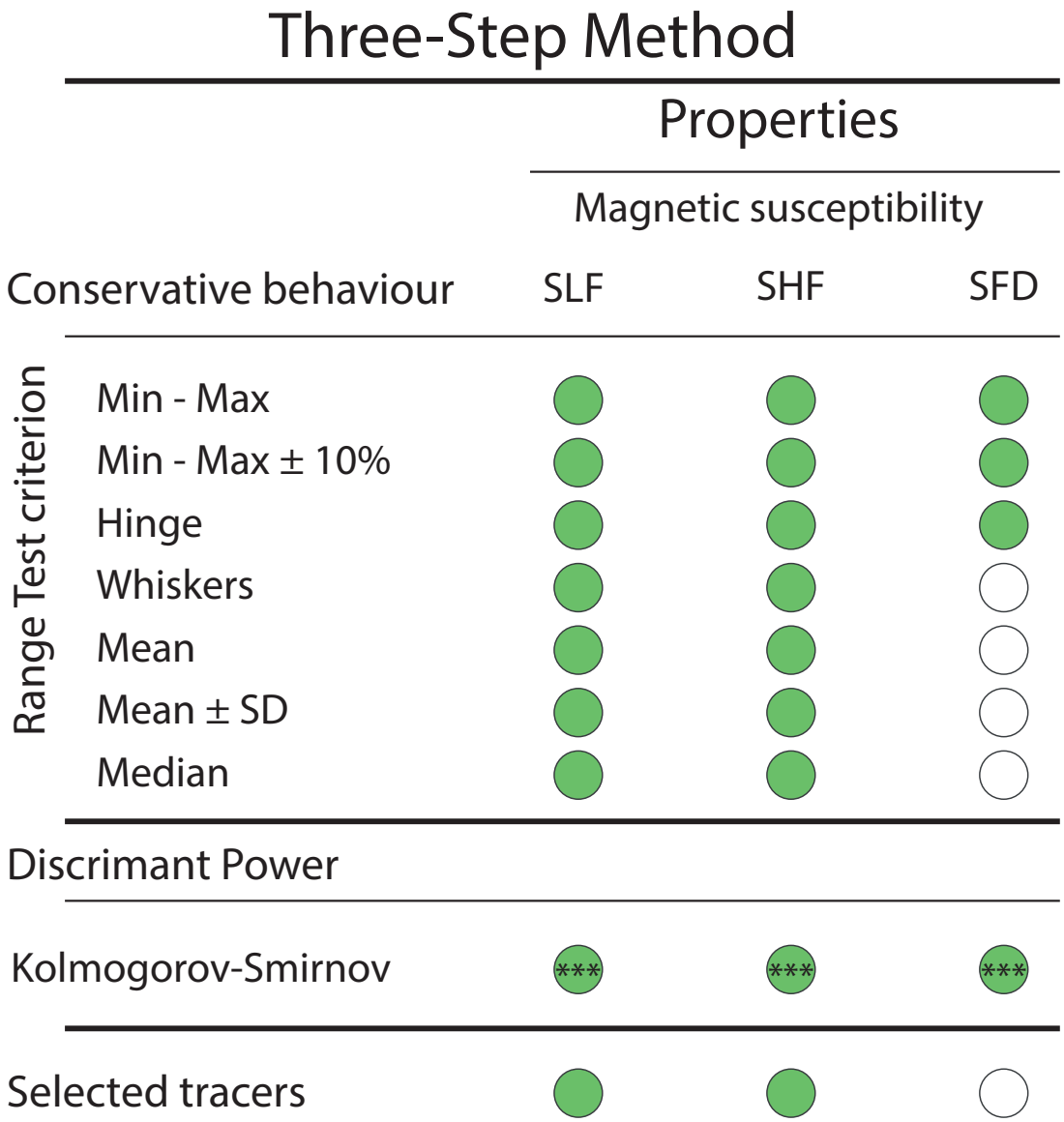

Figure 5.10: Three step method tracer selection results with FingR package

5.8 . Detailed pesticides results

5.8.1 . Herbicides

With the exception of AMPA, all the herbicides were detected from the bottom of the core (5.11). Three periods of application of herbicides may be outlined, with a first generalised usage of herbicides from 1982 to the late 1990s. Then, the use of only a few herbicides, i.e. 2,4-D and S-metholachlor until 2005-2010, before all herbicides rose. 2,4-D, Diuron as well as S-metholachlor were detected in high proportions from 1982 to the late 1990s. Diuron was not detected for the rest of the core. S-metholachlor was low until 2012 before it peaked. Despite a decrease in 1995 and 2015, 2,4-D was observed in larger quantities for the rest of the core with peaks in 2007 and 2012-2014. Simazine, Atrazine, Glyphosate

and AMPA followed the same trends, with the detection of these herbicides from 1982 to 1995 before a decrease and, then, a increase from 2007 for glyphosate and from 2014 for Simazine and AMPA.

5.8.2 . Fungicides

The Tebuconazole fungicide, in the red portion in figure 5.11, was detected in the core from the late 2000s onwards, until reaching a peak in 2015 before starting to decrease. Mainly used in large scale crop-fieds in order to combat different types of plant diseases (Tleuova et al. 2020), this fungicide has been widely used in Brazil in the last two decades (Oliveira Gomes De Assunção et al. 2022).

5.8.3 . Insecticides

Mirex, a widely used insecticide since the 1960s (National Toxicology Program 2021), is found in high levels from 1982 until 1990, when it decreased before peaking again in 1995-1997 and diminishing until 2001. Finally a rise was recorded from 2012 to 2019 and another decline until 2022.

Freely marketed since 1945 (Mellanby 1992) and widely used in the fight against different insects and pests, DDT and it's metabolites, DDD and DDE, are detected from the bottom of the core in 1982 (in the white part in figure 5.11). Significant yet decreasing fluxes of DDT, DDD and DDE are detected until the mid 1990s. DDT reappeared in 2012 until the top of the core. DDD fluxes were lower but kept being recorded until it rose in the same years as DDT, from 2012. DDE remained low until the top of the core.

Several hypotheses may be put forward for explaining the source of DDT and its metabolites along the profile. To test these hypotheses, DDD and DDE, being respectively the anaerobic and aerobic metabolites of DDT, produced depending on the degradation conditions of the pesticide (Sabatier et al. 2014) can provide better insights into the origin of the reappearance of DDT observed from 2012. The fluxes of DDD and DDE show that the fluxes of DDT observed throughout the core correspond to a aerobic and anaerobic degradation until the mid 1990s when anaerobic processes dominated degradation, especially from 2012.

Originally used in attempts to eradicate *Anopheles* and *Aedes aegypti* mosquitoes, the primary vectors of malaria and yellow fever respectively (Simard 2018), DDT was applied in and around potential habitats of these insects from 1948 to the 1970s. Subsequently, Sabatier et al. (2014) demonstrated that herbicide application can lead to increased soil erosion and the remobilisation of legacy pesticides previously retained in soils. Since 2012, considering the evolution of the land uses and land covers described in section 5.3.1, the increase of the proportion of sediments coming from the southern part of the river basin, the increase of herbicides and fluxes of DDD and DDE, this study therefore suggest that the reappearance of DDT could result from the newly cultivation of previously uncultivated areas treated with DDT.

Endosulfan follows the same trends as DDT, with a first peak in 1982-1984, a low detection period until 1988 and a second peak from 1988-1995. From that point on, endosulfan was detected up to the

top of the core in low concentrations and with a high degree of variability. Several factors can explain this drop of endosulfan fluxes in the late 1990s and before the official ban of Endosulfan in 2013 and following the Brazilian Health regulatory agency's recommendations (Pignati et al. 2014). First, during the 1990s, multiple studies were published demonstrating endosulfan's acute toxicity, endocrine-disrupting potential, bioaccumulation, and environmental persistence (Meriel Watts 2011). In 2001, endosulfan was added to the Stockholm Convention on persistent organic pollutants (Janssen 2011). Concurrently, newer insecticides such as neonicotinoids, amongst which Imidacloprid, became available in the same period (Jeschke et al. 2019). These insecticides offered effective pests control with lower persistence and reduced human toxicity (Stockholm Convention on Persistent Organic Pollutants 2011). It is thus hypothesised that they replaced endosulfan for treatments in crops such as cotton, soybean, and coffee in the late 1990's and should to be studied in future studies.

Friponil and Imidacloprid are detected in low levels in the bottom of the core in 1982. Theses insecticides were marketed in 1990 and 1985 respectively, therefore suggesting the occurrence of some diffusion along the profile and this part was not considered for interpretation. Friponil peaked in 1998-2001 and from 2012 to the top of the core. Imidacloprid peaked in 2006-2008 and 2012-2014. The development of these insecticides was initiated in response to the increasing resistance of pesticides to other compounds, as evidenced by (Jeschke et al. 2019). Chlorpyrifos Ethyl, first registered in 1965 in the United States of America (Rauh et al. 2011), is found in the core in high proportions from 1982. Two higher detection periods were identified from 1986 to the mid- 1990s and from 2014-2022. This broad-spectrum insecticide is widely used on various crops, in public health programs, particularly for the control of mosquitoes, ants, cockroaches, and certain disease-carrying tick species. In the sediment core, the first two peaks of Chlorpyrifos-Ethyl coincided with the periods of high input of DDT, andEendosulfan. In 2013–2014, the invasive pest Helicoverpa armigera caused widespread damage, especially in soybean and cotton fields (De Freitas Bueno and Sosa-Gómez 2014). As a result, emergency use authorizations were granted for several banned or restricted pesticides (European and Mediterranean Plant Protection Organization 2013) subsequently maintained or extended to date. The rapid infestation of this pest led the the overuse of insecticides (Pomari-Fernandes et al. 2015). This study therefore suggest that the reappearance of Chlorpyrifos-Ethyl from 2013 could be the consequence of the invasion of this pest in Brazil and the attempts to control it.

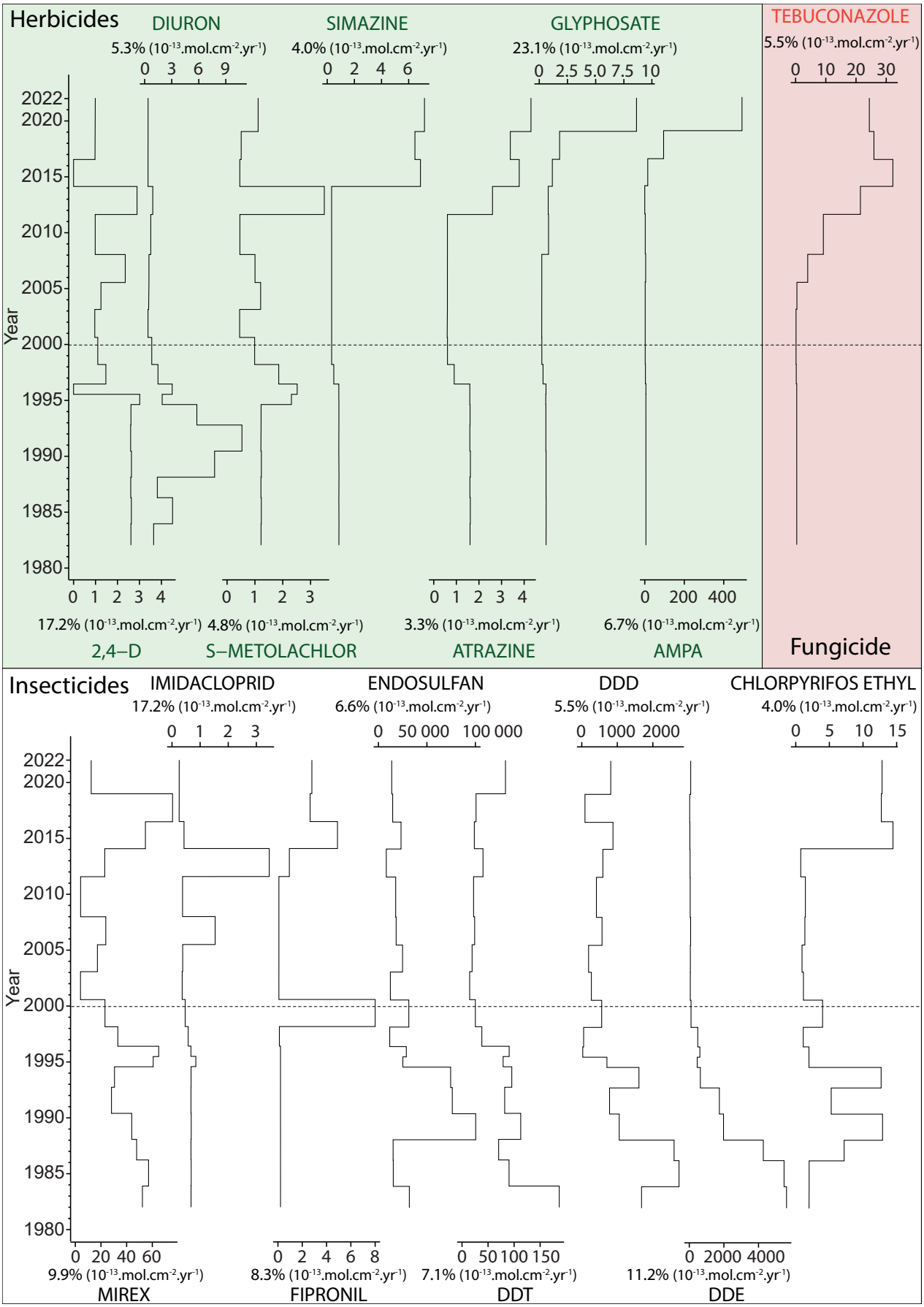

Figure 5.11: Detailed fluxes (in 10^{-13} mol.cm^{-2}.yr^{-1}) of insecticides (grey), herbicides (green), and fungicides (red). Uncertainty for each pesticide is indicated alongside its range.

	2,4-D	Atrazine	Chlorpyrifos Ethyl	Diuron	Fipronil	Imidacloprid	S-Metolachlor	Simazine	Tebuconazole	Endosulfan	DDT	Mirex	Glyphosate	AMPA
Concentration	0.05	0.212	1.03	0.02	0.279	0.015	0.072	0.331	1.72	1276	6.77	1.54	33.34	209.81
$PNEC_{sed}$	2.31	0.20	0.11	0.69	0.017	0.022	0.069	7.82	5.48	3.19	0.01	2100	12577	2709
RCR	0.022	1.062	9.361	0.029	16.44	0.682	1.050	0.042	0.314	399.9	677.1	0.001	0.003	0.077

Table 5.2: Comparison of pesticides concentrations in the top 2 cm of sediments, PNEC values from NORMAN Ecotoxicology Database—Lowest PNECs and Risk Characterisation Ratios (RCR). Values >1 (highlighted in red) indicate potential risk.

5.9 . Detailed Material and Methodology

5.9.1 . Sediment source sampling

Conceição river basin The Conceição River basin (Figure 5.12), located on the basaltic plateau of Rio Grande do Sul and covering approximately 804.3 km^2 is representative of the northern area of the Salto Grande river basin (Ramon 2021). The soils found in the area are mainly Ferrasols (80%) although Nitisols (18%), and Acrisols (2%) can also be found. Altitudes range from 270 to 480 m, and the terrain consists of gentle slopes (9$\%$) at the highest points of the basin and moderate to steep slopes near the river and drainage channels. The land is primarily used for cropland and is mainly cultivated with soybeans (Glycine max) under a no-tillage system in the summer. During the winter, wheat (Triticum aestivum), oats (Avena sativa and Avena strigosa) and ryegrass (Lolium multiflorum) are cultivated for grain production, as feed for dairy cattle feed or to cover the soil (Ramon 2021). However, inadequate soil management in these areas under the no-tillage system has resulted in high erosion rates in recent decades (Didoné et al. 2019). Pastures used for raising cattle occupy 12$\%$ of the river basin's surface area, while forests cover only 5$\%$. Only perennial pastures were sampled in the study.

Ibirapuitã river basin Located in the south of the Salto Grande river basin, the Ibirapuita sub-basin (Figure 5.12) covers an area of 5943 km^2 and is representative of the lower part of the river basin (Ramon 2021).

This basin is comprised between 70 and 370 m of altitudes (only 15% of the river basin is between 280 and 370 m and in the headwaters of the basin). The catchment is dominated by shallow Regosols and sandy Acrisols, which are mainly occupied by the native grasslands that are typical of the Pampa biome (81%, Figure 5.12).

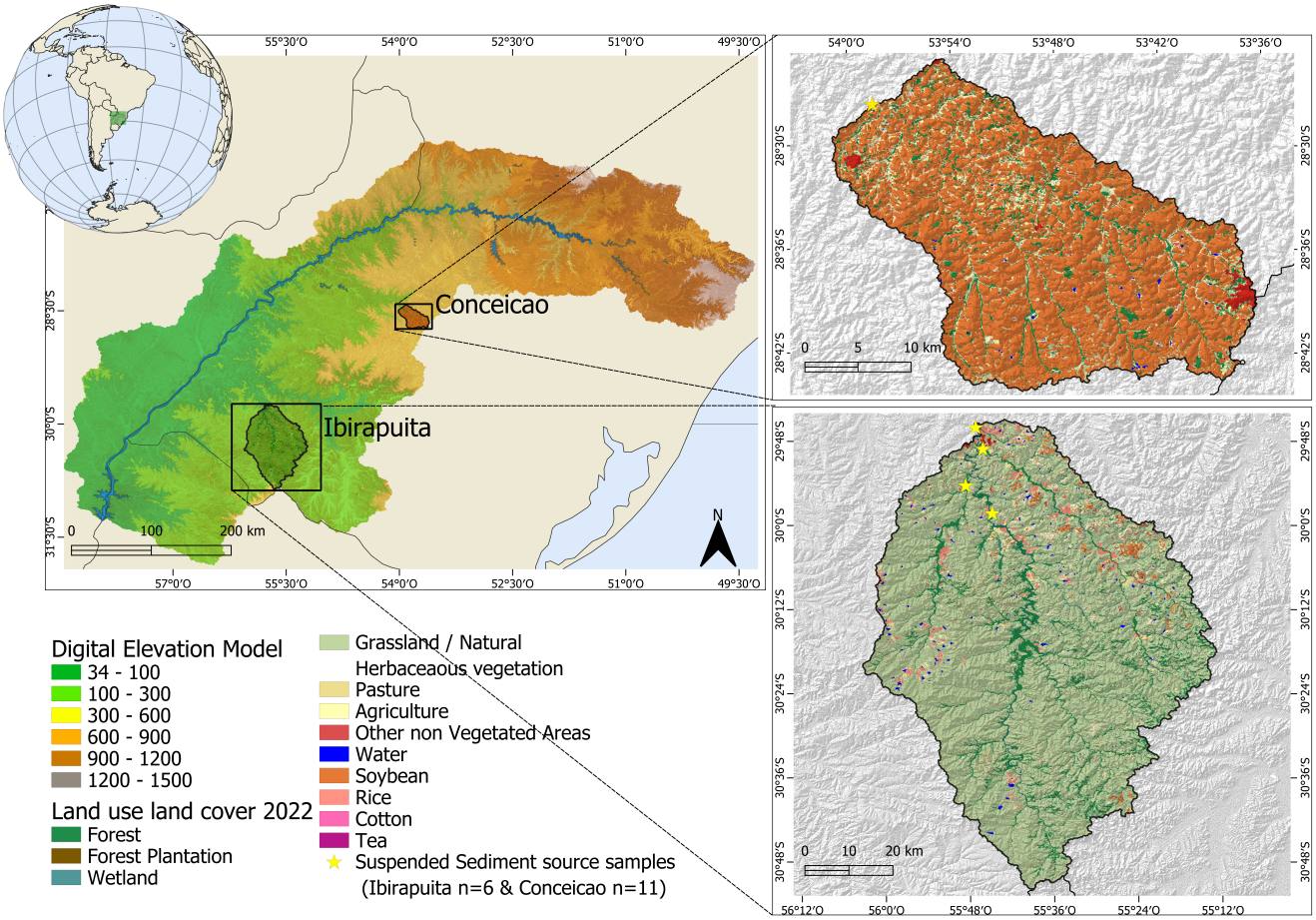

Figure 5.12: Digital elevation model of the Salto Grande, Ibirapuitã and Conceição river basins. Land-use and land-cover and source sample localisation analysed for magnetic susceptibility, background map from OpenStreetMap contributors (2024)

5.9.2 . Particle size analysis

Particle size analysis was conducted on fresh sediment at centimetre-scale resolution using a laser diffraction particle size analyser (Mastersizer 3000 with Hydro LV, Malvern Panalytical). Five replicate measurements were performed on each sediment sample in osmotic water with sonic dispersion applied to reduce particle flocculation. No additional treatment was applied to the sediment. The particle size distribution was assessed over a range of 0.01 µm to 3500 µm and the proportion of particles smaller than 10%, 50% and 90%, respectively, were recorded as D10, D50 and D90 indices.

5.9.3 . Density analysis

Relative density of the sediments was recorded at 0.488 mm intervals using a Computer Tomography scanner (CT-scan), and images were recorded using the GE Discovery CT750 HD equipment available at the DOSEO platform (French Atomic Energy and Alternative Energy Commission, CEA Paris-Saclay, France). Relative density (grey values) was extracted from the recorded images using the free software ImageJ. Discrete Dry Bulk Density (DBD) was measured on seven samples of fresh sediment using a

volume of 1.7 cm^3 (V) in an acrylic cube. The cubes were filled with fresh sediment, and their humid weight (m_{humid} in g) was recorded. Then, they were oven-dried at 40°C for 48 to 96 hours, and their dry weight (m_{dry} in g) was measured. DBD (in $g.cm^3$) was calculated using the following equation 5.3.

$$\rho_b = \frac{m_{\text{dry}}}{V} \tag{5.3}$$

The measured DBD was correlated with the mean relative density values recorded for the samples. The DBD was then reconstructed for the entire sequence following the procedure proposed by Foucher et al. (2021b, 2023).

5.9.4 . Statistics

A change point test was performed on the high-resolution density using the ChangePoint package in R, which is freely available on CRAN (Killick and Eckley (2014), https://CRAN.R-project.org/package=changepoint). This package implements various mainstream and specialised change-point methods for identifying single and multiple change-points within data. This test was performed to identify density shifts and to check whether their occurrence matched with XRF results and the occurrence of contrasting phases of agricultural development in the Salto Grande river basin. This test was performed following the recommendations of Killick and Eckley (2014), using binary segmentation and a penalty value of 0.01.

5.9.5 . Geochemical analysis

The Avaatech XRF Core Scanner, available at the *Laboratoire des Sciences du Climat et de l'Environnement* (Paris-Saclay, France), allows the generation of high-frequency (>1 mm), semi-quantitative (counts per second, cps) elemental profiles across cores. It provides rapid insights into compositional trends, stratigraphic boundaries, and sediment provenance. Nonetheless, it is semi-quantitative, sensitive to matrix and surface variability with a limited accuracy in light and trace elements. Each element was removed when too noisy or filtered for noise using Complete Ensemble Empirical Mode Decomposition method available with R package *Rlibeemd* (Luukko et al. 2016) (parameters : 0.2 noise strength, 100 iterations, considering 2 Intrinsic mode functions and threshold noise score of 0.25 to remove the noisiest elements). Remaining elements Al, Si, P, K, Ca, Ti (10 kV) and Mn, Fe (30 kV) were centered log-ratio (CLR) transformed.

Ti may reflect the terrigenous fraction (Croudace and Rothwell 2015) while Mn likely reflects the lithological composition of the river basin and could be indicating a shift in sediment provenance or change in redox conditions in the lake ((Elbaz-Poulichet et al. 2014)).

5.9.6 . Organic matter analysis

The total organic carbon (TOC) and nitrogen (TN), as well as the stable carbon (δ^{13}C) isotope ratios of organic and clay-bound organic matter were measured in dried SG03 core sediment sampled at 1-cm

intervals. These measurements were performed using a continuous flow Elementar® VarioPyro cube elemental analyzer (EA) coupled to a Micromass® Isoprime Isotope Ratios mass Spectrometer (IRMS) at the Institute of Ecology and Environmental Science of Paris.

Oxygen for combustion was injected at a rate of 30 ml.min^{-1} for 70 s, and the reduction and combustion furnaces were set to temperatures of 850 °C and 1120 °C, respectively (Agnihotri et al. 2014). Analytical precision and repeatability were controlled using tyrosine samples that were calibrated against international standards (Coplen et al. 1983). In the current research, the mean uncertainties amounted to 0.2‰ for TN, 0.18‰ for TOC and 0.1‰ for δ^{13}C. The ^{13}C isotope content is expressed in terms of δ^{13}C against Pee Dee Belemnite (PDB). This is a standard reference for δ^{13}C, measured on the shells of a species of belemnite from the Upper Cretaceous.

5.9.7 . Gamma spectrometry analysis

Gamma spectrometry measurements were conducted using coaxial HPGe detectors (Canberra/Ortec®), which are available at the Laboratoire des Sciences du Climat et de l'Environnement (Gif-sur-Yvette, France). The ^{210}Pb activities were determined at 46.5 keV. $^{210}Pb_{ex}$ was calculated by subtracting the two Radium-226 daughters, Lead-214 (average count at 295.2 and 351.9 keV) and Bismuth-214 (609.3 keV), from the total ^{210}Pb activities detected at 46.5 keV. ^{137}Cs activities were measured at 662 keV. All measurements were corrected for the background level determined every two months as well as for detector and geometry efficiencies. Activities were also decay-corrected to the sampling date.

5.9.8 . Magnetic susceptibility analysis

The magnetic properties of the sediment core and soil source samples were measured using a Bartington MS2B Dual Frequency sensor. Two grams of each sample were measured three times at high and low frequencies (4.7 and 0.47 kHz, respectively) to obtain the mass-specific magnetic susceptibility at high and low frequencies ($\chi_{HF} - m^3kg^{-1}$ and $\chi_{LF} - m^3kg^{-1}$).

5.9.9 . Mineralogical composition

The mineralogical composition of the air-dried fine-earth (ADFE) fraction (<2 mm) was determined by X-ray Diffractometry (XRD) on a Bruker D2 Phaser spectrometer equipped with a Lynxeye™ fast linear detector and the software Diffrac.Suite™. The diffractometer used $CuK\alpha$ radiation (λ = 1.5418 Å) passed through a Ni filter, a current intensity of 10 mA and a power of 30 kVA. Samples containing approximately 600 mg of ADFE fraction were analysed in non-oriented powdered form and irradiated over the °2 θ range from 4 to 50 at a scanning rate of 1°2 θ min^{-1}. The minerals of the ADFE fraction were semi-quantified based on the relative area (RA) of the main reflection of each mineral (e.g., RA-kaolinite), in relation to the total area (TA) of the main minerals present in the samples ($TA = kaolinite_{RA} + quartz_{RA} + feldspar-1_{RA} + feldspar-2_{RA} + anatase_{RA} + hematite_{RA} + goethite_{RA}$) (Oliveira et al. 2020).

The position of the reflections in the XRD and the obtaining of the relative area of the greater intensity reflection for each mineral were acquired by using the software Diffract Suite Eva and interpreted with the aid of tables previously reported by Brown and Brindley (1980).

5.9.10 . Pesticides analysis

The set of samples used for pesticides analysis was freeze-dried in an ALPHA 1-2 LD plus (CHRIST®) freeze dryer for 24 to 48h, depending on the quantity of sample available The pesticides were then extracted using the QuEChERS method; the Quick, Easy, Cheap, Effective, Rugged, and Safe extraction kit and method (Perestrelo et al. 2019). Pesticide concentrations were obtained via Gas and Liquid Chromatography coupled with Mass Spectrometry (GC-MS for Endosulfan, Chlopryrifos Ethyl, DDT,DDD, DDE, and Mirex and LC-MS/MS for S-Metolachlor, Simazine, Atrazine, Diruon, 2.4-D, Tebuconazole, Imidacloriprid and Friponil). Glyphosate and AMPA were analysed using a rapid LC-MS/MS method with a Polypore H+ column without derivatisation, which demonstrated a good selectivity and sensitivity.

Once obtained, the pesticide concentrations ($g.g^{-1}$) were compared with the NORMAN Ecotoxicology Database — Lowest PNECs . This is a collaborative European initiative that compiles environmental quality thresholds or Predicted No Effect Concentration (PNEC). PNEC represents the concentration of a chemical in the environment below which no adverse effects on organisms are expected. It is usually derived from ecotoxicity studies on sensitive organisms (i.e, algae, daphnia, fish) by applying assessment factors to account for uncertainty and interspecies differences. For sediments, the $PNEC_{sediment}$ value represents the threshold protecting benthic organisms and sediment-dwelling communities. The “Lowest PNECs” are values agreed upon by experts, often based on the most conservative available dataset. A risk characterisation ratio (RCR) was calculated (RCR=Sediment concentration / PNEC) on the uppermost centimetres of the core, with pesticides showing a RCR superior to one representing potential ecological risk for benthic communities.

Secondly, the equivalent in moles of pesticides ($mol.g^{-1}$) was calculated by dividing each pesticide’s concentration by its molar mass ($g.mol^{-1}$).

Extensive literature research was conducted, and multiple technical reports were analysed in order to obtain different information on the pesticides, such as their dates of first production/marketing, which is described and used for interpretation in the results and discussion.

Pesticide	Abbreviation	IUPAC name	Familly	Marketed in	Source
2,4-Dichlorophenoxyacetic acid	2,4-D	2,4-Dichlorophenoxyacetic acid	Organic compound	1940	Merotto et al. (2022)
Atrazine	Atrazine	6-chloro-N^2-ethyl-N^4-(propan-2-yl)- 1,3,5-triazine-2,4-diamine	Triazine	1958	(Heri et al. 2008)
Simazine	Simazine	6-chloro-N^2,N^4-diethyl-1,3,5-triazine-2,4-diamine	Triazine	1956	(Heri et al. 2008)
Diuron	DCMU	3-(3,4-dichlorophenyl)-1,1-dimethylurea	Phenylurea	1954	(Woodford 1957)
S-Metolachlor	S-Metolachlor	(S)-2-chloro-N-(2-ethyl-6-methylphenyl)-N-[(2S)-1-methoxypropan-2-yl]acetamide	Urea	1976	(United States Environmental Protection Agency 1995)
Tebuconazole	Tebuconazole	(RS)-1-(4-chlorophenyl)-4,4-dimethyl-3-(1H-1,2,4-triazol-1-ylmethyl)pentan-3-ol	Neonicotinoid	1989	McInnes et al. (2023)
Imidacloprid	IMI	1-[(6-chloro-3-pyridinyl)methyl]-N-nitroimidazolidin-2-ylideneamine	Neonicotinoid	1985	Jeschke et al. (2019)
Endosulfan	Endosulfan	dodecachlorooctahydromethanetriyl benzodioxathiepine oxide	Organochlorine	1954	United States Environmental Protection Agency (2002)
Fipronil	Fipronil	5-Amino-1-[2,6-dichloro-4-(trifluoromethyl)phenyl]-4-(trifluoromethylsulfinyl)-1H-pyrazole-3-carbonitrile	Phenylpyrazole	1990	Jeschke et al. (2019)
Chlorpyrifos Ethyl	Chlorpyrifos Ethyl	O,O-Diethyl O-(3,5,6-trichloropyridin-2-yl) phosphorothioate	Organochlorine	1965	Rauh et al. (2011)
Dichlorodiphényltrichloroéthane	DDT	1,1'-(2,2,2-Trichloroethane-1,1-diyl)bis(4-chlorobenzene)	Organochlorine	1945	Mellanby (1992)
Dichlorodiphényldichloroéthane	DDD	1,1'-(2,2-Dichloroethane-1,1-diyl)bis(4-chlorobenzene)	Metabolite of DDT	-	-
Dichlorodiphényldichloroéthylène	DDE	1,1'-(2,2-Dichloroethene-1,1-diyl)bis(4-chlorobenzene)	Metabolite of DDT	-	-
Glyphosate	Glyphosate	N-(phosphonomethyl)glycine	Phosphonate	1974	Baer and Marcel (2014)
AMPA	AMPA	(Aminomethyl)phosphonic acid	Metabolite of glyphosate	-	-
Mirex	Mirex	dodecachloropentacyclo[5.3.0.0^{2,6}.0^{3,9}.0^{4,8}]decane	Organochlorine	1958	

Table 5.3: Complete list of 16 pesticides with their abbreviations, International Union of Pure and Applied Chemistry (IUAPC) names and classifications. Molecules were found on PubChem (https://pubchem.ncbi.nlm.nih.gov/)

Bibliography

Agnihotri, R., Kumar, R., Prasad, M. V. S. N., Sharma, C., Bhatia, S. K., and Arya, B. C. (2014). Experimental Setup and Standardization of a Continuous Flow Stable Isotope Mass Spectrometer for Measuring Stable Isotopes of Carbon, Nitrogen and Sulfur in Environmental Samples. *MAPAN*, 29(3):195–205.

Andrade, B. O., Dröse, W., Aguiar, C. A. D., Aires, E. T., Alvares, D. J., Barbieri, R. L., Carvalho, C. J. B. D., Bartz, M., Becker, F. G., Bencke, G. A., Beneduzi, A., Silva, J. B., Blochtein, B., Boldrini, I. I., Boll, P. K., Bordin, J., Silveira, R. M. B. D., Martins, M. B., Bosenbecker, C., Braccini, J., Braun, B., Brito, R., Brown, G. G., Büneker, H. M., Buzatto, C. R., Cavalleri, A., Cechin, S. Z., Colombo, P., Constantino, R., Costa, C. F. D., Dalzochio, M. S., Oliveira, M. G. D., Dias, R. A., Santos, L. A. D., Duarte, A. D. F., Duarte, J. L. P., Durigon, J., Da Silva, M. E., Ferreira, P. P. A., Ferreira, T., Ferrer, J., Ferro, V. G., Fontana, C. S., Freire, M. D., Freitas, T. R. O., Galiano, D., Garcia, M., Dos Santos, T. G., Gomes, L. R. P., Gonzatti, F., Gottschalk, M. S., Graciolli, G., Granada, C. E., Grings, M., Guimarães, P. S., Heydrich, I., Iop, S., Jarenkow, J. A., Jungbluth, P., Käffer, M. I., Kaminski, L. A., Kenne, D. C., Kirst, F. D., Krolow, T. K., Krüger, R. F., Kubiak, B. B., Leal-Zanchet, A. M., Loebmann, D., Lucas, D. B., Lucas, E. M., Luza, A. L., Machado, I. F., Madalozzo, B., Maestri, R., Malabarba, L. R., Maneyro, R., Marinho, M. A. T., Marques, R., Marta, K. D. S., Martins, D. D. S., Martins, G. D. S., Martins, T. R., Mello, A. S. D., Mello, R. L., Mendonça Junior, M. D. S., Morais, A. B. B. D., Moreira, F. F. F., Moreira, L. F. B., Moura, L. D. A., Nervo, M. H., Ott, R., Paludo, P., Passaglia, L. M. P., Périco, E., Petzhold, E. S., Pires, M. M., Poppe, J. L., Quintela, F. M., Raguse-Quadros, M., Pereira, M. J. R., Renner, S., Ribeiro, F. B., Ribeiro, J. R. I., Rodrigues, E. N. L., Rodrigues, P. E. S., Romanowski, H. P., Ruschel, T. P., Saccol, S. D. S. A., Savaris, M., Silveira, F. S., Schmitz, H. J., Siegloch, A. E., Siewert, R. R., Silva Filho, P. J. S. D., Soares, A. G., Somavilla, A., Sperotto, P., Spies, M. R., Tirelli, F. P., Tozetti, A. M., Verrastro, L., Vogel Ely, C., Da Silva, A. Z., Zank, C., Zefa, E., and Overbeck, G. E. (2023). 12,500+ and counting: biodiversity of the Brazilian Pampa. *Frontiers of Biogeography*, 15(2).

Baer, K. and Marcel, B. (2014). Glyphosate. In *Encyclopedia of Toxicology*, pages 767–769. Elsevier.

Baeza, S. and Paruelo, J. M. (2020). Land Use/Land Cover Change (2000–2014) in the Rio de la Plata Grasslands: An Analysis Based on MODIS NDVI Time Series. *Remote Sensing*, 12(3):381.

Bernardi, F., Minella, J. P. G., Dambroz, A. P. B., Schlesner, A., Merten, G. H., Mao, L., Evrard, O., Piccilli, D. G. A., Dalmolin, R. S. D., and De Araújo Pedron, F. (2024). Fluvial erosion in a catchment cultivated with no-tillage at the edge of the southern Brazilian plateau. *Environmental Monitoring and Assessment*, 197(1):9.

Berón, L. E. (1990). Features of the limnological behavior of Salto Grande's reservoir (Argentina-Uruguay). *Ecological Modelling*, 52:87–102.

Bizeul, R., Lajoie, O., Cerdan, O., Pak, L. T., Foucher, A., Huon, S., Grangeon, T., and Evrard, O. (2025). Delayed environmental pollution caused by transient landscape storage — An example from the Lesser Antilles. *Environmental Pollution*, 366:125412.

Brown, G. and Brindley, G. W. (1980). X-ray Diffraction Procedures for Clay Mineral Identification. In Brindley, G. W. and Brown, G., editors, *Crystal Structures of Clay Minerals and their X-Ray Identification*, pages 305–360. Mineralogical Society of Great Britain and Ireland, Colchester and London.

Bruel, R. and Sabatier, P. (2020). serac: an R package for ShortlivEd RAdionuclide chronology of recent sediment cores. *Journal of Environmental Radioactivity*, 225:106449.

Cantalice, J. R. B., Souza, W. L. D. S., Bezerra Silva, Y. J. A., Guerra, S. M., Araújo, A. M., Cavalcante, D. M., and Silva, C. M. C. A. C. (2015). Bedload and Suspended Sediment of a Watershed Impacted by Dams. In Hrissanthou, V., editor, *Effects of Sediment Transport on Hydraulic Structures*. InTech.

Chaboche, P.-A. (2021). *Amélioration de la chronologie des retombées initiales de radionucléides pour reconstruire les taux de redistribution de sol dans les bassins versants agricoles d'Amérique du Sud*. phdthesis, Université Paris-Saclay.

Chalar, G. (2006). Eutrophication dynamics on different temporal scales: salto grande reservoir (Argentina-Uruguay). *Eutrophication in South America: causes, consequences and technologies for management and control*.

Chalar, G. (2009). The use of phytoplankton patterns of diversity for algal bloom management. *Limnologica*, 39(3):200–208.

Chalaux-Clergue, T. and Bizeul, R. (2025). FingR: A Support for Sediment Source Fingerprinting Studies. Language: en.

Chalaux-Clergue, T., Bizeul, R., Batista, P. V. G., Martínez-Carreras, N., Laceby, J. P., and Evrard, O. (2024). Sensitivity of source sediment fingerprinting to tracer selection methods. *SOIL*, 10(1):109–138. Publisher: Copernicus GmbH.

Coplen, T. B., Kendall, C., and Hopple, J. (1983). Comparison of stable isotope reference samples. *Nature*, 302(5905):236–238.

Croudace, I. W. and Rothwell, R. G., editors (2015). *Micro-XRF Studies of Sediment Cores: Applications of a non-destructive tool for the environmental sciences*, volume 17 of *Developments in Paleoenvironmental Research*. Springer Netherlands, Dordrecht.

De Freitas Bueno, A. and Sosa-Gómez, D. R. (2014). The Old World Bollworm in the Neotropical Region: The Experience of Brazilian Growers with <I>Helicoverpa Armigera</I>. *Outlooks on Pest Management*, 25(4):261–264.

Derpsch, R., Friedrich, T., Kassam, A., and Hongwen, L. (2010). Current status of adoption of no-till farming in the world and some of its main benefits. *International Journal of Agricultural and Biological Engineering*, 3.

Didoné, E. J., Gomes Minella, J. P., Andres Schneider, F. J., Londero, A. L., Lefèvre, I., and Evrard, O. (2019). Quantifying the impact of no-tillage on soil redistribution in a cultivated catchment of Southern Brazil (1964–2016) with 137Cs inventory measurements. *Agriculture, Ecosystems & Environment*, 284:106588.

Didoné, E. J., Minella, J. P. G., and Evrard, O. (2017). Measuring and modelling soil erosion and sediment yields in a large cultivated catchment under no-till of Southern Brazil. *Soil and Tillage Research*, 174:24–33.

Dinerstein, E., Olson, D., Joshi, A., Vynne, C., Burgess, N. D., Wikramanayake, E., Hahn, N., Palminteri, S., Hedao, P., Noss, R., Hansen, M., Locke, H., Ellis, E. C., Jones, B., Barber, C. V., Hayes, R., Kormos, C., Martin, V., Crist, E., Sechrest, W., Price, L., Baillie, J. E. M., Weeden, D., Suckling, K., Davis, C., Sizer, N., Moore, R., Thau, D., Birch, T., Potapov, P., Turubanova, S., Tyukavina, A., de Souza, N., Pintea, L., Brito, J. C., Llewellyn, O. A., Miller, A. G., Patzelt, A., Ghazanfar, S. A., Timberlake, J., Klöser, H., Shennan-Farpón, Y., Kindt, R., Lillesø, J.-P. B., van Breugel, P., Graudal, L., Voge, M., Al-Shammari, K. F., and Saleem, M. (2017). An Ecoregion-Based Approach to Protecting Half the Terrestrial Realm. *BioScience*, 67(6):534–545.

Elbaz-Poulichet, F., Sabatier, P., Dezileau, L., and Freydier, R. (2014). Sedimentary record of V, U, Mo and Mn in the Pierre-Blanche lagoon (Southern France) – Evidence for a major anoxia event during the Roman period. *The Holocene*, 24(10):1384–1392.

European and Mediterranean Plant Protection Organization (2013). EPPO Global Database.pdf. Technical Report 2543, EPPO.

Evrard, O., Chaboche, P.-A., Ramon, R., Foucher, A., and Laceby, J. P. (2020). A global review of sediment source fingerprinting research incorporating fallout radiocesium (137Cs). *Geomorphology*, 362:107103.

Foley, J. A., DeFries, R., Asner, G. P., Barford, C., Bonan, G., Carpenter, S. R., Chapin, F. S., Coe, M. T., Daily, G. C., Gibbs, H. K., Helkowski, J. H., Holloway, T., Howard, E. A., Kucharik, C. J., Monfreda, C., Patz, J. A., Prentice, I. C., Ramankutty, N., and Snyder, P. K. (2005). Global Consequences of Land Use. *Science*, 309(5734):570–574.

Foucher, A., Chaboche, P.-A., Sabatier, P., and Evrard, O. (2021a). A worldwide meta-analysis (1977–2020) of sediment core dating using fallout radionuclides including ^{137}Cs and ^{210}Pb$_{xs}$. *Earth System Science Data*, 13(10):4951–4966.

Foucher, A., Evrard, O., Cerdan, O., Chabert, C., Lefèvre, I., Vandromme, R., and Salvador-Blanes, S. (2021b). Deciphering human and climatic controls on soil erosion in intensively cultivated landscapes after 1950 (Loire Valley, France). *Anthropocene*, 34:100287.

Foucher, A., Tassano, M., Chaboche, P.-A., Chalar, G., Cabrera, M., Gonzalez, J., Cabral, P., Simon, A.-C., Agelou, M., Ramon, R., Tiecher, T., and Evrard, O. (2023). Inexorable land degradation due to agriculture expansion in South American Pampa. *Nature Sustainability*.

Fuentes-Llanillo, R., Telles, T. S., Soares Junior, D., De Melo, T. R., Friedrich, T., and Kassam, A. (2021). Expansion of no-tillage practice in conservation agriculture in Brazil. *Soil and Tillage Research*, 208:104877.

Gandhi, K., Khan, S., Patrikar, M., Markad, A., Kumar, N., Choudhari, A., Sagar, P., and Indurkar, S. (2021). Exposure risk and environmental impacts of glyphosate: Highlights on the toxicity of herbicide co-formulants. *Environmental Challenges*, 4:100149.

Garcia-Rodrıguez, F., Mazzeo, N., Sprechmann, P., Metzeltin, D., Sosa, F., Renom, M., Scharf, B., and Gaucher, C. (2002). Paleolimnological assessment of human impacts in Lake Blanca, SE Uruguay. *Journal of Paleolimnology*.

Heri, W., Carroll, B., Parshley, T., and Nabors, J. B. (2008). Production, Development, and Registration of Triazine Herbicides. In *The Triazine Herbicides*, pages 31–43. Elsevier.

Hoffmann-Campo, C. B., Oliveira, L. J., Moscardi, F., Gazzoni, D. L., Corrêa-Ferreira, B. S., Lorini, I. A., Borges, M., Panizzi, A. R., Sosa-Gomez, D. R., and Corso, I. C. (2003). Integrated pest management in Brazil. In Maredia, K. M., Dakouo, D., and Mota-Sanchez, D., editors, *Integrated pest management in the global arena*, pages 285–299. CABI Publishing, UK, 1 edition.

Janssen, M. P. M. (2011). Endosulfan. A closer look at the arguments against a worldwide phase out. *National Institute for Public Health and the Environment*.

Jeschke, P., Witschel, M., Krämer, W., and Schirmer, U., editors (2019). *Modern Crop Protection Compounds*. Wiley, 1 edition.

Killick, R. and Eckley, I. A. (2014). **changepoint**: An*R*Package for Changepoint Analysis. *Journal of Statistical Software*, 58(3). Publisher: Foundation for Open Access Statistic.

Kruk, C., Segura, A., Piñeiro, G., Baldassini, P., Pérez-Becoña, L., García-Rodríguez, F., Perera, G., and Piccini, C. (2023). Rise of toxic cyanobacterial blooms is promoted by agricultural intensification in the basin of a large subtropical river of South America. *Global Change Biology*, 29(7):1774–1790.

Londero, A. L., Minella, J. P. G., Schneider, F. J. A., Deuschle, D., Merten, G. H., Evrard, O., and Boeni, M. (2021). Quantifying the impact of no-till on sediment yield in southern Brazil at the hillslope and catchment scales. *Hydrological Processes*, 35(7):e14286.

Luukko, P. J. J., Helske, J., and Räsänen, E. (2016). Introducing libeemd: a program package for performing the ensemble empirical mode decomposition. *Computational Statistics*, 31(2):545–557.

López, S. L., Aiassa, D., Benítez-Leite, S., Lajmanovich, R., Mañas, F., Poletta, G., Sánchez, N., Simoniello, M. F., and Carrasco, A. E. (2012). Pesticides Used in South American GMO-Based Agriculture. In *Advances in Molecular Toxicology*, volume 6, pages 41–75. Elsevier.

Mantovani, J. R., Alcântara, E., Baião, C. F., Pampuch, L., Curtarelli, M. P., Mariano Ribeiro, J. V., Guimarães, Y. C., Londe, L., Massi, K., Marengo, J., Nobre, C. A., Assireu, A. T., Bortolozo, C. A., Simões, S. J., Tomasella, J., Leal De Moraes, O. L., and Park, E. (2025). Unprecedented flooding in Porto Alegre Metropolitan Region (Southern Brazil) in May 2024: Causes, risks, and impacts. *Journal of South American Earth Sciences*, 160:105533.

Mañay, N., Rampoldi, O., Alvarez, C., Piastra, C., Heller, T., Viapiana, P., and Korbut, S. (2004). Pesticides in Uruguay. In Ware, G. W., Albert, L. A., Crosby, D. G., De Voogt, P., Hutzinger, O., Knaak, J. B., Mayer, F. L., Morgan, D. P., Park, D. L., Tjeerdema, R. S., Yang, R. S. H., and Gunther, F. A., editors, *Reviews of Environmental Contamination and Toxicology*, volume 181, pages 111–138. Springer New York, New York, NY.

McInnes, E. F., Papineni, S., Rinke, M., Schorsch, F., and Marxfeld, H. A. (2023). Agrochemicals. In *Haschek and Rousseaux's Handbook of Toxicologic Pathology, Volume 3*, pages 727–763. Elsevier.

Mellanby, K. (1992). *The DDT story*. British Crop Protection Council, Farnham, Surrey, UK.

Meriel Watts (2011). Endosulfan: Supporting documentation for inclusion in Annex A. Technical report, Pesticides action network asia and the pacific.

Merotto, A., Gazziero, D. L. P., Oliveira, M. C., Scursoni, J., Garcia, M. A., Figueroa, R., and Turra, G. M. (2022). Herbicide use history and perspective in South America. *Advances in Weed Science*, 40(spe1):e020220050.

Metcalf, R. L. (2000). Insect Control. In Wiley-VCH, editor, *Ullmann's Encyclopedia of Industrial Chemistry*. Wiley, 1 edition.

National Toxicology Program (2021). mirex.pdf. Scientifique CAS No. 2385-85-5, U.S Department of Health and Human Services.

Oliveira, J. S., Inda, A. V., Barrón, V., Torrent, J., Tiecher, T., and De Oliveira Camargo, F. A. (2020). Soil properties governing phosphorus adsorption in soils of Southern Brazil. *Geoderma Regional*, 22:e00318.

Oliveira, T. E. D., Freitas, D. S. D., Gianezini, M., Ruviaro, C. F., Zago, D., Mércio, T. Z., Dias, E. A., Lampert, V. D. N., and Barcellos, J. O. J. (2017). Agricultural land use change in the Brazilian Pampa Biome: The reduction of natural grasslands. *Land Use Policy*, 63:394–400.

Oliveira Gomes De Assunção, T., Scheffer Thoni, L., Bento Rosa Gomes, F., Rodrigues Castro, S., Manfred Freire Brandt, E., and De Oliveira Pereira, R. (2022). Diurom e tebuconazol no Brasil: Comercialização e ocorrência em águas. *Principia: Caminhos da Iniciação Científica*, 22.

OpenStreetMap contributors (2024). Planet dump retrieved from https://planet.osm.org.

Overbeck, G., Muller, S., Fidelis, A., Pfadenhauer, J., Pillar, V., Blanco, C., Boldrini, I., Both, R., and Forneck, E. (2007). Brazil's neglected biome: The South Brazilian Campos. *Perspectives in Plant Ecology, Evolution and Systematics*, 9(2):101–116.

O'Farrell, I., Bordet, F., and Chaparro, G. (2012). Bloom forming cyanobacterial complexes co-occurring in a subtropical large reservoir: validation of dominant eco-strategies. *Hydrobiologia*, 698(1):175–190.

Palladino, C., García, I., and Fernández, G. (2023). Pesticide dependence and associated risks in Uruguayan agriculture: limitations in its approach. *Agrociencia Uruguay*, 27:e1156.

Perestrelo, R., Silva, P., Porto-Figueira, P., Pereira, J. A., Silva, C., Medina, S., and Câmara, J. S. (2019). QuEChERS - Fundamentals, relevant improvements, applications and future trends. *Analytica Chimica Acta*, 1070:1–28.

Pignati, W., Oliveira, N. P., and Silva, A. M. C. D. (2014). Vigilância aos agrotóxicos: quantificação do uso e previsão de impactos na saúde-trabalho-ambiente para os municípios brasileiros. *Ciência & Saúde Coletiva*, 19(12):4669–4678.

Pomari-Fernandes, A., De Freitas Bueno, A., and Sosa-Gómez, D. R. (2015). Helicoverpa armigera: current status and future perspectives in Brazil. *Current Agricultural Science and Technology*, 21(1).

Powell, R. L. and Still, C. J. (2009). Biogeography of C3 and C4 vegetation in South America. *Anais XIV Simposio Brasileiro de Sensoriamento Remoto, INPE*, pages p. 2935–2942.

Quirós, R. and Luchini, L. (1982). Características Limnológicas del Embalse de Salto Grande, III: Fitoplancton y su Relación con Parámetros Ambientales. *Natura Neotropicalis*, 1(13):49–66.

Ramon, R. (2021). *Quantifying sediment source contributions in contrasted agricultural catchments (Uruguay River, Southern Brazil)*. PhD thesis, Universit{\'e} Paris-Saclay ; Universidade Federal do Rio Grande do Sul (Porto Alegre, Br{\'e}sil).

Ramos, P. V., Inda, A. V., Barrón, V., Teixeira, D. D. B., and Marques, J. (2021). Magnetic susceptibility in the prediction of soil attributes in southern Brazil. *Soil Science Society of America Journal*, 85(1):102–116.

Rauh, V., Arunajadai, S., Horton, M., Perera, F., Hoepner, L., Barr, D. B., and Whyatt, R. (2011). Seven-Year Neurodevelopmental Scores and Prenatal Exposure to Chlorpyrifos, a Common Agricultural Pesticide. *Environmental Health Perspectives*, 119(8):1196–1201. Publisher: Environmental Health Perspectives.

Rodríguez-Bolaña, C., Pérez-Parada, A., Niell, S., Heinzen, H., and De Mello, F. T. (2024). Comparative deterministic and probabilistic approaches for assessing the aquatic ecological risk of pesticides in a mixed land use basin: A case study in Uruguay. *Science of The Total Environment*, 910:168704.

Sabatier, P., Poulenard, J., Fanget, B., Reyss, J.-L., Develle, A.-L., Wilhelm, B., Ployon, E., Pignol, C., Naffrechoux, E., Dorioz, J.-M., Montuelle, B., and Arnaud, F. (2014). Long-term relationships among pesticide applications, mobility, and soil erosion in a vineyard watershed. *Proceedings of the National Academy of Sciences*, 111(44):15647–15652.

Simard, F. (2018). La lutte contre les vecteurs : quel avenir ? *Biologie Aujourd'hui*, 212(3-4):137–145.

Skidmore, M. E., Sims, K. M., and Gibbs, H. K. (2023). Agricultural intensification and childhood cancer in Brazil. *Proceedings of the National Academy of Sciences*, 120(45):e2306003120.

Souza, C. M., Z. Shimbo, J., Rosa, M. R., Parente, L. L., A. Alencar, A., Rudorff, B. F. T., Hasenack, H., Matsumoto, M., G. Ferreira, L., Souza-Filho, P. W. M., De Oliveira, S. W., Rocha, W. F., Fonseca, A. V., Marques, C. B., Diniz, C. G., Costa, D., Monteiro, D., Rosa, E. R., Vélez-Martin, E., Weber, E. J., Lenti, F. E. B., Paternost, F. F., Pareyn, F. G. C., Siqueira, J. V., Viera, J. L., Neto, L. C. F., Saraiva, M. M., Sales, M. H., Salgado, M. P. G., Vasconcelos, R., Galano, S., Mesquita, V. V., and Azevedo, T. (2020). Reconstructing Three Decades of Land Use and Land Cover Changes in Brazilian Biomes with Landsat Archive and Earth Engine. *Remote Sensing*, 12(17):2735.

Stockholm Convention on Persistent Organic Pollutants (2011). UNEP-POPS-NIP-GUID-03-Alternatives-Endosulfan-2011.English.pdf. Technical report, Stockholm Convention.

Tales Tiecher (2015). *Fingerprinting sediment sources in agricultura catchments in Southern Brazil*. PhD thesis, Federal University of Rio Grande do Sul. Publisher: Unpublished.

Tleuova, A. B., Wielogorska, E., Talluri, V. S. S. L. P., Štěpánek, F., Elliott, C. T., and Grigoriev, D. O. (2020). Recent advances and remaining barriers to producing novel formulations of fungicides for safe and sustainable agriculture. *Journal of Controlled Release*, 326:468–481.

United States Environmental Protection Agency (1995). metolachlor.pdf. Reregistration Eligibility Decision (RED) Metolachlor EPA 738-R-95-006, United States Environmental Protection Agency.

United States Environmental Protection Agency (2002). endosulfan_red.pdf. Reregistration Eligibility Decision (RED) Endosulfan EPA 738-R-02-013, United States Environmental Protection Agency.

Wieslaw, L. (2025). The Impact of the EU-MERCOSUR Agreement on Soybean Meal and Corn Feed Markets in the EU and Poland. *EUROPEAN RESEARCH STUDIES JOURNAL*, XXVIII(Issue 3):1016–1032.

Woodford, E. K. (1957). The Toxic Action of Herbicides. *Outlook on Agriculture*, 1(4):145–154.

Zalles, V., Hansen, M. C., Potapov, P. V., Parker, D., Stehman, S. V., Pickens, A. H., Parente, L. L., Ferreira, L. G., Song, X.-P., Hernandez-Serna, A., and Kommareddy, I. (2021). Rapid expansion of human impact on natural land in South America since 1985. *Science Advances*, 7(14):eabg1620.

Zurbriggen, C., González-Lago, M., Baraibar, M., Baethgen, W., Mazzeo, N., and Sierra, M. (2020). Experimentation in the Design of Public Policies: The Uruguayan Soils Conservation Plans. *Iberoamericana – Nordic Journal of Latin American and Caribbean Studies*, 49(1):52–62.

VI

The hidden consequences of agricultural development: Soil degradation and pesticide contamination in the South American Pampa

Chapter 6

The hidden consequences of agricultural development: Soil degradation and pesticide contamination in the South American Pampa.

Analysis of the sediment core collected in the Salto Grande reservoir revealed how the construction of dams, land-use and land-cover transitions, the massive introduction of genetically modified crop monocultures and the shift to no-tillage practices impacted the fluxes of sediments and contaminants in the vast and understudied region of the Pampa biome. This study also revealed a change in the contribution of the sources of sediments in the reservoir associated with the massive changes of land-use in the southern part of the river basin.

Another core was sampled in a river basin draining exclusively areas of the Pampa biome and in one of the oldest reservoirs in South America, the Rincon del Bonete dam reservoir, inaugurated in 1945. Sediment fluxes could therefore be reconstructed since the 1950s in the Pampa region in Uruguay through a multi-proxy analysis including key pesticides used in the region.

Graphical Abstract

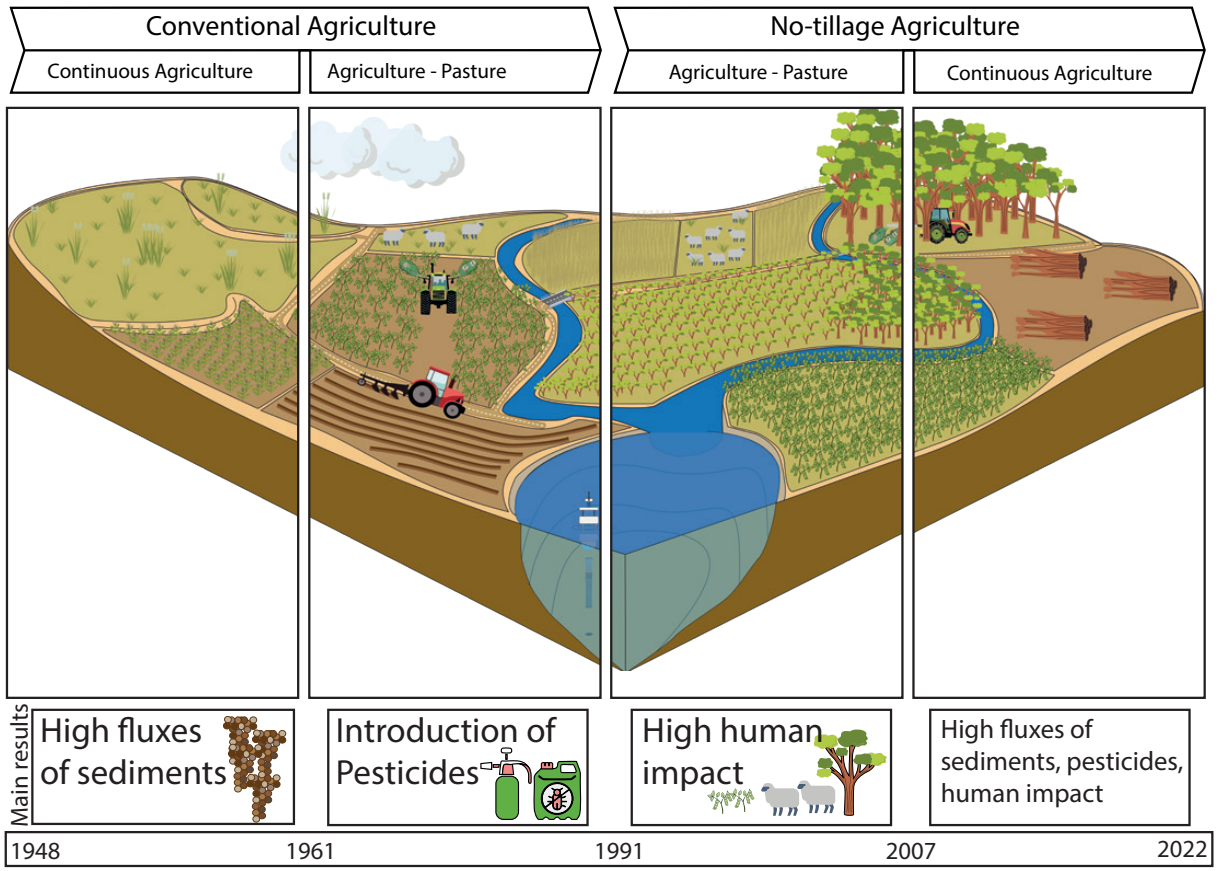

Amaury Bardelle[1], Renaldo Gastineau[2], Floriane Guillevic[3], Anthony Foucher[1], Pierre-Alexis Chaboche[1], José Corcho Alvarado[4], Stefan Röllin[4], Guillermo Chalar[5], Marcos Tassano[6,7], Pierre Sabatier[2], Nathalie Cottin[2], Rosalie Vandromme[8], Olivier Cerdan[8], Christine Alewell[3], Olivier Evrard[1]

[1]Laboratoire des Sciences du Climat et de l'Environnement (LSCE-IPSL), Université Paris-Saclay, UMR 8212 (CEA-CNRS-UVSQ), Gif-sur-Yvette, 91190, France
[2]EDYTEM, Université Savoie Mont Blanc, CNRS, Bâtiment Pôle Montagne, 5 bd de la mer Caspienne, Le Bourget du Lac, 73376, France
[10]Environmental Geosciences, University of Basel, Basel, 4056, Switzerland
[3]University of Basel | UNIBAS, Department of Environmental Sciences, Basel, Switzerland
[4]Nuclear Chemistry Division, Spiez Laboratory, Federal Office for Civil Protection, Austrasse, Spiez, Switzerland
[5]Instituto de Ecología y Ciencias Ambientales, Sección Limnología, Facultad de Ciencias, Universidad de la República, Montevideo, Uruguay
[6]Laboratorio de Radioquímica, Área de Radiofarmacia, Centro de Investigaciones Nucleares. Facultad de Ciencias, Universidad de la República, Montevideo, Uruguay
[7]Instituto de Investigacion Una Salud, Universidad de la República, Montevideo, Uruguay
[8]Risk and Prevention Division, Bureau de Recherches Géologiques et Minières (BRGM), Orléans, F-45060, France
Received 3 May 2025; Received in revised form 19 September 2025; Accepted 20 September 2025



ABSTRACT

Agricultural expansion has led to an acceleration of soil erosion and sediment dynamics in South America in general and in the Pampa biome in particular. This region is a hotspot of land-use and land-cover changes and was marked by important and rapid shifts in farming practices. However, the environmental consequences of these changes remain under-documented.

To address this lack, the current research uniquely reconstructed sediment fluxes since the 1950s in the Pampa region in Uruguay from a sediment archive collected in a dam reservoir inaugurated in 1945. This core was analysed following a multi-proxy approach and fluxes of key pesticides were reconstructed since the 1950s. Results revealed that while early agricultural phases included widespread pesticide use, their impact remained limited due to the limited size of cultivated areas. A transitional period to no-tillage farming and pasture rotation first reduced sediment delivery. Nevertheless, afterwards, large-scale land conversion, combined with intensive pesticide application, has led to another episode of acceleration in soil erosion and an increase in sediment fluxes, largely decoupled from the precipitation variability alone. Notably, a resurgence of the banned DDT pesticide was observed suggesting the possible remobilisation of DDT originating from past applications. These findings provide long-term insights into the environmental consequences of the changes in land-use, land-cover and farming practices since the mid-twentieth century in a relatively understudied region and highlight the need for continued monitoring and for the implementation of measures to mitigate soil erosion and pesticide contamination in the Pampa region.

6.1 . Introduction

South America has experienced significant landscape transformations driven by the expansion of agriculture (pasture, cropland, tree plantations) over the last 70 years. This expansion took place at the expense of natural ecosystems. Since 1985, pasture, cropland, and forest plantation areas have increased by 23%, 160%, and 288%, respectively, often replacing natural vegetation, including natural tree cover (-16% in South America) and natural grasslands (-26% in Southern Brazil) (Oliveira et al. 2017; Zalles et al. 2021). This shift has led to widespread soil degradation, a loss of biodiversity, and natural habitat destruction (Zurbriggen et al. 2020).

The Pampa biome, which is a temperate grassland ecosystem primarily located in Uruguay, southern Brazil and central eastern Argentina, has recently emerged as one of the global hotspots of land-use change (Baeza et al. 2022). These changes threaten soil and water resources as well as biodiversity in a biome that stores large quantities of carbon and supports unique ecosystems (Andrade et al. 2023). The Brazilian Pampa covers slightly over 2% of Brazil's surface area, but it holds about 9% of its total biodiversity (Andrade et al. 2023). Despite the importance of this biome in terms of biodiversity and soil carbon storage, 80% of Uruguayan soils located in the Pampa region were already affected by degradation in 2008 (Chiappe et al. 2008).

The agricultural land expansion and the changes in farming practices from a conventional tillage-based system to a no-tillage-based agriculture in Uruguay started in the 1990s, and they then accelerated in the early 2000s with the aim of reducing soil degradation and erosion. This change has been made possible following the decrease in the cost of herbicides along with the introduction of genetically modified herbicide-resistant crops (Merotto et al. 2022). Accordingly, this shift from a tillage-based to a no-tillage agriculture created a heavy reliance of farmers on the use of pesticides in general, and on glyphosate in particular. Locally, continuous soybean monoculture replaced the traditional crop-pasture rotation, reducing biodiversity and altering weed populations (Merotto et al. 2022). Regionally, the expansion of genetically modified crops, especially glyphosate-resistant soybean, led to a surge in herbicide use, causing ecological shifts such as the expansion of herbicide-resistant weeds, which now represents a major threat for agriculture in Uruguay (Merotto et al. 2022).

Locally, some studies have quantified soil redistribution rates in the region. For instance, Cabrera et al. (2023) reported median net erosion rates of 1.4 to 19.3 $t.ha^{-1}.yr^{-1}$ in contrasting river basins (covering 19.8 to 171.1 km^2) in Uruguay. They used ^{137}Cs and excess lead-210 ($^{210}Pb_{ex}$) measurements to reconstruct soil losses over different periods and under contrasted land-uses at sites that started to be intensively cultivated before the 1960s. Furthermore, an average soil redistribution rate of 7 $t.ha^{-1}$ was found at sites characterised by extensive cattle ranching. Subsequently, soil losses and soil health degradation can lead to regional and basin-scale impacts. Indeed, nutrient-enriched runoff has been linked to toxic cyanobacteria blooms that have prevented water from meeting public health standards

since 2010 (Kruk et al. 2023).

More generally, in addition to the increases in soil losses and sediment/nutrient transfers to water bodies, the use of pesticides in modern agriculture was shown to contaminate soil, water and the vegetation, and it was proved to be toxic for both biodiversity (Aktar et al. 2009) and human populations. Accordingly, Skidmore et al. (2023) demonstrated a statistically significant increase in paediatric leukaemia following soybean crop production expansion in the region, with an increased exposure of the populations to pesticides that may occur via the contamination of the water supply.

However, there is a lack of historical records to reconstruct these pesticide-related pressures. Moreover, few quantitative data are available for the period of agricultural expansion, since the mid-twentieth century, on the impact of the changes in land-use and in farming practices on the evolution of soil and water quality along with soil loss at the regional scale and for the period of agricultural expansion since the mid-twentieth century.

In this context, the objective of the current research is to understand how changes in land-use and agricultural practices, i.e. the shift from natural to anthropogenic landscapes, the transition from conventional to no-tillage farming, and the application of pesticides— may have impacted sediment transfers in the Pampa Biome region since the onset of modern agricultural development.

To this end, retrospective studies using reservoir sediment cores may provide a powerful means to reconstruct long-term environmental changes in the absence of continuous monitoring, as demonstrated by Foucher et al. (2023). These approaches have also been used to reconstruct contaminant and pesticide transfers across different contexts and timescales (Garcia-Rodrıguez et al. 2002).

In South America in general, and in the Pampa biome in particular, such reconstructions are associated with major challenges, including the limited number of lakes and reservoirs suitable for sediment coring operations. Additional parameters, such as the reservoir size, the extent of its drainage area, and the year of reservoir construction, must also be considered when selecting potential sampling sites.

Foucher et al. (2023) successfully identified a reservoir in Uruguay that meets these criteria and collected a sediment core to investigate the impacts of landscape modifications on sediment production. However, their analysis was restricted to the recent period comprised between 1990 and 2020 as they could not investigate earlier changes in land-use, land-cover and agricultural practices (i.e., tillage transition and increasing pesticide use).

To address this gap, the present study analysed a longer sediment core retrieved from the same site, the Rincón del Bonete reservoir, draining a 39,500 km^2 transnational catchment from Uruguay and Southernmost Brazil. This core, which reached the reservoir's bottom, is expected to cover the full period since the dam construction (i.e. 1945), allowing to reconstruct the impact of land-use and agricultural practices on sediment dynamics since World War II, which is almost unique in this part of the world where limited historical archive/data have been made available to date. Furthermore, the originality of this study

lies in the extensive multi-proxy analysis conducted to reconstruct sediment dynamics and relate this data to global and socio-economic trends. Among the analyses performed, a combination of radionuclides including plutonium isotopes were analysed and used to validate the chronology of the sediment core.

More specifically, the study's objectives were threefold: (1) to establish an accurate chronology of the sediment core and validate it, (2) to quantify sediment fluxes and compare them with historical phases of agricultural development in Uruguay, and (3) to reconstruct pesticide fluxes during the successive phases of agricultural expansion and outline their potential impacts on sediment transfers.

6.2 . Materials and Methods

6.2.1 . Study site

The Rincón del Bonete catchment is transboundary with 9% of its surface area being located in Brazil and 91% in Uruguay. It is located within the Pampa biome, mainly in the central and northern regions of Uruguay (figure 6.1) with a geomorphology of hilly to rolling landscapes.

The Rincón del Bonete catchment has two major tributaries including Rio Tacuarembó and Rio Negro (figure 6.1). These two rivers drain very contrasting landscapes with distinct reliefs, geologies and soil types, reflecting the occurrence of different ecoregions (Arocena et al. 2022). On the one hand, the Rio Negro, in the western part of the river basin, drains a region characterised by the presence of mudstones and limestones that support the formation of Mollisols, dark soils, which are rich in organic matter, silt, and clay and that are mainly used for crop cultivation. In contrast, the Rio Tacuarembó drains a region mainly composed of Alfisols, underlied by sandstones, characterised by leached and weathered acidic soils with low organic matter content, showing the country's lowest fertility, or shallow sandy or coarser soils with rock outcrops and loose stones on the surface, predominantly used for forest plantations (Arocena et al. 2022).

Overall, land-use in the Rincón del Bonete catchment remained dominated by natural herbaceous vegetation (61%) in 2023. in addition, the catchment was also occupied with cropland cultivated using no-tillage practices (14%), forest plantations (11%), natural forests (5%), wetlands (4%), water bodies (3%) and non-vegetated areas (1%) (figure 6.1).

Moreover, the Rincón del Bonete catchment drains into a reservoir which surface area varies between 465-1495 km^2 (1140 km^2 in optimal conditions). Built in 1937 and inaugurated in 1945, this reservoir is used to generate electric power in Uruguay. Importantly, the Rincón del Bonete reservoir has never been emptied or dredged since its creation. This reservoir is the largest freshwater body in Uruguay (5 km^3 of water storage) with a ratio of 25-33 km^2 of drainage basin per km^2 of reservoir, thereby exceeding the storage capacity of the other reservoirs in the country, including the large Salto Grande and Palmar dams, with respective reservoir surfaces of 783 and 320 km^2 (World Lake Database - 2025).

The climate in Uruguay is considered as humid subtropical according to the Koppen Climate Classi-

fication (World Meteorological Organization - Clasificación climática). Precipitation in the Rivera municipality, a meteorological station located in the Northern part of the catchment, amounted for an annual mean of 1525 $mm.yr^{-1}$ for the 1991-2020 period. The monthly precipitation is the lowest in June, July and August with 79 $mm.mth^{-1}$ on average. During the rest of the year, precipitation is higher and more constant with an average of 143 $mm.mth^{-1}$. The month with the highest precipitation in the Rivera municipality is April, with an average of 180 mm for the 1991-2020 period (World Meteorological Organization - Tablas estadísticas).

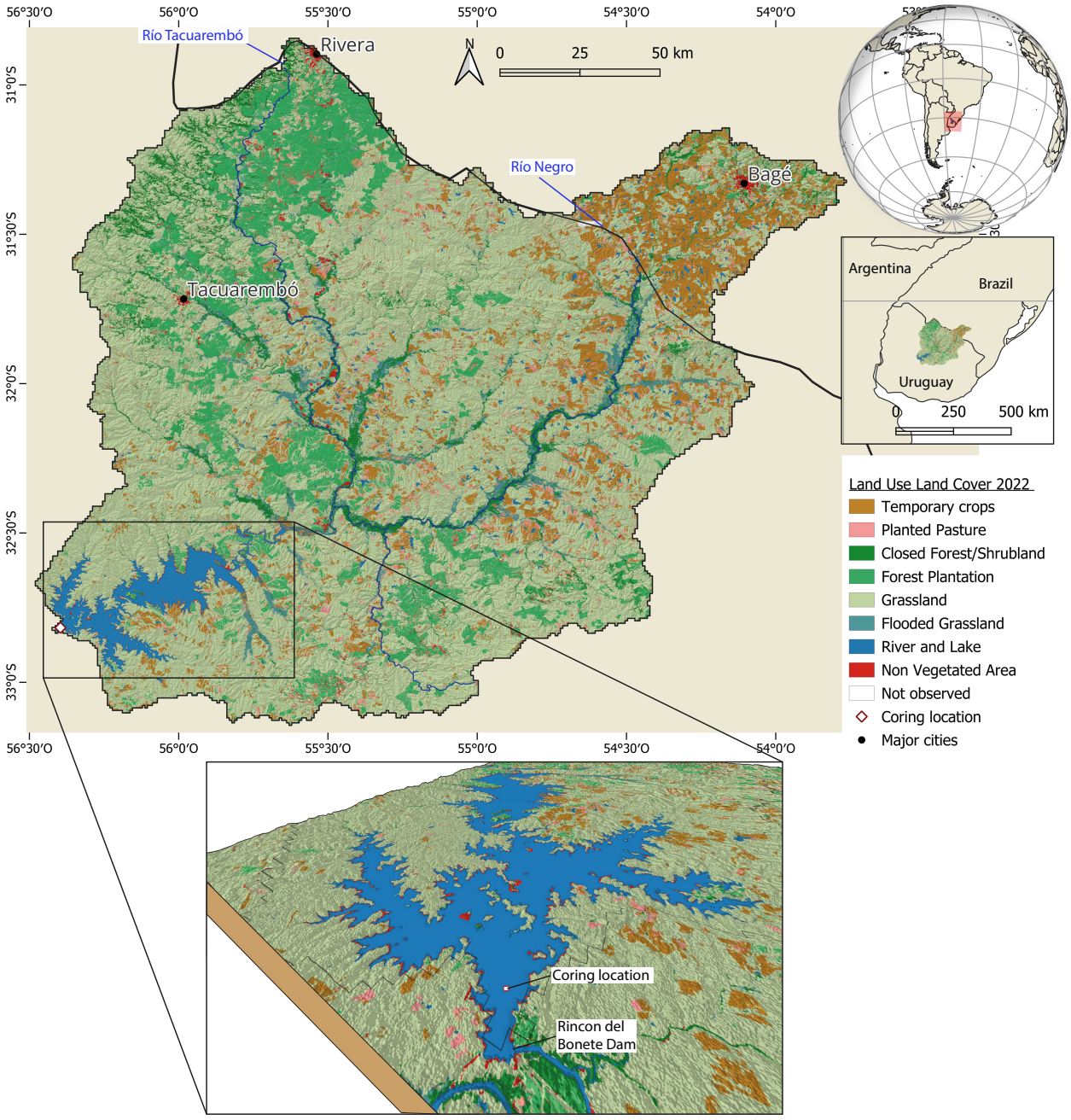

Figure 6.1: Location of the Rincón del Bonete River basin in South America, coring location (S32°49.072', W56°24.008') and map of land-uses and covers in 2022 (MapBiomas Pampa), background map from OpenStreetMap

6.2.2 . Data sources

Land-use was reconstructed in the investigated catchment using the set of maps provided by the MapBiomas network (MapBiomas Pampa) for the Pampa biome for the 1985-2022 period (Baeza et al. 2022). The river basin data were retrieved from the maps published for each year during this period. In the last version of MapBiomas, a distinction was made between permanent pasture and temporary crops. Permanent pastures were defined by MapBiomas as the "cultivation of perennial herbaceous forage species, that persist for more than one year", while temporary crops were defined as the "cultivation of annual herbaceous species that are planted and harvested within one year". Increase and decrease percentages were calculated following equation 6.1.

$$\text{Variation (\%)} = \left(\frac{\text{New value} - \text{Old value}}{\text{Old value}} \right) \cdot 100 \tag{6.1}$$

Rainfall was reconstructed at the scale of the investigated river basin using the climate knowledge portal database (https://climateknowledgeportal.worldbank.org/) and the Climate Engine solution with TerraClimate precipitation calculations (https://app.climateengine.org). This database available at the catchment scale covers the period 1958-2023, at a monthly resolution. This dataset was chosen as is the longest that could be found over the river basin.

To compare the precipitation variations with the reconstructed fluxes of sediments obtained, the mean precipitation per month for each year was calculated. Periods of multiple years with higher precipitation than the calculated median for the whole sequence were also identified.

A 48 cm long sediment (22-BONETE-03) core was collected in December 2022 in the Rincón del Bonete reservoir (IGSN number: 10.58052/IEFOU002D) by local researchers using a Uwitec gravity corer available at the Universidad de la República (Montevideo, Uruguay) equipped with 90 mm PVC liners on a floating platform and by hammering. The sediment core was collected in the original Rio Negro river channel. This channel was identified with a sonar, at 2.5 km from the dam (figure 6.1, under 20 m water depth) to ensure a reconstruction of the complete sedimentation history since the dam creation.

6.2.3 . Methodology

The analysis conducted, their resolution and the associated units were summarized in appendix 6.5. Readers can refer to this table for a fast and clear understanding of all the measurements carried out.

Particle size analysis

Particle size analysis was performed on fresh sediment at a centimetric resolution with a laser diffraction particle size analyser (Mastersizer 3000 with Hydro LV, Malvern Panalytical) in osmotic water on fresh sediment with sonic dispersion to minimise particle flocculation. Each sediment sample was analysed five times. The particle size distribution was measured in the range from 0.01 µm to 3500 µm, and the

fraction indices D10, D50, D90 corresponding to the proportion of particles smaller than 10%, 50% and 90% were extracted. Besides sonic dispersion, no other treatment was conducted on the sediment.

Density analysis

Relative density of the sediment was recorded with a Computer Tomography scanner (CT-scan) every 0.625mm. Images were recorded via a GE Discovery CT750 HD instrument available on the DOSEO platform (French Atomic Energy and Alternative Energy Commission, CEA Paris-Saclay, France). Relative density (grey values) measured with the CT scan were extracted from the reconstructed images via the Free software ImageJ.

Bulk density (ρ_b) was then measured on 8 samples of fresh sediment using a 1.7 cm^3 (V) acrylic cube. The cubes were filled with fresh sediment, the humid weight (m_{humid} in g) was reported, then oven-dried at 40°C for 48 to 96 hours, and the dry weight (m_{dry} in g) was finally measured. The bulk density (ρ_b in $g.cm^3$) was calculated following equation 6.2.

$$\rho_b = \frac{m_{\text{dry}}}{V} \tag{6.2}$$

The mean values of the Ct scan relative density (Hounsfield) over the samples were correlated to the bulk density, and density was reconstructed for the whole sequence following the procedure proposed by Foucher et al. (2023).

Organic matter analysis

One-half of the core was subsampled following depth increments of 1 cm. The sediment was dried at 40°C for 48 h and ground before total organic carbon (TOC) concentration, nitrogen concentration (TN) measurements and stable C (δ^{13}C) isotope ratios were determined.

The %TOC, %TN and δ^{13}Corg contents were measured using an elemental analyser (Flash HT 2000) coupled to an isotope ratio mass spectrometer Advantage delta V via a conflow IV interface from Thermo Scientific. The EA-IRMS instrument was calibrated against two standards (i.e., EMAP2 and USGS24). Analytical precision and repeatability were assessed via the analysis of reference material (Low Organic Standard and High Organic Standard). In the current research, the mean uncertainties amounted to 0.01% for TN, 0.06% for TOC, 0.1 ‰ for δ^{13}C. The ^{13}C isotope content is expressed as δ^{13}C in against Pee Dee Belemnite (PDB). This is a standard reference for δ^{13}C, measured on shells of a species of belemnite from the Upper Cretaceous.

Gamma spectrometry analysis

Gamma spectrometry measurements were conducted on 1-cm layers of dried and ground sediment samples using a 'well' type HPGe detector (Canberra/Ortec®) available at the Modane underground lab-

oratory, a subterranean low-background laboratory located within the Fréjus Road Tunnel, near Modane, France. This laboratory is shielded from cosmic radiation by 1700 m of rocks and is only equipped with very low activity materials and copper-lead shielded detectors to achieve ultra-low background in order to analyse low-radioactivity samples in the best conditions. The activities of lead-210 in excess ($^{210}Pb_{ex}$) were calculated by subtracting the two Radium-226 daughters, Lead-214 (average count at 295.2 and 351.9 keV) and Bismuth-214 (609.3 keV), from the total ^{210}Pb activities detected at 46.5 keV. ^{137}Cs activities were measured at 662 keV and decay-corrected to the sampling date.

All measurements were corrected for background levels determined every two months and for detector and geometry efficiencies.

Plutonium analysis

Based on the vertical distribution of ^{137}Cs activities in the sediment core, 16 samples among those analysed in gamma spectrometry were selected for additional plutonium analyses (^{239}Pu, ^{240}Pu). Measurements were conducted at the Spiez Laboratory in Switzerland following the methodology established by Röllin et al. (2022). Pu isotopes were measured using ICP-MS and MC-ICP-MS after a series of purification and separation steps. The samples were fused, dissolved and filtered to remove silicates, and then Pu was extracted using TEVA, UTEVA, and DGA resins. The isotopes were then quantified using high-sensitivity ICP-MS techniques, correcting for interferences and validating the results with certified reference materials.

Pesticide analysis

A total of 16 pesticides and their metabolites (Appendix 6.4), which were commonly reported in the literature for the Pampa region, were measured at EDYTEM Laboratory (Univ. Savoie Mont-Blanc, France) (Mañay et al. 2004; Palladino et al. 2023).

In order to conduct the pesticide analyses, the second half of the core collected as described above was sampled following depth increments of 2 cm from 0 to 20 cm and then following depth increments of 4 cm from 20 cm to 45 cm. This second set of samples was freeze-dried in an ALPHA 1-2 LD plus (CHRIST®) freeze dryer for 24 to 48h, depending on the sample quantity available.

Pesticides were then extracted via the QuEChERS method; the Quick, Easy, Cheap, Effective, Rugged, and Safe extraction kit and method (Perestrelo et al. 2019). Pesticide concentrations were obtained via Gas and Liquid Chromatography coupled with Mass Spectrometry (GC-MS for Endosulfan, Chlopryrifos Ethyl, DDT,DDD, DDE, and Mirex and LC-MS/MS for S-Metolachlor, Simazine, Atrazine, Diruon, 2.4-D, Tebuconazole, Imidacloriprid and Friponil). Glyphosate and AMPA were analyzed by a rapid LC-MS/MS method with a Polypore H+ column without derivatisation, with a good selectivity and sensitivity.

Once the concentration of pesticides was obtained ($g.g^{-1}$), the equivalent in moles of pesticides

($mol.g^{-1}$) was calculated by dividing each pesticide's concentration by its molar mass ($g.mol^{-1}$).

Extensive research was conducted in the literature and multiple technical reports were analysed in order to obtain different information on the pesticides, such as their dates of first production/marketing and are described and used for interpretation in the results and discussion, section 6.3.6.

Age model and Sediment fluxes

Sediment core chronology was established using $^{210}Pb_{ex}$ activities measured in a set of 29 samples. The *serac* R package for ShortlivEd RAdionuclide Chronology (Bruel and Sabatier 2020) was used for the establishment of the age model via the Constant Flux Constant Sedimentation (CF:CS) model. The age model was validated by identifying the transition from coarser particles to finer sediments at the base of the core, which was associated with the level of the Rio Negro paleochannel corresponding to the dam impoundment period (age model date 1948 $\pm$ 3 years, inauguration of the dam in December 1945). In addition, artificial radionuclides fallout (^{137}Cs, $^{240+239}Pu$ activities, and the associated $^{240/239}Pu$ ratios) from past nuclear weapon tests were used as an independent time-marker to validate the age model (Chaboche et al. 2022). The age-depth model was validated by radionuclide deposition chronology/-pattern affecting South America, including the onset of global detection of nuclear test fallout in 1954, the peak of maximum fallout in the Southern Hemisphere in 1964–1965, and specific nuclear bomb signatures such as those associated with several French nuclear tests conducted in Polynesia between 1966–1974 (UNSCEAR 2008 Report).

Sediment fluxes (MAR, Mass Accumulation Rate,$g.cm^{-2}.yr^{-1}$) were reconstructed by multiplying SAR ($cm.yr^{-1}$) obtained from the CF:CS age model with high-resolution densities calibrated from the CT scan values ($g.cm^{-3}$); equation 6.3.

Mean fluxes of sediment were calculated based on the high frequency MAR records. The different values of MAR for each year were added and divided by the number of observations available for each year.

$$\mathrm{MAR}\ (\mathrm{g\,cm^{-2}\,yr^{-1}}) = \mathrm{Sedimentation\ rate}\ (\mathrm{cm\,yr^{-1}}) \cdot \mathrm{DBD}\ (\mathrm{g\,cm^{-3}}) \tag{6.3}$$

Pesticides fluxes were derived from the sediment fluxes. To this end, the moles of pesticides were converted into fluxes by multiplying the quantities of pesticides with the MAR (equation 6.4).

$$\mathrm{Fluxes\ of\ pesticides}\ (\mathrm{mol\,cm^{-2}\,yr^{-1}}) = \mathrm{Pesticides}\ (\mathrm{mol\,g^{-1}}) \cdot \mathrm{MAR}\ (\mathrm{g\,cm^{-2}\,yr^{-1}}) \tag{6.4}$$

Statistical tests

The Mann-Kendall Test was applied to identify generally positive or negative (p-values < 0.5) trends in precipitation using the R trend package. The result of the test, 'tau', varies between -1 and 1; it is positive

when the trend increases and negative when the trend decreases. In addition, the breaking point test (Hurtado et al. 2020) available in R (https://CRAN.R-project.org/package=BreakPoints) was performed to identify MAR shifts and to check whether their occurrence matched with contrasted phases of agricultural development as documented in the literature for Uruguay.

In order to identify when the data undergoes a significant change, a breakpoint test is performed on the data series. A breakpoint is validated when the *p*-value was sufficiently low (in the present case, p-value < 0.05). Three breakpoints are searched for in the MAR values to identify the four contrasting periods of sediment inputs identified in the literature (and described in section 6.3.1). Each period has to represent at least three years, taking into account the uncertainty associated with the age model, for a complete period to be considered. Finally, the test is applied using the statistical methods established by Pettit (Pettitt 1979) and Buishand (Buishand 1982). The reason for choosing these two statistical methods is that, as Hurtado et al. (2020) demonstrated, they exhibit a high ability to reproduce the date of the breakpoints when they occurred in the middle of a time series, which is of interest here.

In order to compare and characterise the periods identified in the sediment fluxes with the breakpoint test, a series of tests is applied using the rstatix, Stats, PMCMRplus and FSA packages in R. First, the normality of the data is tested using a Shapiro-Wilk test. Then, a Kruskal-Wallis rank sum test, a non-parametric alternative to ANOVA, is applied to compare the medians across the periods identified in the sediment fluxes. Finally, a Dunn's post hoc test with the commonly used Bonferroni correction is applied for pairwise comparisons to specify which groups differed from each other.

6.3 . Results and discussion

All the data produced during this study, the variable description and metadata are available on Zenodo (Physico-chemical properties of a sediment core collected in the Rincon del bonete dam reservoir, Uruguay to reconstruct environmental changes (1945-2023).

6.3.1 . Evolution of the land-use land-cover

MapBiomas data shows an overall prediction accuracy of 76–79%, depending on the year under consideration (Baeza et al. (2022), MapBiomas - Methodology Collection 4). For the last collection released, a robust classification approach combining spectral and temporal data was applied to distinguish between pasture and cropland. Given their often similar appearance on satellite imagery, especially during certain growing stages, misclassification may occur. The methodology uses annual mosaics, phenological indicators, and post-classification temporal filters to reduce these potential misclassifications. These filters improve temporal consistency by penalizing inter-annual land-use changes that are unlikely to occur in reality, ensuring that transitions reflect real dynamics. This data provided valuable insights into the reconstruction of agricultural expansion, deforestation, tree plantation, and changes in other human activities across the Pampa biome's ecosystems. The temporal resolution of the dataset is also well suited for tracking long-term patterns and assessing policy impacts on land use.

From 1985 to 2022, land-use changes in the Rincón del Bonete basin followed two main axes and mainly affected the natural grasslands. Forest plantations expanded in the northwestern and southeastern regions, while agriculture and pasture increased in the northeast (Figure 6.2). The central part of the basin remained relatively intact. This expansion, originating from the Northern part of the river basin, in Brazil, spread southwards along the Río Negro, primarily targeting fertile Mollisol regions for farming and grazing. In parallel, forest plantations developed along the western Río Tacuarembó in Alfisol-dominated areas, where poor soil quality limited agricultural use (Arocena et al. 2022).

More specifically, forest plantations covered less than 1% of the catchment surface area in 1985. This proportion increased to more than 10% in 2022 (figure 6.2), an increase of 1573% in 37 years. Several periods of accelerated forest plantation are observed, such as those that took place between 1999 and 2005 (increase of 195%) and, more recently, between 2014 and 2019 (increase of 18% of the catchment area).

Permanent pastures increased by more than 169% from 1985 to 2022. 2018 is the year with the maximum area under pasture representing 4.6% of the river basin's area. This progression follows three rising periods(1995-2000, 2003-2005 and 2011-2014). Finally, a slowdown of this trend is observed since 2015 (figure 6.2).

Moreover, the area covered by temporary crops increased from 2.5% of the catchment area in 1985 to more than 10% in 2022. A steady increase is observed between 1985 and 2005, followed by a sharper

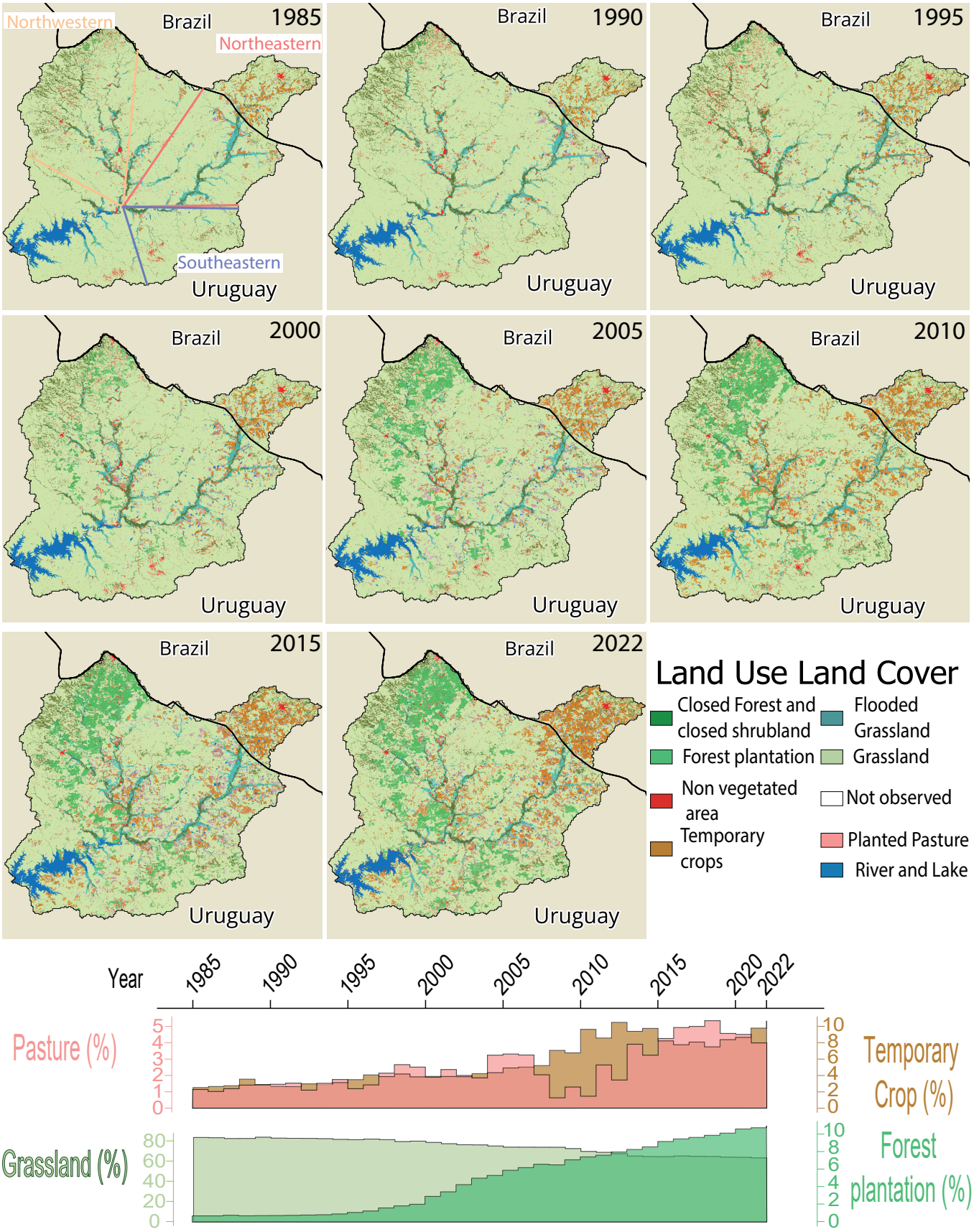

Figure 6.2: Evolution of land-use and land-covers from 1985 to 2022 (MapBiomas Pampa) and representing area (in %) of pasture, grassland, temporary crop and forest plantation extracted from the MapBiomas dataset, background map from OpenStreetMap. The northwestern, southeastern and northeastern parts of the basin are shown for the 1985 map in light orange, red and blue

rise until 2013. It then slows down again before re-accelerating from 2019 to 2022 (Figure 6.2).

In parallel, the area occupied by natural grassland decreased by 25%, as it represented 83% of the Rincón del Bonete river basin surface in 1985 but only 63% in 2022. A strong period of reduction of the surfaces devoted to natural grasslands is observed in 2002-2005 (figure 6.2). These results are comparable with those found by Oliveira et al. (2017) in the nearby Brazilian Pampa. These authors found indeed that the area under natural pastures decreased by 26% since 1975. In parallel, cultivated forests and temporary crops showed the highest growth between 1985-2005, particularly during the second half of this period, from 1995 to 2005.

Natural forests (mean 5.0%), wetlands (mean 3.3%), non-vegetated areas (mean 1.2%), as well as water surfaces (mean 3.0%) remained constant throughout the period ($\pm$ 1-2%).

Based on the land-use and land-cover changes as well as historical records, four periods of agricultural development in Uruguay were identified and described. The first period, from the 1950s until the 1960s, was characterized by continuous cultivation with minimal technological advancements (Hudson et al. 1992). It was then followed by a second period, from the 1970s until the 1990s, marked by the adoption of extensive pesticide use, and the introduction of a crop-pasture rotation system (Merotto et al. 2022), however, most of the catchment area remained largely unexploited (90% of the river basin was then occupied by natural landscapes, i.e. shrublands, wetlands and grasslands), except for the Brazilian uppermost portion (figure 6.2).

From 1990 onwards, a transition occurred as the government voted a law, which granted tax exemptions and even subsidized forestry plantations to initiate and encourage the implementation of these technologically advanced farming techniques (Zurbriggen et al. 2020). A drastic expansion of the area of soybean was also observed, permitted in Uruguay by the authorisation of planting genetically modified soybean seeds and the land leasing law that encouraged short-term leases from 1996. This expansion was accompanied by a transition towards no-tillage agriculture (Garcia-Préchac et al. 2004). As shown by Derpsch et al. (2010), 32% of cropland was cultivated under no-tillage in 2000-2001 compared to 82% in 2006-2007). This third period, from the 1990s to 2002 initially maintained the crop-pasture rotation system, with the implementation of soil conservation practices (Zurbriggen et al. 2020). However, in the subsequent fourth period, from 2002 onwards, this system was abandoned in favour of continuous cultivation and double cultivation (i.e. the planting of two or more crops on the same plot and during the same year), consisting in an intensification of agricultural practices (Rizzo et al. 2021).

As shown in the literature (Hudson et al. 1992; Derpsch et al. 2010; Zurbriggen et al. 2020), changes in land-use and practices across the river basin were influenced by political shifts in the country.

6.3.2 . Sediment analyses

The 22-BONETE-03 sequence is characterised by homogeneous fine brown-coloured sediment. No specific facies or layers could be visually observed when opening the core. However, the layer corre-

sponding to the Rio Negro River channel deposits that took place before the dam impoundment can be visually observed at the base of the core, with the occurrence of coarser sand particles as well as vegetation debris.

Above this facies transition, the D10 index varies between 0.25 and 5.2 $\pm$ 1.2 µm along the core, whereas the D50 index varies between 7.0 and 25.2 $\pm$ 4.6 µm, and D90 varies between 45.0 and 179.8 $\pm$ 41.5 µm (figure 6.3).

Two minima in grain size values are observed, with D10 and D50 indices of 0.3 $\pm$ 0.009 µm and 7.1 $\pm$ 0.1 µm at 5 cm, and 0.25 $\pm$ 0.01 µm and 7.2 $\pm$ 0.3 µm at 10 cm, respectively. D90 amounted to 7.2 $\pm$ 2.9, and 46.1 $\pm$ 13.8 µm at 5 and 10 cm, respectively.

From grain size data as well, the results indicate that the sediment core exhibits a high degree of homogeneity.

TOC values varies from 2.8% at 12 cm to 4.9% at the bottom of the core (44-45 cm) above the pre-dam facies, with an average value of 3.2 $\pm$ 1% (figure 6.3). Three peaks are observed at 38, 32 and 10 cm, with values of 3.8$\%$, 3.6$\%$, and 3.7$\%$, respectively. δ^{13}C remains stable throughout the core (from -18.8 to -22.6‰), except for two minima found at 30 and 11 cm depths, with values of -20.5 and -22.6 ‰, respectively.

δ^{13}C values observed in the sediment sequence reflect the type of plants that grew in soils eroded across the river basin and transported to the reservoir. Overbeck et al. (2007) found the coexistence of C_3 and C_4 plants in the Southern Brazilian grasslands of Rio Grande do Sul (in which the northernmost part of Rincón del Bonete river basin is located). Higher values of δ^{13}C around -16 to -10‰ correspond to the signature of C_4 plants, while lower values of δ^{13}C, between -33 and -24‰ correspond to C_3 plants. This region was predicted to be covered by 50 to 70% of C_4 plants, with values of δ^{13}C around -20‰ by Powell and Still (2009). Bueno et al. (2021) found similar mean values between -19.73 ± 0.35‰ and -18.58 ± 0.55‰. They also found the same trends with a decrease of values in the uppermost layer with values of -23.26‰ and -23.53‰ , which are consistent with those values found in the core analysed in the current research.

The TOC/TN ratio varies between 7 and 11, with an average value of 9$\pm$0.3. Overall, this parameter remains stable along the core, following the same trends as TOC. The minimum value is observed at the top of the core and the maximum is found at 38 cm depth (with values of 7.2 and 10.9, respectively). The TOC/TN ratio shows the same trends as those observed for TOC, with peaks at 38, 30 and 11 cm depths, with respective values of 10.9, 10.9 and 9.5.

The analysis of the TOC/TN ratio provides insights into the provenance of the organic matter, categorised as allochthonous (originating from the catchment) or autochthonous (resulting from biological activity within the reservoir). Terrestrial plants, part of the allochthonous matter, generally show values of TOC/TN above 12 (Lamb et al. 2006) while autochthonous matter is usually characterised by values

below 10. Organic matter in the reservoir therefore appears to consist of a mix of allochtonous and autochthonous material.

A correlation of r^2 = 0.7 is obtained between the measured density and the CT-scan value (Appendix 6.8). The density obtained from calibrating CT-scan values ranges between 0.19 and 0.58 $\pm$ 0.05.

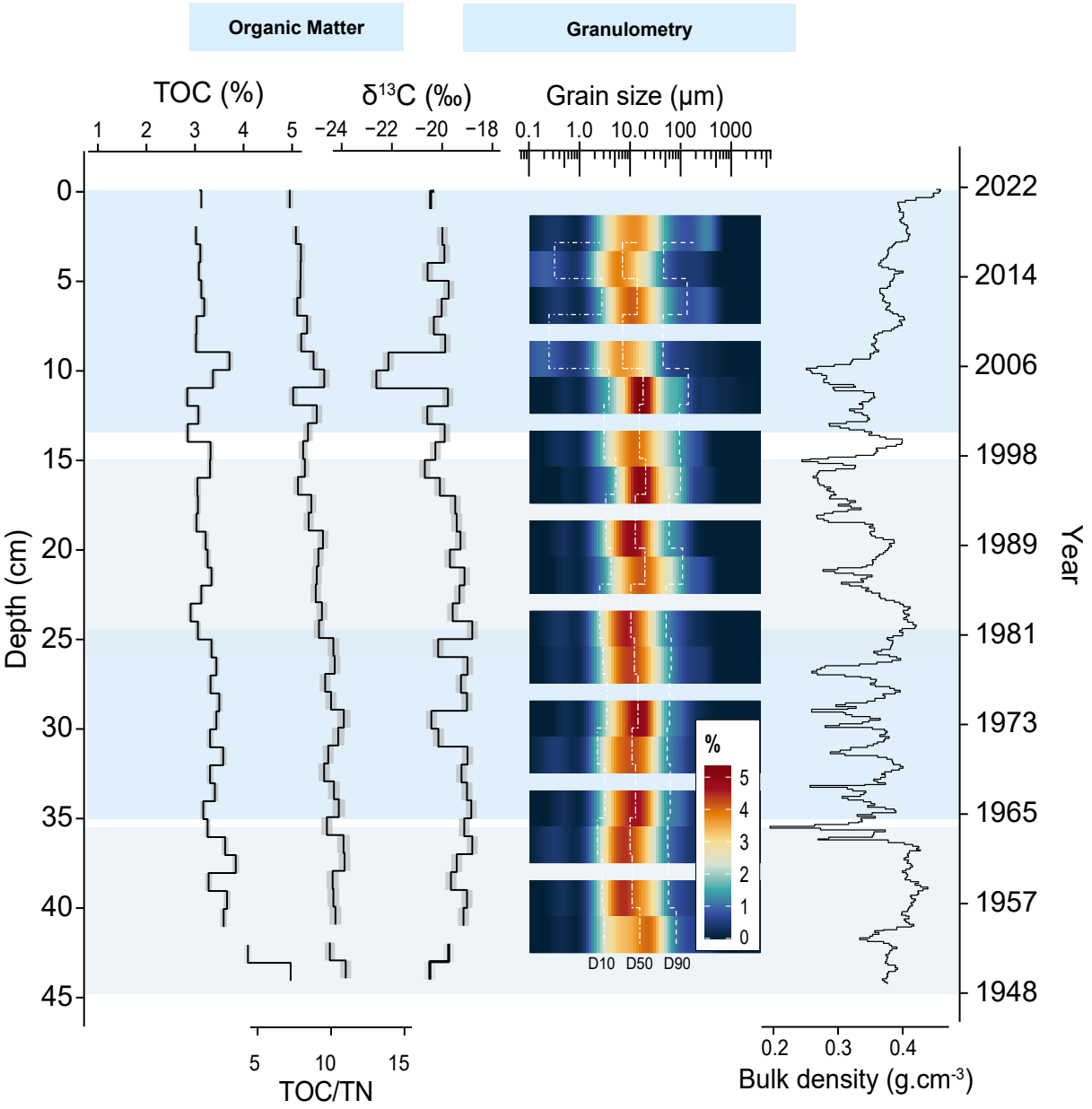

Figure 6.3: Results of Rincón del Bonete core analyses, including organic matter properties (TOC in % and TOC/TN), grain size distribution with D10, D50 and D90 values (dashed white lines) and bulk density values.

6.3.3 . Radionuclide analyses and age model

Gamma spectrometry

The $^{210}Pb_{ex}$ activity along the core decreases following a well-constrained linear trend (r^2 = 0.96) when plotted using a logarithmic scale (figure 6.4). ^{137}Cs activities vary from negligible levels ($<$ 0.6 Bq.kg^{-1}) at the base of the sequence to 12$\pm$0.6 Bq.kg^{-1}. The highest activities of ^{137}Cs are detected between

30 and 35 cm depths, and they are attributed to the peak of the maximum ^{137}Cs bomb fallout generally dated to 1964–1965 in the Southern Hemisphere (Foucher et al. 2021).

Plutonium Analysis

^{240}Pu/^{239}Pu ratios are found to vary between 0.069 and 0.264 ($\pm$ 0.066) along the core. According to the values of this ratio and their variations with time, four periods are identified with first, at the bottom of the core, high ratio values ranging between 0.232 and 0.264 (1948-1956) followed by a decrease in this ratio down to 0.180 (1961-1966). A low ratio between 0.069 and 0.101 is then measured from 1968 to 1981. Finally, a slight increase in this ratio is observed again in the upper part of the core, with corresponding ratio values of 0.114 and 0.096 for the period occurring between 2012 and 2018.

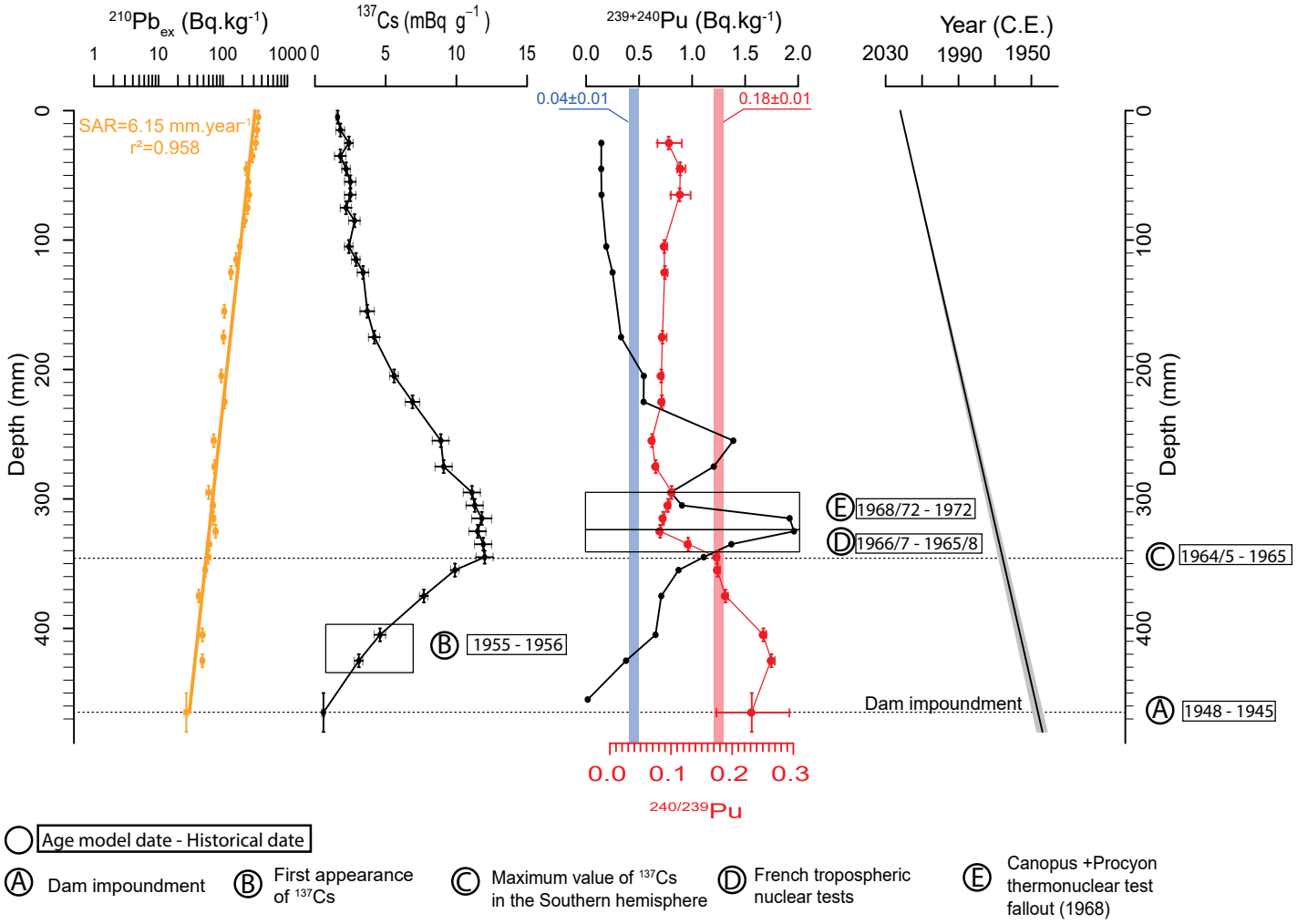

Figure 6.4: Rincón del Bonete core profile with $^{210}Pb_{ex}$, ^{137}Cs, $^{239+240}Pu$ activities ($Bq.kg^{-1}$), $^{240/239}Pu$ ratio and CFCS derived age model. Letters corresponding to historical events were added as well as the associated year

Corresponding letter	Depth (cm)	Year attributed ($^{210}Pb_{ex}$ age model ±3 yr)	^{240}Pu/^{239}Pu ($Bq.kg^{-1}$)	Historical nuclear test events	Events
E	33 - 30	1968-1970	0.101 ± 0.002	1968-1972	Canopus / Procyon nuclear test fallout (launched 1968)
D	34 - 33	1965-1968	0.128 ± 0.001	1966-1967	French tropospheric nuclear test
C	35	1965	0.176 ± 0.003	1964-1965	Peak emissions of ^{137}Cs in the Southern hemisphere
B	42 - 40	1953 - 1956	0.251 ± 0.003	1955	First detection of ^{137}Cs

Table 6.1: Comparison between the $^{210}Pb_{ex}$ age model and historical nuclear test events attributed on the basis of plutonium-related data as well as corresponding letters from figure 6.4.

Age model

Age modelling of sediment cores is often achieved using the $^{210}Pb_{ex}$ method, with this initial model validation typically relying on ^{137}Cs activities, a radionuclide released during nuclear bomb tests conducted between 1945 and 1963 by the United States of America (USA), the Former Soviet Union (FSU) and the United Kingdom (UK). Along with ^{137}Cs, other radionuclides such as ^{239}Pu and ^{240}Pu were deposited globally during this period (UNSCEAR 2000 Report).

Age modelling or validation using ^{137}Cs in sediment cores collected in part of South America is controversial. Some studies have shown that the use of this radionuclide as an input for the validation of age models could be associated with significant uncertainties, given the wide shape of the peak observed in some sediment cores collected in this part of the world (Magand and Arnaud 2007). Other radionuclides than ^{137}Cs may be used as stratigraphic markers (Ferreira et al. 2016). In this context, Chaboche et al. (2022) demonstrated that ^{240}Pu/^{239}Pu ratio could provide a powerful additional tool to validate the age model obtained with $^{210}Pb_{ex}$ and ^{137}Cs.

Application of the constant flux: constant sedimentation (CF:CS) model (Figure 6.4) allowed dating the base of this 48-cm-long sequence to 1948 (±3 yr), which is in good agreement with the commissioning of the dam (1945), with an average sedimentation accumulation rate (SAR) of $6.15 \pm 0.25 mm.yr^{-1}$. The first detection of ^{137}Cs in 1955 is dated to 1953 - 1956 ($\pm 3yr$, table 6.1), which corresponds well to the common milestones used for dating in the literature (Foucher et al. 2021). The classical $^{210}Pb_{ex}$ approach allows for a good overall dating of the core, with the attribution of the bottom sediment layer to the creation of the dam reservoir in 1948. However, the ^{137}Cs maximum fallout attributed to 1964-1965 is not easy to identify in this core, as the peak between 30 - 35 cm is too wide to be attributed to sediment deposition during a single year. This maximum ^{137}Cs peak activity is dated with the $^{210}Pb_{ex}$ age model to 1965-1975. However, the $^{240/239}Pu$ allows to refine the position of the ^{137}Cs peak emissions in the Southern

hemisphere to 35cm corresponding to 1965 with the CF:CS model and with a global fallout signature of $^{240/239}Pu$ of 0.18±0.01. In contrast, the rest of the peak is associated with the typical French nuclear test fallout signature (0.04±0.01).

As a complement, variations in $^{240}Pu/^{239}Pu$ atom ratios and $^{239+240}Pu$ activities provide insightful information about the differentiated timing of radioactive fallout sources of emission, therefore allowing the overall validation of the age model. Indeed, depending on the type of bomb used and the usage period, as they changed with time, contrasted $^{240/239}Pu$ atom ratios were obtained (Koide et al. 1985). USA, FSU and UK bomb testing contributed to a pre-moratorium global fallout signature of 0.18 (Chaboche et al. 2022), which corresponds to the mean $^{240/239}Pu$ ratio of fallout that was emitted in the atmosphere from 1945 to 1963. French nuclear bomb testing in the Southern Hemisphere started later in 1966-1974 and was found to be detectable in South America (Chamizo et al. 2011). This can explain the wider peak of ^{137}Cs observed in the core, likely consisting of the mix of the bomb fallout peak commonly attributed to 1963 (or 1964-65) followed by the significantly lower $^{240/239}Pu$ signatures (around 0.04) fallout levels associated with French bomb testing conducted in French Polynesia (1966-1974). During this later phase among which the French troposphere nuclear tests (1966-1967) are likely observed in the core from 34-33 cm, with a change from higher to lower $^{240/239}Pu$ ratios (attributed to 1965-1968) and the first H bomb nuclear test fallout, Canopus and Procyon (1968-1972) observed in the core from 33-30 cm and attributed to 1968-1970. These events were identified based on findings published by Chaboche et al. (2022) and are summarised in table 6.1.

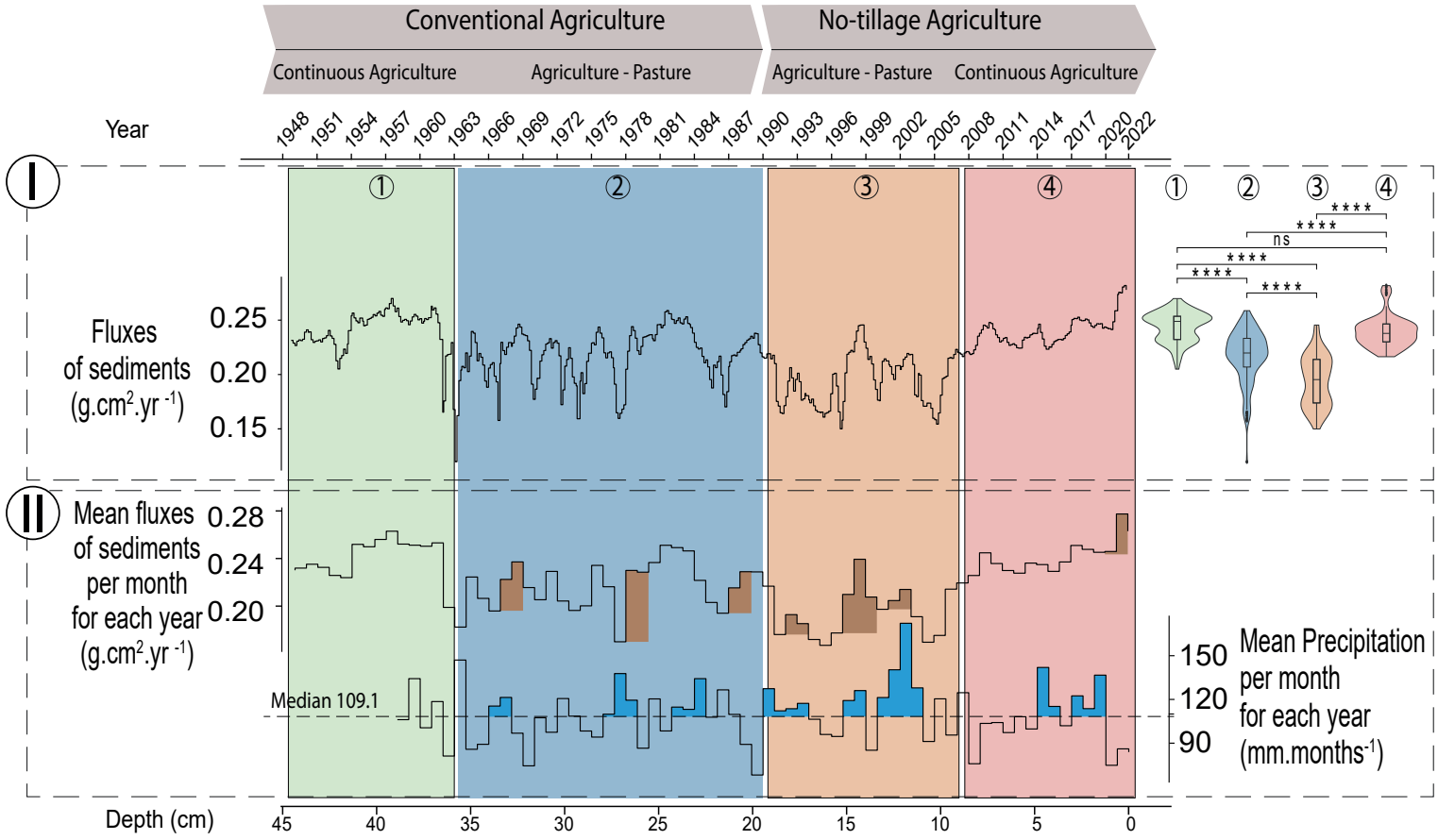

Figure 6.5: Fluxes of sediments (MAR, I) and result of Dunn test on the MAR for the different periods of sediment delivery (I) and mean annual fluxes of sediment and precipitation (II). Periods of sediment delivery identified with the breakpoint test and their corresponding agricultural phases were added, in green, conventional continuous cultivation, in blue, conventional cultivation with rotation (agriculture-pasture). In orange, no-tillage cultivation with rotation (agriculture-pasture) and in red, no-tillage continuous cultivation.

6.3.4 . Rainfall evolution

TerraClimate rainfall data in the Rincón del Bonete catchment during the 1958-2023 period shows large variations between 817 and 2067 mm.yr^{-1} (Appendix 6.9).

The Mann-Kendall trend test reveals a positive trend in rainfall with a τ of 0.02, although with a p-value of 0.79 for the 1958-2023 period.

The mean precipitation per month for each year of the precipitation dataset as well as the final median for the mean precipitation was calculated. Periods of multiple years with higher precipitation than the median were identified in the precipitation dataset. The reconstructed rainfall shows periods of higher mean precipitation than the median for multiple years in 1967-1968, 1977-1978, 1981-1984, 1986-1987, 1990-1993, 1997-1998, 2000-2003, 2014-2015 and 2017-2019 (figure 6.5, II).

6.3.5 . Fluxes of sediments

The MAR ranges between 0.12 and 0.28 $\pm$ 0.06 $g.cm^2.yr^{-1}$ (figure 6.5I). These values are similar to those found by Foucher et al. (2023), in which values ranged from 0.10 to 0.20 and from 0.13 to 0.19

$g.cm^{-2}.yr^{-1}$ for the Rincón del Bonete and Palmar (reservoir located a bit further downstream on the Rio Negro river) sediment cores, respectively. However, higher maximum values are found in this study (maximum 0.28 $\pm g.cm^{-2}.year^{-1}$).

The breakpoint tests applied to the MAR suggest the occurrence of the three breakpoints in 1962, 1990 and 2007 (table 6.2).

Test	**Breakpoints date - p value**		
Pettit	1962 - $3.2e^{-27}$	1991 - $8.6e^{-11}$	2008 - $4.0e^{-15}$
Buishand	1962 - 0	1991 - 0	2006 - 0
Historical dates	$\approx$ **1970**	$\approx$ **1990**	$\approx$ **2002**

Table 6.2: Results of statistical breakpoint test on MAR via the breakpoints package (Hurtado et al. 2020)

Although the Shapiro test result was close to 1 (table 6.3), the probability of observing the result under null hypothesis was too low (p<0.0001), thus violating the normality assumption. Therefore, a Kruskal-Wallis test was chosen instead of the well-known ANOVA test to compare the different periods.

The Kruskal-Wallis test on the four different periods (conventional and no-tillage with and without pasture, table 6.3) shows that a least one of the period significantly differs from the others and post hoc test were therefore conducted.

Post hoc analysis reveals significant differences between pairwise comparisons (table 6.3).

Based on the historical records and the existing literature identified in section 6.3.1, these four periods of sedimentation identified align well with the distinct phases in Uruguay's agricultural development. The four distinct periods of sedimentation identified are characterised first by a plateau with high MAR values is observed (average value of 0.24 $\pm$ 0.01 $g.cm^{-2}.yr^{-1}$) between 1948 and 1962, followed by a period of strong variations between 1962 and 1990 (average value of 0.22 $\pm$ 0.02 $g.cm^{-2}.yr^{-1}$, overall range: 0.11 - 0.26 $g.cm^{2}.yr^{-1}$). The 1991-2002 period is then characterised by a decrease in sediment inputs (mean: 0.19, $\pm$ 0.02 $g.cm^{-2}.yr^{-1}$), whereas the period between 1991 and 2022 shows a new acceleration (mean: 0.23, $\pm$ 0.01 $g.cm^{-2}.yr^{-1}$). Notably, the recent years (2019-2022) display the highest values observed along the entire sediment core (mean: 0.26, $\pm$ 0.01 $g.cm^{-2}.yr^{-1}$, max: 0.28 in 2021).

The transition dated to 1962 took place somewhat earlier compared to the expected history in Uruguay, where the transition to conventional agriculture with pasture rotation took place between 1970 and 1980. However, it can be hypothesised that sediment delivery was influenced by the processes that occurred in the Brazilian part of the river basin, which started it's intensification already in the 1960s (Pereira et al. 2012).

The largest difference is observed between the MAR during the conventional period with continuous cultivation and the MAR during the no-tillage period with pasture rotation (p.adj $< 2.45e^{-36}$), with

no-tillage practices showing significantly lower sediment fluxes. Similarly, the no-tillage period with continuous cultivation has a significantly lower MAR compared to most other groups (p.adj $< 5.13e^{-19}$).

A smaller but still significant difference is observed between the MAR during the conventional period with pasture rotation and the MAR during the no-tillage period with continuous cultivation with p.adj = 0.0079 (table 6.3). This suggests that incorporating pasture into conventional systems contributed to reduce sediment flux, but not as much as the change to no-tillage practices.

Shapiro-Wilk	Normality Test	W = 0.98	$p < 0.0001$	Data	violated	normality	
Kruskal-Wallis	Comparison	$\chi^2(3) = 218.26$	$p < 2.2e^{-16}$	Significant	differences	in groups	
Dunn							
Periods Compared		**Number of observation**		**Statistic**	**p**	**p.adj**	**p.adj.signif**
C-Ct	C-PR	81	181	-8.65	$4.91e^{-18}$	$2.95e^{-17}$	****
C-Ct	NT-PR	81	101	-12.86	$7.00e^{-38}$	$4.2e^{-37}$	****
C-Ct	NT-Ct	81	91	-1.74	$8.18e^{-02}$	$4.91e{-}01$	ns
C-PR	NT-PR	181	101	-6.13	$8.52e^{-10}$	$5.11e^{-09}$	****
C-PR	NT-Ct	181	91	6.93	$4.06e^{-12}$	$2.43e^{-11}$	****
NT-PR	NT-Ct	101	91	11.43	$2.70e^{-30}$	$1.62e{-}29$	****

Table 6.3: Results of statistical tests Shapiro-Wilk (W measures how closely data follows a normal distribution, the closer to 1 the more normally distributed are the data and p the probability of observing the result under the null hypothesis), Kruskal-Wallis (χ^2 from 0 to infinite, the closer to 0 the more similar are the medians of the groups tested, and p the probability of obtaining a test statistic equal to or more extreme than the observed χ^2) and Dunn (Statistic gives the difference between mean ranks of two groups from negative to positive infinite, p the p-value measured from statistic, p.adj the p adjusted from Bonferroni method and p.ajd.signif the significance annotation from non significative, ns, to highly significative, *****) on the MAR. **C** and **NT** stand for the conventional and no-tillage periods. **-Ct** and **-PR** stand for continuous cultivation or cultivation with pasture rotation respectively.

Despite the lack of historical data for the Rincón del Bonete reservoir prior to 1985, the history of agriculture in Uruguay suggests that more land was likely cultivated or used for ranching during the first period compared to the second, with conditions similar to those of the third period (Hudson et al. 1992). High sediment fluxes were observed during this initial period of conventional tillage, followed by a reduction associated with the introduction of conservation measures in 1981 (Law No. 15239) (Zurbriggen et al. 2020), pasture-crop rotation and a reduction in cultivated areas.

The transition to no-tillage practices and afforestation in the early 1990s further reduced sediment fluxes, although as cultivated areas increased. Continued use of pasture–crop rotation and afforestation contributed to temporary reductions in sediment delivery, despite the ongoing expansion of agriculture.

However, from 2007 onward, sediment fluxes increased again, coinciding with a shift toward continuous and double cultivation systems, intensification of land use, and increased wood harvesting. Land-use and land-cover changes during this period were driven not only by national agricultural policy but also by global trade dynamics. Nearly 80% of land-use land-cover changes since 1995 are linked to rising exports from Latin America, Africa, and Southeast Asia (Cabernard et al. 2024). This period also saw a significant expansion of genetically modified soybean cultivation (Foucher et al. 2023). These findings

confirm the acceleration of sedimentation rates identified in recent years by Foucher et al. (2023), and highlight the impact of agricultural intensification on erosion.

Based on the δ^{13}C, some events were identified. During the second peak of δ^{13}C (2004-2005), the observed values exhibit a tendency to reach lower levels than the first peak (i.e.-22.6 ‰). This phenomenon could be indicative of the incorporation of more C_3 photosynthetic pathway plants from the river basin, corresponding to the implementation of soybean and eucalyptus or the removal of previous paddy fields cultivated with rice.

Some rice was still cultivated in the river basin in 2020/2021 (Ministerio de Ganadería, Agricultura y Pesca) and used to be widely cultivated in the river basin in the past. Therefore, this second peak of δ^{13}C, could correspond to the removal of previous paddy fields cultivated with rice.

Conversely, this second peak of δ^{13}C coincides with that of temporary crops observed in the river basin in 2004-2006 (with a 21% increase from 2003 to 2004-2006), which tends to rather confirm the first hypothesis of the massive introduction of soybean in the river basin.

This soybean expansion, which took place in the aftermath of the 2002-2004 economic crisis in Uruguay, could be explained by the high taxation of agriculture in neighbouring Argentina, as this policy included elevated soybean export taxes (Zurbriggen et al. 2020). In the absence of such taxation in Uruguay, it granted a favourable financial climate for soybean cultivation in this country.

Furthermore, exotic trees and mainly eucalyptus - another C_3 plant - were known to have been harvested during the same period (Foucher et al. 2023). Therefore, in a context of a mix of $C_3 - C_4$ plants, the peak of δ^{13}C that we observe could correspond to the massive introduction of C_3 plants, either corresponding to the expansion of the soybean area or the planting of eucalyptus trees in the river basin, or to both.

In addition to the land-use and land-cover, the potential impact of the precipitation factor on the sediment dynamics was also investigated.

Since the fluxes of sediments and precipitation were not sampled with the same frequency, comparison was complex, therefore the mean annual fluxes of sediments per months were calculated, and when compared with the mean precipitation per month for each year, different temporal patterns are found for distinct periods (figure 6.5II). Precipitation were found only from 1958 and no period of multiple years with higher precipitation than the median (wet period) was considered between 1958-1964. The second period (1964-1990) shows some correlation between both variables. The different wet periods investigated likely generated events associated with higher sediment delivery, while drier periods were likely correlated with periods of lower sediment delivery. Supplementary analyses were conducted to quantify the impact of precipitation on sediment fluxes. However, the irregular rate frequency of sediment fluxes did not allow for quantification of the impact of each individual rainfall event identified in the precipitation sequence.

During the third phase (1990-2007), two wet periods are found in the precipitation, which probably impacted the sediment fluxes. However, it can be seen that the wet intervals only has a limited influence, if any, on the fluxes of sediment during this second phase.

In contrast, the fourth and final phase (2007-2023) is characterized by a clear decoupling between sediment fluxes and precipitation variability. Indeed, the wet period observed in 2017-2019 had a disproportionate effect on the fluxes of sediments with a much higher sediment peak observed for rainfall episodes although they remained of the same order of magnitude as those recorded during the previous phase.

The precipitation dataset was selected to cover the longest period possible. However, its monthly resolution limited the ability to analyse short-term, high-intensity erosion-prone rainfall events, which may represent a significant source of variability in sediment fluxes. Future studies could benefit from incorporating higher-resolution daily precipitation datasets available for more recent periods, enabling a more detailed assessment of the relationship between extreme rainfall and sediment dynamics.

6.3.6 . Pesticides

Of the 16 pesticides analysed, 13 substances were detected in the core with various concentrations and fluxes ($mol.cm^{-2}.yr^{-1}$, figure 6.6). Post-depositional mobility may be an issue for all pesticides. Therefore, the first detection depth and production date of each compound as well as the comparison with historical events, such as field trials and usage recommendations in Uruguay (Nuevos herbicidas para cultivos de invierno) were used to select those substances with minimal mobility along the profile. Glyphosate and its metabolite AMPA are excluded from this discussion due to excessive diffusion, as shown in the supplementary material (Appendix 6.10). Mirex is not detected in the core. All the pesticides data treated in this section (3.6) are shown in figure 6.6.

Herbicides

With the exception of Diuron, which is detected from 1955 onwards, all herbicides (in the green portion in figure 6.6) are found from the 1975-1985 period. The fluxes of Diuron (marketed from 1954 (Woodford 1957)), similar to those of Simazine and Atrazine (marketed from 1956 and 1958, respectively (Heri et al. 2008)), decline from the 1980/1990s before reappearing from 2010 to 2022. After the first widespread use of herbicides observed in the 1970s, their usage decrease and they are only significantly used again from 2005 onwards. After it's first introduction, S-Metolachlor, marketed from 1976 (United States Environmental Protection Agency - Reregistration Eligibility Decision (RED) Metolachlor), is found in low levels until 2018 when high fluxes are detected again. Diuron is used to control undesirable grasses and other annual and evergreen broadleaf weeds. This herbicide usage was first reported in Uruguay in 1967 (Merotto et al. 2022). Therefore, the first peak of Diuron in 1955 to 1960 probably corresponds to diffusion. However, the second peak from 1967 corresponds with the first reported use of this herbicide

in Uruguay. It is detected in the core during a period devoid of afforestation. Therefore, this herbicide detection might be attributed to the initial disturbance of the Pampa, mainly in the Northern part of the river basin in order to remove annual grasses. In the 1970s, Diuron was also recommended in Uruguay to be used for cultivating winter wheat (Nuevos herbicidas para cultivos de invierno). Nevertheless, no cultivation of wheat was documented in the river basin. Otherwise, some rice was still cultivated in the river basin in 2020/2021 (Ministerio de Ganadería, Agricultura y Pesca) and used to be cultivated in the river basin in the past. Therefore, Diuron might also have been used as a pre-emergence herbicide in paddy fields in order to control annual weeds. This could also explain the detection of the first peak of δ^{13}C observed in 1973 (around 30cm; Figure 6.3) corresponding to the degradation of paddy fields through the use of Diuron and the supply of C_3 plant residues to the reservoir.

2,4-D, which was first tested in the 1940s (Merotto et al. 2022) in Uruguay, is detected in the core from 1950 onwards. This herbicide was likely used to destroy the weeds under the crops. It is detected in greater quantities simultaneously with the appearance of S-Metolachlor, Simazine and Atrazine, which are detected in the sediment core from 1975, periods during which all the herbicides started to be generally used in Uruguay. These herbicides were likely used for pre- and post-emergent treatments of annual weeds (Merotto et al. 2022). The rise in multiple herbicides in the 1970s could be related to the cereal and oilseed boom period that took place in Uruguay at that time for land preparation and weed control (Merotto et al. 2022). Furthermore, the rise of Atrazine from 2007 could be linked with the increase in temporary crops and the preparation of the grasslands to plant soybean.

Diuron is the first herbicide to be detected in the core in significant quantity and it's concentration decreases from the 1970, which corresponds to the rise in multiple other herbicides (S-Metolachlor, Simazine, Atrazine and 2,4D). Therefore, it can be hypothesised that Diuron was replaced from the 1970 with the other herbicides detected afterwards.

Fungicides

The Tebuconazole fungicide (in the red portion in figure 6.6) starts to be detected significantly in the core from the late 1980s onwards, with increasingly higher fluxes until 2018. This fungicide has been mainly used in large scale crop-fields to prevent different types of plant diseases (Tleuova et al. 2020) and could be representative of the implantation of soybean cultivation for which this fungicide has been recommended for. Furthermore, this detection is in good agreement with the massive expansion of soybeans that took place from 1990 in the river basin, as shown by Foucher et al. (2023).

Insecticides

The insecticide DDT was freely marketed from 1945 (Mellanby 1992) to 1968 when it was banned in Uruguay (Mañay et al. 2004). This insecticide and its metabolites, DDE and DDD, are detected from 1948

($\pm$3) in the core (in the grey part in figure 6.6). Three peaks of DDT are measured, the first from 1948 to 1970, the second in the 1990's and, finally, the third from 2005. DDD and DDE fluxes increase until 1985 when they dropped, before increasing again from 2005 and 2010 respectively. They remain high along the sediment profile, except for a drop observed before the 2000s and an increase afterwards. DDT is considered to diffuse at a rate of $10^{-8} cm^2.s^-1$ (Logan et al. 1989), but this movement generally takes place downward and not upward. The peaks of DDT and it's metabolites observed therefore correspond to events that occurred in the river basin and not to post depositional mobility.

Several hypotheses may be put forward for explaining the source of DDT and its metabolites along the profile. To test these hypotheses, DDD and DDE, respectively the anaerobic and aerobic metabolites of DDT, produced depending on the degradation conditions of the pesticide (PubChem - DDT) can provide better insights into the origin of the second and thirds peaks observed in the 1990s and after 2007.

First, the DDT may have been supplied during the same period of original application before the 1970s when attempts to eradicate yellow fever, malaria and other vector-borne diseases were put in place. In fact as reported in Severo (1955), the plan to eradicate both *Anopheles* and *Aedes aegypti* mosquitoes, the primary vectors of malaria and yellow fever, respectively, initiated in Brazil as early as in 1932, was generalised to the whole continent at the end of World War II. From 1948 to the early 1970s, DDT was used extensively in and around potential habitats of the insect in an attempt to eradicate it. Therefore, the reappearance of DDT from 2007 could be due to the erosion of previously undisturbed soils that had been contaminated with DDT, corroborating the rise in herbicide use, such as Atrazine, since 2007.

This study suggests that the secondary peak of DDT observed in the sediment core may be due to a newly applied insecticide, rather than the remobilisation of a previously applied substance.

In fact, Dicofol, an organochlorine insecticide (PubChem - Dicofol), marketed since 1955 and structurally similar to DDT world health organization - food and agriculture organization of the united nations, which was not analysed in this study, was detected as a source of DDT contamination in previous studies (Turgut et al. 2009). As Dicofol can be synthesized using DDT, large amounts of DDT impurities may be found in Dicofol. Turgut et al. (2009) found between 0.3 to 14.3% of DDT in the Dicofol that they analysed. Barra et al. (2006) reported the use of Dicofol in South America. For example, in 2000, Brazil imported 111 tonnes of Dicofol and produced 209 tonnes of this substance. Furthermore, according to Travis et al. (2020), one commercial formulation of Dicofol was approved for use in the country and they also showed the presence of Dicofol residues on children wrists in Uruguay. Despite the fact that no specific link could yet be made between Dicofol and DDT exposure in Uruguay (Travis et al. 2020), the impurities found in Dicofol and its potential use in Uruguay could be the cause of the second peak of DDT and its metabolites observed in the core in the 1990's.

However, more investigation is required to verify the hypothesis of an indirect DDT contamination due to the use of Dicofol in the river basin.

Endosulfan is also detected in 1948 and the associated fluxes decrease until 1980. Two peaks are then observed in 1990-2000 and, more recently, from 2010 onwards, with a maximum recorded after 2015. Endosulfan was used for general pest control. In the 1990s, organochlorine insecticides were banned in Uruguay (Boroukhovitch 1998). Endosulfan was an exception (Boroukhovitch 1998) and may therefore have provided an alternative to all these banned insecticides. The second peak observed in the core after 2010 probably corresponds to the use of the remaining stocks of Endosulfan after it was banned in 2011 (Registro Nacional de Leyes y Decretos).

Chlorpyrifos Ethyl, first registered in 1965 in the United States of America (Rauh et al. 2011), is found in the core in high proportions from 1975. This broad-spectrum insecticide is widely used on various crops, in public health programs, particularly for the control mosquito, ants, cockroaches, and certain disease-carrying tick species. In the sediment core, the rise of Chlorpyrifos-Ethyl coincided with the decline of DDT, suggesting it may have been adopted as a replacement substance following the ban on DDT.

Finally, Imidacloprid and Friponil are first detected in 1975 and the associated fluxes continued to increase until nowadays. Friponil peaks between 2010 and 2018 whereas Imidacloprid increases from 2000 to 2022. Imidaclopride was the first neonicotinoid discovered in 1985 and Friponil, a phenylpyrazole, was discovered in the 1990. These insecticides were developed in response to increasing pesticide resistance to other compounds (Jeschke et al. 2019). Both insecticides are used as seed coating and could have been introduced in the river basin during the increase of temporary crops observed from 1985. However, some diffusion associated with these substances can be observed in the profile and care was therefore taken when interpreting the temporal evolution of the fluxes of these insecticides.

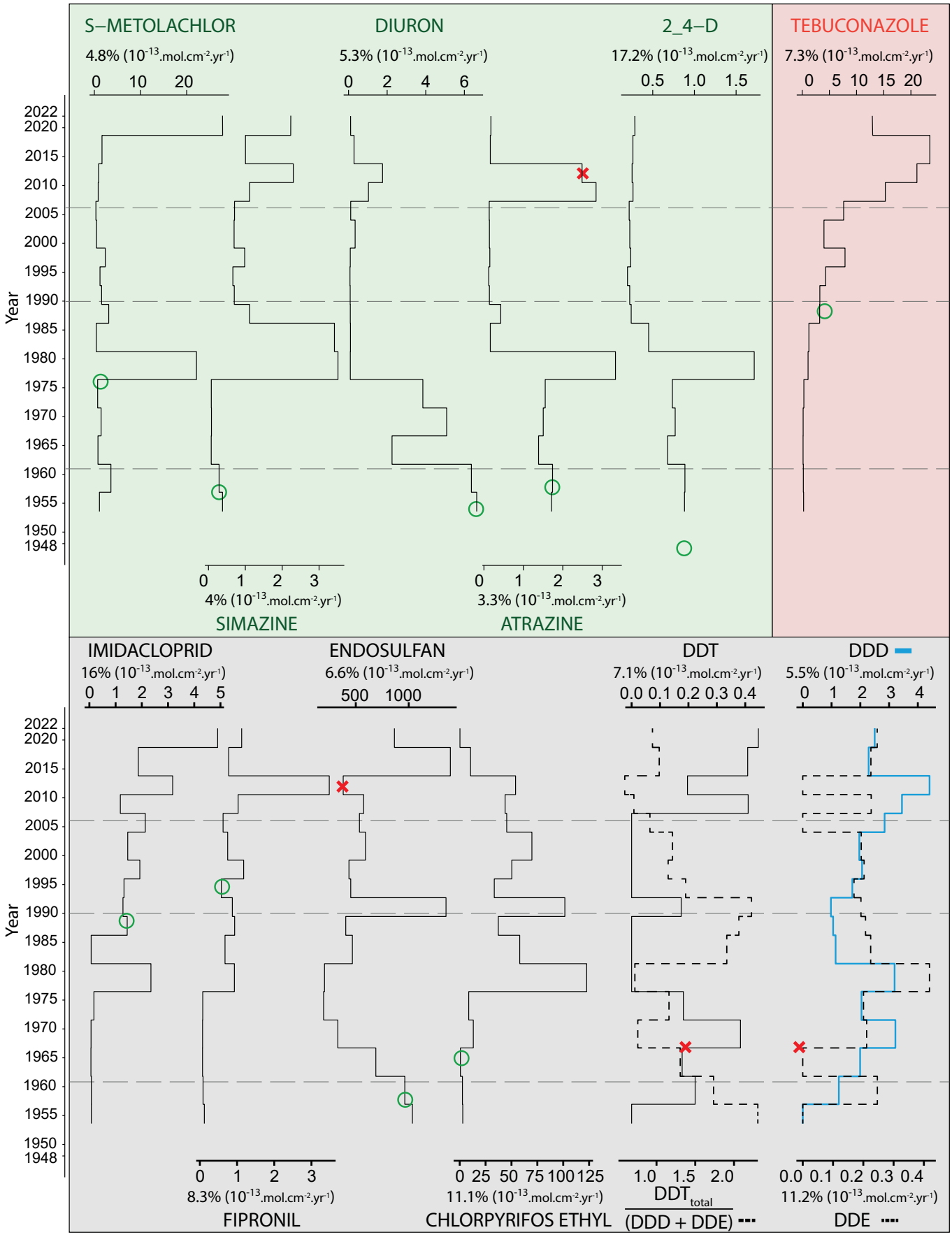

Figure 6.6: Fluxes (in 10^{-13} mol.cm^{-2}.yr^{-1}) of insecticides (grey), herbicides (green), and fungicides (red). Uncertainty for each pesticide is indicated alongside its range. The date of production is marked with a green circle, and the date of ban with a red cross

6.4 . Conclusions

Key findings of the study have been summarised and illustrated in Figure 6.7. Each result has been categorised by period and expressed on a scale ranging from low to very high.

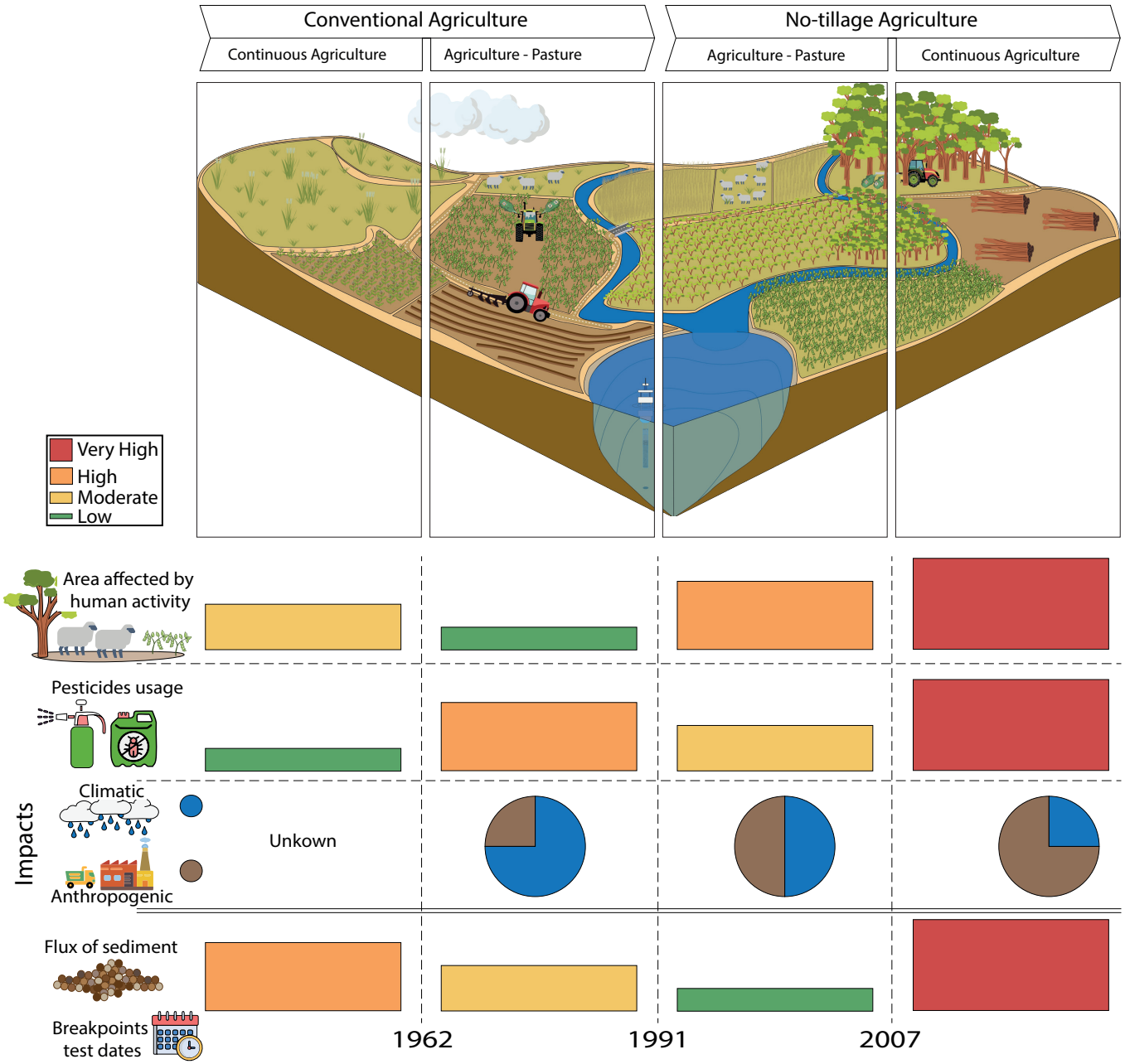

Figure 6.7: Synthesis of the main findings of this study and conceptual representation. The **Area affected by human activity** was derived from land-use land-cover analysis, **pesticide usage** from the pesticide analyses, **climatic and anthropogenic impacts** from the sediment flux/precipitation comparison, and the **sediment flux** and **breakpoint test dates** from MAR analysis. Results were categorised by period and expressed on a scale ranging from low to very high.

Through a comprehensive and original multi-proxy approach, this study revealed how changes from natural to human-dominated landscapes with massive introduction of monocultures and shifts in agricultural practices, have significantly affected sediment transport in the Uruguayan river basin, reflecting the

trends observed across the Pampa biome.

- **Sediment fluxes** were found to **evolve concomitantly** with the **pesticide consumption** as well as the **land-use and land-cover change**, influenced in part by the **precipitation factor** in the early stages, and then dominantly controlled by the **anthropogenic actions** later on.
- The shift to **no-tillage** and **pasture rotation** briefly **reduced sediment fluxes**, despite the large amounts of herbicides required for this practice. However, the **intensification of agriculture** and **wood harvesting** later **reversed this trend**.
- Notably, two periods of **resurgence** of the banned **DDT** pesticide were observed in **recent years** (in 1990-1995 and from 2007). The present study suggests a possible **contamination** from a DDT-derived pesticide known as **Dicofol** followed by the **remobilisation** of previously applied DDT possibly resulting from the widespread use of this insecticide in attempts to eradicate the vector-borne malaria and yellow fever diseases after World War II.
- The **increase** in **sediment delivery** over the most recent period (**2008-2023**) is likely due to the **conversion of 12% of grassland over 14 years**, while 60% remain either natural or used for extensive ranching. As previously highlighted, large-scale land-use changes across South America are driven by the growing global demand for agricultural commodities. A striking example is the new UPM (UPM Uruguay) wood processing facility that has been built near the Rincón del Bonete dam, inaugurated in 2023 as the largest in Uruguay and one of the world's biggest factories of this type. With additional plants under construction, Uruguay's production capacity will continue to expand, emphasizing the fact that the environmental degradation observed in the river basin reflects wider international market forces and requires global attention.

In future research, the contrasting landscapes (i.e. geology, soil types) and land-use of the Rincón del Bonete basin's two main tributaries deserve further investigation. Sampling at the outlet of each river and/or applying sediment fingerprinting techniques could help differentiate sediment sources and their potential variations with time, offering a more accurate understanding of erosion dynamics and land-use impacts within this river basin, representative of the situation observed across the wider Pampa biome.

6.5 . supplementary material

Pesticide	Abbreviation	IUPAC name	Familly
2,4-Dichlorophenoxyacetic acid	2,4-D	2,4-Dichlorophenoxyacetic acid	Organic compound
Atrazine	Atrazine	6-chloro-N^2-ethyl-N^4-(propan-2-yl)- 1,3,5-triazine-2,4-diamine	Triazine
Simazine	Simazine	6-chloro-N^2,N^4-diethyl-1,3,5-triazine-2,4-diamine	Triazine
Diuron	DCMU	3-(3,4-dichlorophenyl)-1,1-dimethylurea	Phenylurea
S-Metolachlor	S-Metolachlor	(S)-2-chloro-N-(2-ethyl-6-methylphenyl)-N-[(2S)-1-methoxypropan-2-yl]acetamide	Urea
Tebuconazole	Tebuconazole	(RS)-1-(4-chlorophenyl)-4,4-dimethyl-3-(1H-1,2,4-triazol-1-ylmethyl)pentan-3-ol	Neonicotinoid
Imidacloprid	IMI	1-[(6-chloro-3-pyridinyl)methyl]-N-nitroimidazolidin-2-ylideneamine	Neonicotinoid
Endosulfan	Endosulfan	dodecachlorooctahydromethanetriyl benzodioxathiepine oxide	Organochlorine
Fipronil	Fipronil	5-Amino-1-[2,6-dichloro-4-(trifluoromethyl)phenyl]-4-(trifluoromethylsulfinyl)-1H-pyrazole-3-carbonitrile	Phenylpyrazole
Chlorpyrifos Ethyl	Chlorpyrifos Ethyl	O,O-Diethyl O-(3,5,6-trichloropyridin-2-yl) phosphorothioate	Organochlorine
Dichlorodiphényltrichloroéthane	DDT	1,1'-(2,2,2-Trichloroethane-1,1-diyl)bis(4-chlorobenzene)	Organochlorine
Dichlorodiphényldichloroéthane	DDD	1,1'-(2,2-Dichloroethane-1,1-diyl)bis(4-chlorobenzene)	Metabolite of DDT
Dichlorodiphényldichloroéthylène	DDE	1,1'-(2,2-Dichloroethene-1,1-diyl)bis(4-chlorobenzene)	Metabolite of DDT
Glyphosate	Glyphosate	N-(phosphonomethyl)glycine	Phosphonate
AMPA	AMPA	(Aminomethyl)phosphonic acid	Metabolite of glyphosate
Mirex	Mirex	dodecachloropentacyclo[5.3.0.$0^{2,6}$.$0^{3,9}$.$0^{4,8}$]decane	Organochlorine

Table 6.4: Complete list of 16 pesticides with their abbreviations, International Union of Pure and Applied Chemistry (IUAPC) names and classifications. Molecules were found on PubChem (https://pubchem.ncbi.nlm.nih.gov/)

Analysis conducted	Studied parameters	Resolution	Units
Particle size analysis	D10, D50, D90	1 cm	μm
CT-scanner	Relative density	0.625 mm	Hounsfield
Bulk density	Bulk density	1 cm	$g.cm^{-3}$
Organic matter analysis	TOC, TN, δ^{13}Corg	1 cm	% + ‰
Gamma spectrometry analysis	$^{210}Pb_{ex}$, ^{137}Cs	1 cm	$Bq.kg^{-1}$
Plutonium analysis	^{239}Pu, ^{240}Pu	1 cm	$Bq.kg^{-1}$
Pesticide analysis	See Appendix 6.4 for full list	2-4 cm	$mol.cm^{-2}.yr^{-1}$
Fluxes of sediments	MAR	0.625 mm	$g.cm^{-2}.yr^{-1}$

Table 6.5: Summary of analysis conducted, parameters studied, resolution of the data, and units.

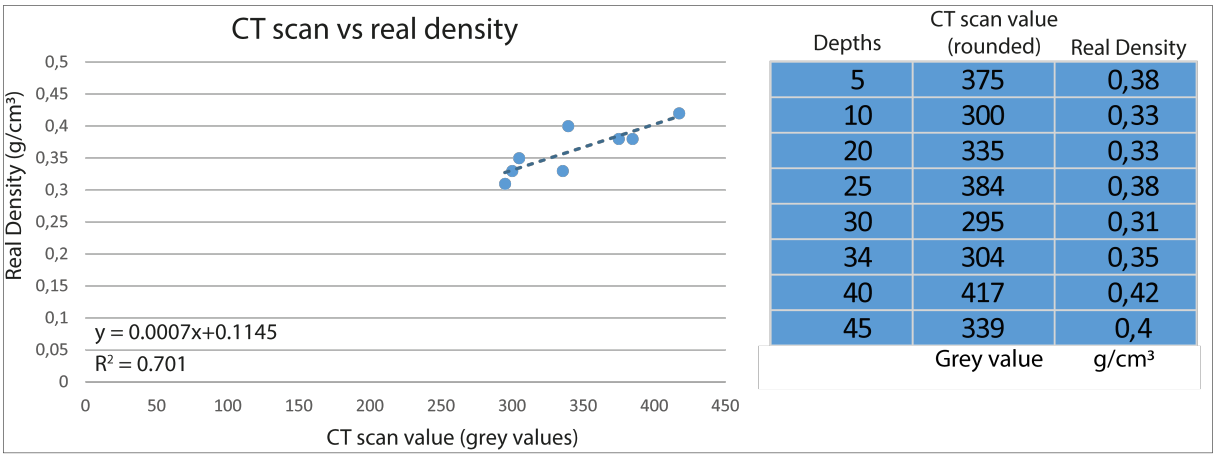

Depths	CT scan value (rounded)	Real Density
5	375	0,38
10	300	0,33
20	335	0,33
25	384	0,38
30	295	0,31
34	304	0,35
40	417	0,42
45	339	0,4
	Grey value	g/cm³

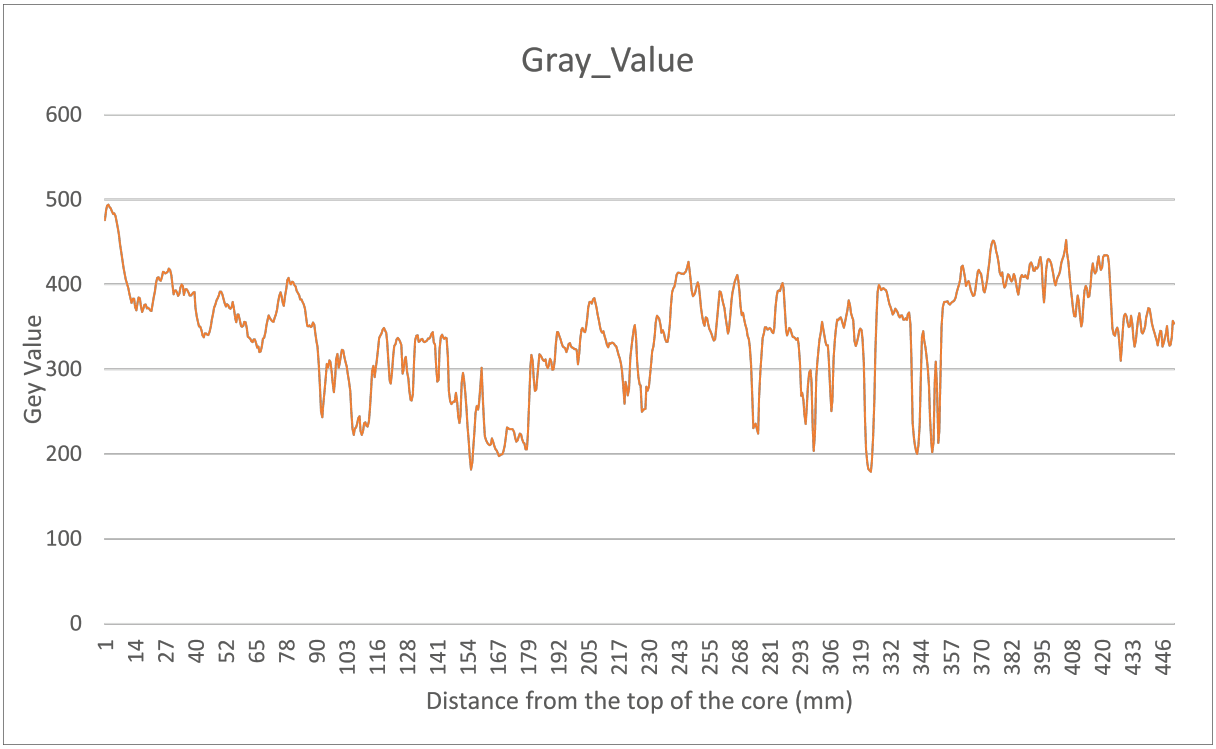

Figure 6.8: Correlation between measured density and CT scan values in blue in the top and CT scan values obtained in orange on the bottom part

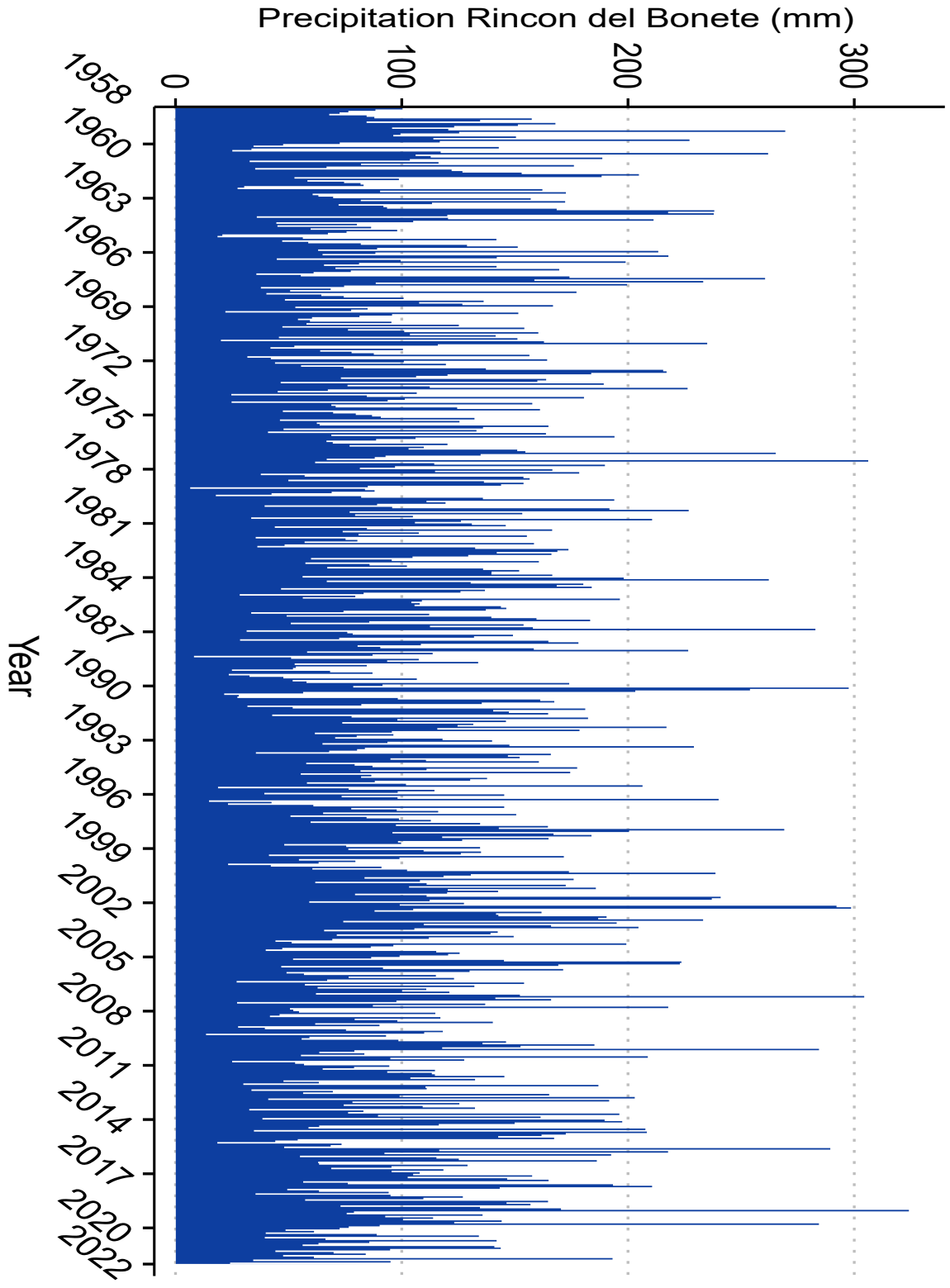

Figure 6.9: Monthly precipitation in the Rincon del Bonete river basin as recorded in the TerraClimate dataset

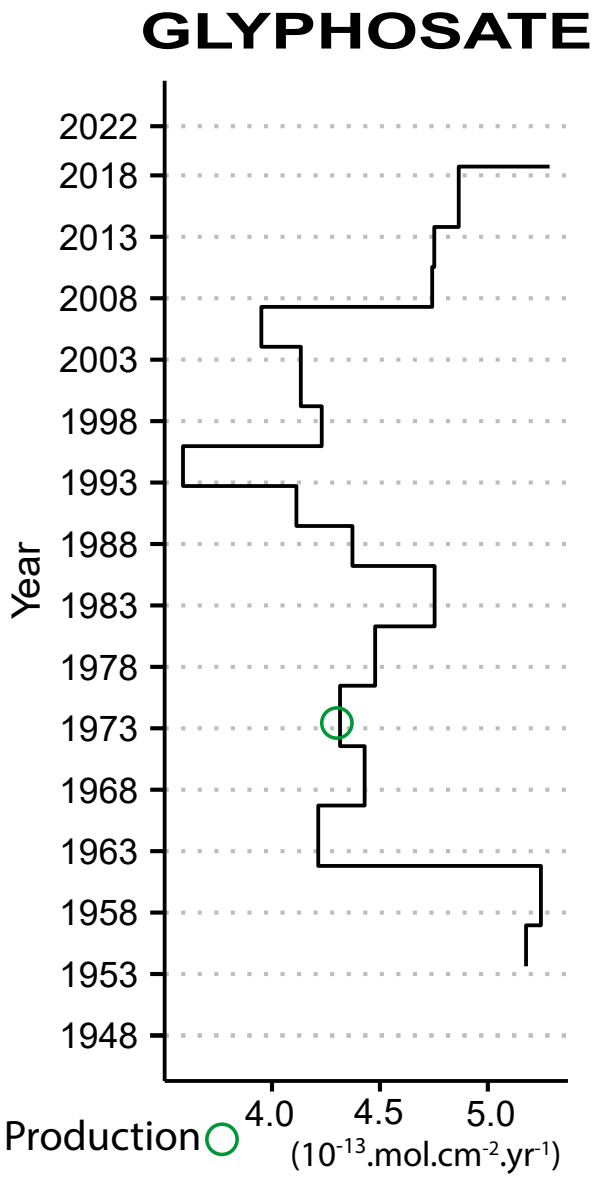

Figure 6.10: Fluxes of Glyphosate in $10^{-13}.mol.cm^{-2}.yr^{-1} \pm 23.1\%$

Bibliography

Aktar, W., Sengupta, D., and Chowdhury, A. (2009). Impact of pesticides use in agriculture: their benefits and hazards. *Interdisciplinary Toxicology*, 2(1):1–12.

Andrade, B. O., Dröse, W., Aguiar, C. A. D., Aires, E. T., Alvares, D. J., Barbieri, R. L., Carvalho, C. J. B. D., Bartz, M., Becker, F. G., Bencke, G. A., Beneduzi, A., Silva, J. B., Blochtein, B., Boldrini, I. I., Boll, P. K., Bordin, J., Silveira, R. M. B. D., Martins, M. B., Bosenbecker, C., Braccini, J., Braun, B., Brito, R., Brown, G. G., Büneker, H. M., Buzatto, C. R., Cavalleri, A., Cechin, S. Z., Colombo, P., Constantino, R., Costa, C. F. D., Dalzochio, M. S., Oliveira, M. G. D., Dias, R. A., Santos, L. A. D., Duarte, A. D. F., Duarte, J. L. P., Durigon, J., Da Silva, M. E., Ferreira, P. P. A., Ferreira, T., Ferrer, J., Ferro, V. G., Fontana, C. S., Freire, M. D., Freitas, T. R. O., Galiano, D., Garcia, M., Dos Santos, T. G., Gomes, L. R. P., Gonzatti, F., Gottschalk, M. S., Graciolli, G., Granada, C. E., Grings, M., Guimarães, P. S., Heydrich, I., Iop, S., Jarenkow, J. A., Jungbluth, P., Käffer, M. I., Kaminski, L. A., Kenne, D. C., Kirst, F. D., Krolow, T. K., Krüger, R. F., Kubiak, B. B., Leal-Zanchet, A. M., Loebmann, D., Lucas, D. B., Lucas, E. M., Luza, A. L., Machado, I. F., Madalozzo, B., Maestri, R., Malabarba, L. R., Maneyro, R., Marinho, M. A. T., Marques, R., Marta, K. D. S., Martins, D. D. S., Martins, G. D. S., Martins, T. R., Mello, A. S. D., Mello, R. L., Mendonça Junior, M. D. S., Morais, A. B. B. D., Moreira, F. F. F., Moreira, L. F. B., Moura, L. D. A., Nervo, M. H., Ott, R., Paludo, P., Passaglia, L. M. P., Périco, E., Petzhold, E. S., Pires, M. M., Poppe, J. L., Quintela, F. M., Raguse-Quadros, M., Pereira, M. J. R., Renner, S., Ribeiro, F. B., Ribeiro, J. R. I., Rodrigues, E. N. L., Rodrigues, P. E. S., Romanowski, H. P., Ruschel, T. P., Saccol, S. D. S. A., Savaris, M., Silveira, F. S., Schmitz, H. J., Siegloch, A. E., Siewert, R. R., Silva Filho, P. J. S. D., Soares, A. G., Somavilla, A., Sperotto, P., Spies, M. R., Tirelli, F. P., Tozetti, A. M., Verrastro, L., Vogel Ely, C., Da Silva, A. Z., Zank, C., Zefa, E., and Overbeck, G. E. (2023). 12,500+ and counting: biodiversity of the Brazilian Pampa. *Frontiers of Biogeography*, 15(2).

Arocena, R., Castro, M., and Chalar, G. (2022). Ecological integrity assessment of streams in the light of natural ecoregions and anthropic land use. *Environmental Monitoring and Assessment*, 194(10):748.

Baeza, S., Vélez-Martin, E., De Abelleyra, D., Banchero, S., Gallego, F., Schirmbeck, J., Veron, S., Vallejos, M., Weber, E., Oyarzabal, M., Barbieri, A., Petek, M., Guerra Lara, M., Sarrailhé, S., Baldi, G., Bagnato, C., Bruzzone, L., Ramos, S., and Hasenack, H. (2022). Two decades of land cover mapping in the Río de la Plata grassland region: The MapBiomas Pampa initiative. *Remote Sensing Applications: Society and Environment*, 28:100834.

Barra, R., Colombo, J. C., Eguren, G., Gamboa, N., Jardim, W. F., and Mendoza, G. (2006). Persistent Organic Pollutants (POPs) in Eastern and Western South American Countries. In Ware, G. W., Nigg, H. N., and Doerge, D. R., editors, *Reviews of Environmental Contamination and Toxicology*, volume 185, pages 1–33. Springer New York, New York, NY. Series Title: Reviews of Environmental Contamination and Toxicology.

Boroukhovitch, M. (1998). Uruguay -Current State of Chlorine Containing Pesticides in Uruguay.

Bruel, R. and Sabatier, P. (2020). serac: an R package for ShortlivEd RAdionuclide chronology of recent sediment cores. *Journal of Environmental Radioactivity*, 225:106449.

Bueno, C., Alves, F., Pinheiro, L., Perez, L., Agostini, V., Fernandes, E., Möller, O., Weschenfelder, J., Pinho, G., Wallner-Kersanach, M., Moura, R., Durán, J., Etchevers, I., Costa, L., Werlang, C., Bortolin, E., Machado, E., Figueira, R., Ferreira, P., Andrade, C., Fornaro, L., and García-Rodríguez, F. (2021). The effect of agricultural intensification and water-locking on the world's largest coastal lagoonal system. *Science of The Total Environment*, 801:149664.

Buishand, T. A. (1982). Some methods for testing the homogeneity of rainfall records. *Journal of Hydrology*, 58(1):11–27.

Cabernard, L., Pfister, S., and Hellweg, S. (2024). Biodiversity impacts of recent land-use change driven by increases in agri-food imports. *Nature Sustainability*, 7(11):1512–1524.

Cabrera, M., Sanabria, R., González, J., Cabral, P., Tejeda, S., Zarazua, G., Melgar-Paniagua, E., and Tassano, M. (2023). Using 137Cs and 210Pbex to assess soil redistribution at different temporal scales along with lithogenic radionuclides to evaluate contrasted watersheds in the Uruguayan Pampa grassland. *Geoderma*, 435:116502.

Chaboche, P.-A., Pointurier, F., Sabatier, P., Foucher, A., Tiecher, T., Minella, J. P., Tassano, M., Hubert, A., Morera, S., Guédron, S., Ardois, C., Boulet, B., Cossonnet, C., Cabral, P., Cabrera, M., Chalar, G., and Evrard, O. (2022). 240Pu/239Pu signatures allow refining the chronology of radionuclide fallout in South America. *Science of The Total Environment*, 843:156943.

Chamizo, E., García-León, M., Peruchena, J., Cereceda, F., Vidal, V., Pinilla, E., and Miró, C. (2011). Presence of plutonium isotopes, 239Pu and 240Pu, in soils from Chile. *Nuclear Instruments and Methods in Physics Research Section B: Beam Interactions with Materials and Atoms*, page S0168583X11003727.

Chiappe, M., Carambula, M., and Fernandez, E. (2008). *El campo uruguayo: una mirada desde la sociología rural./*. Departamento de Publicaciones de la Facultad de Agronomía„ Montevideo;.

Derpsch, R., Friedrich, T., Kassam, A., and Hongwen, L. (2010). Current status of adoption of no-till farming in the world and some of its main benefits. *International Journal of Agricultural and Biological Engineering*, 3.

Ferreira, P. A. D. L., Figueira, R. C. L., Siegle, E., Asp Neto, N. E., Martins, C. D. C., Schettini, C. A. F., Maciel, P. M., García-Rodriguez, F., and Mahiques, M. M. D. (2016). Using a cesium-137 (137 Cs) sedimentary fallout record in the South Atlantic Ocean as a supporting tool for defining the Anthropocene. *Anthropocene*, 14:34–45.

Foucher, A., Chaboche, P.-A., Sabatier, P., and Evrard, O. (2021). A worldwide meta-analysis (1977–2020) of sediment core dating using fallout radionuclides including ^{137}Cs and ^{210}Pb$_{xs}$. *Earth System Science Data*, 13(10):4951–4966.

Foucher, A., Tassano, M., Chaboche, P.-A., Chalar, G., Cabrera, M., Gonzalez, J., Cabral, P., Simon, A.-C., Agelou, M., Ramon, R., Tiecher, T., and Evrard, O. (2023). Inexorable land degradation due to agriculture expansion in South American Pampa. *Nature Sustainability*.

Garcia-Préchac, F., Ernst, O., Siri-Prieto, G., and Terra, J. A. (2004). Integrating no-till into crop–pasture rotations in Uruguay. *Soil and Tillage Research*, 77(1):1–13.

Garcia-Rodrıguez, F., Mazzeo, N., Sprechmann, P., Metzeltin, D., Sosa, F., Renom, M., Scharf, B., and Gaucher, C. (2002). Paleolimnological assessment of human impacts in Lake Blanca, SE Uruguay. *Journal of Paleolimnology*.

Heri, W., Carroll, B., Parshley, T., and Nabors, J. B. (2008). Production, Development, and Registration of Triazine Herbicides. In *The Triazine Herbicides*, pages 31–43. Elsevier.

Hudson, R. A., Meditz, S. W., Weil, T. E., and Library of Congress, editors (1992). *Uruguay: a country study*. Number 550-97 in Area handbook series. Federal Research Division, Library of Congress : For sale by the Supt. of Docs., U.S. G.P.O, Washington, D.C, 2nd ed edition.

Hurtado, S. I., Zaninelli, P. G., and Agosta, E. A. (2020). A multi-breakpoint methodology to detect changes in climatic time series. An application to wet season precipitation in subtropical Argentina. *Atmospheric Research*, 241:104955.

Jeschke, P., Witschel, M., Krämer, W., and Schirmer, U., editors (2019). *Modern Crop Protection Compounds*. Wiley, 1 edition.

Koide, M., Bertine, K. K., Chow, T. J., and Goldberg, E. D. (1985). The 240Pu / 239Pu ratio, a potential geochronometer. *Earth and Planetary Science Letters*, 72(1):1–8.

Kruk, C., Segura, A., Piñeiro, G., Baldassini, P., Pérez-Becoña, L., García-Rodríguez, F., Perera, G., and Piccini, C. (2023). Rise of toxic cyanobacterial blooms is promoted by agricultural intensification in the basin of a large subtropical river of South America. *Global Change Biology*, 29(7):1774–1790.

Lamb, A. L., Wilson, G. P., and Leng, M. J. (2006). A review of coastal palaeoclimate and relative sea-level reconstructions using 13C and C/N ratios in organic material. *Earth-Science Reviews*, 75(1-4):29–57.

Logan, B. E., Steele, J. A., and Arnold, R. G. (1989). Computer Simulation of Ddt Distribution in Palos Verdes Shelf Sediments. *Journal of Environmental Engineering*, 115(1):221–238.

Magand, O. and Arnaud, F. (2007). Response on the comment from Ribeiro Guevara and Arribere on the article 'Radionuclide dating (Pb-210, Cs-137, Am-241) of recent lake sediments in a highly geodynamic setting (Lakes Puyehue and Icalma–Chilean Lake District)'. *Science of The Total Environment*, 385(1-3):312–314.

Mañay, N., Rampoldi, O., Alvarez, C., Piastra, C., Heller, T., Viapiana, P., and Korbut, S. (2004). Pesticides in Uruguay. In Ware, G. W., Albert, L. A., Crosby, D. G., De Voogt, P., Hutzinger, O., Knaak, J. B., Mayer, F. L., Morgan, D. P., Park, D. L., Tjeerdema, R. S., Yang, R. S. H., and Gunther, F. A., editors, *Reviews of Environmental Contamination and Toxicology*, volume 181, pages 111–138. Springer New York, New York, NY.

Mellanby, K. (1992). *The DDT story*. British Crop Protection Council, Farnham, Surrey, UK.

Merotto, A., Gazziero, D. L. P., Oliveira, M. C., Scursoni, J., Garcia, M. A., Figueroa, R., and Turra, G. M. (2022). Herbicide use history and perspective in South America. *Advances in Weed Science*, 40(spe1):e020220050.

Oliveira, T. E. D., Freitas, D. S. D., Gianezini, M., Ruviaro, C. F., Zago, D., Mércio, T. Z., Dias, E. A., Lampert, V. D. N., and Barcellos, J. O. J. (2017). Agricultural land use change in the Brazilian Pampa Biome: The reduction of natural grasslands. *Land Use Policy*, 63:394–400.

Overbeck, G., Muller, S., Fidelis, A., Pfadenhauer, J., Pillar, V., Blanco, C., Boldrini, I., Both, R., and Forneck, E. (2007). Brazil's neglected biome: The South Brazilian Campos. *Perspectives in Plant Ecology, Evolution and Systematics*, 9(2):101–116.

Palladino, C., García, I., and Fernández, G. (2023). Pesticide dependence and associated risks in Uruguayan agriculture: limitations in its approach. *Agrociencia Uruguay*, 27:e1156.

Pereira, P. A. A., Martha, G. B., Santana, C. A., and Alves, E. (2012). The development of Brazilian agriculture: future technological challenges and opportunities. *Agriculture & Food Security*, 1(1):4.

Perestrelo, R., Silva, P., Porto-Figueira, P., Pereira, J. A., Silva, C., Medina, S., and Câmara, J. S. (2019). QuEChERS - Fundamentals, relevant improvements, applications and future trends. *Analytica Chimica Acta*, 1070:1–28.

Pettitt, A. N. (1979). A Non-Parametric Approach to the Change-Point Problem. *Journal of the Royal Statistical Society. Series C (Applied Statistics)*, 28(2):126–135. Publisher: [Royal Statistical Society, Oxford University Press].

Powell, R. L. and Still, C. J. (2009). Biogeography of C3 and C4 vegetation in South America. *Anais XIV Simposio Brasileiro de Sensoriamento Remoto, INPE*, pages p. 2935–2942.

Rauh, V., Arunajadai, S., Horton, M., Perera, F., Hoepner, L., Barr, D. B., and Whyatt, R. (2011). Seven-Year Neurodevelopmental Scores and Prenatal Exposure to Chlorpyrifos, a Common Agricultural Pesticide. *Environmental Health Perspectives*, 119(8):1196–1201. Publisher: Environmental Health Perspectives.

Rizzo, G., Monzon, J. P., and Ernst, O. (2021). Cropping system-imposed yield gap: Proof of concept on soybean cropping systems in Uruguay. *Field Crops Research*, 260:107944.

Röllin, S., Corcho-Alvarado, J. A., Sahli, H., Putyrskaya, V., and Klemt, E. (2022). High-resolution records of cesium, plutonium, americium, and uranium isotopes in sediment cores from Swiss lakes. *Environmental Science and Pollution Research*, 29(57):85777–85788.

Severo, O. P. (1955). Eradication of the Aedes Aegypti Mosquito from the Americas. *Jefferson History and Publications*.

Skidmore, M. E., Sims, K. M., and Gibbs, H. K. (2023). Agricultural intensification and childhood cancer in Brazil. *Proceedings of the National Academy of Sciences*, 120(45):e2306003120.

Tleuova, A. B., Wielogorska, E., Talluri, V. S. S. L. P., Štěpánek, F., Elliott, C. T., and Grigoriev, D. O. (2020). Recent advances and remaining barriers to producing novel formulations of fungicides for safe and sustainable agriculture. *Journal of Controlled Release*, 326:468–481.

Travis, S. C., Aga, D. S., Queirolo, E. I., Olson, J. R., Daleiro, M., and Kordas, K. (2020). Catching flame retardants and pesticides in silicone wristbands: Evidence of exposure to current and legacy pollutants in Uruguayan children. *Science of The Total Environment*, 740:140136.

Turgut, C., Gokbulut, C., and Cutright, T. J. (2009). Contents and sources of DDT impurities in dicofol formulations in Turkey. *Environmental Science and Pollution Research*, 16(2):214–217.

Woodford, E. K. (1957). The Toxic Action of Herbicides. *Outlook on Agriculture*, 1(4):145–154.

Zalles, V., Hansen, M. C., Potapov, P. V., Parker, D., Stehman, S. V., Pickens, A. H., Parente, L. L., Ferreira, L. G., Song, X.-P., Hernandez-Serna, A., and Kommareddy, I. (2021). Rapid expansion of human impact on natural land in South America since 1985. *Science Advances*, 7(14):eabg1620.

Zurbriggen, C., González-Lago, M., Baraibar, M., Baethgen, W., Mazzeo, N., and Sierra, M. (2020). Experimentation in the Design of Public Policies: The Uruguayan Soils Conservation Plans. *Iberoamericana – Nordic Journal of Latin American and Caribbean Studies*, 49(1):52–62.

VII

General discussion, conclusion and perspectives

Chapter 7

General discussion, conclusion and perspectives

Overall, this thesis explored how changes in land use, agricultural practices and socio-economic drivers have modified sediment dynamics, contaminant transfers, and environmental pressures in large agricultural basins of Southern South America. By combining reservoir sediment records, fallout radionuclide inventory measurements along cultivated hillslopes, and soil redistribution modelling, it quantified these changes across complementary spatial and temporal scales.

Reservoir sediment cores provide long-term archives of environmental changes at the catchment scale and their integrated record downstream. This is particularly useful in catchments where continuous monitoring data are limited or lacking such as that of the Uruguay River. By accumulating sediments exported from the river basin, reservoirs were shown to preserve records of sediment fluxes, contaminant inputs, eutrophication, and changes in sediment provenance. However, these records represent integrated signals at the scale of the basin. They do not directly identify the local processes or connectivity pathways responsible for the observed changes.

This limitation highlights the need to further link reservoir-scale reconstructions with field- and hillslope-scale observations in the upper catchment. Erosion, deposition, and contaminant mobilisation are controlled by local processes, but their downstream expression depends on whether eroded material is supplied to the river network and is ultimately transferred to reservoirs. This discussion therefore examines how agricultural changes modified sediment production, sediment connectivity, and contaminant transfers, and how combining reservoir archives, hillslope measurements, and a process-based erosion model can assist and improve their interpretation.

7.1 . Fluxes of sediments and historical contextualisation

Understanding the past and current processes taking place within the river basin requires a clear characterisation of the agricultural context of Southern South America. Agricultural development in the region has followed specific trajectories that must be considered to properly interpret recent environmental changes. The historical development of agriculture in the two main countries contributing to the Uruguay River basin (Brazil and Uruguay) was therefore examined and synthesised in the following section along with the results of the dynamics of the fluxes of sediments of each reservoir.

7.1.1 . Brazil and the Salto Grande dam river basin

Agriculture in southern Brazil, has undergone profound transformations over the last century (Selma Simões de Castro and José Pereira de Queiroz Neto 2009), driven by both socio-economic development and technological innovation. Early agricultural systems in the region were largely based on diversified family farming introduced by European immigrants during the nineteenth century, combined with extensive cattle ranching on the natural grasslands of the Pampa biome. From the second half of the twentieth

century onward, however, Brazilian agriculture experienced a rapid process of modernisation and territorial expansion associated with mechanisation, improved crop varieties, and the intensification of crop production. This transformation was particularly marked by the rapid expansion of soybean cultivation and grain production (Oliveira et al. 2017), which accelerated land-use changes and integrated the region into global agricultural markets. While these developments significantly increased agricultural productivity, they also generated major environmental pressures, notably soil degradation and accelerated erosion processes linked to land-use change and intensive agricultural practices. Soil erosion has become one of the most widespread forms of land degradation in Brazil, with some agricultural areas experiencing extremely high soil losses depending on soil characteristics, rainfall erosivity, and land management practices (Guerra et al. 2014). In southern Brazil, including Rio Grande do Sul, the conversion of natural grasslands and the intensification of cropping systems have been identified as key drivers of soil degradation, contributing to sediment transfer within watersheds and affecting soil fertility and long-term agricultural sustainability (Oliveira et al. 2017; Merten and Minella 2013; Guerra et al. 2014).

In the large Salto Grande river basin, sediment fluxes decreased by 61% while the contribution of the southern part of the basin increased by 75% since the early 2000s. This decline is consistent with that outlined by studies carried out in other parts of the world demonstrating that dam construction can substantially reduce downstream sediment fluxes at regional to global scales (Syvitski et al. 2005; Syvitski and Milliman 2007; Walling 2006). In this basin, this period corresponds to the construction of several large dams in the northern sector (2000, 2002, 2006, 2006, 2010), supporting a temporal coincidence between sediment flux reduction and sediment trapping. In contrast to the decrease in sediment flux observed in this study, Heathcote et al. (2013) showed increasing sediment accumulation rates in agricultural systems under intensifying land use, even in the presence of soil conservation measures. This apparent discrepancy highlights that sediment supply and sediment flux at the basin outlet may respond differently to land-use change, depending on the relative influence of sediment storage, connectivity, and trapping processes.

The sediment fingerprinting results demonstrate a shift in sediment provenance towards the southern part of the basin since the early 2000s. This shift is consistent with the expansion of agriculture in the southern part of the basin, which may have enhanced sediment supply by increasing soil disturbance, reducing vegetation cover, and promoting runoff-driven erosion processes as documented in the literature (Montgomery 2007). In parallel, the widespread adoption of no-tillage practices, while generally reducing soil loss, may have modified runoff pathways and sediment connectivity, leading to complex responses in sediment and contaminant fluxes (Didoné et al. 2019). These patterns highlight the difficulty of attributing sediment flux changes to single drivers at large spatial scales, where multiple sources and transfer processes are integrated at the catchment scale (Walling 1983).

7.1.2 . Uruguay and the Rincon del Bonete dam river basin

Historically, the natural grasslands of Uruguay were exploited for extensive ranching throughout most of the 20th century. From the 1950s until the 1980s, agriculture was marked by a stagnation of production levels (Hudson et al. 1992), attributed to a lack of technologically advanced production methods. During this period, despite the presence of pesticide use, its impact on sediment transfer likely remained limited due to the relatively small extent of cultivated areas.

A transition began in the late 1980s, when the government promoted new land uses through policies supporting forestry plantations (Zurbriggen et al. 2020). This phase was followed, in the late 1990s, by a drastic expansion of soybean cultivation and a transition from conventional tillage to no-tillage systems, enabled by the authorisation of genetically modified soybean seeds and the 1996 land leasing law (Zurbriggen et al. 2020). From 2002 onward, no-tillage became dominant (32% of cropland in 2000–2001 compared to 82% in 2006–2007; (Derpsch et al. 2010)). This transitional period, marked by the adoption of no-tillage and pasture rotation, coincided with a reduction in sediment delivery. This decrease is consistent with the expected effects of these practices under light to moderate grazing, which can reduce soil disturbance, maintain surface cover, and limit raindrop impact and sheet erosion (Pimentel et al. 1995; Trimble and Mendel 1995; Durán Zuazo and Rodríguez Pleguezuelo 2008).

From the early 2000s to the present, agricultural intensification has been accompanied by a strong increase in pesticide use, ranging between 3.9 and 10.6 tons of imported products between 2000 and 2021, with a maximum recorded in 2014 (Palladino et al. 2023), and herbicides representing 89% of the increase in 2021. During this period, large-scale land conversion and the expansion of cropping systems led to a renewed increase in soil erosion and sediment fluxes in the Rincón del Bonete catchment, largely decoupled from precipitation variability alone.

This unprecedented agricultural expansion and intensification had significant environmental impacts, contributing to soil degradation at the national scale (Foucher et al. 2023). In response, soil and water conservation measures were introduced in 1981 (law No. 15239), although their full implementation only occurred after 2013 with the Soil Use and Management Plans (SUMP). These plans require that erosion rates, estimated using RUSLE, remain below 7 $t.ha^{-1}.yr^{-1}$ for farms larger than 0.5 km^2 (representing 16,000 km^2 of cropland in 2019), highlighting the recognition of soil erosion as a major environmental issue in Uruguay (Zurbriggen et al. 2020).

The analysis of both cores, from the Rincon del Bonete and Salto Grande reservoirs, therefore suggests that sediment dynamics in these large agricultural basins were strongly influenced by the interaction between land-use change and evolving agricultural practices, which is consistent with the results of other studies conducted in the region (Foucher et al. 2023; Le Gall et al. 2017). Together, these changes appear to have modified both the magnitude of sediment accumulation and the dominant source areas contributing to reservoir deposits.

The decline in sediment accumulation rates after 2000 in the Salto Grande reservoir may partly reflect sediment disconnection caused by upstream dam construction in the northern part of the basin. Such reductions are consistent with the role of dams in trapping sediments and altering downstream sediment budgets (Vörösmarty et al. 2003; Syvitski et al. 2005). Furthermore, integrating both the Salto Grande and Rincon del Bonete studies suggest that this apparent reduction in sediment fluxes does not only reflect a simple decrease in erosion but also a change in sediment sources with first a dominance of the northern part that switched to that of the southern part of the catchment. More specifically, sediment fluxes shifted from a dominance of the basaltic plateau and forest biome to a stronger contribution from the Pampa. The Rincón del Bonete records clearly reflect the agricultural development of the southern basin, with a marked acceleration since 2008.

7.2 . Integrating hillslope-scale variability to reservoir sediment records

Many applications of FRN technique rely on sampling strategies that implicitly assume a high degree of local spatial uniformity in radionuclide inventories, although spatial variability and associated uncertainties have long been recognized (Walling and He 1999; Mabit et al. 2008). Zhang and Busteed (2024) demonstrated pronounced small-scale variability in ^{137}Cs distributions and identified it as a major source of uncertainty in soil redistribution estimates. In order to quantify this uncertainty in southern Brazil, a high-density fallout radionuclide sampling strategy was applied within two 12 m × 12 m midslope plots to assess the representativeness of individual soil cores for estimating soil redistribution in cultivated hillslopes in southern Brazil. The combined use of ^{137}Cs and $^{210}Pb_{ex}$ inventories, together with the implementation of several conversion models, allowed a detailed evaluation of spatial variability (Chapter 3). Radionuclide inventories and modelled soil redistribution rates exhibit strong variability over short distances, highlighting pronounced small-scale heterogeneity. In this context, $^{210}Pb_{ex}$ provided complementary insights into recent soil redistribution and farming-practice effects, particularly where ^{137}Cs signals are difficult to interpret due to past land-use change or soil disturbances. Consistent patterns emerged, with more heterogeneous inventories under conventional tillage and lower, more homogeneous redistribution rates under no-tillage. However, uncertainties remain regarding the reference inventories and their representativity, as well as the assumptions of the conversion models such as the complete and uniform mixing within the plough layer, simplified descriptions of radionuclide depth distributions and post-depositional redistribution, and should be further investigated. Large uncertainties also remain on the history of nuclear bomb testing fallout. While the temporal fallout records was adapted to the local inventories, the records of ^{137}Cs fallout used in this thesis were inferred from a station several hundred kilometres away and based on ^{90}Sr measurements and should be further constrained. These results still underline the value of combining radionuclides to better constrain soil redistribution processes and emphasize the need for sampling strategies that explicitly account for fine-scale spatial variability when

upscaling them to the hillslope scale.

Together, the hillslope soil inventory and reservoir sediment core studies showed that investigating sediment dynamics in these agricultural basins should not be based on the examination of a single spatial scale. The hillslope scale study demonstrated that erosion and redistribution are highly variable at the field scale, while the reservoir cores recorded the cumulative sediment delivery, storage, and remobilisation at the basin scale. This contrast reflects well-established scale effects in sediment systems, whereby hillslope measurements capture highly variable, event-driven erosion processes, while downstream sediment records integrate the effects of sediment connectivity, temporary storage, and remobilisation across the catchment (Walling 1983; de Vente and Poesen 2005; Fryirs and Brierley 2012; Bracken et al. 2015). This multi-scale perspective supports the broader interpretation that apparent decreases in downstream sediment fluxes may coexist despite unchanged or even intensified local erosion, change in processes, variations in sediment sources (Tales Tiecher 2015), and increased contaminant connectivity in upper catchments.

These findings also support the need for approaches that can better represent the current spatial impacts of changes in agricultural practices, erosion processes, and land use. In this context, application of so-called distributed erosion models such as WaterSed could provide spatially-distributed information to better identify the areas that are most likely to produce, store, or deliver sediment to the river network (Vandromme et al. 2023). By integrating information on topography, land use, agricultural practices, drainage structure and also the possibilities of adding soft hydraulics measures (terraces, hedges, grass strip and buffer basin), a distributed erosion model could also help identifying areas where sediment connectivity has likely increased or decreased through time. This is particularly relevant in landscapes where no-tillage, terracing, crop expansion, soil compaction, and gully development may modify runoff pathways and sediment delivery independently of average erosion rates.

The main limitation of this type of modelling lies in the requirement for a robust and spatially-distributed dataset for model parametrisation and evaluation. This requirement is particularly important for distributed erosion models such as WaterSed, which rely on multiple input variables describing rainfall events, soil properties, topography, land use, and management practices.

In this study, modelling was initially envisaged to be conducted at the scale of the entire Uruguay River basin, with a focus on the Rincón del Bonete subcatchment. However, the lack of consistent and long-term monitoring data in the entire basin, particularly regarding discharge and suspended sediment load prevented the reliable parametrisation and validation of the model. In this context, the long-term monitoring conducted between 2014 and 2017 at a smaller spatial scale, at the outlet of the Conceição catchment, provided valuable information on hydrological dynamics and suspended sediment load under current land-use conditions. The modelling work carried out on the Conceição catchment provides useful insights into both the capabilities and current limitations of the approach. The partial parametrisa-

tion and subsequent fine-tuning of key parameters, particularly those controlling soil water storage and evapotranspiration, allowed the model to reproduce the general magnitude and variability of event-scale runoff, although discrepancies remain at the individual event level. The persistence of event-dependent deviations, with both over- and underestimation depending on event magnitude, highlights the sensitivity of the system to antecedent moisture conditions and storage capacity. The results are an initial step toward model calibration and demonstrate that the model is capable of capturing first-order hydrological behaviour, while also underlining the need for more extensive datasets and a more systematic calibration strategy to better constrain key processes. Extending this approach to longer time series and larger spatial scales would require sustained monitoring efforts and a dedicated investigation, which would constitute a substantial research effort beyond the scope of this study.

Other studies conducted in a nearby area monitored an experimental zero-order catchments under no-till systems with similar climatic and soil conditions and successfully applied modelling, providing complementary insights into runoff, sediment dynamics, and soil water processes (Londero et al. 2021; Hörbe et al. 2021; Schneider et al. 2025).

Model applications in this catchment show that runoff dynamics can be reproduced with a good agreement, whereas sediment yield simulations remain less accurate and require careful calibration (Schneider et al. 2025). Model performance is particularly sensitive to some parameters, including saturated hydraulic conductivity, surface roughness, and soil cohesion, and varies between calibration and validation phases as well as depending on the spatial scale considered. Field observations indicate strong event-to-event variability in runoff and sediment responses, even under similar rainfall conditions (Londero et al. 2021). Experimental comparisons within the catchment further show that terraces increase soil water availability and crop yields, while modifying runoff dynamics (Hörbe et al. 2021). Taken together, these results indicate that, even under controlled and well-monitored conditions, hydrological responses and sediment transfer remain highly variable, and model performance is constrained by parameter sensitivity and process representation.

7.3 . Agricultural intensification and conservation practices

Analysis of both reservoirs converges on the central role of agricultural expansion and intensification, particularly the widespread adoption of herbicide-resistant cropping systems and the integration of no-tillage without complementary conservation practices.

Initially introduced to reduce soil loss, no-tillage appears to have contributed to a temporary decline in sediment production, which is consistent with the patterns described in chapters 5 & 6 and the literature (Minella et al. 2017; Didoné et al. 2014). Yet, over longer timescales, the results suggest that its simplified implementation often accompanied by monocropping or continuous cropping systems and without complementary measures such as crop rotation or contour farming may still lead to excessive soil

compaction, reduced infiltration, and enhanced surface runoff (Londero et al. 2021; Didoné et al. 2014; Merotto et al. 2022). Therefore, this can affect the sediment redistribution dynamics and enhance flow concentration, leading to increased subsurface erosion. Both the Rincon del Bonete and Salto Grande reservoirs recorded the recent resurgence of banned pesticide compounds. This resurgence could be attributed to the expansion of agriculture on previously treated and uncultivated areas. Another explanation could be the remobilisation of the contaminants stored in soils through this increased subsurface erosion. In parallel, contaminant records show a strong increase, particularly for herbicides such as glyphosate after the 2000s. This reflects the intensification of agricultural practices and increased chemical inputs, which are widely reported in South American agroecosystems (in 2019, the average glyphosate application rate was estimated at 1440 $g.ha^{-1}$) (Aktar et al. 2009; Merotto et al. 2022).

On the contrary, the decline in insecticide concentrations was unexpected and could be attributed to the implementation of integrated pest management (Hoffmann-Campo et al. 2003), which might have allowed the reduction of the use of insecticides. Another explanation could be the expansion of soybean cropping, which requires lower insecticides input. In parallel, national insecticide imports increased (FAO Statistics) and the decline of the concentrations of insecticides in the cores may be attributable to the limited set of compounds that were analysed, which may have excluded substitute or more recent insecticides.

Both studies therefore support the idea that conservation practices may have short-term benefits but long-term deleterious consequences, particularly in systems under monoculture, therefore explaining the apparent contradiction between decreasing sediment fluxes at certain periods and increasing hydrological connectivity and contaminant transport.

Furthermore, since its creation in 1979, the Salto Grande reservoir has exhibited persistent eutrophic conditions (Quirós and Luchini 1982; Berón 1990), reflecting chronic nutrient enrichment and recurrent phytoplankton blooms. These conditions have intensified since the early 2000s (Chalar 2006, 2009), likely in response to the expansion of intensive agriculture and livestock production across the basin. In parallel, Beaulieu et al. (2019) have shown that increasing eutrophication in lakes and reservoirs can enhance methane emissions through the stimulation of organic matter production and anaerobic degradation. Conservation agriculture can promote soil organic carbon accumulation, particularly when no-tillage is combined with complementary measures such as residue retention, cover crops, and diversified rotations. Although the magnitude and persistence of carbon sequestration remain strongly site-dependent, it might help mitigating the overall impact of agriculture (FAO soils portal). However, in the current context, the observed intensification of eutrophication may contribute to increased greenhouse gas emissions from the reservoir, highlighting an additional pathway through which agricultural intensification can influence biogeochemical functioning beyond sediment and nutrient transfers.

7.4 . Socio-economic drivers, water resource and future trajectories

This thesis also showed the explicit connection between global economic drivers and local environmental changes. The expansion of export-oriented agriculture, reinforced by regional and inter-regional trade frameworks such as Mercosur and the EU-Mercosur agreements, represents a major external driver that may intensify land-use change and agricultural intensification in the Pampa region. Soybean and soybean-derived products account for roughly 20–25% of Argentina's export revenue (World Bank Group 2022). It also constitutes the largest component of Brazil's export value and dominates its agribusiness exports, which account for nearly half of total exports of Brazil (World Bank Group 2025). Furthermore, in 2019, Uruguay produced 0.54 million tonnes carcass weight equivalent (cwe) of beef and exported 0.42 million tonnes cwe in 2019, roughly 80% of its beef production (Greenwood 2021). These trade agreements allow reducing export costs, harmonising regulations, and attracting foreign investments. Consequently, they could create strong incentives for the further intensification and expansion of export-oriented agriculture in Brazil, particularly in the soybean-dominated agricultural regions such as that of Rio Grande do Sul. This could also lead to the further conversion of the Pampa's grasslands and other natural habitats into agricultural fields.

To go further, Dogliotti et al. (2026) revisited the relationship between afforestation and water yield in the Pampa region, showing that although afforestation generally leads to reductions in runoff, the magnitude and spatial expression of this effect remain highly variable. Their analysis demonstrates that forest cover alone is insufficient to explain streamflow decline, and that hydrological responses emerge from the interaction between vegetation structure, management practices, and intrinsic catchment sensitivity. In particular, runoff reductions can reach substantial levels in specific configurations, highlighting a trade-off between biomass production and water availability (Dogliotti et al. 2026).

In this context, the expansion of industrial forestry associated with the development of a massive wood processing facility (constructed by the UPM group, standing for United Paper Mills, UPM Uruguay) near the Rincón del Bonete dam, together with additional plantations under development, is likely to further increase forest cover in Uruguay and across the Pampa. Rather than inducing uniform hydrological changes, such expansion may amplify water stress in hydrologically sensitive catchments, particularly under climatic constraints such as droughts. This is consistent with previous studies showing that afforestation reduces water yield primarily through increased evapotranspiration, although the magnitude of this effect depends on climate and catchment characteristics (Farley et al. 2005).

These interactions became particularly evident during the 2022–2023 drought, when water resources in Uruguay were severely depleted (Diacre 2024). Reservoir levels dropped to critical thresholds, leading the government to declare a state of water emergency for several months and to switch water supply to the Río San José, which is hydraulically connected to the Río de la Plata estuary. As a result, the drinking water supplied to Montevideo, the capital of Uruguay, exceeded recommended thresholds for chloride



Figure 7.1: Localisation of the major Brazilian soybean producing states

and sodium concentrations, reflecting the intrusion of saline water into the supply system. This example illustrates how, under a changing climate with more frequent and intense extremes, shifts in water balance may reduce the buffering capacity of catchments, thereby increasing their vulnerability and limiting their capacity to sustain water supply during drought periods, with direct implications for water availability and supply.

Furthermore, Li et al. (2026) showed that - from 1982 to 2018 - tree evaporation in the Amazon contributed about one-third of growing-season precipitation across major Brazilian soybean-producing states (Paraná, Santa Catarina, Rio Grande do Sul, São Paulo, Mato Grosso do Sul, Mato Grosso, Goiás, Figure 7.1) with large consequences on the crop yields (reduced by 227kton, or 6% loss in Rio Grande do Sul). This reflects a strong atmospheric moisture recycling mechanism, whereby trees take up water from the soil and return it to the atmosphere through transpiration and evaporation of intercepted rainfall. The resulting water vapour is transported and can subsequently condense and fall as precipitation over the basin and in downwind regions Li et al. (2026). This process creates a land–atmosphere feedback in which forest cover contributes to maintaining regional rainfall. As air masses move across the basin, moisture can be recycled multiple times, so that a significant fraction of precipitation is derived from terrestrial evapotranspiration rather than coming directly from oceanic sources.

The modelled reduction in precipitation over southern Brazil, combined with decreased water avail-

ability associated with afforestation, suggests the occurrence of an increasing pressure on regional water resources and highlights the need for further assessment.

Besides the overall decrease of growing-season precipitation, in 2024, extreme flooding in the Guaíba river basin (435 mm of rainfall were recorded in a 31 hour period Minella et al. (2026)) submerged large areas of Porto Alegre (Mantovani et al. 2025), the capital and largest city of Rio Grande do Sul, depositing potentially contaminated sediments across the metropolitan region. (Neto et al. 2025) found that unplanned urbanization and extensive agricultural practices significantly contributed to flooding, with human activities reducing the land's natural ability to absorb and manage rainwater, causing widespread inundation. As a result, over 2.3 million people were displaced and there were substantial economic losses.

Climate change and the likely increase of extreme events including droughts and very wet periods combined with the intensification of human activities driven by global market demand could create extreme conditions for the environment and for humans in the region, and future sediment and contaminant dynamics studies should consider economic and political contexts not only in individual countries but also globally. Projections of continued expansion in soybean cultivation and forestry suggest that current trends of increasing connectivity and increasing water consumption/evapotranspiration are likely to intensify, possibly aggravating the impacts of extreme events such as flooding and droughts that could previously be buffered in the catchment. This interpretation is consistent with evidence from the South American plains showing an increasing occurrence of flooding in agricultural areas over the past two decades, associated with a transition from deeper to shallower groundwater systems that respond more rapidly to intense precipitation (Houspanossian et al. 2023). Similarly, large-scale afforestation has been shown to substantially increase evapotranspiration and reduce regional water availability, contributing to declining water resources and increased drought risk in Southwest China (Xiao et al. 2020).

In light of the environmental challenges identified in this study and the projected land-use and land-cover changes, this thesis outlines the need for clear and more environmental-friendly agricultural policies, alongside the improved monitoring of land use and management, to support the adoption of more sustainable agricultural practices. In Brazil, such practices have been formalised within a conservation agriculture system referred to as 'Sistema de Plantio Direto na Palha com Qualidade' (SPD), which is based on minimal soil disturbance, permanent soil cover, and crop rotation and optimally with terraces. This framework provides a structured basis for soil conservation and improved water retention at the field scale. However, its effectiveness depends on a consistent implementation. In many soybean-dominated systems, simplified rotations and intensive input use may limit these benefits, highlighting the need for stronger governance and monitoring to ensure that conservation principles are effectively applied in practice such as the soil and water conservation plan in Uruguay (Zurbriggen et al. 2020) or the recent 226/025 decree supporting ecosystem-based biomonitoring advances (Teixeira-de Mello et al. 2026).

By integrating both complementary large and small scale studies, this thesis shows that changes in land use and agricultural practices have modified both erosion processes and contaminant transfers in the large agricultural basins of Southern South America. The sedimentary records reveal the combined influence of contemporary agricultural pressures and legacy contamination, while the fallout radionuclide modelling study highlights the strong spatial heterogeneity of soil redistribution at the hillslope scale and under different agricultural practices. A major conclusion is that reductions in downstream sediment flux should not be interpreted automatically as a sign of the efficiency of soil conservation techniques or as a sign of environmental recovery. In these basins, lower sediment accumulation rates may coincide with changes in sediment sources, increased or decreased sediment connectivity, higher contaminant concentrations, and persistent ecological risks.

Brazil, Argentina, and Uruguay have supported extensive research on agricultural systems and the development of conservation agriculture practices over the past decades, notably through national research institutions and farmer-led innovation networks (amongst others, EMBRAPA (Empresa Brasileira de Pesquisa Agropecuária) in Brazil, INTA (Instituto Nacional de Tecnología Agropecuaria) in Argentina or INIA (Instituto Nacional de Investigación Agropecuaria) in Uruguay). Despite this strong scientific and technical foundation, the expansion of export-oriented agricultural markets has continued to drive the intensification of production systems across these countries. This tension between agronomic knowledge and economic incentives has important implications for soil conservation, and for understanding sediment transfers, and associated environmental impacts. In this context, it is essential that countries benefiting from these agricultural commodities recognise their role within global production systems and support continued international collaboration. Such cooperation may contribute to the development of regulatory frameworks and market incentives that promote more sustainable agricultural practices, rather than reinforcing trajectories towards lower environmental standards. A recent example is the European Regulation on Combating Deforestation and Forest Degradation (EUDR), adopted in 2023, which seeks to restrict the import of commodities associated with deforestation and forest degradation in producing countries, thereby linking market access to environmental performance.

7.5 . Limitations and Perspectives for future research

This thesis addressed long-standing questions, persisting for more than a decade, such as that of the provenance of sediments in the Salto Grande reservoir, while also highlighting the limitations of current approaches, including the lack of long-term datasets and monitoring for large-scale studies, as well as the high spatial variability and complexity of soil erosion and redistribution processes.

7.5.1 . Methodological limitations

An objective of this thesis was also to explore the potential of environmental DNA (eDNA) to reconstruct recent ecological changes and land-use signals recorded in the reservoir sediment cores, an approach that is increasingly used in aquatic and sedimentary environments (Deiner et al. 2017; Parducci et al. 2017). However, the eDNA data were not retained for further analysis due to several methodological and interpretative limitations. First, taxonomic assignments based on the NCBI and SILVA databases yielded the presence of several taxa that were not consistent with the known biogeographical context of the study area. This raised uncertainties regarding the reliability of species identification, likely reflecting limitations in reference databases and potential misassignments, as discussed in other metabarcoding studies (Taberlet et al. 2018; Porter and Hajibabaei 2018). Second, key emblematic species expected to be detected in the catchment, such as soybean, were not retrieved in the analysed samples. Given the well-documented dominance of these crops in the region, their absence suggests an incomplete detection, a known limitation of eDNA approaches related to preservation, transport, and marker biases (Deiner et al. 2017). An additional explanation may be related to the quantity and pathways of DNA input into the system, as taxa producing lower or more transient biomass, or contributing less efficiently to erosion and particulate transfer, may deliver reduced amounts of DNA to sediments, thereby limiting their detectability (Giguet-Covex et al. 2023). Third, the vertical resolution of the sampling was limited to three discrete depth intervals per core. This low temporal resolution restricted the ability to capture changes in community composition and to robustly link eDNA signals to known shifts in land use and agricultural practices. In addition, the presence of ambiguous sequences in control samples and the incomplete amplification of some plant markers further reduced our confidence in the dataset. Taken together, these limitations prevented a robust ecological interpretation of the eDNA results, and the dataset was therefore not integrated into the Salto Grande dam and Rincon del Bonete dam chapters.

Moreover, during this thesis, and through discussions with colleagues in the team, several methodological aspects requiring further investigation were identified when analysing the sediment cores that were used to reconstruct changes in erosion rates with time. A first issue is related to the difficulty of obtaining accurate and representative high-resolution bulk density measurements. Initially, the protocol relied on CT scanning to derive high-resolution density profiles, which were then calibrated against discrete measurements obtained from 1 cm^3 samples. However, this approach resulted in weak correlations. Consequently, the protocol was revised to calculate bulk density for each sampled layer, which was then compared to the CT-derived signal. Additional tests, including the use of reference materials during measurement, only resulted into limited improvement, and efforts should be made in the future to better constrain this technique. Secondly, discussions within the team highlighted the potential of applying statistical clustering techniques to sediment core datasets. It was further recognised that XRF data analysis is largely based on expert interpretation, which may limit the method reproducibility. This motivated the

development of an R-based workflow to standardise data processing, including denoising, variable selection, clustering, and visualisation of sediment core data, which is described in supplementary material B.

7.5.2 . Perspectives for future research

Future research should expand contaminant monitoring to include emerging compounds. Indeed, (Merotto et al. 2022) highlighted the diversification of herbicide use in South America following the widespread adoption of glyphosate-resistant crops, with the increasing application of compounds such as glufosinate, sulfentrazone, clomazone, ACCase inhibitors (e.g., clethodim, haloxyfop), and ALS inhibitors (e.g., imazethapyr), which were not analysed in this thesis. Furthermore, there ise a need to better quantify the long-term effects of agricultural practices such as no-tillage, and develop multi-proxies analysis, integrating geochemical, hydrological, ecological, and socio-economical analyses. Others studies emerged from the work realised by Foucher et al. (2023) and 5's study on the sources of sediments contributing to the Rincon del Bonete reservoir in Uruguay in response to concerns from farmers and the INIA institute on the exact provenance of the sediment accumulated in the reservoir. Two major tributaries including the Rio Tacuarembó and Rio Negro flow across this catchment and drain very contrasting landscapes with distinct reliefs, geologies and soil types and used for forest plantation and crop cultivation, respectively. A follow-up study is therefore being designed in order to distinguish the relative contributions of agricultural and forestry areas to sediment delivery. This work will deploy sediment fingerprinting techniques and apply them to the sediment core analysed in 5 through the explicit consideration of potential source areas within the Rincon del Bonete catchment drained by these two tributaries.

To further develop this research, alternative sampling strategies should be evaluated to better capture the high spatial variability inherent to soil redistribution processes. In particular, multiple soil cores collected within short distances (e.g., based on the DEM resolution) could be combined by depth interval to produce composite samples, providing a more representative estimate of radionuclide inventories across hillslopes while reducing the analytical workload. The number of cores, their spatial distribution, and the definition of depth intervals should remain adaptable and determined according to catchment characteristics and logistical constraints, or informed by an initial sampling phase used to evaluate variability and guide the optimisation of the sampling design.

In parallel, to address the lack of long-term monitoring data, the record of temporal patterns of sediment transfers assessed from reservoir sediment cores could be used to inform and constrain the parametrisation of distributed based erosion models (Smith et al. 2018) such as WaterSed, particularly with respect to erosion rates, sediment connectivity, and delivery ratios.

Recent developments in low-cost and open-source monitoring technologies also offer opportunities to increase the spatial density of observations and extend monitoring to larger areas (Hamel et al. 2024). In the context of this study, such approaches could help overcoming the current limitations related to

sparse sampling and the strong small-scale variability of sediment redistribution. Deploying a greater number of measurement points across the catchment would improve the representation of hillslope-scale processes and connectivity patterns that are not captured by limited core sampling alone. In addition, a higher spatial coverage would support a more robust comparison between point-based sediment records and spatially-distributed erosion estimates, thereby strengthening the interpretation of sediment sources, pathways, and storage processes within the catchment.

Unmanned aerial vehicles (UAVs) equipped with sensors such as LiDAR or high-resolution photogrammetric systems should also be considered to acquire detailed topographic and surface data. These approaches enable the rapid data acquisition at high spatial resolution, allowing for the characterisation of microtopography, erosion features, and sediment redistribution patterns which is not possible with coarser datasets.

At the scale of larger river basins, satellite-based observations may also provide a complementary perspective. Freely available products, such as those derived from the MapBiomas initiative, can be used to reconstruct land-use dynamics, while remote sensing approaches (Wang et al. 2023) allow the assessment of soil degradation through both direct indicators (e.g., mineral composition, soil organic matter, surface roughness, and moisture content) and indirect proxies (e.g., vegetation condition and land-use/land-cover changes).

The combined use of UAV and satellite data may therefore offer a multi-scale framework in which high-resolution, local observations could be used to calibrate and interpret broader-scale patterns derived from satellite imagery. Such integration is particularly relevant in this study, as it would support the extrapolation of hillslope-scale processes identified from sediment cores and field measurements to the scale of larger river basins, while accounting for spatial heterogeneity in erosion and sediment transfers.

Bibliography

Aktar, W., Sengupta, D., and Chowdhury, A. (2009). Impact of pesticides use in agriculture: their benefits and hazards. *Interdisciplinary Toxicology*, 2(1):1–12.

Beaulieu, J. J., DelSontro, T., and Downing, J. A. (2019). Eutrophication will increase methane emissions from lakes and impoundments during the 21st century. *Nature Communications*, 10(1):1375. Publisher: Nature Publishing Group.

Berón, L. E. (1990). Features of the limnological behavior of Salto Grande's reservoir (Argentina-Uruguay). *Ecological Modelling*, 52:87–102.

Bracken, L. J., Turnbull, L., Wainwright, J., and Bogaart, P. (2015). Sediment connectivity: a framework for understanding sediment transfer at multiple scales. *Earth Surface Processes and Landforms*, 40(2):177–188. _eprint: https://onlinelibrary.wiley.com/doi/pdf/10.1002/esp.3635.

Chalar, G. (2006). Eutrophication dynamics on different temporal scales: salto grande reservoir (Argentina-Uruguay). *Eutrophication in South America: causes, consequences and technologies for management and control*.

Chalar, G. (2009). The use of phytoplankton patterns of diversity for algal bloom management. *Limnologica*, 39(3):200–208.

de Vente, J. and Poesen, J. (2005). Predicting soil erosion and sediment yield at the basin scale: Scale issues and semi-quantitative models. *Earth-Science Reviews*, 71(1):95–125.

Deiner, K., Bik, H. M., Mächler, E., Seymour, M., Lacoursière-Roussel, A., Altermatt, F., Creer, S., Bista, I., Lodge, D. M., de Vere, N., Pfrender, M. E., and Bernatchez, L. (2017). Environmental DNA metabarcoding: Transforming how we survey animal and plant communities. *Molecular Ecology*, 26(21):5872–5895.

Derpsch, R., Friedrich, T., Kassam, A., and Hongwen, L. (2010). Current status of adoption of no-till farming in the world and some of its main benefits. *International Journal of Agricultural and Biological Engineering*, 3.

Diacre, A. (2024). La crise de l'eau en Uruguay: Compréhension des causes et impacts. *Hal*.

Didoné, E. J., Gomes Minella, J. P., Andres Schneider, F. J., Londero, A. L., Lefèvre, I., and Evrard, O. (2019). Quantifying the impact of no-tillage on soil redistribution in a cultivated catchment of Southern Brazil (1964–2016) with 137Cs inventory measurements. *Agriculture, Ecosystems & Environment*, 284:106588.

Didoné, E. J., Minella, J. P. G., Reichert, J. M., Merten, G. H., Dalbianco, L., de Barrros, C. A. P., and Ramon, R. (2014). Impact of no-tillage agricultural systems on sediment yield in two large catchments in Southern Brazil. *Journal of Soils and Sediments*.

Dogliotti, G., Hirigoyen, A., Birgand, F., Gonzalez-Talice, J., and Cook, R. (2026). How much is too much forest? Catchment sensitivity and silvicultural controls on water yield in temperate grassland afforestation. *Forest Ecology and Management*, 618:124002.

Durán Zuazo, V. H. and Rodríguez Pleguezuelo, C. R. (2008). Soil-erosion and runoff prevention by plant covers. A review. *Agronomy for Sustainable Development*, 28(1):65–86.

Farley, K. A., Jobbágy, E. G., and Jackson, R. B. (2005). Effects of afforestation on water yield: a global synthesis with implications for policy. *Global Change Biology*, 11(10):1565–1576.

Foucher, A., Tassano, M., Chaboche, P.-A., Chalar, G., Cabrera, M., Gonzalez, J., Cabral, P., Simon, A.-C., Agelou, M., Ramon, R., Tiecher, T., and Evrard, O. (2023). Inexorable land degradation due to agriculture expansion in South American Pampa. *Nature Sustainability*.

Fryirs, K. A. and Brierley, G. J. (2012). *Geomorphic Analysis of River Systems: An Approach to Reading the Landscape*. Wiley, 1 edition.

Giguet-Covex, C., Jelavić, S., Foucher, A., Morlock, M. A., Wood, S. A., Augustijns, F., Domaizon, I., Gielly, L., and Capo, E. (2023). The Sources and Fates of Lake Sedimentary DNA. In Capo, E., Barouillet, C., and Smol, J. P., editors, *Tracking Environmental Change Using Lake Sediments*, volume 21, pages 9–52. Springer International Publishing, Cham. Series Title: Developments in Paleoenvironmental Research.

Greenwood, P. L. (2021). Review: An overview of beef production from pasture and feedlot globally, as demand for beef and the need for sustainable practices increase. *Animal*, 15:100295.

Guerra, A. J. T., Fullen, M. A., Jorge, M. d. C. O., and Alexandre, S. T. (2014). Erosão e conservação de solos no Brasil. *Anuário do Instituto de Geociências*, 37(1):81–91.

Hamel, P., Ding, N., Cherqui, F., Zhu, Q., Walcker, N., Bertrand-Krajewski, J.-L., Champrasert, P., Fletcher, T. D., McCarthy, D. T., Navratil, O., and Shi, B. (2024). Low-cost monitoring systems for urban water management: Lessons from the field. *Water Research X*, 22:100212.

Heathcote, A. J., Filstrup, C. T., and Downing, J. A. (2013). Watershed Sediment Losses to Lakes Accelerating Despite Agricultural Soil Conservation Efforts. *PLOS ONE*, 8(1):e53554. Publisher: Public Library of Science.

Hoffmann-Campo, C. B., Oliveira, L. J., Moscardi, F., Gazzoni, D. L., Corrêa-Ferreira, B. S., Lorini, I. A., Borges, M., Panizzi, A. R., Sosa-Gomez, D. R., and Corso, I. C. (2003). Integrated pest management in Brazil. In Maredia, K. M., Dakouo, D., and Mota-Sanchez, D., editors, *Integrated pest management in the global arena*, pages 285–299. CABI Publishing, UK, 1 edition.

Houspanossian, J., Giménez, R., Whitworth-Hulse, J. I., Nosetto, M. D., Tych, W., Atkinson, P. M., Rufino, M. C., and Jobbágy, E. G. (2023). Agricultural expansion raises groundwater and increases flooding in the South American plains. *Science*, 380(6652):1344–1348. Publisher: American Association for the Advancement of Science.

Hudson, R. A., Meditz, S. W., Weil, T. E., and Library of Congress, editors (1992). *Uruguay: a country study*. Number 550-97 in Area handbook series. Federal Research Division, Library of Congress : For sale by the Supt. of Docs., U.S. G.P.O, Washington, D.C, 2nd ed edition.

Hörbe, T., Minella, J. P. G., Schneider, F. J. A., Londero, A. L., Gubiani, P. I., Merten, G. H., and Schlesner, A. (2021). Managing runoff in rainfed agriculture under no-till system: potential for improving crop production. *Revista Brasileira de Ciência do Solo*, 45:e0210015.

Le Gall, M., Evrard, O., Dapoigny, A., Tiecher, T., Zafar, M., Minella, J. P. G., Laceby, J. P., and Ayrault, S. (2017). Tracing Sediment Sources in a Subtropical Agricultural Catchment of Southern Brazil Cultivated With Conventional and Conservation Farming Practices. *Land Degradation & Development*, 28(4):1426–1436. _eprint: https://onlinelibrary.wiley.com/doi/pdf/10.1002/ldr.2662.

Li, H., Lesk, C. S., Zhu, L., Crowther, T. W., Chen, M., Ray, D. K., and Mueller, N. D. (2026). Amazon deforestation reduces precipitation and soybean yields across Southern Brazil. *Proceedings of the National Academy of Sciences*, 123(24):e2525378123.

Londero, A. L., Minella, J. P. G., Schneider, F. J. A., Deuschle, D., Merten, G. H., Evrard, O., and Boeni, M. (2021). Quantifying the impact of no-till on sediment yield in southern Brazil at the hillslope and catchment scales. *Hydrological Processes*, 35(7):e14286.

Mabit, L., Benmansour, M., and Walling, D. E. (2008). Comparative advantages and limitations of the fallout radionuclides 137Cs, 210Pbex and 7Be for assessing soil erosion and sedimentation. *Journal of Environmental Radioactivity*, 99(12):1799–1807.

Mantovani, J. R., Alcântara, E., Baião, C. F., Pampuch, L., Curtarelli, M. P., Mariano Ribeiro, J. V., Guimarães, Y. C., Londe, L., Massi, K., Marengo, J., Nobre, C. A., Assireu, A. T., Bortolozo, C. A., Simões, S. J., Tomasella, J., Leal De Moraes, O. L., and Park, E. (2025). Unprecedented flooding in Porto Alegre Metropolitan Region (Southern Brazil) in May 2024: Causes, risks, and impacts. *Journal of South American Earth Sciences*, 160:105533.

Merotto, A., Gazziero, D. L. P., Oliveira, M. C., Scursoni, J., Garcia, M. A., Figueroa, R., and Turra, G. M. (2022). Herbicide use history and perspective in South America. *Advances in Weed Science*, 40(spe1):e020220050.

Merten, G. H. and Minella, J. P. G. (2013). The expansion of Brazilian agriculture: Soil erosion scenarios. *International Soil and Water Conservation Research*, 1(3):37–48.

Minella, J. P., Merten, G. H., Barros, C. A., Ramon, R., Schlesner, A., Clarke, R. T., Moro, M., and Dalbianco, L. (2017). Long-term sediment yield from a small catchment in southern Brazil affected by land use and soil management changes. *Hydrological Processes*, 32(2):200–211. _eprint: https://onlinelibrary.wiley.com/doi/pdf/10.1002/hyp.11404.

Minella, J. P. G., Buligon, L., Silva, C. C. D., Londero, A. L., Dambroz, A. P. B., Silva, P. R. B. D., Feyh, G. A., Saatkamp, E. D., Schlesner, A., Fernando, E., Merten, G. H., Carvalho, L. F. D. D., Papalia, D., and Rubert, T. (2026). Extreme hydrological and erosive processes during the April 2024 event: A small catchment-monitoring experience in southern Brazil. *Revista Brasileira de Ciência do Solo*, 50.

Montgomery, D. R. (2007). Soil erosion and agricultural sustainability. *Proceedings of the National Academy of Sciences*, 104(33):13268–13272.

Neto, J. B. F., Freitas, M. S., Simões, P. S. M., Pereira, G., Leão, H. S., Calmon, A. V. V., and Gücker, B. (2025). Impact of April and May, 2024 extreme precipitation on flooding in Rio Grande do Sul, Brazil. *Urban Climate*, 61:102487.

Oliveira, T. E. D., Freitas, D. S. D., Gianezini, M., Ruviaro, C. F., Zago, D., Mércio, T. Z., Dias, E. A., Lampert, V. D. N., and Barcellos, J. O. J. (2017). Agricultural land use change in the Brazilian Pampa Biome: The reduction of natural grasslands. *Land Use Policy*, 63:394–400.

Palladino, C., García, I., and Fernández, G. (2023). Pesticide dependence and associated risks in Uruguayan agriculture: limitations in its approach. *Agrociencia Uruguay*, 27:e1156.

Parducci, L., Bennett, K. D., Ficetola, G. F., Alsos, I. G., Suyama, Y., Wood, J. R., and Pedersen, M. W. (2017). Ancient plant DNA in lake sediments. *New Phytologist*, 214(3):924–942. _eprint: https://nph.onlinelibrary.wiley.com/doi/pdf/10.1111/nph.14470.

Pimentel, D., Harvey, C., Resosudarmo, P., Sinclair, K., Kurz, D., McNair, M., Crist, S., Shpritz, L., Fitton, L., Saffouri, R., and Blair, R. (1995). Environmental and Economic Costs of Soil Erosion and Conservation Benefits. *Science*, 267(5201):1117–1123. Publisher: American Association for the Advancement of Science.

Porter, T. M. and Hajibabaei, M. (2018). Scaling up: A guide to high-throughput genomic approaches for biodiversity analysis. *Molecular Ecology*, 27(2):313–338. _eprint: https://onlinelibrary.wiley.com/doi/pdf/10.1111/mec.14478.

Quirós, R. and Luchini, L. (1982). Características Limnológicas del Embalse de Salto Grande, III: Fitoplancton y su Relación con Parámetros Ambientales. *Natura Neotropicalis*, 1(13):49–66.

Schneider, F. J. A., Minella, J. P. G., Londero, A. L., Deuschle, D., Merten, G. H., Evrard, O., Cerdan, O., and Dambroz, A. P. B. (2025). Surface Runoff and Sediment Yield Modelling Under No-Till: Chiselling and Crop Management Effects. *Hydrological Processes*, 39(12):e70354.

Selma Simões de Castro and José Pereira de Queiroz Neto (2009). Soil Erosion in Brazil from Coffee to the Present-day Soy Bean Production. In *Developments in Earth Surface Processes*, volume 13, pages 195–221. Elsevier. ISSN: 0928-2025.

Smith, H. G., Peñuela, A., Sangster, H., Sellami, H., Boyle, J., Chiverrell, R., Schillereff, D., and Riley, M. (2018). Simulating a century of soil erosion for agricultural catchment management. *Earth Surface Processes and Landforms*, 43(10):2089–2105. _eprint: https://onlinelibrary.wiley.com/doi/pdf/10.1002/esp.4375.

Syvitski, J. and Milliman, J. (2007). Geology, Geography, and Humans Battle for Dominance over the Delivery of Fluvial Sediment to the Coastal Ocean. *The Journal of Geology*, 115(1):1–19.

Syvitski, J. P. M., Vörösmarty, C. J., Kettner, A. J., and Green, P. (2005). Impact of Humans on the Flux of Terrestrial Sediment to the Global Coastal Ocean. *Science*, 308(5720):376–380. Publisher: American Association for the Advancement of Science.

Taberlet, P., Bonin, A., Zinger, L., and Coissac, E. (2018). *Environmental DNA: For Biodiversity Research and Monitoring*. Oxford University Press.

Tales Tiecher (2015). *Fingerprinting sediment sources in agricultura catchments in Southern Brazil*. PhD thesis, Federal University of Rio Grande do Sul. Publisher: Unpublished.

Teixeira-de Mello, F., Barrios, M., Paredes Del Puerto, J. M., Pacheco, M., Díaz, I., Fernández Nion, C., Silvera, N., Suárez, B., Moi, D. A., Gutiérrez, J. M., Heber, E., Rodríguez-Bolaña, C., Meerhoff, M., Castro, M., González-Bergonzoni, I., D'Anatro, A., Fabre, A., Quintans, F., López-Rodríguez, A., Chalar, G., Burwood, M., and Gelós, M. (2026). Enhancing national water quality monitoring through biomonitoring: Insights from Uruguay. *Water Biology and Security*, page 100690.

Trimble, S. W. and Mendel, A. C. (1995). The cow as a geomorphic agent — A critical review. *Geomorphology*, 13(1):233–253.

Vandromme, R., Hayashi, S., Tsuji, H., Evrard, O., Grangeon, T., Landemaine, V., Laceby, J. P., Wakiyama, Y., and Cerdan, O. (2023). Lessons learnt on the impact of an unprecedented soil decontamination program in Fukushima on contaminant fluxes. *Proceedings of the National Academy of Sciences*, 120(43):e2301811120.

Vörösmarty, C. J., Meybeck, M., Fekete, B., Sharma, K., Green, P., and Syvitski, J. P. M. (2003). Anthropogenic sediment retention: major global impact from registered river impoundments. *Global and Planetary Change*, 39(1):169–190.

Walling, D. (2006). Human impact on land–ocean sediment transfer by the world's rivers. *Geomorphology*, 79(3-4):192–216.

Walling, D. E. (1983). The sediment delivery problem. *Journal of Hydrology*, 65(1):209–237.

Walling, D. E. and He, Q. (1999). Improved Models for Estimating Soil Erosion Rates from Cesium-137 Measurements. *Journal of Environmental Quality*, 28(2):611–622. _eprint: https://acsess.onlinelibrary.wiley.com/doi/pdf/10.2134/jeq1999.00472425002800020027x.

Wang, J., Zhen, J., Hu, W., Chen, S., Lizaga, I., Zeraatpisheh, M., and Yang, X. (2023). Remote sensing of soil degradation: Progress and perspective. *International Soil and Water Conservation Research*, 11(3):429–454.

World Bank Group (2022). Argentina - Country Climate and Development Report : Background Note 6 - Strategies to Decarbonize Freight Transport in Argentina : Soybean and Dairy Supply Chains. Technical Report 178458, World Bank Group, Washington, D.C.

World Bank Group (2025). MAXIMIZING INCLUSIVE AND GREEN GROWTH FROM THE EAST-WEST RAILWAY. Technical report, World Bank Group.

Xiao, Y., Xiao, Q., and Sun, X. (2020). Ecological Risks Arising from the Impact of Large-scale Afforestation on the Regional Water Supply Balance in Southwest China. *Scientific Reports*, 10(1):4150. Publisher: Nature Publishing Group.

Zhang, X. C. J. and Busteed, P. R. (2024). Accuracy and sensitivity of soil erosion estimation using 137Cs technology: A statistical perspective. *Geoderma*, 444:116863.

Zurbriggen, C., González-Lago, M., Baraibar, M., Baethgen, W., Mazzeo, N., and Sierra, M. (2020). Experimentation in the Design of Public Policies: The Uruguayan Soils Conservation Plans. *Iberoamericana – Nordic Journal of Latin American and Caribbean Studies*, 49(1):52–62.

VIII

Supplementary material

Chapter A

Supplementary material

A.1 . Thesis timeline

The first part of my PhD was focused on the analysis of the cores collected prior to my PhD in Uruguay in the Salto Grande and Rincon del Bonete dams.

The first months of my PhD were also dedicated to the validation of most of the mandatory doctoral school training (figure A.1). I had the opportunity to attend a thematic school organised by one of my thesis directors, the 'Tracing school 2024', bringing together international researchers working on the subject of sediment fingerprinting, which exposed me to a wide range of scientific and methodological perspectives from the very beginning of my PhD, deepening my curiosity on the subject and inspiring me for my future work.

Part of my doctoral training was also dedicated to the supervision of an apprenticeship, Nathan Martins, during the second year of my PhD and a short term internship, Robin Paillat, during the third year of my PhD (1 afternoon a week during 3 months).

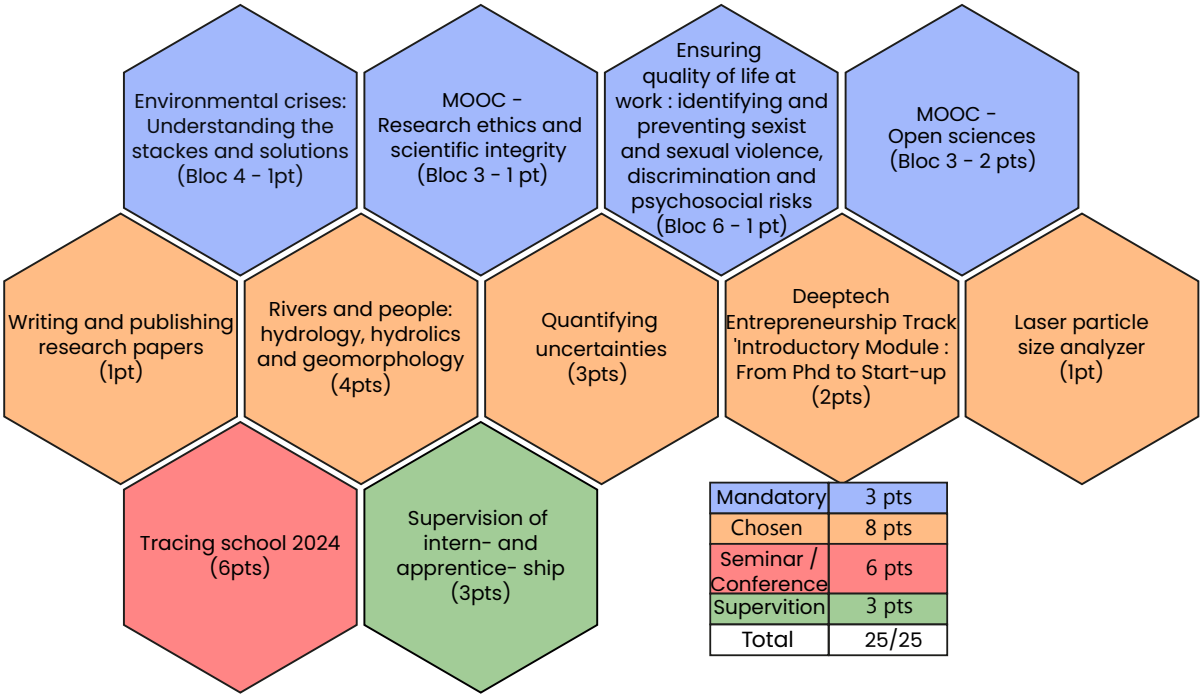

Figure A.1: Doctoral Training

During the end of the first year of my PhD, I had the opportunity to realise a sampling campaign in southern Brazil working on the improvement of the methodologies used to investigate the spatial variability of erosion processes at local scales. For that matter, two erosion sites, along hillslopes cultivated with different farming practices in an intensively cultivated catchment (800 km^2) of the Rio Grande do Sul

region in southernmost Brazil, were sampled. Of note, this sampling campaign, it's preparation, the shipping of the samples to France and their analysis took in total more than two years.

Efforts were also made to disseminate my work. Notably, during the course of my PhD, I was given the opportunity to present my work during two General Assemblies of the European Geoscience Union (EGU) (Bardelle et al. 2025a, 2026b), in PICO sessions (Presenting Interactive COntent), combining 2 min short oral presentation followed by a 'dynamic poster' presentation. Furthermore, I had the opportunity to write an article for 'The Conversation journal', an online broad-public media working directly with researcher to provide high quality vulgarisation of scientific papers, on the subject of the impact of the EU-Mercosur treaty in South-america, Bardelle et al. (2026a). A video was also made by the Observatory of Space Sciences of Grenoble (OSUG) following this article (https://www.youtube.com/watch?v=yykgB50sEuw). Bardelle et al. (2025b)'s article was also disseminated through CEA and CNRS short communications.

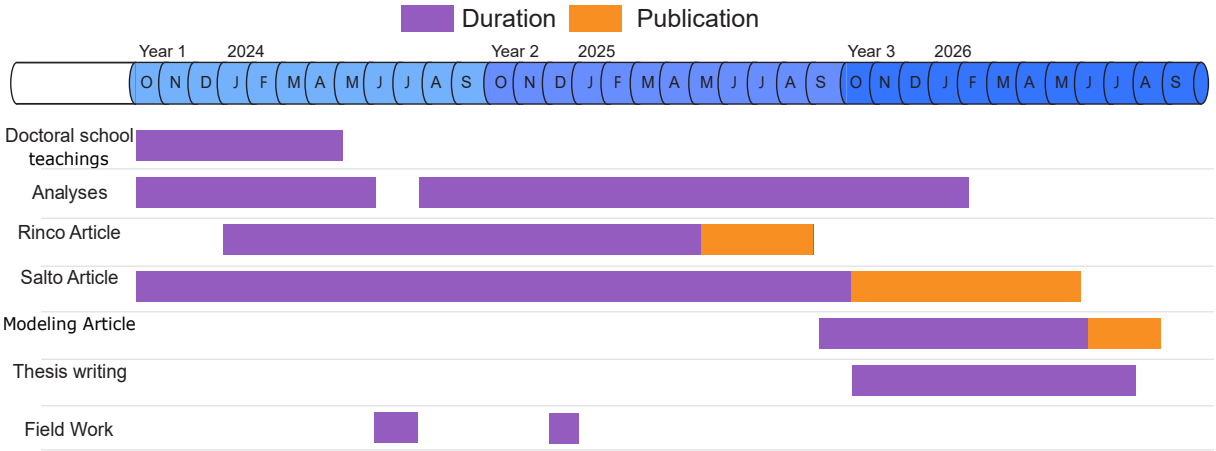

Figure A.2: Timeline of the PhD thesis

Bibliography

Bardelle, A., Gastineau, R., Evrard, O., Foucher, A., Chaboche, P.-A., and Sermondadaz, S. (2026a). Accord UE-Mercosur : quand la radiochronologie retrace l'histoire agricole de la Pampa en Amérique du Sud.

Bardelle, A., Gastineau, R., Foucher, A., Guillevic, F., Chaboche, P.-A., Chalar, G., Tassano, M., Sabatier, P., Cottin, N., Cerdan, O., and Evrard, O. (2025a). Evolution of the impact of land use changes and agricultural practices on sediment delivery in the Uruguayan Pampa. Technical Report EGU25-11054, Copernicus Meetings. Conference Name: EGU25.

Bardelle, A., Gastineau, R., Guillevic, F., Foucher, A., Chaboche, P.-A., Corcho-Alvarado, J. A., Röllin, S., Chalar, G., Sabatier, P., Tassano, M., Cottin, N., Vandromme, R., Cerdan, O., Alewell, C., and Evrard, O. (2025b). The hidden consequences of agricultural development: Soil degradation and pesticide contamination in the South American Pampa. *Science of The Total Environment*, 1002:180584.

Bardelle, A., Gastineau, R., Tiecher, T., Chalar, G., Cabrera, M., Tassano, M., Minella, J. P. G., Inda, A. V., Cottin, N., Sabatier, P., Foucher, A., Cerdan, O., Alewell, C., and Evrard, O. (2026b). Dynamics of sediment and associated pesticide transfers in cultivated southernmost Brazil since 1982. Technical Report EGU26-6446, Copernicus Meetings. Conference Name: EGU26.

Chapter B

SedimentR: Identifying major structures in sediment cores through clustering of XRF geochemical data.

Romain Ducruet[1], Amaury Bardelle[1], Pierre-Alexis Chaboche[1], Anthony Foucher[1], Pierre Sabatier[2], Olivier Evrard[1]

[1]Laboratoire des Sciences du Climat et de l'Environnement (LSCE, IPSL), Université Paris-Saclay, UMR 8212 (CEA, CNRS, UVSQ),Gif-sur-Yvette,91190,France
[2]EDYTEM, Université Savoie Mont Blanc, CNRS, Bâtiment Pôle Montagne, 5 bd de la mer Caspienne, Le Bourget du Lac,73376, France

Accepted: Under review

Published: Under review

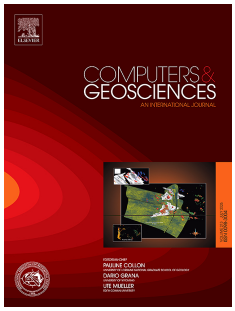

Corresponding author: romain.ducruet@lsce.ipsl.fr (R. Ducruet)

Graphical abstract

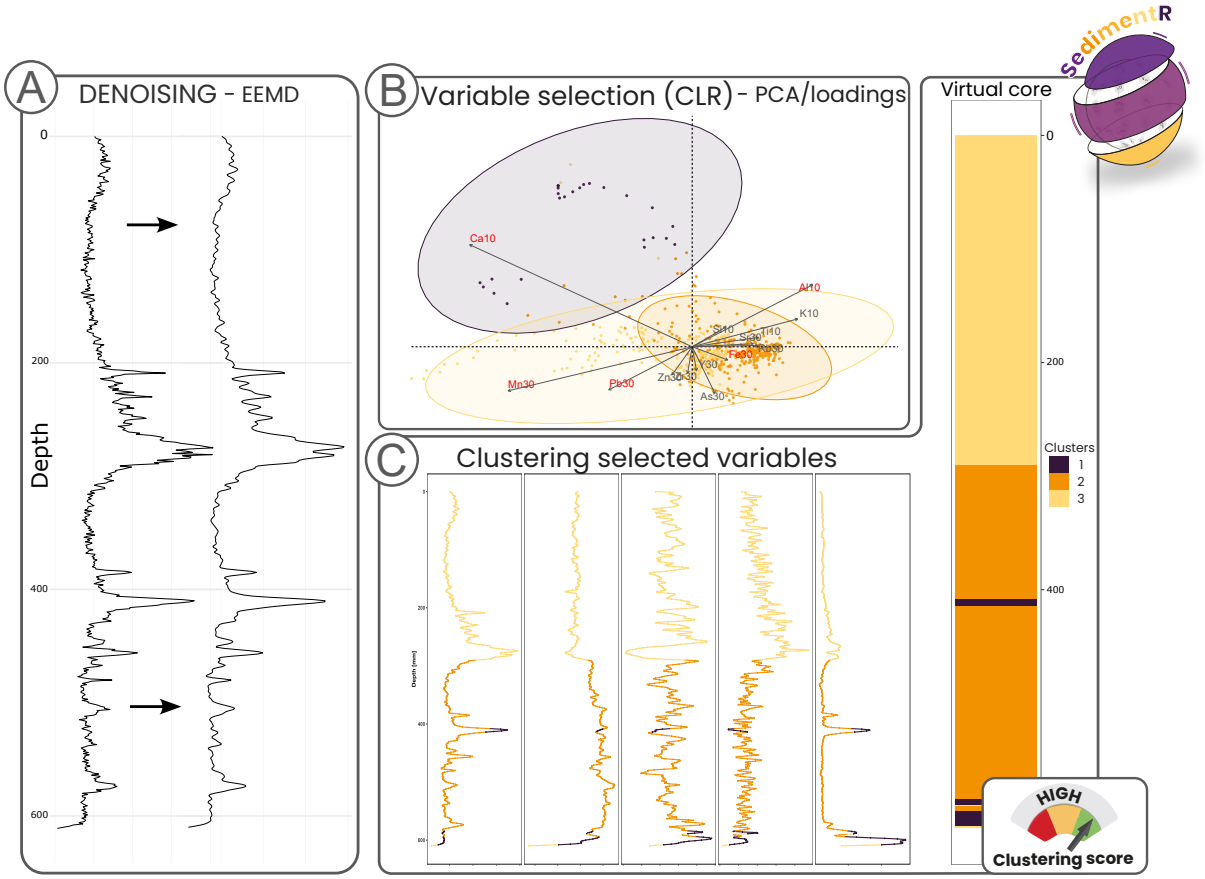

Abstract

Retrospective studies using sediment cores are powerful tool for reconstructing long-term environmental and climate changes. However, interpretation of sediment core records is mainly based on expert knowledge and may lack of reproducibility. Therefore, this study proposes the implementation of

the SedimentR package to facilitate the processing and interpretation of geochemical data analysed in sediment cores. This protocol was first specifically developed for the processing and analysis of sediment cores threw X-ray fluorescence (XRF), a procedure becoming routine in sedimentology.It enables the identification and the exclusion of highly noisy elements, ensuring that only the correctly measured variables are retained for further analysis. Principal component analysis (PCA) is then applied to identify the most influential variables through loadings, followed by clustering of selected variables using k-means or hierarchical methods. As a proof-of-concept, the SedimentR package procedure was applied to two contrasted sediment cores for which the associated data has been previously published and including, both long-term changes and event deposits. Its use was shown to validate previous interpretations. This protocol demonstrated its usefulness and practicality for partitioning distinct and robust clusters that were consistent, statistically validated, and representative of meaningful structures despite the underlying multivariate geochemical variability.

B.1 . Introduction to the package

Recent technological advances have significantly improved our understanding of natural phenomena, particularly through the development of high-resolution measurement tools such as X-ray fluorescence (Xrf) core scanners. Compared to traditional approaches, these instruments enable the rapid acquisition of sediment geochemistry at a sub-millimeter resolution (down to 0.5 mm), opening up new possibilities for detailed sedimentary and paleo environmental reconstructions. However, the increased accessibility and ease of use of this technique generates extensive and complex datasets, the interpretation of which previously required substantial expertise. The increasing accessibility of this technique, including to users with limited expertise may result in an increased likelihood of misinterpretation and methodological bias. Indeed, the XRF datasets are high-dimensional and compositional, and are often affected by measurement noise, matrix effects, and inter-element correlations. As a consequence, a careful preprocessing and the implementation of statistically robust analytical approaches are required. Nevertheless, XRF datasets are often interpreted through the visual inspection of elemental profiles and qualitative comparisons with other published data records (Croudace & Rothwell 2015), even in the framework of expert-based applications.

These approaches are inherently subjective and may not adequately account for the multivariate structure and noise characteristics of the data. Visual inspection alone can lead to the over-interpretation of noisy signals, the neglection of co-varying elements, and a limited reproducibility. These limitations raise the need for standardized, quantitative workflows for XRF data treatment. In this study, we present SedimentR, a reproducible analytical framework integrating signal denoising, objective variable selection, and the clustering of depth-resolved geochemical signals. By combining these successive steps within a consistent workflow, SedimentR facilitates the extraction of statistically robust patterns from complex sediment core datasets, thereby improving the reproducibility and transparency of geochemical interpretations.

`SedimentR` consists of six main functions, which can be each used independently according to the user's needs. Each function performs a specific operation in the XRF data processing workflow. However, to obtain reliable results, it is recommended to follow a precise sequence when using these functions successively. To simplify the processing and minimize errors associated with the succession of these steps, SedimentR also provides a workflow via the function `sedicore()`. This function automatically integrates all individual functions into a meaningful sequence, enabling the systematic processing of the data within a single execution. This optimized workflow reduces the risk of errors. SedimentR thus offers flexibility for users who want to customize each step, as well as simplicity for those who prefer a fully automated, end-to-end processing approach.

B.1.1 . Fully automated workflow: `sedicore`

Code 1: Workflow

```
Example:

sedicore( )
```

The fully guided function, automatically integrates all individual functions above in the correct sequence, enabling the systematic processing of the data within a single execution.

B.1.2 . First step: `charger`

Code 2: Dataset Loading

```
Example:
charger("folder/file.xlsx",sheet="X")

charger("path/to/file.csv", sep = ",", fileEncoding = "UTF-8")

charger( )
```

The `charger` function (shown in Code 2) allows importing data from CSV or Excel (.xlsx) files into R as a DataFrame either through providing the path to the files or through selecting it via a window popup if no path is given. It automatically handles the conversion of numeric columns, and in the case of Excel files, allow the user to select the sheet to be read.

Once the file containing the data has been selected, the user can apply a data denoising option to the data based on the Empirical Mode Decomposition (EEMD) method. This allow the selection of the least noisy data for subsequent analyses. This option is integrated into the `charger` function, but can also be used as a standalone function by calling `xrf_noise()`. The entire function is described in the section B.1.2

After loading the data and implementing the denoising option, the function `charger` provides the option to create log-transformed ratios between user-selected columns (e.g., Fe/Ti, Ca/K, etc.) interactively. These ratios are used as sedimentary and climatic proxies (according to Croudace & Rothwell (2015)). It also includes the interactive handling of missing values, allowing the user to remove specific rows or to exclude certain columns. The resulting DataFrame, optionally enriched and cleaned, is then ready for further analyses and all operations conducted can be saved in .txt files.

Loading the data

Input data can be added from ".csv" and ".xlsx" file formats and must include a column with the depth, the different elements measured by XRF . Any type of depth-resolved proxy records used in environmental and sedimentary reconstructions can be added. Importantly, the data must be provided within a single sheet.

Denoising

Code 3: Noisy variables

```
Example:
```

Intregrated in `charger` (in this case it's an option)

```
xrf_noise(X)

xrf_noise()
```

To improve signal reliability and analysis reproducibility, this package implements an optional semi-automated denoising procedure via the `xrf_noise` function. This procedure performs noise detection and filtering using Ensemble Empirical Mode Decomposition (EEMD). Although originally developed in the context of XRF data processing, the EEMD approach was designed in the package to be applicable to a broad range of depth-resolved signals.

Empirical Mode Decomposition (EMD), as described by Huang et al. (1998), provides an adaptive and data-driven framework for decomposing signals into a finite set of intrinsic mode functions (IMFs). IMFs represent intrinsic oscillatory components of the signal and are ordered from high to low frequencies. However, EMD is subject to mode mixing (i.e. an unclear separation of signals with different characteristics). Therefore, Wu & Huang (2009) created the Ensemble Empirical Mode Decomposition (EEMD), which addresses this issue by adding controlled white noise and averaging across multiple realizations. This results in more stable and physically interpretable decompositions.

Within this workflow, geochemical data (i.e. XRF) can be decomposed into IMFs enabling the adaptive separation of high-frequency stochastic noise from structured environmental variability, without making assumptions about linearity or stationarity. For each variable, the contribution of noise is quantified using a normalized noise score, defined as the ratio between the variance of selected high-frequency (often referred to as noise) IMFs and the total variance of the original signal. This metric provides an objective and reproducible criterion for evaluating signal quality across multiple variables.

Denoised signals are reconstructed by removing the identified high-frequency IMFs and summing the remaining components. This preserves low-frequency trends and meaningful variability while minimizing fluctuations induced by the noise. IMF1 therefore contains the highest-frequency contribution and typically captures instrumental noise and short-scale fluctuations. Subsequent IMFs progressively represent structured signal components. The workflow also produces a filtered dataset containing only variables that fall below a user-defined noise threshold. This approach therefore constitutes a flexible computational framework for assesing the quality of high-resolution geoscientific datasets and is broadly applicable to depth-resolved proxy records used in environmental and sedimentary reconstructions.

More generally, EEMD is widely recognized in the geoscientific literature as a powerful method for analyzing non-linear and non-stationary signals (Zhang et al. 2020), which are characteristic of many

geochemical or geophysical profiles. Unlike classical approaches such as Fourier or wavelet transforms, EEMD does not rely on predefined basis functions, allowing the decomposition to adapt directly to the data (Huang et al. 1998). Its principal strength is its ability to mitigate mode mixing through noise-assisted ensemble averaging, thereby improving the stability and interpretability of the extracted IMFs (Wu & Huang 2009). This makes it particularly effective for preserving multi-scale variability.

It is important to consider several limitations in EEMD when applying it to geoscientific signals. The method is computationally intensive due to the ensemble averaging procedure, which can become a limitation for large datasets. In addition, EEMD is sensitive to key user-defined parameters, particularly the amplitude of the added noise and the number of ensemble realizations, for which there are no universal selection criteria (Wu & Huang 2009; Huang et al. 1998). More fundamentally, EEMD inherits structural limitations from Empirical Mode Decomposition (EMD), which relies on local extrema detection and cubic spline interpolation to construct signal envelopes. This procedure can introduce interpolation-induced distortions, including overshoot and undershoot effects, which may manifest as artificial oscillations or 'pre' and 'post' peak fluctuations in the reconstructed signal (Rato et al. 2008; Kopsinis & Stephen 2009). These artifacts are particularly pronounced in signals containing sharp gradients or intermittent structures, where the envelope fitting becomes unstable. As a result, high-frequency IMFs may contain a mixture of noise and physically meaningful signal components, leading to potential distortion when these modes are removed during denoising. Furthermore, mode mixing is only partially mitigated in EEMD, as closely spaced frequency components may still be distributed across multiple IMFs, reducing the overall interpretability (Flandrin et al. 2004; Mandic et al. 2013). The method also suffers from edge effects and variability across ensemble realizations, which can affect the stability of the decomposition and the physical consistency of IMFs. Consequently, while EEMD significantly improves upon classical EMD by stabilizing the decomposition through noise-assisted averaging, residual artifacts, parameter sensitivity, and IMF ambiguity remain issues.

Ratio calculations

Multiple elemental ratios are often used in XRF-based studies. This package compiles those proposed by Croudace & Rothwell (2015), allowing users to select the most appropriate ratios according to their research objectives. To reduce skewness and handle multiplicative effects, the charger function can be used o apply a log transformation to the calculated ratios.

$$\mathrm{f_i} = \log\left(\frac{\mathrm{x_i}}{\mathrm{y_i}}\right), \text{ if } \mathrm{y_i} \neq 0 \text{ and } \mathrm{x_i}, \mathrm{y_i} \neq \mathrm{Na} \tag{B.1}$$

B.1.3 . Second or Third step: `scale_data`

Code 4: Data scaling

```
Example:
scale_data(X)
scale_data()
```

A cache with the created datasets is maintained in the background so that users can specify a dataset containing all the filtered or denoised variables and ratios generated in the previous step using the `xrf_noise` function, or select a cached dataset.

The `scale_data` function facilitates the selection, normalization, and export of user-defined XRF datasets. Before processing, it allows the user to interactively remove unwanted columns, such as depth measurements at different energies or elements that were identified to be associated with high noise levels.

After selecting the columns, the function applies centered log-ratio (CLR) normalization to all columns except those representing pre-computed log ratios, which are left unchanged. The resulting dataset combines the CLR-transformed variables with the retained log ratio columns, producing a dataset ready for multivariate analyses such as PCA.

$$\mathrm{y_{ij}} = \log\left(\frac{\mathrm{x_{ij}}}{\mathrm{g_i}}\right), with\ \mathrm{g_i} = \left(\prod_{\mathrm{j=1}}^{\mathrm{q}} \mathrm{x_{ij}}\right)^{1/\mathrm{q}} \tag{B.2}$$

- x_{ij} = raw value of element j at depth i
- q = number of elements used in the CLR transformation at depth i
- g_i = geometric mean of all elements measured at the same depth i
- y_{ij} = CLR-transformed value for element j at depth i

B.1.4 . Fourth step: `prop.select`

Code 5: PCA analysis

```
Example :
prop.select(X)
prop.select()
```

A cache of the created datasets is maintained in the background so that users can specify either the dataset containing all the scaled variables and ratios generated in the previous step using the `scale_data` function, or select the cached dataset.

The `prop.select` function performs a Principal Component Analysis (PCA) on the dataset of normalized variables to identify the most informative elements. By examining the contribution of each variable to the selected principal components, the function identifies those that best capture the structure and variance of the data. Users can choose the number of components to retain using cumulative variance, broken-stick, or manual selection methods and can define a percentile threshold to automatically select the most significant variables. Overall, `prop.select` provides an interactive workflow to reduce dimensionality and extract key variables for subsequent analyses, such as clustering or pattern identification.

Cumulative variance

1. The proportion of variance is calculated for each components j :

$$\lambda_j = \frac{\sigma_j^2}{\sum_{i=1}^{p} \sigma_i^2} \tag{B.3}$$

   where σ_j^2 is the eigenvalue (i.e., the square of the standard deviation σ_j of the j-th principal component), and p, the total number of components (or initial number of properties).

2. The cumulative variance is then calculated until the k component :

$$V_k = \sum_{j=1}^{k} \lambda_j \tag{B.4}$$

3. The smallest integer k is chosen so that :

$$V_k \geq \theta$$

   where θ is the threshold chosen by the user (example : $\theta = 0.9$ for 90%)

The number of principal components to retain is computed from the calculated cumulative variance and based on the user's given threshold.

Broken-stick method

As mentioned, the number of components to retain can also be computed using the broken-stick method implemented in the package.

The proportion of variance is calculated for each components j :

$$E(\lambda_j) = \frac{1}{k}\sum_{i=j}^{k}\frac{1}{i} \tag{B.5}$$

where E(λ_j) is the expected proportion of variance for each j component (out of k).

This method is based on the comparison of the observed eigenvalues to those expected under a null model where the total variance is randomly distributed among components (serving as a reference baseline to determine whether the observed results are significantly different from randomness or whether a meaningful structure or effect can be detected in the data). Only components with an explained variance that exceeded the corresponding broken stick expectation are considered significant and retained (Frontier 1976; Jackson 1993; Jol).

Selection of the most influential properties

The contribution of each variable to the retained components is then evaluated through their loadings, allowing the identification of the most influential variables. L_{ij} is defined as the *loading* of the i variable on the j principal component in the PCA. The most influential properties (in absolute value) are then identified for each components j, .

To this end, the following method is applied :

1. The absolute weight of the loadings on each j components is calculated :

$$w_{ij} = |L_{ij}| \tag{B.6}$$

2. The S_j threshold is determined based on the percentile of the weights

$$\mathrm{S_j} = Quantile_p(w_{1j}, w_{2j}, \ldots, w_{nj}) \tag{B.7}$$

where p is the chosen percentile. For example, for the 90^{e} percentile of the weights, $p = 0.90$

3. Finally, the i variables are selected such as :

$$w_{ij} \geq S_j$$

Thus, only the variables with a contribution equal to or greater than the user-defined threshold are retained for each component.

B.1.5 . Fifth step: `xrf_clust`

Code 6: Cluster analysis

```
Example :
xrf_clust(X)
xrf_clust()
```

A cache with the created datasets is maintained in background, so that the user can either specify the dataset containing all the selected variables and ratios generated in the previous step using `xrf_clust` function or select the cached dataset.

The `xrf_clust` function performs a clustering analysis on the dataset of selected variables. This helps to determine the optimal number of clusters, classify observations within the clusters, analyze cluster drivers, and provide multiple visualization options. The main enhancement of this approach is the coupling of variable selection from PCA with the estimation of the optimal number of clusters. The optimal cluster number is determined using a comprehensive set of validity indices available in the `NbClust` package (Charrad et al. 2014), providing a robust, data-driven method for clustering via the k-means or hierarchical clustering.

The user can visualize the clustering in the PCA graph.

They can also manually select the number of clusters, for example based on the number of sedimentary facies visually identified in the core. Both approaches (i.e., automatic and manual clustering) are fully supported. However, to assess the robustness of the clustering solution, several validation metrics can be computed. Comparing the automatic and manually selected numbers of clusters helps determining which configuration yields the most reliable and interpretable results. To assess the robustness of the clusters, four complementary indices are calculated: Silhouette, Davies–Bouldin, Bootstrap Stability, and Calinski-Harabasz.

B.1.6 . Internal validation and stability assessment for clustering quality

To ensure the robustness and interpretability of the clustering results, several complementary internal validation indices were computed using the standard clustering validation tools available. These indices

quantify different and non-redundant aspects of clustering quality, including geometric separation, compactness, reproducibility under resampling, and global structural consistency. Rather than relying on a single metric, a multi-criteria validation framework was adopted in order to reduce methodological bias and improve the interpretability of the cluster structure. Specifically:

- the Silhouette index evaluates how well each observation fits within its assigned cluster relative to neighboring clusters, providing a measure of boundary sharpness and assignment confidence;
- the Davies-Bouldin index quantifies cluster similarity by comparing intra-cluster dispersion to inter-cluster centroid separation, thereby assessing redundancy between clusters;
- the Bootstrap stability index measures the reproducibility of cluster assignments under repeated resampling, allowing discrimination between statistically stable clusters and sampling artefacts;
- the Calinski-Harabasz index evaluates the global structure of the clustering solution by comparing between-cluster variance to within-cluster variance. It is commonly used for selecting the optimal number of clusters.

Taken all together, these complementary criteria provide a hierarchical validation strategy combining geometric quality assessment, statistical robustness and structural interpretability. This approach ensures that the retained clustering solution reflects a meaningful partition of the multivariate geochemical space rather than an artifact of the clustering algorithm or sampling variability.

Silhouette Index

The Silhouette measures cohesion and separation of clusters. For each point i:

$$s(i) = \frac{b(i) - a(i)}{\max(a(i), b(i))} \tag{B.8}$$

where:

- $a(i)$ = average distance between point i and all other points in the same cluster
- $b(i)$ = minimum average distance between point i and points in other clusters

The mean Silhouette over all points gives an overall assessment:

$$\bar{s} = \frac{1}{n} \sum_{i=1}^{n} s(i) \tag{B.9}$$

Interpretation:

- Values near 1 $\rightarrow$ well-separated clusters
- Values around 0 $\rightarrow$ overlapping clusters
- Negative values $\rightarrow$ possible misclassification

Davies–Bouldin Index

Measures cluster similarity. For each cluster pair i, j:

$$R_{ij} = \frac{S_i + S_j}{M_{ij}} \tag{B.10}$$

where:

- $S_i = \frac{1}{|C_i|} \sum_{x \in C_i} \|x - \mu_i\|$ = intra-cluster dispersion
- $M_{ij} = \|\mu_i - \mu_j\|$ = distance between cluster centers

For cluster i, take the worst-case ratio:

$$R_i = \max_{j \neq i} R_{ij} \tag{B.11}$$

The Davies–Bouldin index is the mean over all clusters:

$$DBI = \frac{1}{k} \sum_{i=1}^{k} R_i \tag{B.12}$$

where:

- k = number of clusters

Interpretation:

- Lower values are better
- $DBI < 0.5 \rightarrow$ well-separated clusters
- $DBI > 1 \rightarrow$ overlapping clusters

Bootstrap Stability

Assesses how reproducible clusters are under resampling. For cluster C_i:

$$\text{Stability}_i = \frac{1}{B}\sum_{b=1}^{B} \text{Jaccard}(C_i, C_i^{(b)}) \tag{B.13}$$

where:

- B = number of bootstrap resamples
- $C_i^{(b)}$ = cluster obtained on the bth bootstrap sample
- $\text{Jaccard}(C_i, C_i^{(b)}) = \frac{|C_i \cap C_i^{(b)}|}{|C_i \cup C_i^{(b)}|}$ = similarity between original and bootstrap cluster assignments

Average stability over all clusters:

$$\bar{\text{Stability}} = \frac{1}{k}\sum_{i=1}^{k} \text{Stability}_i \tag{B.14}$$

where:

- k = number of clusters

Interpretation:

- $> 0.8 \rightarrow$ stable clusters
- $< 0.4 \rightarrow$ unstable clusters, possibly artefacts

Calinski–Harabasz Index

Evaluate the quality of a clustering by comparing between-cluster dispersion to within-cluster cohesion.

Calinski–Harabasz (CH) index for k clusters is defined as follows:

$$CH(k) = \frac{BCSS/(k-1)}{WCSS/(n-k)} \tag{B.15}$$

where:

- $BCSS = \sum_{j=1}^{k} n_j \|\bar{x}_j - \bar{x}\|^2$ = between-cluster sum of squares
- $WCSS = \sum_{j=1}^{k} \sum_{x_i \in C_j} \|x_i - \bar{x}_j\|^2$ = within-cluster sum of squares
- k = number of clusters
- n = total number of observations
- n_j = number of points in cluster C_j
- $\bar{x}_j$ = centroid of cluster C_j
- $\bar{x}$ = global centroid of the dataset

Interpretation:

- Higher CH values indicate better-defined clusters (high separation and high cohesion)
- Commonly used to select the optimal number of clusters by maximizing $CH(k)$

B.1.7 . Sixth step: `visual.clust`

Code 7: Visualization

```
Example :

visual.clust(data_final)

visual.clust( )
```

A cache with the created datasets is maintained in background, so that the user can either specify the dataset containing all the selected variables and ratios and clusters generated in the previous step using `xrf_clust` function or select the cached dataset.

The `visual.clust` function allows to integrate and visualize multivariate geochemical profiles, clustering results, and stratigraphic context within a single interactive and reproducible framework. The procedure was designed to support exploratory analysis and final figure generation for sediment core interpretation, combining elemental profiles, cluster assignments, and optional chronological and visual annotations.

Data structure and preprocessing

The input dataset consists of depth-resolved measurements (e.g., XRF peak areas), alongside an optional categorical cluster assignment. Prior to visualization, the data are reshaped from a wide format to a long format to enable the consistent handling of multiple elemental variables. Each observation is associated with a depth coordinate, an element identifier, and a measured intensity value. Users may select either all available variables, a predefined subset derived from multivariate preprocessing (e.g., PCA-selected variables), or a manual selection. When PCA-based selection is available, only the variables identified that are the most representative of the multivariate structure are retained for plotting. Depth is treated as the primary stratigraphic axis and is consistently plotted in reverse order to reflect sediment accumulation (from top to bottom).

Handling of stratigraphic discontinuities

To preserve stratigraphic integrity, depth irregularities are explicitly detected by comparing successive depth intervals. When deviations exceed approximately twice the median sampling resolution, discontinuities are flagged and used to segment profiles. This prevents artificial interpolation across hiatuses or sampling gaps, ensuring that line segments are only drawn within stratigraphically coherent intervals.

Optional transformation and scaling

As geochemical variables often exhibit strong differences in magnitude and skewed distributions, an automatic scaling diagnostic is performed. For variables exhibiting high dynamic range (orders of mag-

nitude differences), a log10 transformation can be optionally applied. This ensures comparability across elements and improves visual discrimination of both low- and high-amplitude signals. Otherwise, axis scaling is adaptive, using either linear or logarithmic breaks depending on the data structure.

Cluster integration and color encoding

When clustering information is available, each observation is color-coded according to its cluster assignment. A default perceptually balanced palette is provided, although users may specify custom color schemes for publication-quality figures. Clusters are used as a stratigraphic overlay to highlight compositional regimes within each elemental profile. This allows direct visual comparison between geochemical variability and unsupervised grouping structure.

Geochemical profile visualization

Elemental profiles are displayed as faceted horizontal, log-style plots, where each facet corresponds to a single element. Within each facet, geochemical intensity is plotted against depth using connected line segments and points (data can be visualized in CLR by accepting the creation of the `Sediment_Geochem_Clusters_Analysis` tab and using the `visual.clust()` function) at the end of the workflow). Faceting ensures that each element is displayed on an independent scale while preserving stratigraphic alignment across all variables. The resulting visualization provides a high-resolution representation of vertical geochemical variability and facilitates identification of co-variation patterns, abrupt transitions, and stratigraphic boundaries.

Virtual core representation

To provide a synthetic stratigraphic overview, cluster assignments are grouped into contiguous depth intervals. These intervals are defined by changes in clusters and stratigraphic discontinuities. The resulting “virtual core” representation collapses multivariate information into a simplified lithostratigraphic-style column, with each segment corresponding to a homogeneous cluster interval. This representation enables direct comparison between geochemical profiles and inferred compositional units, improving the interpretability of clustering results in a stratigraphic context.

Integration of age–depth models

An optional age–depth model can be incorporated by linking depth-matched chronological data to the geochemical dataset. When provided, the system incorporates the chronological data based on depth and generates a secondary temporal axis. This enables geochemical variability to be visualized simultaneously of in both the depth and age domains. Users can also define specific key points (ages or

depths) to be projected onto the stratigraphy using nearest-neighbor matching. This allow the addition of reference horizons across both depth and timescales.

Sediment core imagery

To support geological interpretation, core photographs can be integrated directly into the visualization layout. The images are scaled to match the depth interval of the dataset and are aligned with the stratigraphic axis. This allow direct visual comparison between physical sedimentary structures and geochemical or cluster-based patterns.

Output and export

All visual outputs are generated using a modular framework and combined using patchwork layouts when multiple panels (profiles, virtual core, age–depth model, imagery) are needed. Figures can be exported in publication-ready formats (PNG or PDF) with modular dimensions and resolution, ensuring compatibility with journal submission requirements. The full Sediment_Geochem_Clusters_Analysis tab with the different datasets created can also be exported in .csv and .xlsx.

B.2 . Case studies using SedimentR

To order understand how the package can be used, methodologies and potential interpretation of the results, two cases studies were carried out based on previous studies conducted on a sediment core collected in a reservoir (Péguières) draining a burned catchment in Southeastern France (Ducruet et al. 2026) and on a core collected in a lake (Allos) of the French Alps (Wilhelm et al. 2012).

B.2.1 . Peguières case study:

The site of Peguières is composed of three small ponds within the Estérel Massif in Southern France. Over the past 50 years, the area has been affected by two major wildfires (1987 and 2003). The core PEG07, selected for inclusion in the package, was collected from a lake impacted by the 2003 wildfire. Ducruet et al. (2026) show that wildfires lead to increased erosion in Mediterranean watersheds, but that this response varies greatly among sites. In some cases, particularly following the 2003 fire, erosion rates remain high for several decades, indicating a sustained disruption of sediment dynamics. In others, however, a trend toward the gradual recovery and conditions close to the pre-fire state is observed. The study thus highlights a long-term post-fire response, challenging the hypothesis of a rapid return to pre-fire conditions.

The objective for using the sedimentR package is to evaluate whether the same structural interpretations as those described in Ducruet et al. (2026) can be recovered through this reproducible statistical framework with an XRF core-scanner dataset. The aim is to assess whether such an unsupervised ap-

proach can reproduce the main findings of the study, particularly the characterisation of the long-term impact of wildfires on sedimentary dynamics in Mediterranean ecosystems. Particular attention is also given to manganese (Mn), in order to evaluate its robustness as a discriminant variable emerging from the PCA selection. The goal is to determine whether Mn consistently contributes to the clustering structure, thereby supporting the conclusions of Ducruet et al. (2026) regarding its potential role as a tracer for identifying wildfire-related disturbances in Mediterranean environmental systems.

Method, interpretability and results with SedimentR

Denoising Level Selection Signal denoising was performed using the Ensemble Empirical Mode Decomposition (EEMD) framework. Two denoising levels were considered:

- reliable denoising: removal of the first intrinsic mode function (IMF1)
- strong denoising: removal of the first two intrinsic mode functions (IMF1–IMF2)

The following parameters were used during the EEMD decomposition:

- Noise strength: 0.2
- EEMD iterations: 100
- Noise IMFs removed: 1 (reasonable denoising)

Noise Score Interpretation The noise score was computed for each variable in order to quantify the proportion of signal variance associated with the highest-frequency IMFs. This score provides an objective indicator of signal contamination with high frequency noise. A high noise score (close to 1) indicates that most of the variance is dominated by noise, whereas a low noise score (close to 0) indicates a predominantly structured signal component. Variables were retained using a noise-score threshold of 0.3. The dataset initially contained 31 elemental XRF variables. After applying the noise-score threshold (noise score < 0.3), 18 variables were retained and 13 variables were discarded. This resulted in a reduced feature space that is richer in structurally informative geochemical signals, making it better suited to subsequent dimensionality reduction and clustering analyses.

CLR Transformation After noise filtering and negative-value screening, the dataset contained 18 variables, including depth. For the CLR transformation, the following variables (depth, Mn(10 KeV), Inco, Co) were excluded prior to compositional transformation. These exclusions were performed for methodological consistency with compositional data analysis requirements and to avoid redundancy or non-geochemical signal contamination:

- Depth was removed because it represents a stratigraphic coordinate rather than a compositional variable. Including depth in a CLR transformation would violate the assumptions of compositional data analysis, in which only components closed of a geochemical system should be transformed. Depth is therefore preserved as an external explanatory axis for stratigraphic interpretation.
- Mn10 was excluded due to redundancy with Mn30. Both variables represent manganese intensities measured at different acquisition settings; howerver, Mn30 (30KeV) provides a more stable and energetically reliable signal for downstream multivariate analysis. Retaining both would introduce artificial weighting of the same geochemical process in PCA space.
- Incoherent scattering (Inco) and Coherent scattering (Co) were removed because they are not elemental concentrations but physical scattering signals primarily related to matrix effects. While they can be usefull for quality control or normalization strategies in some workflows, they are not appropriate components of compositional transformations such as CLR, as they can distort the geochemical structure when treated as elemental variables.

The final dataset used for PCA therefore contained 14 compositional variables, ensuring a statistically coherent feature space that focused on structurally meaningful geochemical variability and minimizing redundancy prior to multivariate structure extraction.

Principal Component Analysis (PCA) and loadings threshold Principal Component Analysis was applied to this dataset to identify the dominant multivariate geochemical structures. A threshold was retained based on a cumulative explained variance criterion of 90%. In this case, four components were sufficient to exceed this threshold, collectively explaining 93.54% of the total variance. In practice, this means that the PCA model was configured to retain enough components to explain at least 90% of the total variance present in the dataset after transformation.

Beyond component retention, variable contribution was assessed using a 90th percentile threshold applied to absolute loading values. In PCA, loadings represent the correlation between the original variables and the principal components. High absolute loadings indicate variables that strongly influence the orientation of a given component in multivariate space. By selecting variables above the 90th percentile, the analysis isolates only the most influential geochemical signals. The variables that exceeded this threshold (i.e., Ca, Mn, Al, Fe and Pb), therefore represent the dominant geochemical drivers of the system. Their repeated strong absolute loadings across multiple components suggest that they structure the dataset multi-dimensionally rather than being confined to a single independent process.

The fact that only five variables dominate the high-loading tail indicates a high degree of effective dimensional compression. Although 14 variables are retained, the system's structure is largely governed by a small subset of chemically meaningful elements. This is a key result, because it implies that subsequent clustering or interpretation steps are driven by a reduced and physically interpretable geochemical core rather than diffuse multivariate noise.

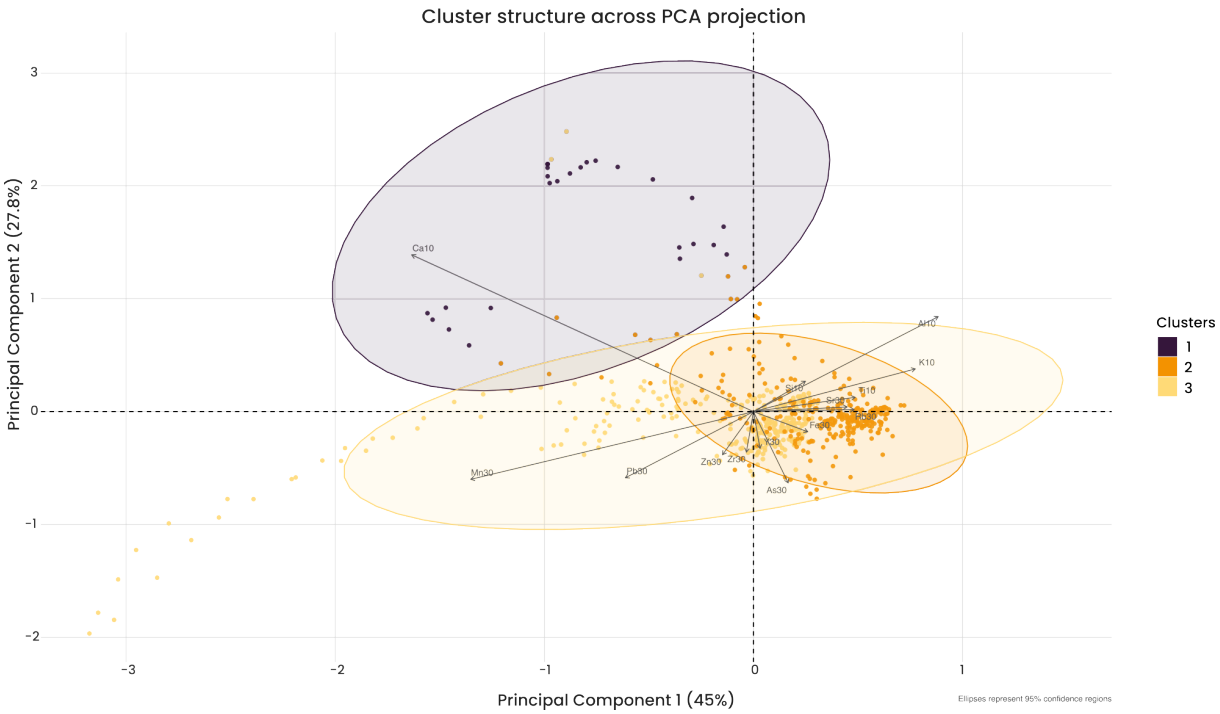

Figure B.1: PCA of the Peguières core dataset showing the first two principal components (PC1 and PC2). Samples are grouped according to the identified clusters, with 95% confidence ellipses illustrating the dispersion of each cluster.

Clustering application The clustering structure was determined using a k-means framework, where the optimal number of clusters was inferred using the NbClust decision procedure. Rather than relying on a single validation criterion, this method evaluates a large set of internal clustering indices, of which provides an independent estimate of the optimal number of clusters. In this case, the selection of the optimal number of clusters is based on an explicit majority-rule aggregation of index votes. The distribution of recommendations obtained from NbClust is as follows: 2 indices suggested k = 2; 15 indices supported k = 3; 1 index proposed k = 4; 3 indices suggested k = 7; and isolated indices proposed k = 9 and k = 10, respectively. This voting structure cleraly favours the solution k = 3, which received the most methodological support of all the tested configurations.

Once the optimal number of cluster (k=3) had been established, the interpretability of the clustering solution was assessed through cluster driver analysis using ANOVA-based F-statistics. This approach evaluates how strongly each variable contributes to differentiating clusters by comparing inter-cluster variance to intra-cluster variance. Variables with high F-values therefore represent strong discriminators of cluster membership, meaning that their distributions differ significantly across the identified groups. The results show that Fe and Ca overwhelmingly dominate the clustering structure, with extremely high F-values (1381.5 and 864.9 respectively) and highly significant p-values. This indicates that these two elements are the primary axes along which the dataset is partitioned. Pb also plays a significant discriminating role, although to a lesser extent, while Mn and Al contribute to a lower extent, although with some statistically significant separation power. Cluster 1 is characterized by elevated Ca and Al concentrations together with high Mn and Fe levels and relatively low Pb levels. Cluster 2 shows a contrasting signature dominated by high Fe and Pb concentrations, combined with a depletion in Ca and Mn. Cluster 3 is strongly enriched in Mn and Pb while exhibiting lower levels of Al and Fe.

Overall, the k-means solution reveals a structurally robust partitioning of the dataset into three geochemically interpretable clusters. Rather than representing arbitrary statistical divisions, the clusters correspond to coherent multivariate geochemical regimes, which are controlled by a limited number of dominant elemental drivers. In this case, Fe and Ca act as the principal axes of separation, while Pb and Mn refine secondary geochemical differentiation.

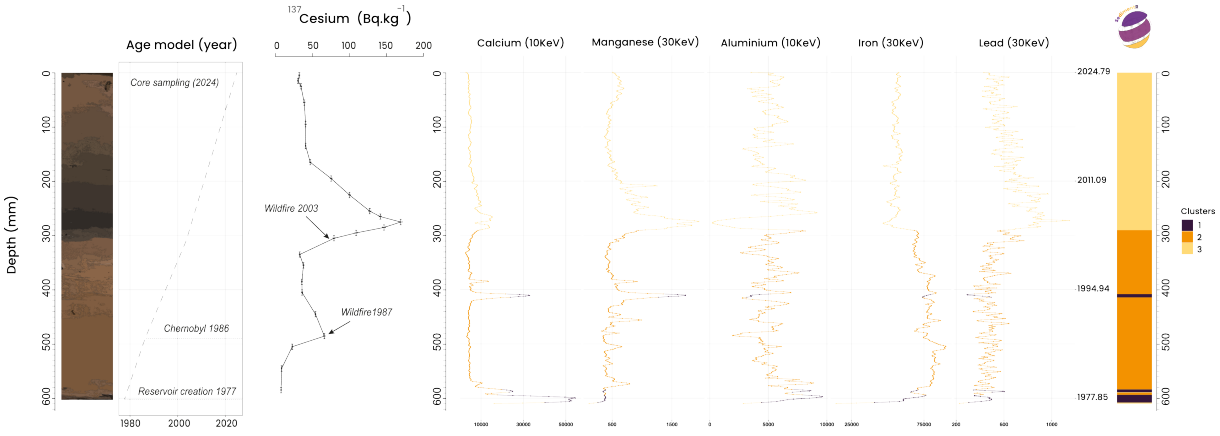

Figure B.2: Results of the clustering workflow applied to the Peguières core dataset. The figure combines(i) a photo from the sediment archive; (ii) the sediment core age-depth model; (iii) Cesium-137 (^{137})Cs activity profiles used for chronological reconstruction; (iv) multi-proxy geochemical profiles relative to depth, alongside the associated clustering results; and (v) the clustered virtual core reconstruction. Together, these elements provide an integrated view of the sedimentary sequence, linking chronological information, geochemical variability, and data-driven stratigraphic clustering.

Clustering application Clustering robustness was assessed using a set of complementary internal validation metrics, each capturing a different aspect of cluster quality. These metrics jointly evaluate statistical stability, geometric separation, and compactness of the resulting partitions together, providing a multi-dimensional diagnostic of clustering reliability rather than relying on a single criterion.

Bootstrap stability, with a value of 0.944, indicates a very high level of reproducibility of the clustering solution under resampling. This means that when the dataset is repeatedly perturbed and reclustered, the assignment of observations to clusters remains highly consistent. Such a high value suggests that the identified clusters are not sensitive to sampling variability and are therefore likely to reflect a stable underlying structure in the data rather than random fluctuations.

The Calinski–Harabasz index, which reached 1128.0, evaluates the ratio between 'between-cluster' dispersion and 'within-cluster' dispersion. A high value indicates that the clusters are both internally compact and well separated from each other in the feature space. In this case, the magnitude of the index is indicativeof a very strong global clustering structure, where the variance between groups far exceeds the variance within groups.

The Silhouette index, equal to 0.681, provides a point-wise measure of how well each observation fits within its assigned cluster compared to neighboring clusters. Values in this range indicate a good separation between clusters, meaning that most observations are significantly closer to their own cluster centroid than to alternative clusters. While not indicating perfect separation, this value confirms a well-defined partition with limited overlap between groups.

The Davies–Bouldin index, with a value of 0.577, measures the average similarity between each cluster and its most similar counterpart, based on within-cluster dispersion and inter-centroid distance. Lower

values correspond to better clustering quality. In this case, the value indicates relatively limited overlap between clusters and satisfactory compactness, which is consistent with a well-structured partitioning of the data.

Collectively, these results demonstrate that the clustering solution is both statistically stable and geometrically meaningful. Indeed, the analysis supports the conclusion that the PCA-reduced XRF compositional space is partitioned into three distinct and robust geochemical groups. These groups are not only statistically validated but also structurally coherent, reflecting a meaningful organization of the underlying multivariate geochemical variability. This clustering result is consistent with the results of Ducruet et al. (2026). Indeed, starting from the wildfire event, the analysis highlights a marked structural change across the watershed. This shift appears to be significant, as the change in clustering remains stable until the top of the core, suggesting that the system has not returned to its pre-wildfire state. This result indicates a long-term change rather than a transient disturbance. In a second step, the objective was to evaluate the hypothesis that manganese (Mn) is a relevant tracer of wildfire in Mediterranean ecosystems. The results of the PCA-based selection confirm that Mn plays a significant role in the data structure, as it is included among the contributing variables. Although it is not the most dominant element in terms of its relative contribution, it shows a marked enrichment in the cluster associated with the post-fire period. This pattern futher supports its potential as a geochemical indicator of fire impacts.

B.2.2 . Validation of the clustering workflow using random variables

To demonstrate the importance and robustness of the entire workflow for variable selection and achieving the most reliable clustering possible, an additional test was conducted on the same sediment core. The same pre-processing steps were applied, including noise reduction and variable removal. The main difference occurred during the variable selection phase via PCA. While the initial approach relied on k-means clustering applied to a subset of five variables, the second analysis used all fourteen available variables. The results of this comparison are summarized below. They demonstrate that selecting and reducing dimensionality by retaining only the most informative variables significantly reduces the complexity of the dataset and therefore improves the quality of the clustering.

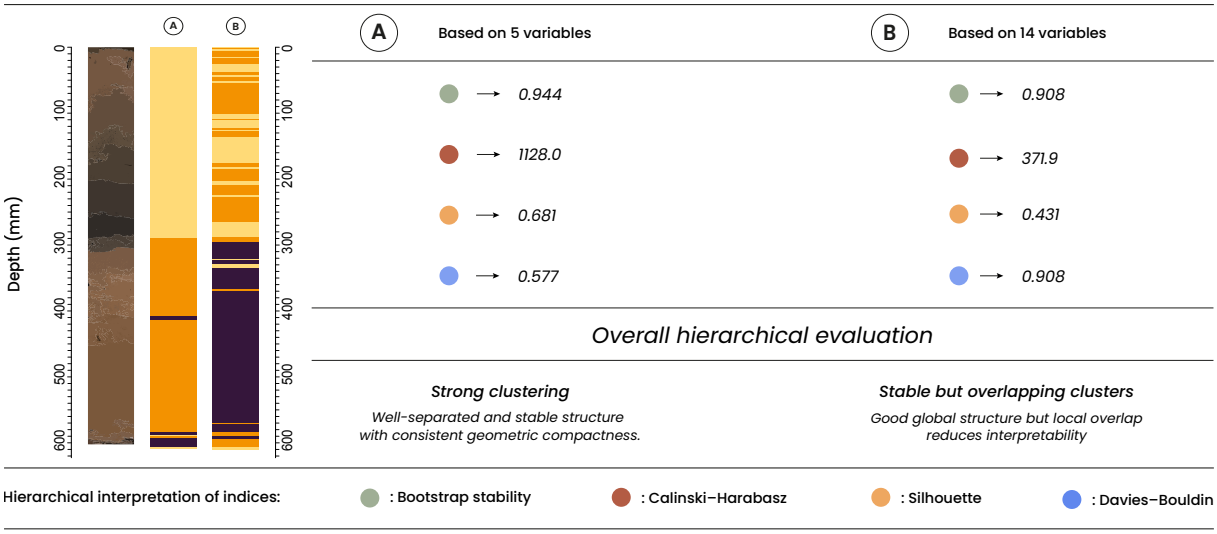

Figure B.3: Comparison of clustering results obtained with and without PCA-based variable selection. The first approach retained the most influential variables according to cumulative explained variance and loading threshold criteria (A), whereas the second approach used the full dataset (B).

B.2.3 . Allos case study:

In this second example,Wilhelm et al. (2012) presents an in-depth study of flood events that have occurred in the French Alps over the past 1,400 years. The study is based on an analysis of sediment cores from the Lake Allos. Analysis of core ALO09P12 revealed distinct sedimentary layers that correspond to periods of extreme precipitation events. Each specific layer is characterized by a sharp, coarse basal part with an upward normal grading; high density; low total organic carbon (TOC) content; the presence of terrestrial plant remains; and systematic calcium (Ca) enrichment (Wilhelm et al. 2012) and all layers are correlated across the different lake basins (Wilhelm et al. 2015).

A chronology based on short-lived radionuclides and radiocarbon associated, alongside multi-proxy analyses, has made it possible to correlate these event deposits with major precipitation events over the last 1,400 years. This has revealed an increased flood frequency between 1,300 and 1,900 AD, corresponding to the Little Ice Age (LIA). Indeed, on a multi-centennial timescale, the flood frequency at Lake Allos is consistent with the general moisture, large river hydrology, and temperature patterns found in the north-western Mediterranean region and corresponding to a low flood activity during the Medieval Warm Period (MWP) and a high flood activity during the cold/wet LIA. Over the Holocene, human activities have also impacted the flood records (Brisset et al. 2017)

Here, the objective was to test the SedimentR package on XRF geochemical variables measured to identify flood deposits and then to compare them with the proposed initial layering. SedimentR analysis effectively reduced the dimensionality of the geochemical signal while preserving information relevant to sedimentary interpretation. Of the 11 initially measured variables, only 8 were retained after noise filtering; subsequently, 3 major elements (Ca, Mn and Fe, Figure 4) were identified as accounting for the

bulk of the variance (81.77%) and thus as the dominant tracers of flood deposits within this sedimentary archive. From these three elements, the k-means clustering method identified three optimal clusters. The first cluster is characterized by a low calcium content and very high concentrations of manganese and iron. The second cluster exhibits a very high calcium content, while manganese and iron concentrations remain low. The third cluster represents an intermediate state between the two former, with relatively high concentrations of all three elements (Ca, Mn, and Fe).

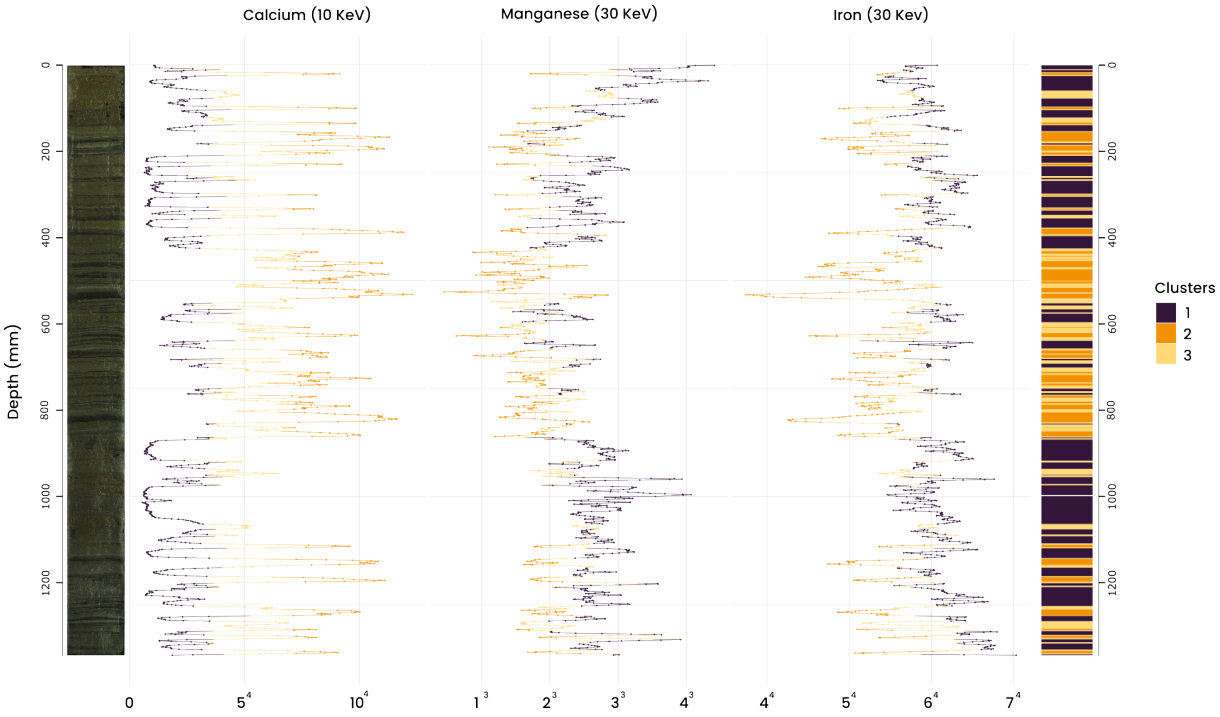

Figure B.4: Results of the Allos clustering workflow implemented in the SedimentR package. The figure combines (i) a photo of the sediment core; (ii) geochemical profiles as a function of depth, alongside the associated clustering results; and (iii) the clustered virtual core reconstruction.

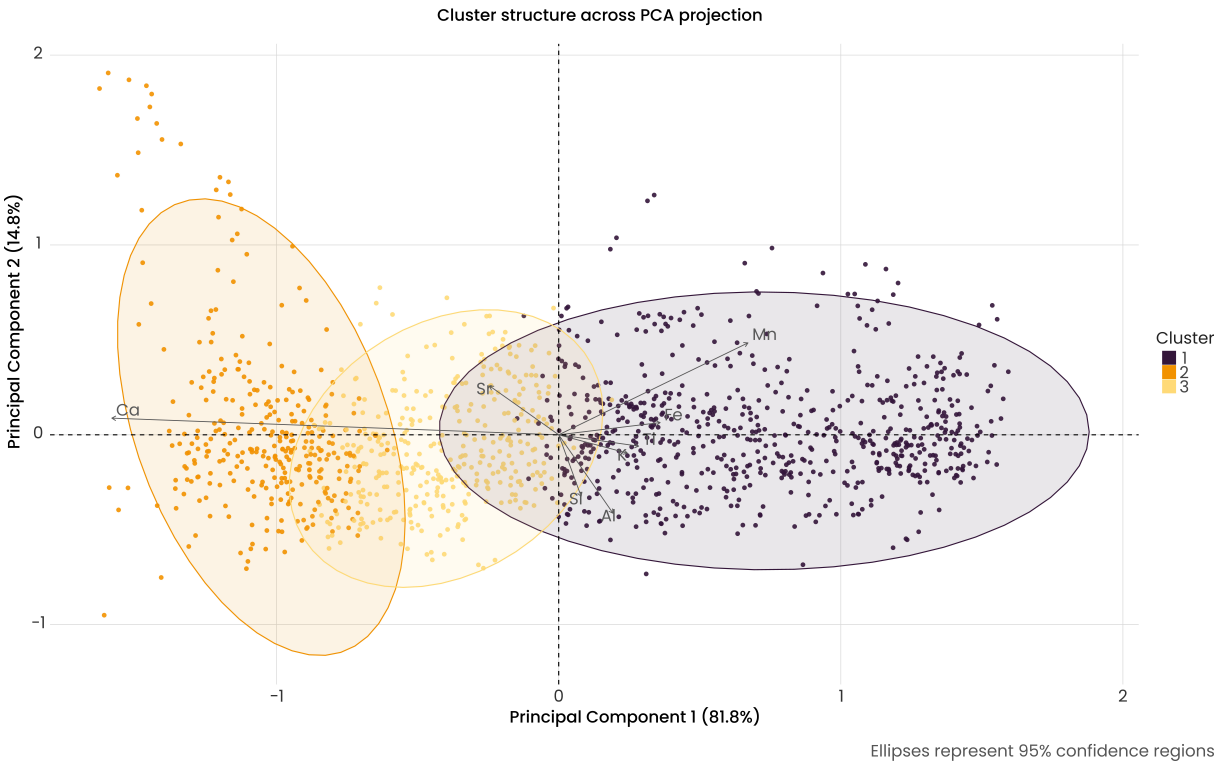

Figure B.5: PCA of the Allos core dataset showing the first two components, with 95% confidence ellipses showing the dispersion of each cluster. Samples are grouped according to the identified clusters.

Clusters are statistically supported by very high validation indices (bootstrap = 0.949; Calinski–Harabasz >5,000), indicating robust and genuine structures. Separation is considered good to moderate (Silhouette = 0.583; Davies-Bouldin = 0.544), which is consistent with natural systems where transitions between different facies are rarely strictly discrete.

Analysis of variance (ANOVA) confirms that Ca is the primary discriminating factor, followed by Fe and Mn. This result is consistent with the conclusions of the previous study, which identified interbedded layers characterized by systematic Ca enrichment and interpreted them as flood event deposits over the past 1,400 years (Wilhelm et al. 2012). Cluster 2 and 3, as identified by the unsupervised workflow, correspond closely to this geochemical signature. This agreement supports the ability of the geochemical signal alone to detect flood-related deposits in this lake sediment, that were previously identified using more resource-intensive multi-proxy approaches. It also highlights the relevance of Ca as a key proxy for flood events in this system.

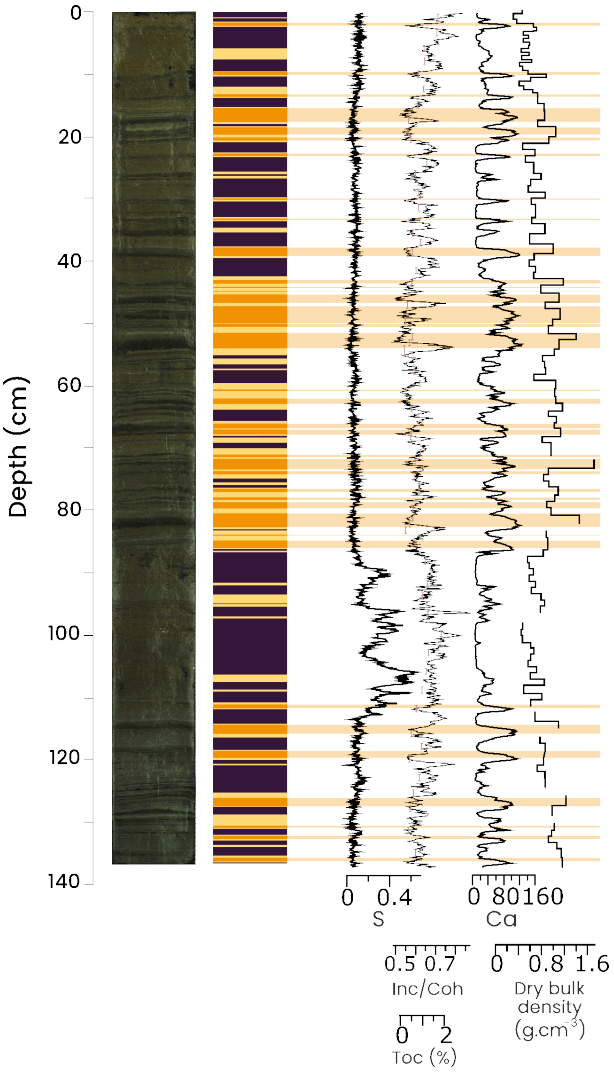

Figure B.6: Allos comparison between the clustering result to identify flood events (orange square cluster 2/3) and the result from the previous study of Wilhelm et al. (2012)in light orange bands.

The package therefore supported the automated detection of events. Historical flood deposits (thick, graded layers) were identified exclusively on the basis of the statistical structure of the data, without making prior assumptions. Geochemical clustering robustly highlighted historical flood deposits, particularly through Cluster 2/3, which is characterized by Ca enrichment, as detailed in Wilhelm et al. (2012). This approach closely reproduced the results of an independent multi-proxy study, offering an automated methodology, high resolution, and proving its applicability to diverse sedimentary archives. Finally, the package complemented the multi-proxy approach rather than replacing it. It enabled rapid, high-resolution screening, and facilitated interpolation between dated levels. It also provided a powerful means to extend the reconstructions across space and time.

B.3 . Conclusions

Using a robust and reproducible framework for the denoising, selection of the dataset's driving variables, and multiple statistical indices, the SedimentR package provides a new and statistical protocol for the clustering of depth-revolved variables.

The advantages of the package result from several key features. First, it enables objective thresholding and classification. Unlike the visual or empirical identification of layers, clustering provides a quantitative and reproducible identification of events. Secondly, it simplifies the data by condensing variables into key indicators, allowing for a simplified, yet robust, interpretation of the underlying processes.

This protocol was applied to two different datasets and demonstrated its usefulness in partitioning distinct and robust geochemical groups that were coherent and statistically validated, and reflected a meaningful organization of the underlying multivariate geochemical variability. Notably, the protocol was capable of detecting clusters corresponding to historical flood deposits, extreme events such as wildfires and their long-term impacts, and smaller-scale floods and events. Efforts will be made in the future to maintain this package and users are invited to explore other datasets in order to validate the capacity of this protocol to detect a large variety of events and their impacts that could possibly be missed with visual inspection only.

B.4 . Supplementary Materials

Hierarchical interpretation of indices (with cut-offs):

1. **Bootstrap stability**

   → Question: Do the clusters really exist? Statistical credibility filter.

   < 0.40 = very unstable (artefactual)

   0.40–0.60 = weak stability

   0.60–0.75 = moderate stability

   0.75–0.85 = stable

   > 0.85 = very stable

2. **Calinski–Harabasz**

   → Question: Is there a real global cluster structure in the data? Structural existence filter.

   < 100 = no clear structure

   100–200 = weak structure

   200–500 = moderate structure

   500–1000 = good structure

   > 1000 = excellent structure

3. **Silhouette**

   → Question: Are the cluster boundaries geometrically sharp? Refinement of separation quality.

   < 0.20 = very poor / heavy overlap

   0.20–0.40 = weak separation

   0.40–0.60 = moderate separation

   0.60–0.75 = good separation

   > 0.75 = excellent separation

4. **Davies–Bouldin**

   → Question: How much do clusters overlap? Refinement of geometric compactness and redundancy.

   Cut-offs:

< 0.50 = excellent (very compact, well separated)

0.50–0.75 = good separation

0.75–1.00 = moderate separation

1.00–1.25 = weak separation

> 1.25 = poor / strong overlap

Bibliography

(). Jolliffe, I. T. (2002). Principal Component Analysis (2nd ed.). New York Springer-Verlag. - References - Scientific Research Publishing. URL: https://www.scirp.org/reference/referencespapers?referenceid=2528917.

Brisset, E., Guiter, F., Miramont, C., Troussier, T., Sabatier, P., Poher, Y., Cartier, R., Arnaud, F., Malet, E., & Anthony, E. J. (2017). The overlooked human influence in historic and prehistoric floods in the European Alps. *Geology*, *45*, 347–350. URL: https://doi.org/10.1130/G38498.1. doi:10.1130/G38498.1.

Charrad, M., Ghazzali, N., Boiteau, V., & Niknafs, A. (2014). NbClust: An R Package for Determining the Relevant Number of Clusters in a Data Set. *Journal of Statistical Software*, *61*, 1–36. URL: https://doi.org/10.18637/jss.v061.i06. doi:10.18637/jss.v061.i06.

Croudace, I. W., & Rothwell, R. G. (Eds.) (2015). *Micro-XRF Studies of Sediment Cores: Applications of a non-destructive tool for the environmental sciences* volume 17 of *Developments in Paleoenvironmental Research*. Dordrecht: Springer Netherlands. URL: https://link.springer.com/10.1007/978-94-017-9849-5. doi:10.1007/978-94-017-9849-5.

Ducruet, R., Foucher, A., Chaboche, P.-A., & Evrard, O. (2026). Pre- and post-wildfire erosion dynamics as derived from sediment core analyses in Mediterranean ecosystems (Var, Southern France). *Geomorphology*, *503*, 110278. URL: https://www.sciencedirect.com/science/article/pii/S0169555X26001212. doi:10.1016/j.geomorph.2026.110278.

Flandrin, P., Rilling, G., & Goncalves, P. (2004). Empirical mode decomposition as a filter bank. *IEEE Signal Processing Letters*, *11*, 112–114. URL: https://ieeexplore.ieee.org/document/1261951. doi:10.1109/LSP.2003.821662.

Frontier, S. (1976). Etude de la decroissance des valeurs propres dans une analyse en composantes principales: Comparaison avec le modele du baton brise. *Journal of Experimental Marine Biology and Ecology*, *25*, 67–75. URL: https://www.sciencedirect.com/science/article/pii/0022098176900769. doi:10.1016/0022-0981(76)90076-9.

Huang, N. E., Shen, Z., Long, S. R., Wu, M. C., Shih, H. H., Zheng, Q., Yen, N.-C., Tung, C. C., & Liu, H. H. (1998). The empirical mode decomposition and the Hilbert spectrum for nonlinear and non-stationary time series analysis. *Proceedings of the Royal Society A: Mathematical, Physical and Engineering Sciences*, *454*, 903–995. URL: https://doi.org/10.1098/rspa.1998.0193. doi:10.1098/rspa.1998.0193.

Jackson, D. A. (1993). Stopping Rules in Principal Components Analysis: A Comparison of Heuristical and Statistical Approaches. *Ecology*, *74*, 2204–2214. URL: https://www.jstor.org/stable/1939574. doi:10.2307/1939574.

Kopsinis, Y., & Stephen, M. (2009). Development of EMD-Based Denoising Methods Inspired by Wavelet Thresholding. *Signal Processing, IEEE Transactions on*, *57*, 1351–1362. doi:10.1109/TSP.2009.2013885.

Mandic, D. P., Rehman, N. u., Wu, Z., & Huang, N. E. (2013). Empirical Mode Decomposition-Based Time-Frequency Analysis of Multivariate Signals: The Power of Adaptive Data Analysis. *IEEE Signal Processing Magazine*, *30*, 74–86. URL: https://ieeexplore.ieee.org/document/6633076. doi:10.1109/MSP.2013.2267931.

Rato, R. T., Ortigueira, M. D., & Batista, A. G. (2008). On the HHT, its problems, and some solutions. *Mechanical Systems and Signal Processing*, *22*, 1374–1394. URL: https://www.sciencedirect.com/science/article/pii/S0888327007002701. doi:10.1016/j.ymssp.2007.11.028.

Wilhelm, B., Arnaud, F., Sabatier, P., Crouzet, C., Brisset, E., Chaumillon, E., Disnar, J.-R., Guiter, F., Malet, E., Reyss, J.-L., Tachikawa, K., Bard, E., & Delannoy, J.-J. (2012). 1400 years of extreme precipitation patterns over the Mediterranean French Alps and possible forcing mechanisms. *Quaternary Research*, *78*, 1–12. URL: https://www.sciencedirect.com/science/article/pii/S0033589412000294. doi:10.1016/j.yqres.2012.03.003.

Wilhelm, B., Sabatier, P., & Arnaud, F. (2015). Is a regional flood signal reproducible from lake sediments? *Sedimentology*, *62*, 1103–1117. URL: https://onlinelibrary.wiley.com/doi/abs/10.1111/sed.12180. doi:10.1111/sed.12180. _eprint: https://onlinelibrary.wiley.com/doi/pdf/10.1111/sed.12180.

Wu, Z., & Huang, N. E. (2009). Ensemble empirical mode decomposition: a noise-assisted data analysis method. *Advances in Adaptive Data Analysis*, *01*, 1–41. URL: https://www.worldscientific.com/doi/abs/10.1142/S1793536909000047. doi:10.1142/S1793536909000047.

Zhang, X., Li, J., Liu, X., & Chen, Z. (2020). Improved EEMD-based standardization method for developing long tree-ring chronologies. *Journal of Forestry Research*, *31*, 2217–2224. URL: https://doi.org/10.1007/s11676-019-01002-y. doi:10.1007/s11676-019-01002-y.

université PARIS-SACLAY

ÉCOLE DOCTORALE
Sciences de l'Environnement d'Île-de-France (SEIF)

Titre : Reconstruction des impacts des changements d'usage des sols sur les transferts de sédiments et de contaminant dans le sud du Brésil et en Uruguay durant l'Anthropocène

Mots clés : datation, traçage sédimentaire, modélisation, érosion des sols, radionucléides

Résumé : L'Amérique du Sud en général et les biomes de la Pampa et de la Forêt Atlantique en particulier (Brésil, Argentine, Uruguay), ont connu une expansion et une intensification agricoles rapides depuis la fin du XXe siècle. Ces transformations incluent la conversion de paysages naturels en terres cultivées, l'adoption généralisée du semis direct et une augmentation marquée de l'utilisation de pesticides. Depuis 1985, les surfaces consacrées aux pâturages, aux terres cultivées et aux plantations forestières ont augmenté respectivement de 23 %, 160 % et 288 % en Amérique du Sud. Malgré leur ampleur, l'impact de ces changements sur l'érosion des sols et le transfert des sédiments reste insuffisamment quantifié, en raison de l'absence de suivi instrumental à long terme et d'archives permettant la reconstruction des processus passés. Cette thèse visait ainsi à reconstituer la redistribution des sols et les transferts de contaminants associés à différentes échelles spatiales et temporelles dans le sud de l'Amérique du Sud, en combinant des approches multi-proxies. Elle a permis d'évaluer la représentativité et la fiabilité de la méthode des inventaires de radionucléides pour quantifier l'érosion à l'échelle du versant, en analysant la variabilité spatiale, les potentiels biais et incertitudes méthodologiques de la méthode, et en comparant ces estimations à celles issues d'un modèle d'érosion distribué et évènementiel. L'impact des changements d'utilisation des sols a pu être étudié à partir de l'analyse d'archives prélevées dans deux lacs-réservoirs contrastés du bassin du fleuve Uruguay. Le réservoir de Salto Grande, situé à l'aval d'un bassin fortement anthropisé, permet d'étudier les dynamiques récentes (1980-2023) du transfert sédimentaire et de contaminants. À l'inverse, le réservoir de Rincón del Bonete fournit un enregistrement à plus long terme (1945-2025) de la transition entre paysages naturels et agricoles, en ce comprise l'évolution des pratiques culturales et de l'usage des pesticides. Les résultats montrent une forte variabilité spatiale de la redistribution des sols à l'échelle de la parcelle, avec des inventaires de radionucléides et des estimations d'érosion contrastées pour des profils collectés à proximité immédiate. Le choix du modèle de conversion impacte tant l'intensité reconstruite de la redistribution de sol que son signe (érosion ou accumulation). Dans le bassin de Salto Grande, les flux sédimentaires ont diminué de 61 % depuis les années 1980, tandis que la contribution de la partie sud du bassin aux sédiments du barrage a augmenté de 71% depuis les années 2000, en lien avec les aménagements hydrauliques, l'expansion agricole et la généralisation du semis direct. Une augmentation concomitante des flux de pesticides a également été observée. À plus long terme, l'archive sédimentaire de Rincón del Bonete indiquent l'occurrence d'une phase agricole initiale ayant un impact limité sur l'érosion des sols (1945–1991), suivie d'une diminution des apports sédimentaires lors de l'adoption du semis direct et de rotations avec pâturages (1991–2007), puis une augmentation récente de l'érosion et des flux sédimentaires (2007–2023) associée à l'intensification agricole et dissocié d'une variabilité naturelle. La détection de pesticides interdits, tels que le DDT, suggère une remobilisation de contaminants historiques liée à cette hausse récente de l'érosion. Ces travaux contribuent à améliorer la reconstruction des dynamiques d'érosion et de transfert sédimentaire dans une région où les données restent limitées, et soulignent la nécessité d'un suivi continu et de mesures agro-environnementales visant à limiter l'érosion des sols et la contamination par les pesticides.

Title : Reconstructing the impacts of changes in land use on the transfers of sediments and contaminants in Southern Brazil and in Uruguay during the Anthropocene

Keywords : dating, sediment tracing, modelling, soil erosion, radionuclides

Abstract : South America in general, and the Pampa and Atlantic Forest biomes (Uruguay, Argentina and Brazil) in particular, have undergone a rapid agricultural expansion and intensification since the late 20th century. These changes include the conversion of natural landscapes to cropland, the widespread adoption of no-tillage systems, simplification of landscapes and a marked increase in pesticide use. Since 1985, pasture, cropland, and forest plantation areas have increased by 23%, 160%, and 288%, respectively. Despite their magnitude, the implications of these transformations for soil erosion and sediment transfers remain insufficiently quantified, mainly because of the limited availability of long-term monitoring for their retrospective reconstruction. This thesis deployed multi-proxy approaches to reconstruct soil redistribution and sediment-associated contaminant transfers across a range of spatial and temporal scales in southern South America. A first objective was to evaluate the representativeness and reliability in fallout radionuclide inventory approaches for reconstructing erosion processes at the hillslope scale. This included assessing spatial variability and methodological limitations of radionuclide-based estimates, and comparing these estimates with outputs from a distributed erosion model. A second objective was to assess the impact of land-use change and agricultural intensification on sediment transfer dynamics investigating two contrasting reservoir systems within the Uruguay River basin. The Salto Grande reservoir, constructed in 1980, and draining a catchment already largely under agricultural use, was investigated to identify sediment sources and associated contaminant fluxes and examine the effects of no-tillage expansion and soybean monocropping (1980-2023). In contrast, the Rincón del Bonete reservoir, constructed in 1945 in a predominantly uncultivated basin, provides a longer-term record (1945-2023) of the transition from rather natural to more anthropogenic landscapes, including agricultural changes in tillage practices and increasing pesticide application. Results highlight substantial spatial variability in soil redistribution at the hillslope scale, with neighbouring cores yielding contrasting radionuclide inventories and erosion estimates. The choice of conversion model was found to significantly impact both the magnitude and the sign of soil redistribution. In the Salto Grande basin, sediment fluxes decreased by 61% since the 1980s, while the contribution from the southern part of the basin increased by 75% since the 2000s. These changes can be explained by the construction of dams upstream, agricultural expansion downstream, and the widespread adoption of monocropping no-tillage practices. Furthermore, an associated increase in pesticide fluxes was recorded. Over longer timescales, sediment records from Rincon del Bonete indicate an initial phase of limited impact despite the initiation of pesticide use (1945-1991), followed by a reduction in sediment delivery during the transition to no-tillage and pasture rotation (1991-2007), and subsequently (2007-2023) a renewed increase in sediment fluxes linked to large-scale land conversion and intensified herbicides application, largely decoupled from natural variability. The detection of banned pesticide compounds such as DDT further suggests the recent remobilisation of legacy contaminants. Overall, this work contributes to improving the reconstruction of soil erosion and sediment transfers in a data-scarce region since the onset of modern agriculture in South America and provides a framework for combining sediment archives, radionuclide tracers, and modelling tools. These results support a more robust assessment of the environmental impacts of agricultural development and highlight the need for continued monitoring and for the implementation of agri-environmental measures to mitigate soil erosion and pesticide contamination in Southern South America.